Report
R-16-02
February 2016

Initial modelling of the near-field hydrogeology

Exploring the influence of host rock characteristics and barrier properties

Report for the safety evaluation SE-SFL

Elena Abarca
Diego Sampietro
Mariona Miret
Henrik von Schenck

SVENSK KÄRNBRÄNSLEHANTERING AB

SWEDISH NUCLEAR FUEL
AND WASTE MANAGEMENT CO

Box 250, SE-101 24 Stockholm
Phone +46 8 459 84 00
skb.se

SVENSK KÄRNBRÄNSLEHANTERING

ISSN 1402-3091
SKB R-16-02
ID 1514526
February 2016

Initial modelling of the near-field hydrogeology

Exploring the influence of host rock characteristics and barrier properties

Report for the safety evaluation SE-SFL

Elena Abarca, Diego Sampietro, Mariona Miret
Amphos[21] Consulting S.L.

Henrik von Schenck, Svensk Kärnbränslehantering AB

Summary

The present work is part of the SFL safety evaluation and deals with the hydrological conditions in the repository near-field. The term near-field refers to the rock vaults, their components and barriers, as well as the surrounding rock in the vicinity of the repository.

In order to provide input to the site selection process for SFL the safety evaluation aims at evaluating the proposed repository concept (Elfwing et al. 2013) at a representative site in Sweden. The evaluation will be performed with existing data from SKB's site investigation programs for the nuclear fuel repository in Laxemar and Forsmark and from less extensive investigations performed at a few other sites. In the present work, geological data from the Laxemar area has been used to represent typical Swedish bedrock. An existing regional hydrogeology simulation (Vidstrand et al. 2010) has been used as input to supply initial and boundary conditions to the near-field hydrology model.

A central objective has been to investigate the influence of host rock characteristics on the groundwater flow through the repository. Near-field simulations have been performed to sample two different rock domains at three different depths (300 m, 500 m, and 700 m depth). Models and results have been analysed with respect to the hydraulic conductivity of the rock, the presence of fracture zones, the effect of groundwater salinity, and the direction of the local flow system relative to the orientation of the rock vaults. In addition, the groundwater flow through repository has been evaluated assuming different scenarios of barrier degradation, as well as repository closure approaches.

Sammanfattning

Följande arbete utgör en del av säkerhetsvärderingen för SFL och rör hydrologiska förhållanden i förvarets närområde. Termen närområde avser bergsalar, deras komponenter och barriärer samt det omgivande berget, i förvarets närhet.

I syfte att ge underlag till platsvalsprocessen för SFL är målsättningen i säkerhetsvärderingen att utvärdera det föreslagna förvarskonceptet (Elfwing et al. 2013) på en representativ plats i Sverige. Utvärderingen kommer genomföras med befintliga data från SKB:s platsundersökningsprogram för Kärnbränsleförvaret i Laxemar och Forsmark och från mindre omfattande undersökningar som genomförts på ytterligare några platser. I följande arbete har geologiska data från Laxemar-området använts för att representera en typisk svensk berggrund. En existerande simulering av den regionala hydrogeologin (Vidstrand et al. 2010) har använts för att tillhandahålla initial- och radvillkor åt modellen över närområdets hydrologi.

Ett huvudsyfte med detta arbete har varit att undersöka påverkan av bergets egenskaper på grundvattenflödet genom förvaret. Simuleringar av närsområdeshydrologin har därför utförts vid flera olika positioner i berget; två bergvolymer har undersökts på tre olika djup (300 m, 500 m och 700 m djup). Modeller och resultat har analyserats med avseende på bergets konduktivitet, närvaron av sprickzoner, påverkan av grundvattnets salthalt samt riktningen hos grundvattenflödet i förhållande till orienteringen av bergsalarna. Vidare har flödet genom förvaret utvärderats under olika antagande rörande barriärdegradering, såväl som för olika förslutningsalternativ.

Contents

1 Introduction

SKB plans to dispose of long-lived low and intermediate level waste in SFL. The waste comprises waste from the operation and decommissioning of the Swedish nuclear power plants, legacy waste from the early research in the Swedish nuclear programmes, and smaller amounts of waste from hospitals, industry and research. The long-lived low and intermediate level waste from the nuclear power plants consists of neutron-irradiated components and control rods. The total quantity of long-lived waste planned for SFL is estimated to approximately 16,000 m^3, of which about one third originates from the nuclear power plants. The remainder comes from AB SVAFO and Studsvik Nuclear AB, who manage the legacy waste and the waste from hospitals, industry and research.

In the proposed concept (Elfwing et al. 2013), SFL is as a deep geological repository with two storage vaults:

- one vault for the metallic waste from the nuclear power plants, and
- one vault for legacy waste from AB SVAFO and Studsvik Nuclear AB.

The vault for the metallic waste (BHK) is designed with a concrete barrier. The waste is segmented, after which the parts are deposited in steel tanks and stabilized with grout. The steeltanks are emplaced in the repository. This section of the repository is backfilled with concrete, which acts as a barrier against groundwater flow and contributes to a low diffusion rate and high sorption of many radionuclides. The concrete in the barrier will create an alkaline environment in the repository section, reducing the corrosion rate of the steel and thus limiting the release rate of radionuclides.

The vault for the legacy waste (BHA) from AB SVAFO and Studsvik Nuclear AB is designed with a bentonite barrier. The waste is deposited in containers designed for SFL and stabilized with grout. These containers are emplaced in the repository. The section is backfilled with bentonite. The bentonite acts as a barrier by limiting the groundwater flow, thereby making diffusion the dominant transport mechanism for radionuclides through the bentonite. Bentonite clay also has the ability to efficiently filter colloids.

Figure 1-1 shows a schematic representation of the repository design, with the BHA vault in the foreground and the BHK vault in the background.

In order to provide input to the site selection process for SFL the safety evaluation aims at evaluating the proposed repository concept (Elfwing et al. 2013) at a representative site in Sweden. The evaluation will be performed with existing data from SKB's site investigation programs for the nuclear fuel repository in Laxemar and Forsmark and from less extensive investigations performed at a few other sites. In the present work, geological data from the Laxemar area has been used to represent typical Swedish bedrock.

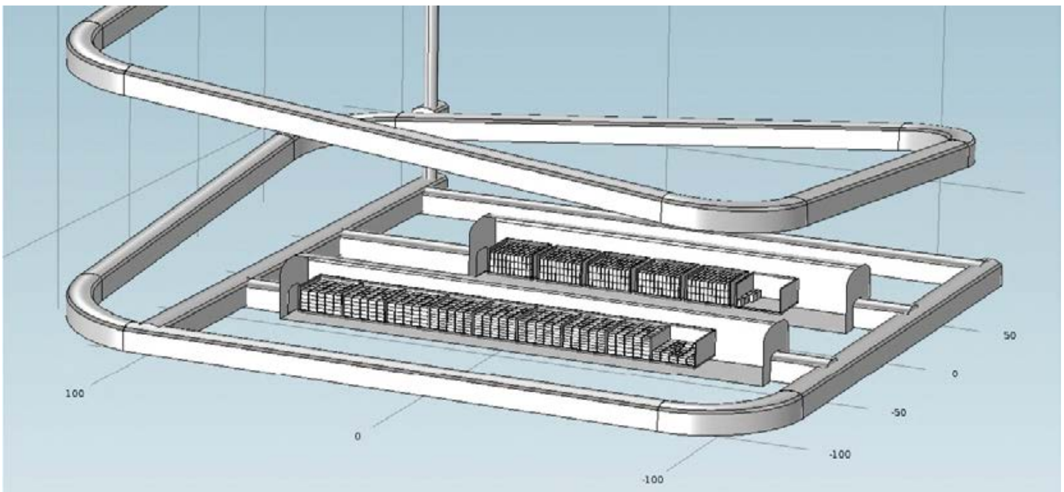

Figure 1-1. *SFL repository design with BHA vault (front) and BHK vault (back).*

1.1 Objectives

1.1.1 Influence of the host rock

A central objective of this work has been to investigate the influence of the host rock on the flow through the SFL repository. Numerical models of the SFL near-field have been analysed with respect to the:

- Presence of deterministic and stochastic fractures.
- Water salinity.
- Direction of the local flow system.
- Flow through vaults and waste domains.

1.1.2 Influence of repository orientation

A second objective has been to analyse the influence of repository orientation relative to the direction of the groundwater flow. This can affect flow through the vaults and waste as well as the interaction between vaults.

1.1.3 Influence of barrier degradation and alternative repository closure

Finally, it has been an objective of this work to assess the groundwater flow through SFL assuming different scenarios for barrier degradation, as well as alternative repository closure approaches.

1.2 Outline of the report

Chapter 2 describes the repository scale model used for the groundwater flow simulations. The geometry and material properties of the engineered structures and the rock in the repository near-field are presented. The chapter also details the model equations solved and the boundary conditions. An overview of the result presentation is provided.

Chapter 3 presents results related to the influence of host rock characteristics on the flow through the SFL vaults and waste. Two rock domains in the Laxemar area have been investigated at 300 m, 500 m, and 700 m depth. Results illustrate the local groundwater flow fields at the different locations as well the potential interaction between vaults.

Chapter 4 is concerned with the influence on vault and waste flow as affected by repository orientation relative to the direction of groundwater flow. In one case the groundwater flow is mainly vertical, and in as second case the flow is mainly horizontal. Indicators of vault interaction are presented.

Chapter 5 presents results of vault and waste flow affected by changing hydraulic conductivity in the backfill materials of BHA and BHK. Degraded states of bentonite and concrete are analysed as well as an alternative initial state.

Chapter 6 concerns the closure of the repository, when the repository tunnels and shafts are sealed. A base case closure assumes that plugs will be installed in the ramp and shaft, intended to limit groundwater flow through the tunnels. The base case is compared to a closure alternative with no plugs as well as an alternative with an extended sealing of the access tunnels, at vault depth. The effect of alternative closures is analysed in terms of vault and waste flows and as changes in local flow conditions.

2 Description of the repository scale model

2.1 Repository geometry and materials

Two storage vaults are planned for SFL; one vault for legacy waste (BHA), and one vault for the metallic waste from the nuclear power plants (BHK). The BHA vault will be backfilled with bentonite and the BHK vault will be backfilled with concrete. Figure 2-1 and Figure 2-2 show schematic cross-sections of BHA and BHK, respectively.

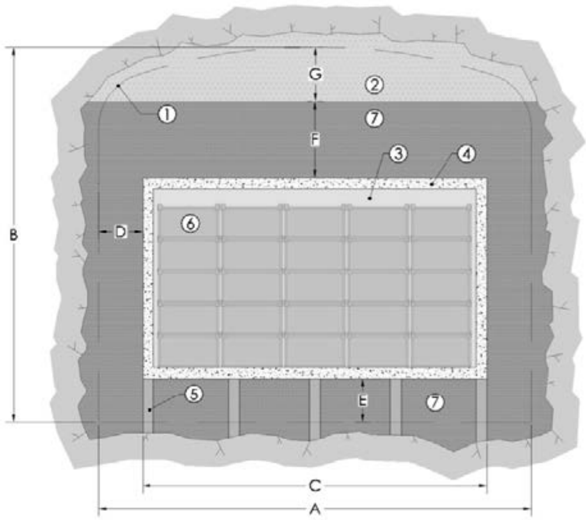

Figure 2-1. *Schematic cross-sectional layout of BHA (from Elfwing et al. 2013). Legend: 1.) Theoretical tunnel contour. 2) Bentonite pellets. 3) Grout. 4) Concrete structure (0.5 m). 5) Granite pillars. 6) Waste packages. 7) Bentonite blocks. Approximate dimensions: A = 20.6 m, B = 18.5 m, C = 16 m, D = 2.3 m, E = 2.4 m, F = 4 m, G = 3.7 m.*

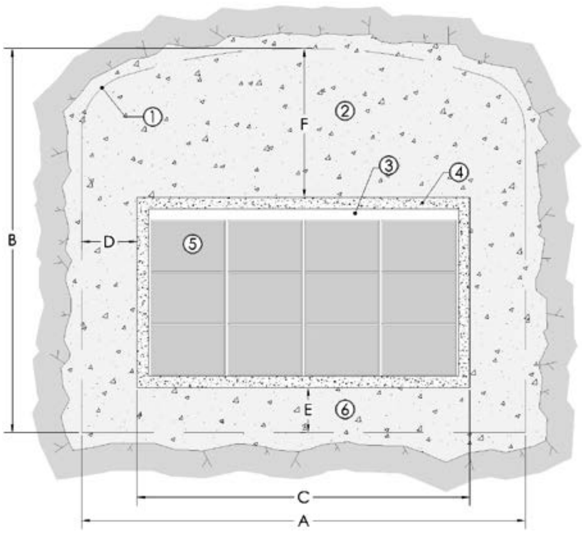

Figure 2-2. *Schematic cross-sectional layout of the BHK vault for metallic waste (from Elfwing et al. 2013). Legend: 1.) Theoretical tunnel contour. 2) Concrete backfill. 3) Grout. 4) Concrete structure. (0.5 m). 5) Steel tanks. 6) Concrete. Approximate dimensions: A = 20.6 m, B = 19.6 m, C = 15 m, D = 2.8 m, E = 2.4 m, F = 8.8 m.*

Waste containers are emplaced in concrete structures that serve as radiation barriers during operation. The backfill materials are installed upon repository closure. The ramp and access tunnels will be filled with crushed rock or similar material. Bentonite plugs and seals will be placed in the tunnel sections connecting the vaults and access tunnels, in the vertical shaft and in the access ramp Figure 2-3.

The values of the hydraulic conductivity, permeability, effective diffusivity and porosity of repository materials are given in Table 2-1. The assignment of hydraulic conductivities to the model materials is illustrated in Figure 2-4. The waste domain is defined to include the waste containers, the waste compartment volume and the concrete structure. Properties of a single composite material are set to represent this ensemble.

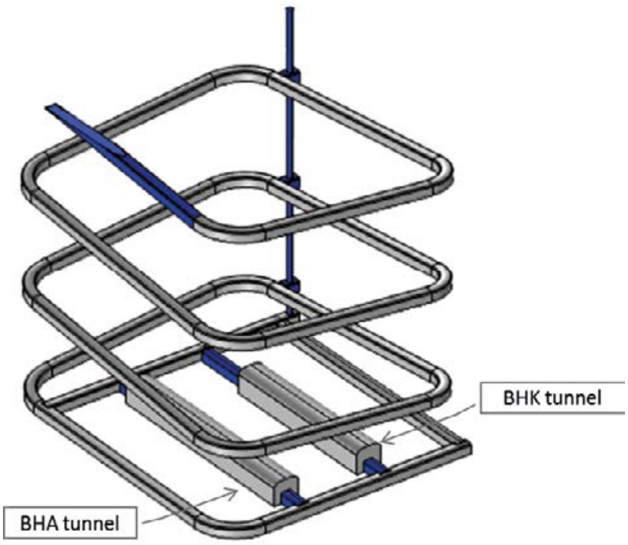

***Figure 2-3.** Sealing sections (blue) installed at closure in the tunnel sections connecting the vaults and access tunnels, the vertical shaft and in the access ramp.*

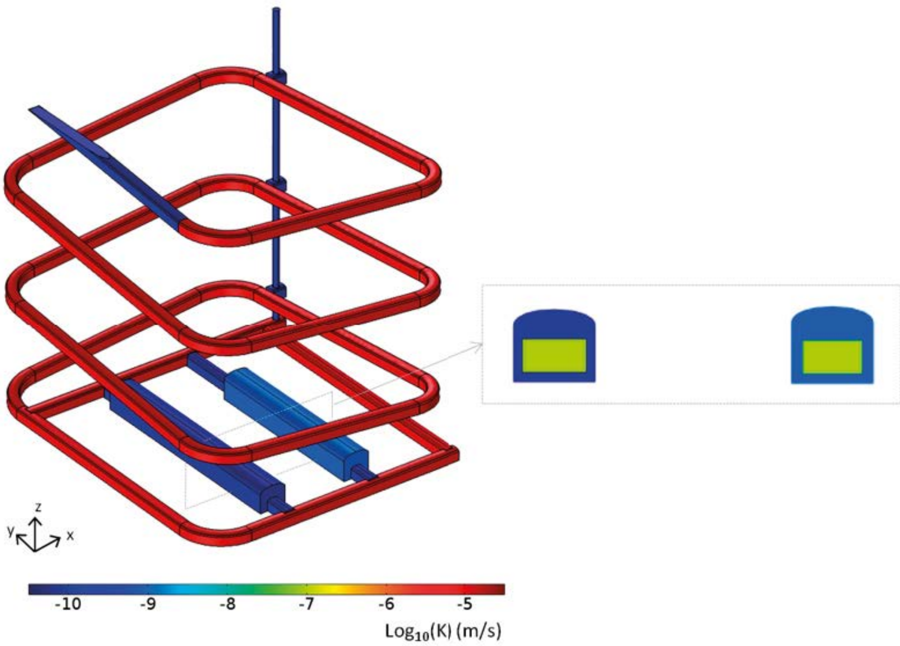

***Figure 2-4.** Assignment of hydraulic conductivity to the materials in the SFL model domains.*

Table 2-1. Characteristics of the repository materials.

Material	K (m/s)	k (m^2) (*)	De (m^2/s)	ϕ	References
Access tunnels backfill	1.0E−05	2.0E−12	6.0E−10	0.30	SKB 2001
Waste domain	1.0E−07	2.0E−14	3.5E−10	0.30	SKB 2014
Bentonite sealing sections	1.0E−10	2.0E−17	1.6E−10	0.46	SKB 2010
BHK vault backfill	8.3E−10	1.7E−16	3.5E−12	0.11	SKB 2014
BHA vault backfill	1.0E−10	2.0E−17	1.6E−10	0.46	SKB 2010

(*) Calculated assuming the density (ρ) and viscosity (μ) reference values of ρ=1,000 kg/m^3 and μ=0.002 Pa·s.

2.2 Representation of the host rock

Geological data from the Laxemar area has been used to represent typical Swedish bedrock for the SFL safety evaluation. The area is well characterized with high data density, having been considered as a potential site for the final repository for spent nuclear fuel (SKB 2011). Figure 2-3 shows the focus area and layout of the final repository for spent nuclear fuel. As indicated, deformation zones delimit several rock domains.

In this work, rock domains 1 and 4 have been selected for further analysis, as they represent the lowest and highest permeability volumes, respectively. In a given rock domain, test locations have been selected at 300 m, 500 m and 700 m depth. At each depth the near-field model has been positioned to avoid the major deformation zones (see Figure 2-6 through Figure 2-8).

The Laxemar area belongs to a geological unit called the Transscandinavian Igneous Belt. This unit is formed by igneous intrusive rocks (granite-syenitoid-dioritoid-gabbroid). These formations show different deformation structures from ductile (weak foliation, ductile-shear zones, etc.) to brittle, generated along multiple strain events. Most of the structures observed in Laxemar area were formed by brittle strain episodes. The location of these structures is related to old ductile structures.

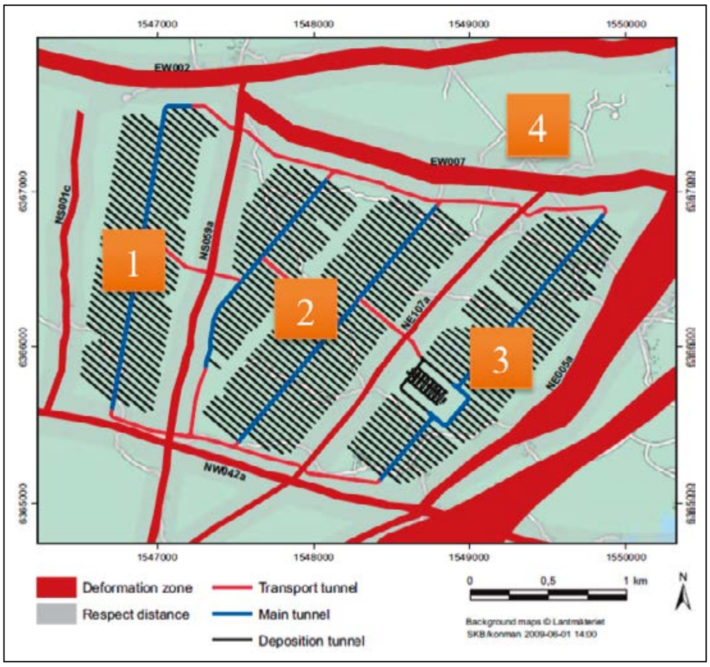

Figure 2-5. Laxemar focus area (modified from SKB 2011). Four rock domains delimited by deformation zoned are indicated.

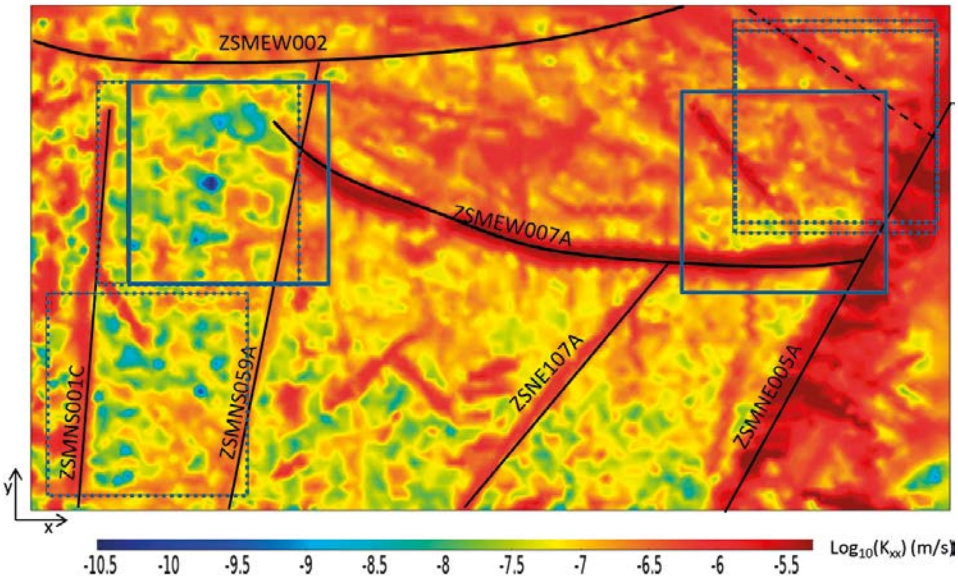

Figure 2-6. *Rock hydraulic conductivity K_{xx} field represented in a xy-plane at 300 m depth. Model domains at 300 m are represented by bold squares in rock domain 1 (left) and in rock domain 4 (right). The model domains at other depths are represented by dotted squares.*

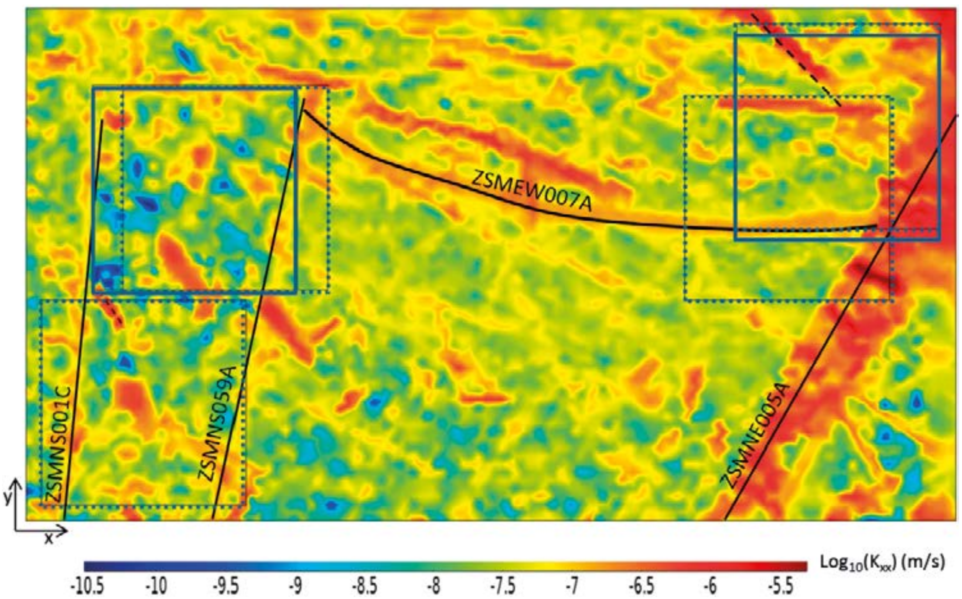

Figure 2-7. *Rock hydraulic conductivity K_{xx} field represented in a xy-plane at 500 m depth. Model domains at 500 m are represented by bold squares in rock domain 1 (left) and in rock domain 4 (right). The model domains at other depths are represented by dotted squares.*

Four sets of vertical deformation zones outcrop at the surface (Rhén and Hartley 2009). Two of them show northnortheast-southsouthwest and northeast-southwest strikes (with subvertical dip and sinistral strike-slip displacements). The other two sets are an east-west strike (presenting north or south pronounced dip and with higher deformation than the other families) and a north-south set (with pronounced west dip with a sinistral strike-slip component). Related to these deformation zones, cataclasites, faults and breccias can be observed. Deformation zones have hydraulic relevance as planar elements with high hydraulic conductivity. Also diorite dykes are present with variable length and thickness in the study area. Dykes act as hydraulic barriers due to the low hydraulic conductivity of diorite. However, the igneous bedrock shows high alteration around the dykes, where hydraulic conductivity is higher.

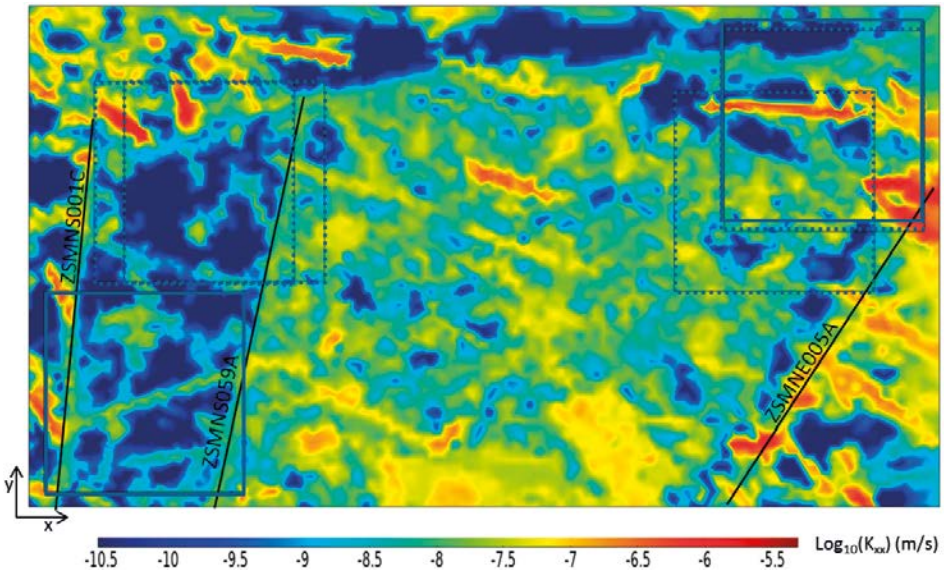

Figure 2-8. *Rock hydraulic conductivity K_{xx} field represented in a xy-plane at 700 m depth. Model domains at 700 m are represented by bold squares in rock domain 1 (left) and in rock domain 4 (right). The model domains at other depths are represented by dotted squares.*

Three domains are differentiated in the regional hydrogeological model of the area (Rhén and Hartley 2009):

- Hydraulic soil domains: Quaternary deposits overlying the igneous bedrock. They are formed by till in the upper areas and river-glacial deposits in the valleys.
- Hydraulic conductor domains: Related to deformation zones. They are the most transmissive areas, although transmissivity decreases with depth (Rhén et al. 2008) as is shown in Figure 2-6 through Figure 2-8.
- Hydraulic rock mass domains: Formed by intrusive igneous materials (bedrock) that present a low transmissivity and are associated with fractures whose density decreases with depth. These materials show a high density of subhorizontal fractures the first 150 metres, generating high values of transmissivity.

Groundwater flow occurs predominantly through the fracture network. The hydraulic properties of the rock mass are determined by the heterogeneity and anisotropy of the fractured system which is described in the regional model (Vidstrand et al. 2010).

Deterministic deformation zones from Vidstrand et al. (2010) have been identified in each rock domain. Two parallel northeast-southwest deformation zones, ZSMNS059A and ZSMNS001C, limit rock domain 1. Rock domain 4 is limited by the northeast-southwest ZSMNE005A deformation zone to the east; the west-east ZSMEW007A deformation zone to the south; the northeast-southeast ZSMNS059A deformation zone to the west, and the east-west ZSMEW002 deformation zone to the north (Figure 2-5 and Figure 2-6).

The depth of the deformation zones is related to each family system. The north-south and north-northeast-southsouthwest sets reach deeper than the east-west set, which show a lower dip (Figure 2-6 through Figure 2-8). Thus, deformation zones identified as ZSMNS001C, ZSMNS059A and ZSMNE005A are found at 300 m, 500 m and 700 m depths. Deformation zone ZSMEW007A is clearly identified at 300 m depth (Figure 2-6) but it is almost negligible at 700 m depth (Figure 2-8).

2.3 Model equations

2.3.1 Density dependent flow

The repository models have been implemented using the *Subsurface Flow Module* of COMSOL Multiphysics (COMSOL 2013), which is tailored for modelling groundwater flow in fractured and porous media. A stationary density dependent flow problem has been set up. The *Darcy's Law* interface solves for the flow and the *Molal solute transport* interface for the transport of dissolved salts (Nardi et al. 2014). The system of coupled partial differential equations is presented below.

Fluid mass conservation is given by:

$$\nabla \cdot (\rho \mathbf{u}) = 0 \tag{2-1}$$

$$\mathbf{u} = -\frac{k}{\mu}(\nabla \mathrm{p} + \rho g \nabla \mathrm{D}) \tag{2-2}$$

where ρ is the density (kg/m^3), μ is the dynamic viscosity (Pa·s), $\mathbf{u}$ is the Darcy velocity (m/s), k is the permeability of the porous medium (m^2), p is the water pressure (Pa), g is the acceleration of gravity (9.81 m/s^2) and D is the elevation (m).

The stationary species transport equation is given by:

$$0 = -\psi q_l \nabla c + \nabla \cdot (\psi D_l \nabla c) - c\nabla \cdot \rho_l D_l \omega_l^w - f_{ch}^w c \tag{2-3}$$

where:

$\omega = \phi S_l \rho_l \omega_l^w$

and

$\psi = \rho_l \omega_l^w$

Above, ϕ is the porosity (m^3/m^3), S_l is the liquid saturation (m^3/m^3), ρ_l is the water density (kg/m^3) and ω_l^w is the mass fraction of pure water in the liquid (kgw/kg). The species concentration (mol/kgw) is denoted by c and D_l is the sum of the effective dispersion D_{disp} (m^2/s) and diffusion D_{diff} (m^2/s) tensors.

A linear equation of state relates fluid density with salinity:

$$\rho = \rho_0(1 + \varepsilon S) \tag{2-4}$$

where S is the fluid salinity in percentage of mass fraction, ε is the linear salinity coefficient and ρ_0, the density of freshwater (1,000 kg/m^3). In accordance with Vidstrand et al. (2010), ε is set to 0.0078.

2.3.2 Tracer transport

Tracer transport simulations have been implemented using the *Subsurface Flow Module* of COMSOL Multiphysics (COMSOL 2013). A stationary non-reactive solute transport problem has been solved using the *Solute transport* interface.

The transport equation is expressed as:

$$\nabla[-(D_D + D_e)\nabla c] + \mathbf{u}\nabla c = R + S \tag{2-5}$$

Above, c is the tracer concentration (kg/m^3), D_D is the dispersion (m^2/s) and D_e the effective diffusivity (m^2/s). The Darcy velocity (m/s) is denoted by $\mathbf{u}$.

The dispersion coefficient is defined as:

$$D_D = \frac{(\alpha_L \cdot u^2 + \alpha_T \cdot v^2 + \alpha_T \cdot w^2)}{\sqrt{(u^2 + v^2 + w^2)}} \tag{2-6}$$

Above, α_L (m) is the transversal dispersivity and α_T (m) is the longitudinal dispersivity. The components of the velocity field are given by u, v and w (m/s).

2.4 Initial and boundary conditions

Regional hydrogeological simulations by (Vidstrand et al. 2010), performed using the DarcyTools software (Svensson and Ferry 2010, Svensson 2010), have provided input data to the near-field hydrology models. Driving pressure and salinities have been extracted by means of the iDC interface (Abarca et al. 2013) and used as initial and boundary conditions for the repository-scale model. A linear interpolation function onto the COMSOL model mesh has been used assign the property fields. A benchmark exercise illustrating the consistent coupling of near-field and regional models is presented in Appendix A.

The DarcyTools driving pressure, p_{DT} (Pa), is converted into absolute pressure by correcting for the gravitational term, assuming a freshwater density of ρ_0 = 1,000 kg/m^3.

$$p = p_{DT} - \rho_0 g \nabla D \tag{2-7}$$

The pressure at the rock boundaries has been used to specify the flow through the boundaries using a Cauchy boundary condition on the following form:

$$q' = \lambda\left(\frac{p_{DT}}{\rho_0 g} - (\frac{p}{\rho_0 g} + z)\right) \tag{2-8}$$

Above, p_{DT} is obtained from regional model, p is calculated by COMSOL and λ is a conductance proportional to the hydraulic conductivity ($70 \cdot K_{xx}$). The conductance has been set such that the boundary condition is equivalent to a prescribed pressure boundary condition. The advantage of the formulation is that flows through the outer boundaries can be accurately quantified.

For the base case calculation, it assumed the ramp and shaft are sealed with bentonite (see Figure 2-3). A zero flux condition has been specified where the shaft and ramp intersect the outer boundary of the model.

For the salt transport equation, the salinity field from the regional model has been prescribed at the host rock's boundaries as Dirichlet conditions. A concentration equal to zero has been set at the intersection of the ramp and shaft with the outer model boundary.

Two non-reactive tracer transport simulations have also been solved to quantify the interaction between vaults. For the interaction BHK to BHA, a normalized concentration of tracer c_{Tracer_BHK}=1 has been imposed at the BHK vault surfaces (Figure 2-9).

In this case, the solute transport equation has been solved for all model domains except for the BHK waste domain.

For interaction BHA to BHK, a normalized concentration of tracer c_{Tracer_BHA}=1 has been imposed along the BHA vault surfaces.

In both cases, the initial tracer concentration has been set to c_i=0 for the entire model domain.

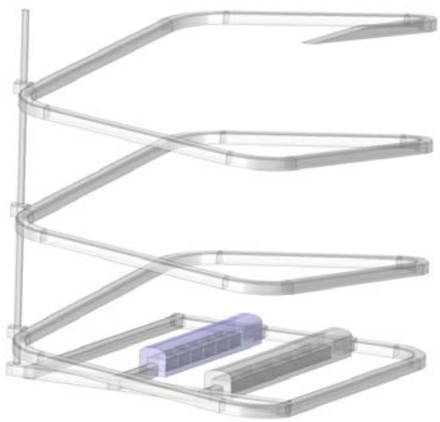

Figure 2-9. *Prescribed concentration of tracer in the BHK vault for solute transport simulations.*

An open boundary condition has been specified at the outer model boundaries. With this condition, the incoming groundwater enters the domain with a tracer concentration of c_i=0 and leaves the rock domain with a tracer concentration resulting from the solved transport equation.

2.5 Model domain and spatial discretisation

It is desirable that the size of the near-field model domain is sufficiently large, such that the hydraulic properties of repository materials can be altered without affecting the regional groundwater flow. It has been found a rock domain of $1,000 \times 1,000 \times 500$ m^3 is adequate in this regard (see Appendix B). As mentioned in Section 2.2, two rock domains in the Laxemar area have been analysed, with the repository located at 300 m, 500 m and 700 m depth.

Each model is identified by a name/ID of the form "depth_j", where:

- *depth* is an integer value that specifies the approximate depth of the repository (300, 500 or 700 m depth),
- *j* is a categorical variable that can take on two values (1 or 4), which in turn identify the rock domain.

The model domain coordinates are summarized in Table 2-2. The repository geometry is set in the centre of the model domain for each location.

Table 2-2. *Model domain coordinates for each repository location.*

Repository location	x_{min}	y_{min}	z_{min}	x_{max}	y_{max}	z_{max}
300_1	7,650	6,750	−550	8,650	7,750	−50
500_1	7,500	6,750	−750	8,500	7,750	−250
700_1	7,250	5,700	−1,300	8,250	6,700	−450
300_4	10,400	6,700	−550	11,400	7,700	−50
500_4	10,650	7,000	−750	11,650	8,000	−250
700_4	10,650	7,050	−950	11,650	8,050	−450

The model geometry has been discretized with an unstructured tetrahedral mesh. A representative model mesh with 1.65×10^6 tetrahedral elements is shown in Figure 2-10.

The model discretization of all investigated locations is presented in Appendix C.

2.6 Observables

2.6.1 Description of the host rock

The regional Laxemar geological and hydrogeological characterization according to Rhén et al. (2008) and Rhén and Hartley (2009) is summarized in Section 2.2. The host rock in the repository near-field is described in Chapter 3. For each location, the hydraulic conductivity of the rock is presented in one horizontal and two vertical planes cutting the BHA and BHK vaults (Figure 2-11). The colour legend and scale for the rock hydraulic conductivity (m/s) is common to all plots.

The anisotropic permeability fields (m^2) of the host rock are calculated in COMSOL by interpolating the corresponding fields from the regional model (Vidstrand et al. 2010). The permeability values are converted into hydraulic conductivity using ρ_0 = 1,000 kg/m^3 as the reference fluid density and μ = 0.002 Pa·s as the reference dynamic viscosity. For the sake of simplicity, the analysis of the hydraulic conductivity of the host rock will focus on the K_{xx} values.

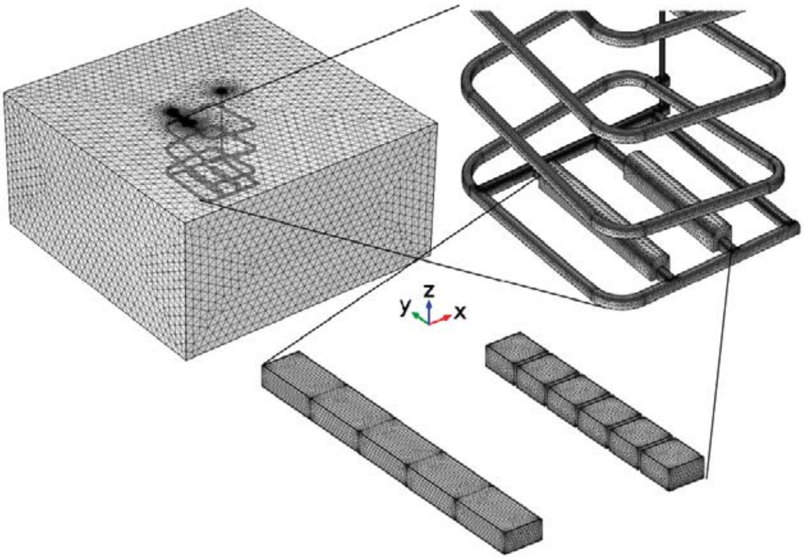

Figure 2-10. *Example of the model mesh at location 300_1, comprising 1.65 × 10^6 tetrahedral elements.*

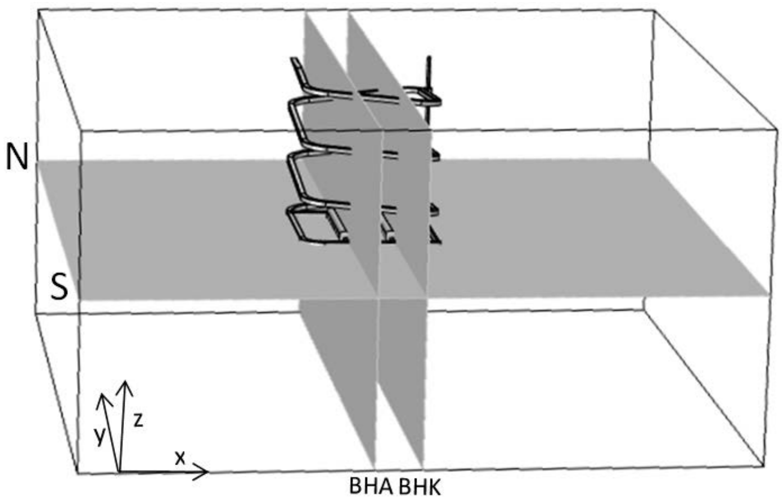

Figure 2-11. *Vertical plot planes cutting BHA vault (left) and BHK vault (right) and horizontal plot plane cutting BHA and BHK vaults.*

The deterministic deformation zones already characterized in the Laxemar area have been identified for the 6 repository locations using the same terminology as in Vidstrand et al. (2010). The stochastic deformation zones have been labelled "Di_Zj", where:

- *i* is an integer value for enumerating the deformation zones. The enumeration order starts at shallow depths and continues up to deeper areas, and
- *j* is a categorical variable that identify the repository location. *j* can take values 1 or 4.

2.6.2 Salinity

Water salinity increases with depth in the Laxemar area. Local groundwater is assumed to be a mixture of 4 reference waters (Rhén and Hartley 2009): altered meteoric water, deep saline water, glacial melt water, and littorina sea water. The salinity variation introduces density variations affecting groundwater flow. Salinity fields are presented for all repository locations with a common colour legend and scale for all plots.

2.6.3 Groundwater flow field

In the presentation of results, the local flow field in the model domain is described qualitatively by means of streamline plots and quantitatively by the computed total flow entering the model domain through the boundaries.

Streamlines are curves tangential to the instantaneous groundwater flow vector field. In this case, the “Magnitude controlled Positioning” option available in COMSOL has been used to limit the maximum and minimum distance between streamlines. The algorithm used for magnitude controlled option places the streamlines so that the flow between each pair of adjacent streamlines is the same throughout the domain, giving more dense streamlines where the magnitude of the groundwater flow is high.

The total flow entering the model domain is calculated by integrating the positive values of the normal Darcy flux over the domain boundaries (Q_{rock_domain} (m^3/yr)):

$$Q_{rock\ domain} = \sum_{(\vec{q}\cdot\vec{n})>0} \iint \vec{q}\cdot\vec{n} \tag{2-9}$$

Where $\vec{q}\cdot\vec{n} = u\cdot n_x + v\cdot n_y + w\cdot n_z$, u, v and w are the Darcy flow components in the x, y and z directions, respectively, and *nx*, *ny* and *nz* the components of the normal vector in the x, y and z directions, respectively.

2.6.4 Flow through vaults and waste control volumes

The flow through the repository is described by the total flow through the BHA and BHK vaults and the flow through a set of waste control volumes.

The total flow through the vaults is calculated by integrating the positive values of the normal Darcy flux over the rock/vault surface (Q_{vault} (m^3/yr)):

$$Q_{Vault} = \sum_{(\vec{q}\cdot\vec{n})>0} \iint \vec{q}\cdot\vec{n} \tag{2-10}$$

Flows are calculated by COMSOL in the Gauss points located at the centre of each element. For post processing the flow through an inner model surface, the flow of one element at either side of the surface is used. Here, as a convention, flow is computed on the low permeability side, as flow perpendicular to stratification is constrained by the lowest permeability material.

The flow through the waste domain has been calculated for a set of control volumes in each vault. The BHK waste is distributed into 6 individual compartments, each defining a control volume. The BHA waste domain has been divided into 5 control volumes of equal size (Figure 2-12).

The waste control volumes are labelled with reference to vault and lengthwise position. The 6 faces of each control volume have been enumerated as shown in Figure 2-12.

For each control volume, groundwater flow is calculated by surface integrals over each of the 6 faces of the volume (Q_{face} (m^3/yr)). Positive values have been added up representing the groundwater flow crossing the control volume ($Q_{control\_volume,out}$(m^3/yr)):

$$Q_{face} = \iint \vec{q}\cdot\vec{n} \tag{2-11}$$

$$Q_{control\_volume,in} = \sum_{Q_{face}<0} Q_{face} \tag{2-12}$$

$$Q_{control\_volume,out} = \sum_{Q_{face}>0} Q_{face} \tag{2-13}$$

The mass balance closing error has been calculated by comparing the positive values with the negative values as:

$$\%\ Clossing\ error = \frac{Q_{control\_volume,out} - Q_{control\_volume,in}}{Q_{control\_volume,in}} \tag{2-14}$$

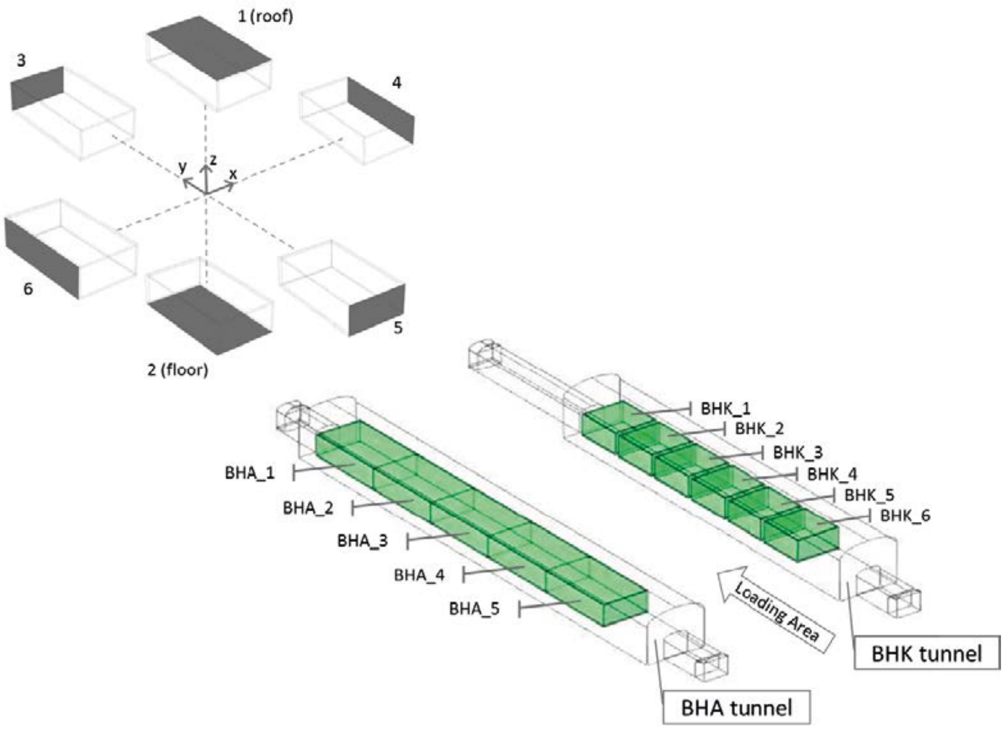

Figure 2-12. *The labelling of waste control volumes and faces in BHA and BHK.*

In addition to these quantitative observables, the description of the flow through the repository is illustrated by 3D plots of streamlines reaching and leaving the BHA and BHK waste volumes, as well as 2D plots of the local flow in the vicinity of the vaults.

2.6.5 Tracer release

Non-reactive tracer transport simulations have been performed to quantify the potential interaction between repository vaults. A tracer is released from the backfill/rock interface of each vault. Under steady state conditions, the mass flux released by a constant source is equal to the surface integral of the mass flow over a closed domain. In this case, the amount of tracer released from the vaults (m_r (kg/yr)) is computed by integrating the mass flux leaving the surfaces of the model domain (positive values):

$$m_r = \sum_{J>0} \iint_{A_{rock}} (-(D_D + D_e)\nabla c + \mathbf{u}c) \cdot \mathbf{n} \cdot dS \qquad (2\text{-}15)$$

Above, A_{rock} is the outer surface of the model domain, D_D is the dispersion coefficient (m^2/s), D_e the effective diffusivity (m^2/s), c is the solute concentration (kg/m^3), $\mathbf{u}$ is Darcy velocity (m/s) and $\mathbf{n}$ is the normal vector of the surface S.

2.6.6 Tracer transfer between vaults

The mass flux of tracer released from a vault that reaches the neighbouring vault (m_v (kg/yr)) is calculated by integrating the total mass flux of tracer over the rock/backfill surface of the receiving vault:

$$m_r = \sum_{J>0} \iint_{A_{vault}} (-(D_D + D_e)\nabla c + \mathbf{u}c) \cdot \mathbf{n} \cdot dS \qquad (2\text{-}16)$$

where A_{vault} is the surface of the interface rock/vault.

2.6.7 Vault to vault interaction

The interaction between BHK and BHA is measured by calculating the ratio:

$$Ratio = \frac{m_v}{m_r} \qquad (2\text{-}17)$$

The extent of the tracer plume is represented in figures by the isosurface delineating 20% of the released concentration.

3 Screening of the host rock

3.1 300_1

3.1.1 Description of the host rock

The host rock at location 300_1 exhibits several high hydraulic conductivity zones or fracture zones (Figure 3-1 through Figure 3-3). A horizontal high hydraulic conductivity zone, running in the north-south direction, is located above the repository at a depth of 150 m (D1_Z1). The hydraulic conductivity of this zone ranges from 4.91×10^{-7} m/s to 1.47×10^{-7} m/s. Another high hydraulic conductivity zone is located under the repository (D2_Z1), sloping downwards toward the south. It has values of hydraulic conductivity between 2.45×10^{-7} m/s and 3.92×10^{-7} m/s (Figure 3-1 and Figure 3-2).

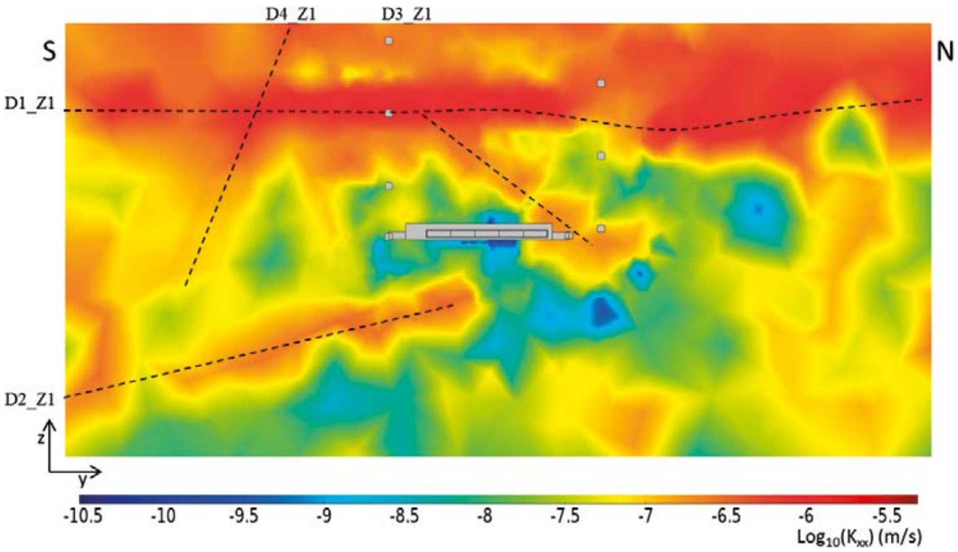

Figure 3-1. *Rock hydraulic conductivity field (K_{xx}) represented in an yz-plane intersecting the BHA vault at location 300_1.*

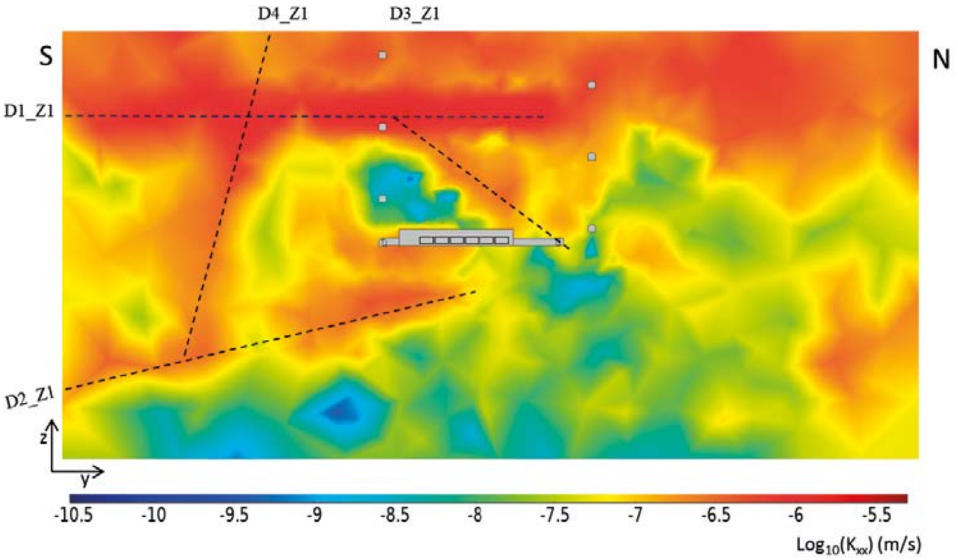

Figure 3-2. *Rock hydraulic conductivity field (K_{xx}) represented in an yz-plane intersecting the BHK vault at location 300_1.*

A vertical high conductivity zone (D3_Z1), dipping 45° north, crosses the repository from northwest to southeast near the BHA vault (Figure 3-1 through Figure 3-3). It has values of hydraulic conductivity around 4.2×10^{-7} m/s. Another vertical high hydraulic conductivity zone (D4_Z1) is observed south of the BHK vault. Its hydraulic conductivity ranges from 4.91×10^{-7} m/s to 2.4×10^{-7} m/s (Figure 3-1 and Figure 3-2).

In a horizontal plane at 300 m depth (Figure 3-3), two families of significant hydraulic conductivity lineaments are identified. The family of the deformation zone ZSMNS059A; with north-south direction, and the family of deformation zone ZSMEW007, with SE-NW direction.

The centre of the host rock is affected by a high hydraulic conductivity zone north of the BHA vault (D3_Z1), and another southeast of BHK vault (D7_Z1). The rest of the BHA is located in a low hydraulic conductivity area. The hydraulic conductivity of the repository area ranges between 4.91×10^{-7} m/s and 2.45×10^{-7} m/s.

3.1.2 Salinity

The salinity variation within the 300_1 model domain is low (Figure 3-4), ranging from 0% to a maximum value of 0.12%. The highest values of salinity are found in the lower part of the domain, at 500 m depth approximately. This salinity variation yields negligible density changes in the 300_1 model domain.

3.1.3 Groundwater flow field

At location 300_1, a preferential groundwater inflow zone is located in the upper southeast area. Water is directed downwards in two preferential directions. The most evident path follows a west-east direction, starting with a downstream component in the west, changing to an upstream component in the east following the ZSMNS059A high hydraulic conductivity zone (Figure 3-5).

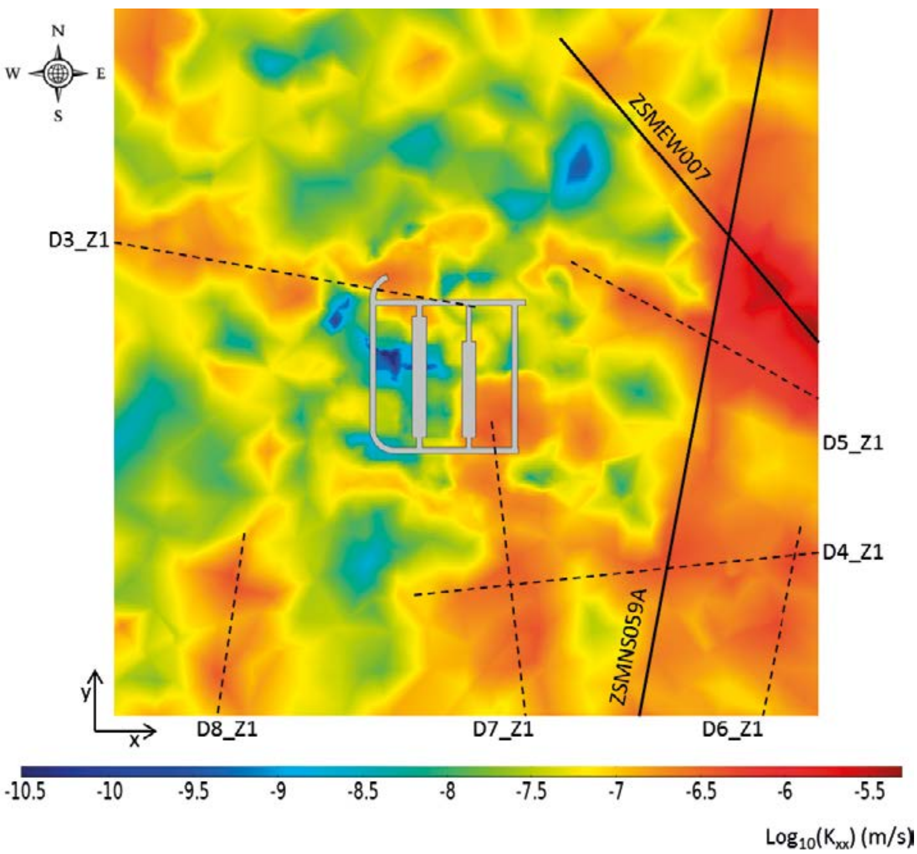

Figure 3-3. *Rock hydraulic conductivity field (K_{xx}) represented in a xy-plane intersecting BHA and BHK at location 300_1.*

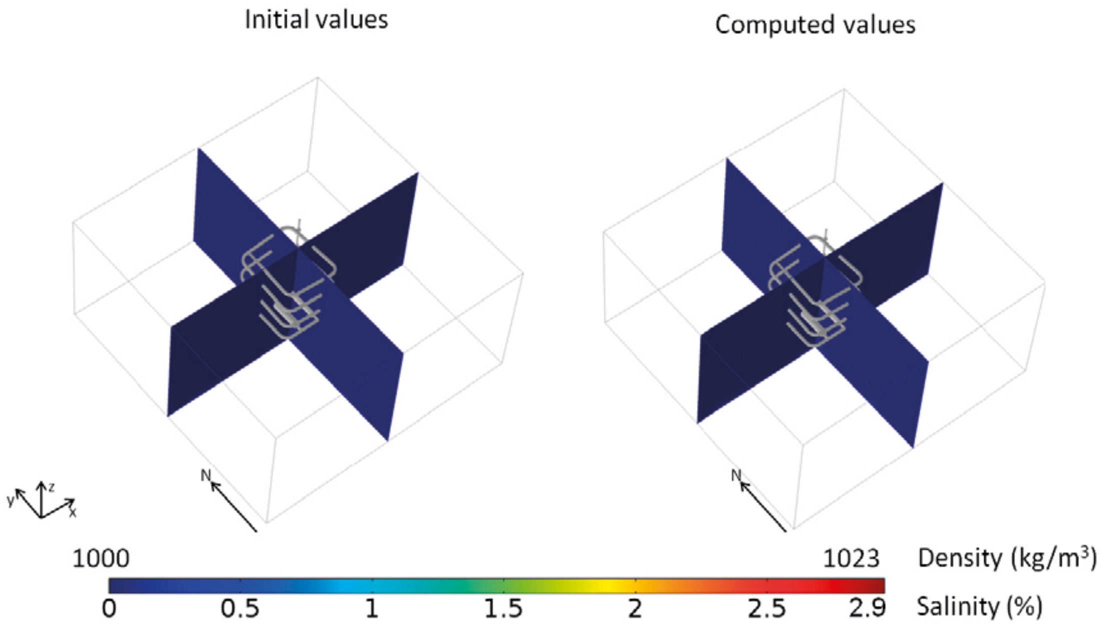

Figure 3-4. *Salinity and density in repository location 300_1, with initial values (left) and computed values (right).*

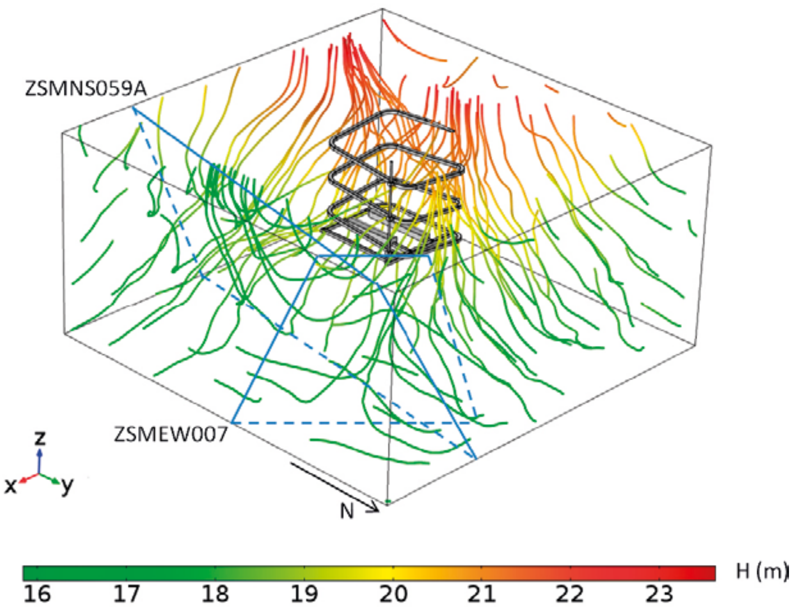

Figure 3-5. *Groundwater streamlines at location 300_1. The colours of the streamlines indicate the local hydraulic head (H). The location of the relevant deformation zones is indicated by blue plane traces.*

The second path has a north-south direction with a downstream component. At the bottom northeast area, some streamlines show a northeast-southwest direction associated with deformation zone ZSMEW007. The calculated total groundwater flow entering model domain 300_1 is 1.34×10^5 m^3/year.

3.1.4 Flow through the vaults and waste

Table 3-1 shows the calculated groundwater flow per waste control volume and the total flow per vault. The calculated groundwater flow through BHK is three times greater than the groundwater flow through BHA (Figure 3-6). Note that the hydraulic conductivity of the BHK backfill is higher than the BHA backfill.

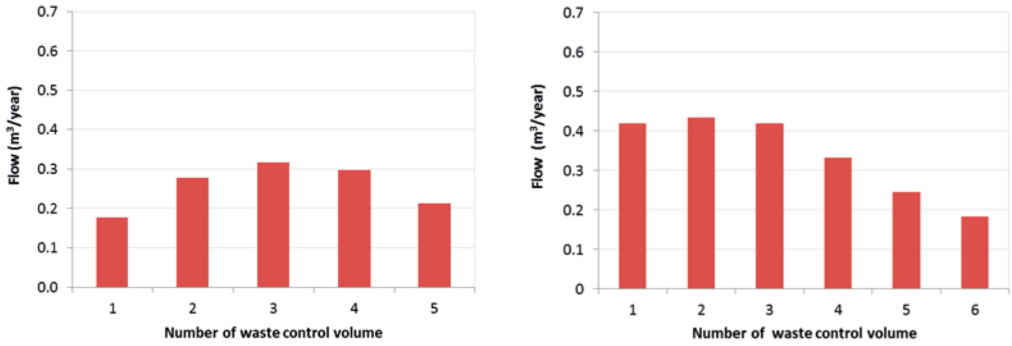

Figure 3-6. *Calculated flow through the waste control volumes of BHA (left) and BHK (right) at location 300_1.*

Table 3-1. Computed flow through waste control volumes and through the BHA and BHK vaults at location 300_1.

			Total flow (m^3/year)	Mass conservation error
BHA	**Waste**	BHA_1	0.177	3.66%
		BHA_2	0.278	0.46%
		BHA_3	0.316	−0.60%
		BHA_4	0.297	−0.55%
		BHA_5	0.212	−2.50%
	Vault	BHA	0.748	3.07%
BHK	**Waste**	BHK_1	0.420	0.96%
		BHK_2	0.434	0.77%
		BHK_3	0.420	0.70%
		BHK_4	0.332	1.01%
		BHK_5	0.245	0.67%
		BHK_6	0.183	0.38%
	Vault	BHK	2.336	2.38%

Of the groundwater flow entering BHA 34% passes through the waste while the corresponding number for BHK is 15%. The calculated flow through the BHA waste control volumes located at the ends of the vault is lower than the flow in the central waste control volumes and shows a higher mass balance closing error. High flows are located in the waste control volumes near low hydraulic conductivity rock. The flow through the BHK waste control volumes decreases towards the loading area, where the rock hydraulic conductivity increases (Figure 3-7). The rock acts as a hydraulic bypass and diverts the horizontal flow protecting the vaults. Moreover, the access tunnels collect the most of flow from west to east. The flow in the BHA vault is longitudinal. However, through the BHK vault, it has a more northwest to southeast direction. Groundwater flow reaching both vaults has a significant vertical component (Figure 3-8).

3.1.5 Tracer transport

The interaction between vaults is analysed based on the results of two simulations of non-reactive tracer transport at location 300_1. Figure 3-9 shows the extent, at steady state, of two tracer plumes leaking from the vault/rock interface. They are delineated by the isosurface representing 20% of the released concentration (c_r). The tracer plumes from BHA (green plume in Figure 3-9) and from BHK (blue plume in Figure 3-9) are driven by the vertical groundwater flow. The BHA vault is located upstream of the BHK vault. However, due to the significant vertical groundwater flow component, the plume from BHA does not interact significantly with BHK.

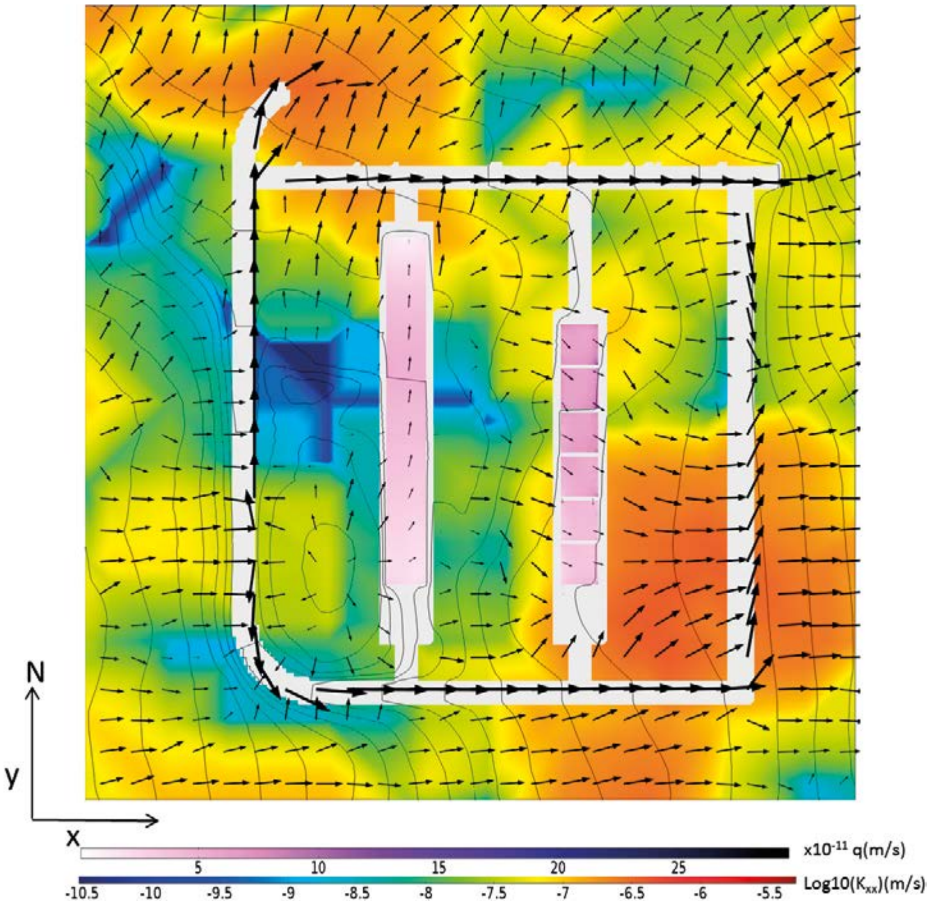

Figure 3-7. *Magnitude of the Darcy velocity through the waste control volumes, hydraulic conductivity of the rock, hydraulic head (isolines) and Darcy velocity (arrows) at location 300_1. Additional cross-section plots are available in Appendix D (Figure D-1, Figure D-2).*

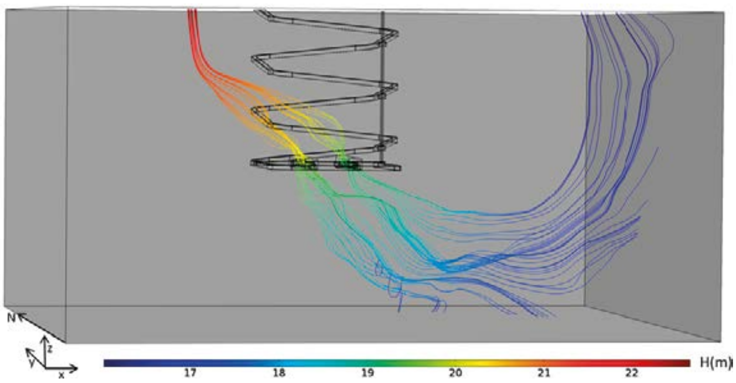

Figure 3-8. *Groundwater flow streamlines crossing the waste control volumes of the BHA and BHK vaults at location 300_1.*

The fraction of tracer mass released from each vault (m_r) reaching the neighbouring vault (m_v) is given in Table 3-2. The BHK vault is not affected by the mass flux released from the BHA vault. The tracer released from the BHK vault is not detected at the BHA vault. This is expected since the BHK vault is located downstream from the BHA.

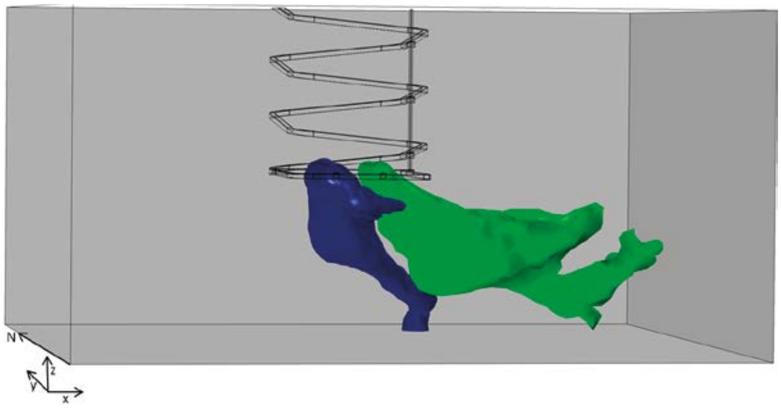

Figure 3-9. Extent of tracer plumes illustrated by the 20% isosurface of the released concentration (c_r) at location 300_1. The tracer plume released from BHK is shown in green and tracer plume from BHA in blue.

Table 3-2. Calculated tracer interaction at location 300_1.

	From BHA to BHK	From BHK to BHA
m_r (kg/yr)	21.6	34.7
m_v (kg/yr)	4.13E−3	1.68E−6
Ratio	0.0002	0.0000

3.2 300_4

3.2.1 Description of the host rock

At location 300_4, the host rock exhibits two main deformation zones with very high hydraulic conductivity values. These deformation zones are identified as ZSMEW007A, which is located to the south of the repository, and ZSMNE005A, which is located south east of the repository (Figure 3-12). This domain has the highest hydraulic conductivity values of all locations.

The superficial zone (D4_Z4) is horizontal with high hydraulic conductivity, as illustrated in Figure 3-10 and Figure 3-11.

The vertical deformation zone D1_Z4 affects both BHA and BHK. D1_Z4 has hydraulic conductivity values around 2.94×10^{-6} m/s when crossing the BHA vault (Figure 3-10) and 4.41×10^{-7} m/s around the BHK vault (Figure 3-11). A subvertical zone of high hydraulic conductivity (D2_Z4) is located above the repository. Another vertical deformation zone (D3_Z4) is found north of the repository vaults and presents hydraulic conductivity values from 9.81×10^{-7} m/s to 1.96×10^{-6} m/s (Figure 3-12).

3.2.2 Salinity

Salinity values are low at location 300_4 with, a maximum of 0.03% (Figure 3-13) resulting in negligible density changes.

3.2.3 Groundwater flow field

At location 300_4 groundwater flow is directed downward from the top southeast zone (Figure 3-14). Reaching repository depth, the water moves subhorizontally towards the northwest. The high hydraulic conductivity areas identified in the host rock (ZSMEW007A) mainly control groundwater flow. The lowest groundwater heads occur at the lower southeast corner where the slope of the downward streamlines increases due to the presence of the ZSMNE005A deformation zone. The calculated total groundwater flow entering model domain 300_4 is 5.14×10^5 m^3/year.

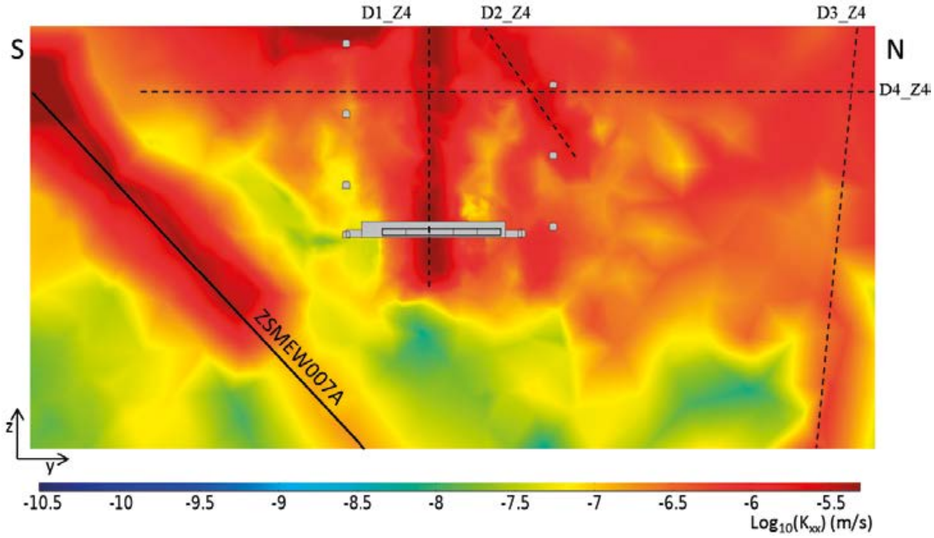

Figure 3-10. *Rock hydraulic conductivity field (K_{xx}) represented in an yz-plane intersecting the BHA vault at location 300_4.*

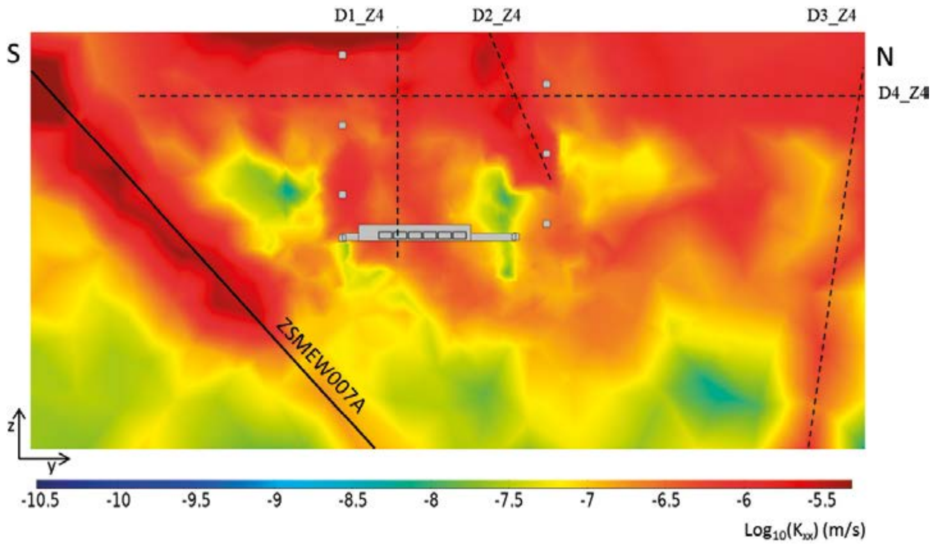

Figure 3-11. *Rock hydraulic conductivity field (K_{xx}) represented in an yz-plane intersecting the BHK vault at location 300_4.*

3.2.4 Flow through the vaults and waste

Table 3-3 and Figure 3-15 show the calculated groundwater flow per waste control volume and the total flow per vault. The total flow through the BHA vault (0.4 m^3/year) is one order of magnitude lower than the flow through the BHK vault (4.7 m^3/year). This result is due to the difference in hydraulic conductivity for the BHK and the BHA backfills (8.3×10^{-10} m/s and 1×10^{-10} m/s, respectively). Around BHA, deformation zone D1_Z4 acts as a preferential flow path, draining groundwater and protecting the vault (Figure 3-16). In addition, access tunnels are collecting the groundwater flow from west to east protecting the vaults.

The calculated flow through the BHA waste control volumes is much lower than in BHK control volumes (Table 3-3 and Figure 3-15). On average, 27% of the groundwater flow through BHA flows through a waste control volume. In the case of BHK, the number is 12%. Groundwater flow through the BHK waste control volumes progressively increases towards the loading area, affected by the D1_Z4 deformation zone.

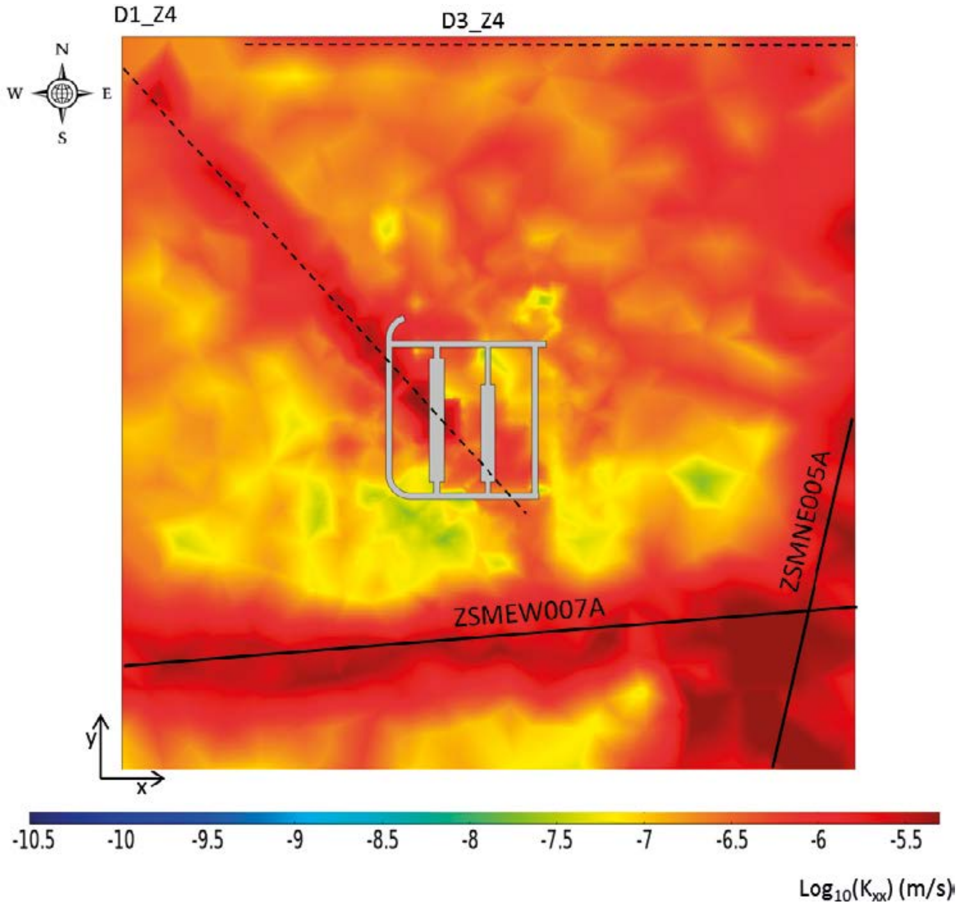

***Figure 3-12.** Rock hydraulic conductivity field (K_{xx}) represented in a xy-plane intersecting BHA and BHK at location 300_4.*

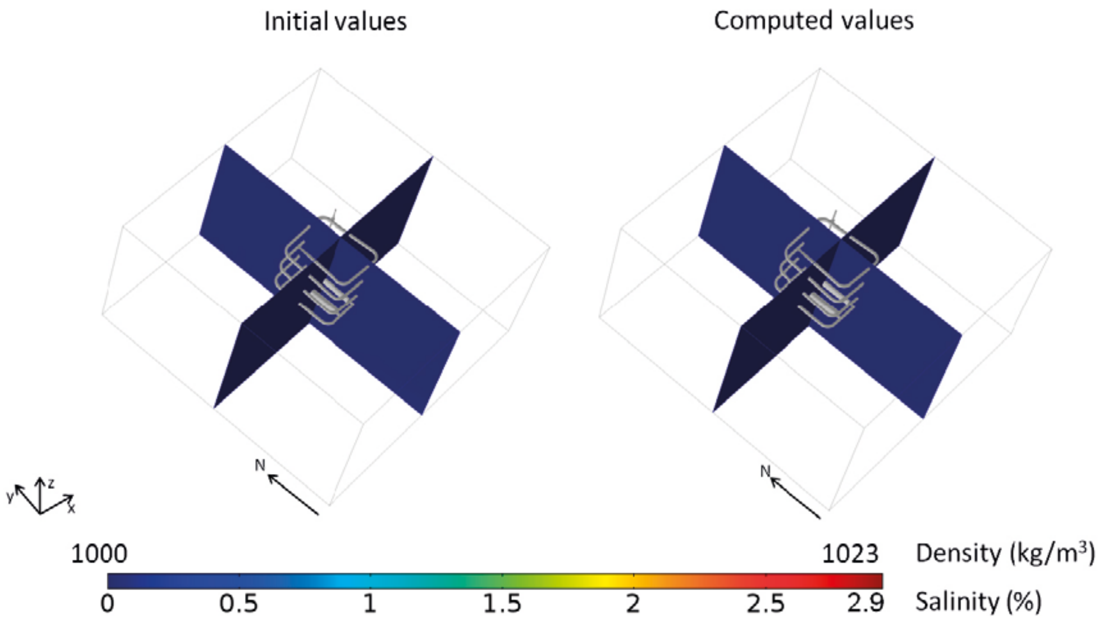

***Figure 3-13.** Salinity and density at repository location 300_4, with initial values (left) and computed values (right).*

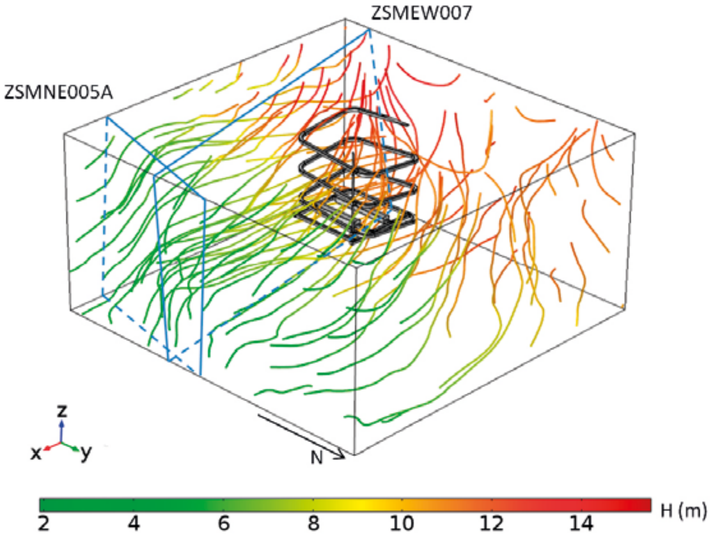

Figure 3-14. Groundwater streamlines at location 300_4. The colour of the streamline indicates the local hydraulic head (H). The location of the relevant deformation zones is indicated by blue plane traces.

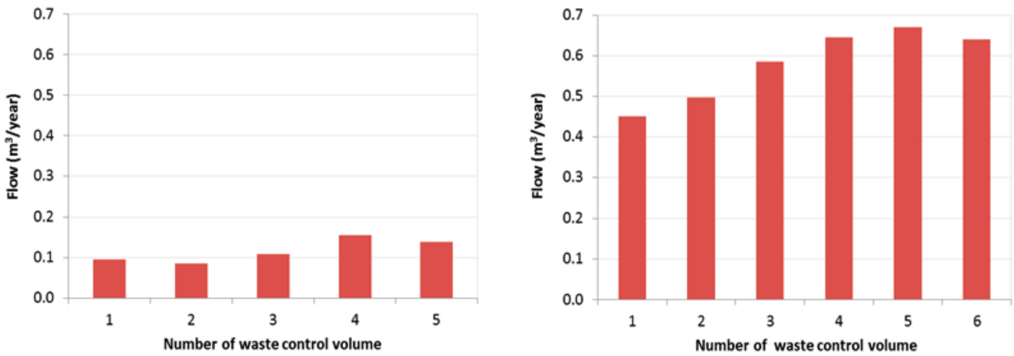

***Figure 3-15.** Calculated flow through the waste control volumes of BHA (left) and BHK (right) at location 300_4.*

The streamlines reaching and leaving the waste control volumes (Figure 3-17) show a strong vertical component in the inflowing water and a horizontal outflow path. The higher density of streamlines reaching BHK illustrates the higher inflow to that vault.

Table 3-3. Computed flow through waste control volumes and through the BHA and BHK vaults at location 300_4.

			Total flow (m^3/year)	Mass conservation error
BHA	**Waste**	BHA_1	0.096	0.02%
		BHA_2	0.086	−4.78%
		BHA_3	0.109	−2.40%
		BHA_4	0.155	−0.71%
		BHA_5	0.138	3.31%
	Vault	BHA	0.427	−1.82%
BHK	**Waste**	BHK_1	0.450	0.32%
		BHK_2	0.498	2.21%
		BHK_3	0.586	0.67%
		BHK_4	0.646	1.69%
		BHK_5	0.671	2.20%
		BHK_6	0.641	1.41%
	Vault	BHK	4.663	1.51%

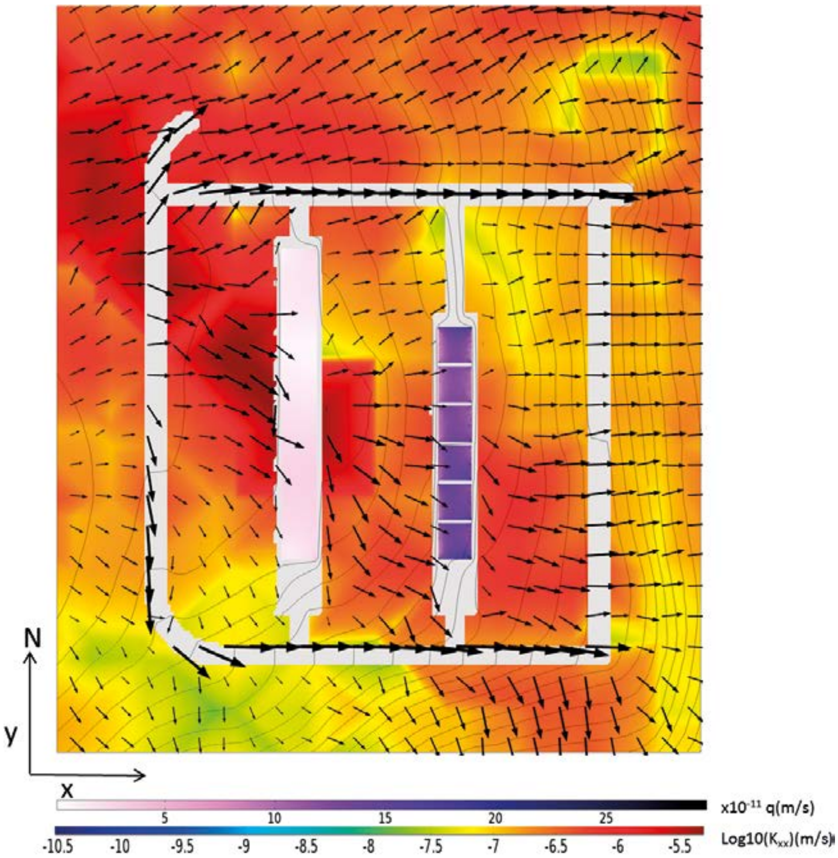

Figure 3-16. Magnitude of the Darcy velocity through the waste control volumes, hydraulic conductivity of the rock, hydraulic head (isolines) and Darcy velocity (arrows) at location 300_4. Additional cross-section plots are available in Appendix D (Figure D-3, Figure D-4).

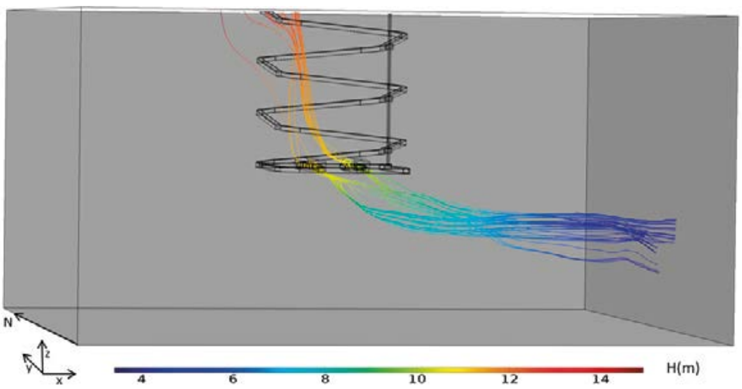

Figure 3-17. Groundwater flow streamlines crossing the waste control volumes of the BHA and BHK vaults at location 300_4.

3.2.5 Tracer transport

Figure 3-18 shows the extent of two tracer plumes released at the vault/rock interface at steady state. They are delineated by the isosurface indicating 20% of the released concentration (c_r). The 300_4 domain presents the highest values of hydraulic conductivity and therefore the highest values of groundwater flow. The tracer plumes generated are extended due to the high groundwater flows. Groundwater flows from west to east with a significant vertical component crossing the BHA vault (blue plume in Figure 3-18) and the BHK vault (green plume). The ratio of interaction between BHA tracer and BHK vault (located downstream) is 0.0002 (Table 3-4). The tracer released from the BHK vault is not detected at the BHA vault. This is expected since the BHK vault is located downstream of the BHA.

Table 3-4. Calculated tracer interaction at location 300_4.

	From BHA to BHK	From BHK to BHA
m_r (kg/yr)	2.24E+1	3.82E+1
m_v (kg/yr)	3.72E−3	8.36E−6
Ratio	0.0002	0.0000

3.3 500_1

3.3.1 Description of the host rock

The host rock at location 500_1 contains fewer deformation zones compared to 300_1. Deformation zone D2_Z1, already identified in the lower area of repository 300_1, is located south of the repository. It reaches a depth of more than 500 m (Figure 3-19 and Figure 3-20). The hydraulic conductivity of this deformation zone decreases with depth down to 2.45×10^{-7} m/s. A horizontal deformation zone (D9_Z1) located near BHK is shown in Figure 3-20. D9_Z1 presents a north-south strike while D2_Z1 and D10_Z1 presents a northwest-southwest strike. Parallel to D10_Z1 is another deformation zone, D5_Z1. Deformation zone ZSMNS059A is far from the BHA and BHK vaults (Figure 3-21).

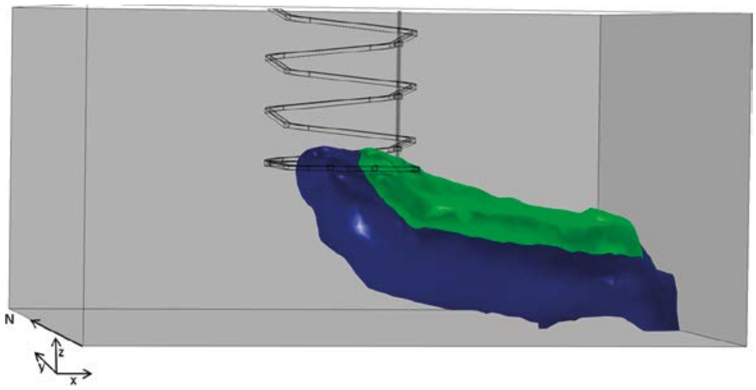

Figure 3-18. Extent of tracer plumes illustrated by the 20% isosurface of the released concentration (c_r) at location 300_4. The tracer plume released from BHK is shown in green and tracer plume from BHA in blue.

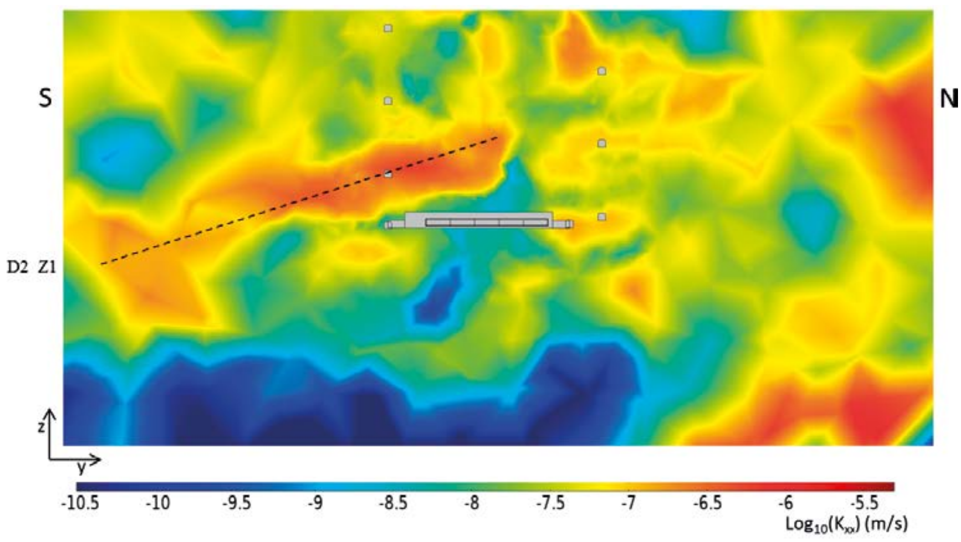

Figure 3-19. Rock hydraulic conductivity field (K_{xx}) represented in a yz-plane intersecting the BHA vault at location 500_1.

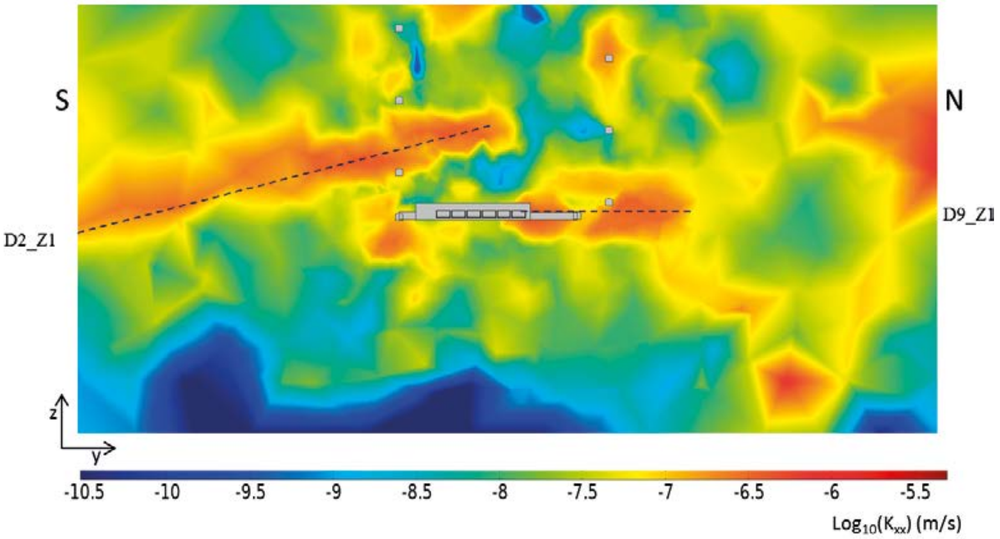

Figure 3-20. *Rock hydraulic conductivity field (K_{xx}) represented in an yz-plane intersecting the BHK vault at location 500_1.*

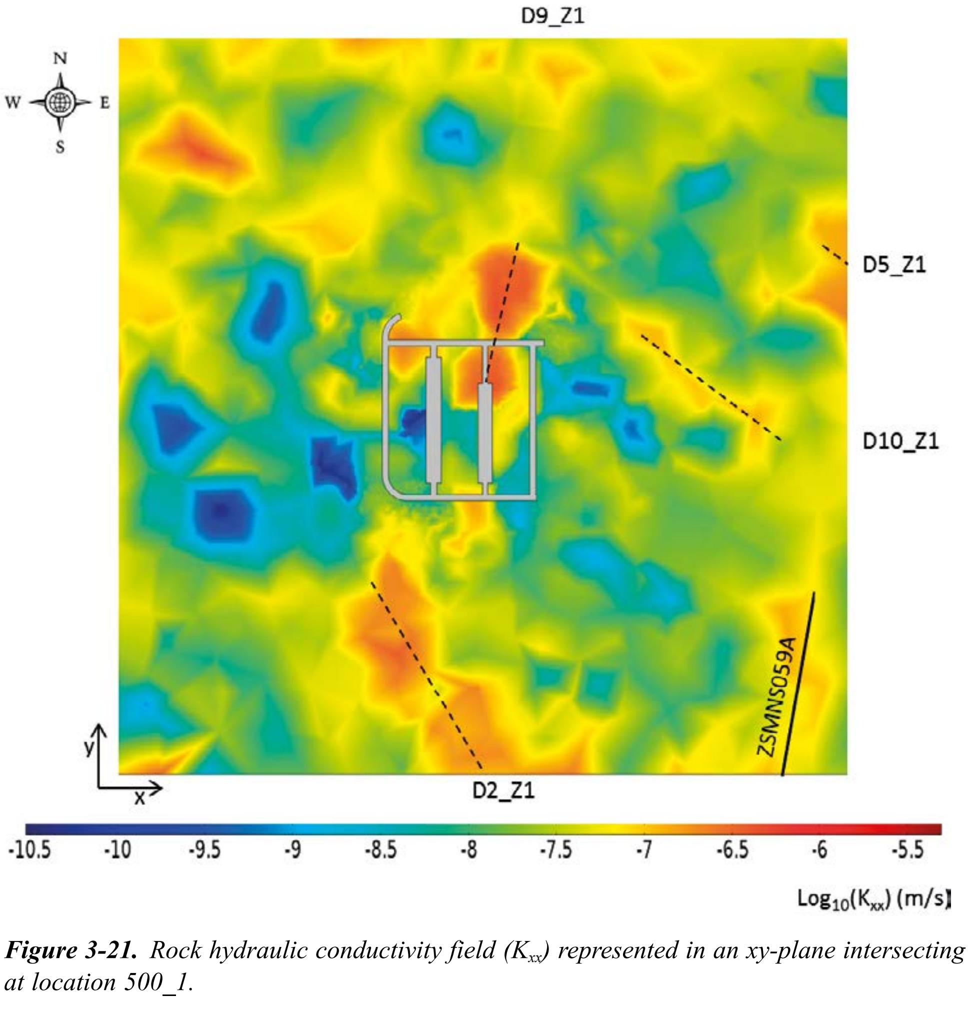

Figure 3-21. *Rock hydraulic conductivity field (K_{xx}) represented in an xy-plane intersecting BHA and BHK at location 500_1.*

3.3.2 Salinity

The salinity variation in this domain is shown in Figure 3-22, and ranges from 0% up to a maximum value of 1.2%. The highest salinity values are found at the lower of the northern edges of the model domain. This variation in salinity requires density variations to be accounted for when calculating the fluid flow.

3.3.3 Groundwater flow field

The streamlines (Figure 3-23) show vertical downward flow with the highest hydraulic heads found at the top south-southwest area. Above the repository, the horizontal component of the flow has a south-southwest to north-northeast direction. At the repository level, associated with the presence of the subhorizontal D2_Z1 deformation zone, flow becomes more horizontal and shifts eastwards. Groundwater flow in lower areas moves in multiple directions (eastwards and northwards). The calculated total groundwater flow entering the model domain 500_1 is 1.74×10^4 m^3/year.

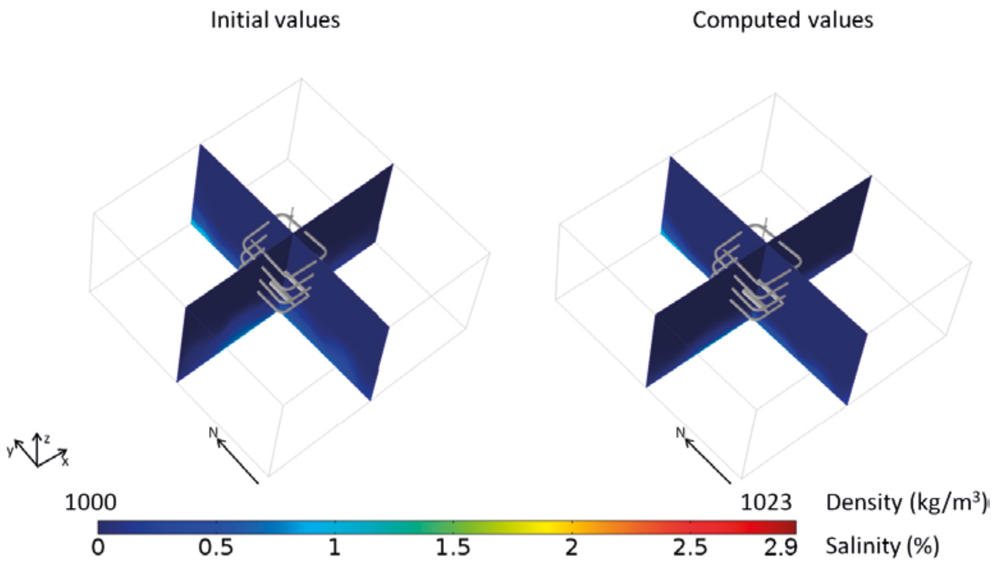

Figure 3-22. *Salinity and density at repository location 500_1, with initial values (left) and computed values (right).*

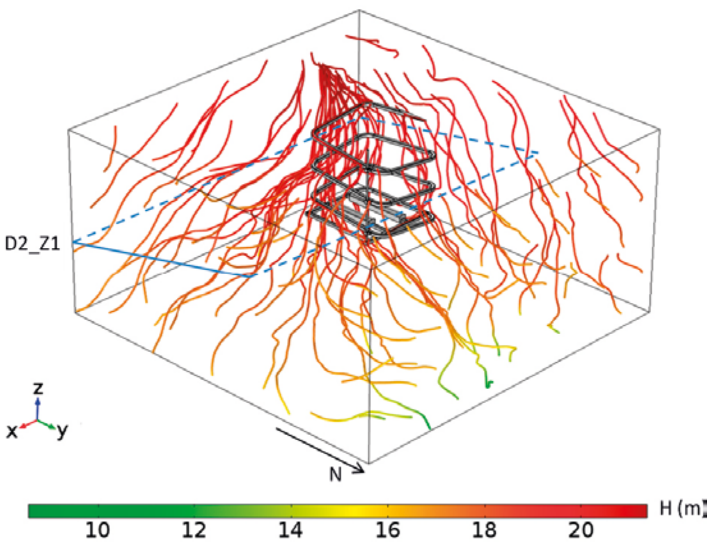

Figure 3-23. *Groundwater streamlines at location 500_1. The colour of the streamlines indicates the local hydraulic head (H). The location of the relevant deformation zones is indicated by blue plane traces.*

3.3.4 Flow through the vaults and waste

Table 3-5 and Figure 3-24 show the calculated groundwater flow per waste control volume and the total flow per vault. The calculated flows through the BHA and BHK vaults are quite similar. 44% of the BHA vault flow passes through the waste sections whereas 10% of groundwater flow through BHK crosses the BHK waste compartments.

Figure 3-25 shows the Darcy velocity field together with the magnitude of the flow entering the waste. This figure illustrates flow from southwest to northeast. Most of that flow is redirected to the more permeable access tunnels (1×10^{-5} m/s) towards D9_Z1 (Figure 3-25). The access tunnels act as a hydraulic ring that protects the vaults from the eastward flow. Deformation zone D9_Z1 collects the groundwater flow from south to north. The waste control volumes surrounded by higher hydraulic conductivity rock experience lower flows. That is the case of waste control volume BHK 1 which is clearly affected by D9_Z1 and has the lowest waste flow. On the other hand, the central waste control volumes of the BHA, surrounded by low hydraulic conductivity rock, show higher flows (Figure 3-25). The flow direction through the waste control volumes in BHA and BHK vaults is from south to north.

Flow through BHA and BHK has a significant vertical component (see Figure D-5 and Figure D-6 of Appendix D). Figure 3-26 shows flow lines reaching and leaving the waste control volumes. The streamlines illustrate the vertical inflow. Water reaches the vaults from the top and leaves through the bottom boundaries. Under the repository the vertical streamlines bend towards the north becoming quasi-horizontal.

Table 3-5. Computed flow through waste control volumes and through the BHA and BHK vaults at location 500_1.

			Total flow (m^3/year)	Mass conservation error
BHA	**Waste**	BHA_1	0.301	4.00%
		BHA_2	0.516	1.38%
		BHA_3	0.616	0.10%
		BHA_4	0.534	−1.57%
		BHA_5	0.314	−4.42%
	Tunnel	BHA	0.676	2.19%
BHK	**Waste**	BHK_1	0.093	−1.92%
		BHK_2	0.145	−0.80%
		BHK_3	0.232	0.36%
		BHK_4	0.224	−0.35%
		BHK_5	0.185	1.65%
		BHK_6	0.149	0.71%
	Tunnel	BHK	0.623	4.12%

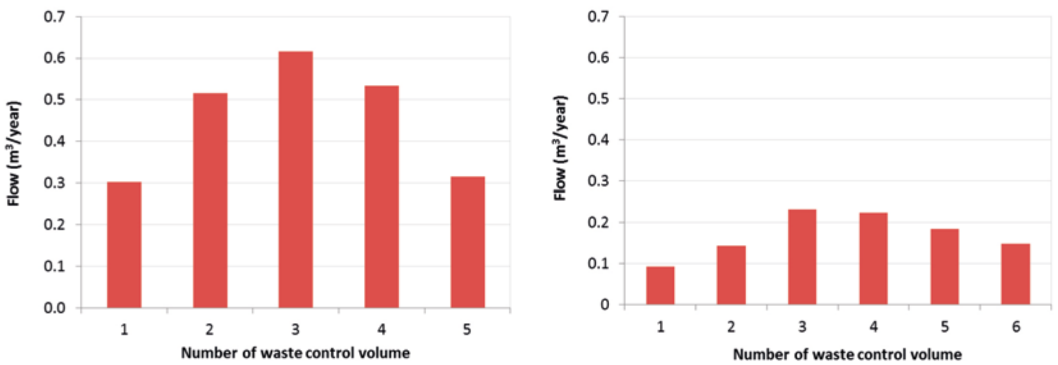

***Figure 3-24.** Calculated flow through the waste control volumes of BHA (left) and BHK (right) at location 500_1.*

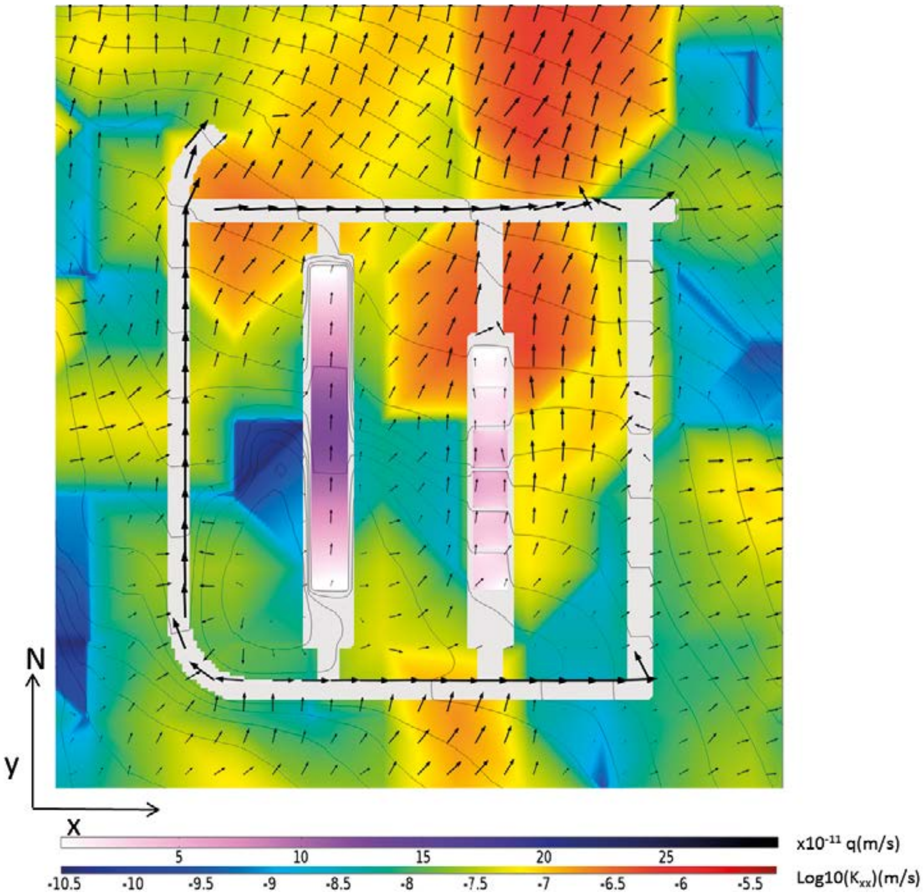

Figure 3-25. *Magnitude of the Darcy velocity through the waste control volumes, hydraulic conductivity of the rock, hydraulic head (isolines) and Darcy velocity (arrows) at location 500_1. Additional cross-section plots are available in Appendix D (Figure D-5 and Figure D-6).*

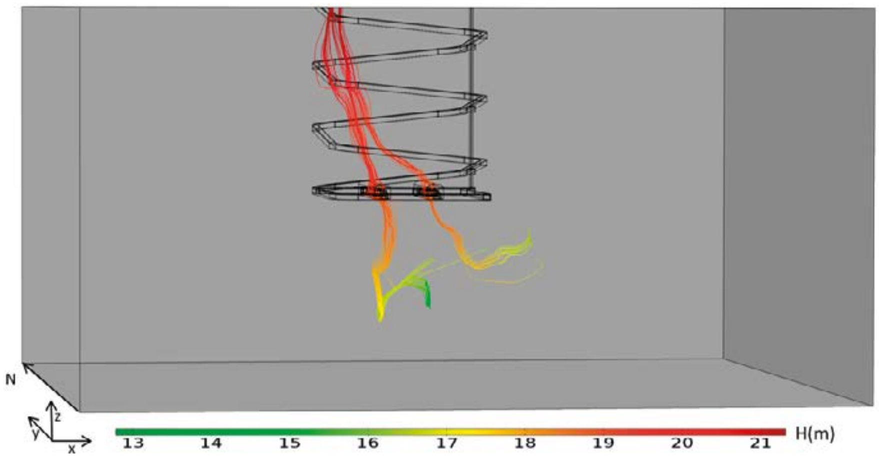

Figure 3-26. *Groundwater flow streamlines crossing the waste control volumes of the BHA and BHK vaults at location 500_1.*

3.3.5 Tracer transport

Figure 3-27 shows the extent of the two tracer plumes released at the vault/rock interface at steady state. They are delineated by the isosurface indicating 20% of the released concentration (c_r). The 500_1 domain is characterized by low groundwater flow values. As a consequence, transport by diffusion becomes important. The two plumes are elongated towards the north following the local groundwater flow (Figure 3-26). The BHA plume (blue) is less extended than the BHK plume due to higher flows through the BHK vault (Figure 3-27). The BHA plume interacts slightly with the BHK vault. The computed ratio m_r/ m_v is 0.0013 (Table 3-6), indicating that 0.13% of the mass released from BHA reaches BHK.

Table 3-6. Calculated tracer interaction at location 500_1.

	From BHA to BHK	From BHK to BHA
mr (kg/yr)	14.43	12.67
mv (kg/yr)	1.93E−02	1.96E−07
Ratio	0.0013	0.0000

3.4 500_4

3.4.1 Description of the host rock

The host rock at location 500_4 contains the two main deformation zones ZSMNEW007A and ZSMNE005A, with associated high hydraulic conductivity values. This location has additional penetrative deformation zones with subvertical dip, like D7_Z4, D6_Z4, D5_Z4 and D8_Z4 as shown in Figure 3-28 and Figure 3-29.

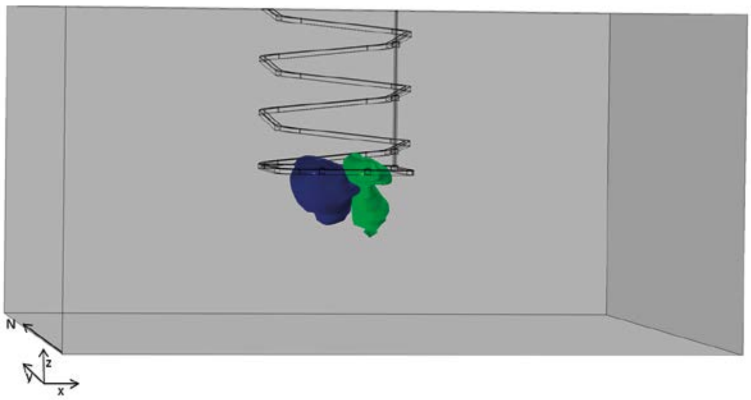

Figure 3-27. *Extent of tracer plumes illustrated by the 20% isosurface of the released concentration (c_r) at location 500_1. The tracer plume released from BHK is shown in green and tracer plume from BHA in blue.*

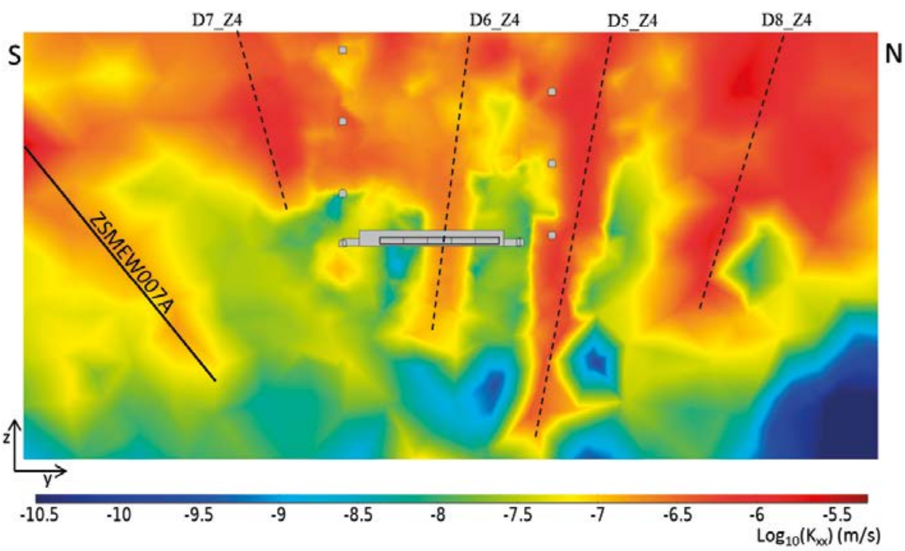

Figure 3-28. *Rock hydraulic conductivity field (K_{xx}) represented in an yz-plane intersecting the BHA vault at location 500_4.*

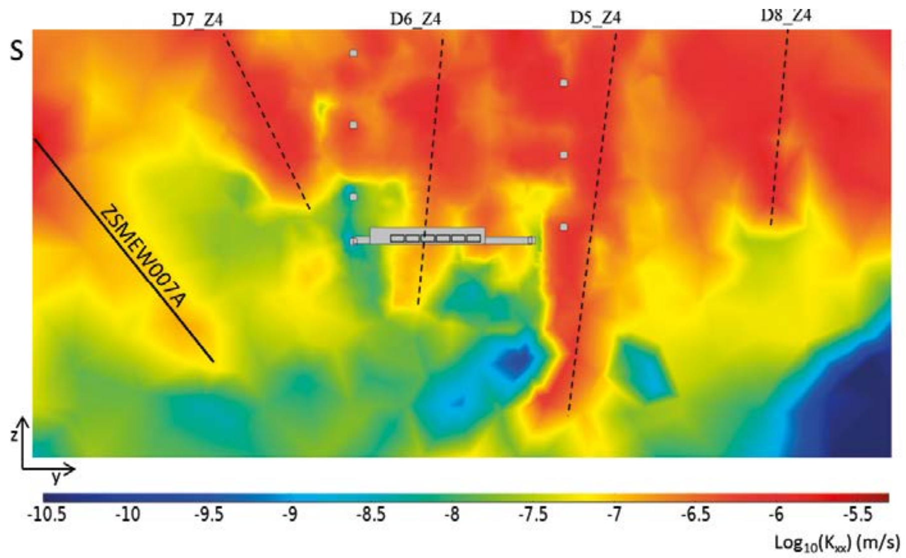

Figure 3-29. *Rock hydraulic conductivity field (K_{xx}) represented in an yz-plane intersecting the BHK vault at location 500_4.*

The deformation zone D6_Z4 intersects both repository vaults. Deformation zones are less permeable near the BHA vault. D8_Z4 and D6_Z4 have a northwest-southeast strike whereas D5_Z4 has an east-west strike (Figure 3-30). D6_Z4 intersects BHA at waste control volume 2 and 3 and BHK at waste control volume 4 and 5.

3.4.2 Salinity

Groundwater salinity computed from the regional model ranges from 0% to a maximum value of 2.2% at location 500_4. The maximum value of salinity is found in the lower northeast corner. This salinity difference is enough to require density dependent flow simulations. The computed salinity distribution agrees well with the initial distribution (Figure 3-31).

3.4.3 Groundwater flow field

At location 500_4, streamlines illustrate a downward flow from the top west area to the southeast area, near the ZSMNE005A deformation zone. Above 500 m depth, the flow has a strong vertical component. However, it becomes subhorizontal at around 500 m due to the presence more saline, deep water. The calculated total groundwater flow entering the model domain 500_4 is 9.37×10^4 m^3/year.

3.4.4 Flow through the vaults and waste

Table 3-7 and Figure 3-33 show the calculated groundwater flow per waste control volume and the total flow per vault. The total flow through BHK is four times greater than for BHA. On average, 44% of flow through BHA passes through a waste control volume. The corresponding number for BHK is 10%.

Waste control volume BHA 4 is surrounded by rock with low hydraulic conductivity and experiences the highest flow values. Groundwater flow through the BHK waste is quite uniform for the six waste control volumes (about 0.33 m^3/year per control volume) (Table 3-7).

Groundwater near the repository flows from west to east mainly through deformation zone D5_Z4 (Figure 3-30). The access tunnels redirect flow, preventing groundwater from entering the vaults (Figure 3-34). The flow from west to east is perpendicular to the vaults. Where the hydraulic conductivity of the surrounding rock is higher, flow circumvents the vaults through the surrounding rock. However, where the surrounding rock hydraulic conductivity is low, part of the eastward flow is forced through the vaults resulting in higher local flow through the waste control volumes.

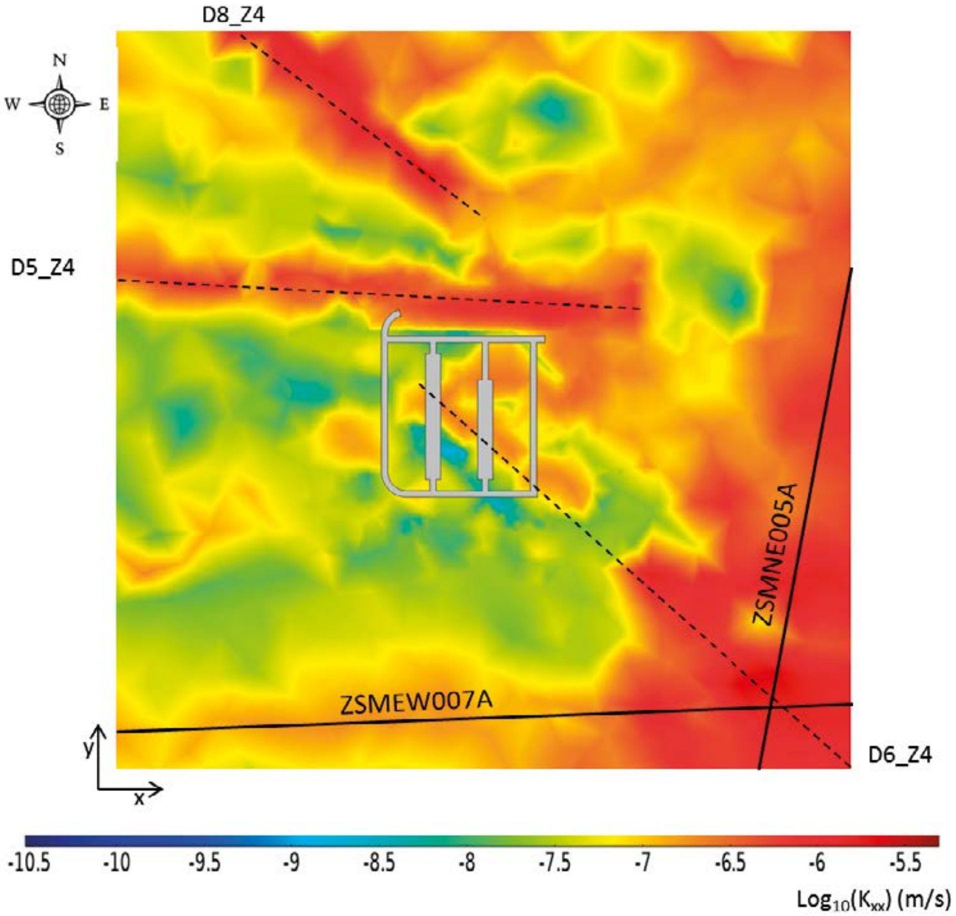

Figure 3-30. *Rock hydraulic conductivity field (K_{xx}) represented in a xy-plane intersecting BHA and BHK at location 500_4.*

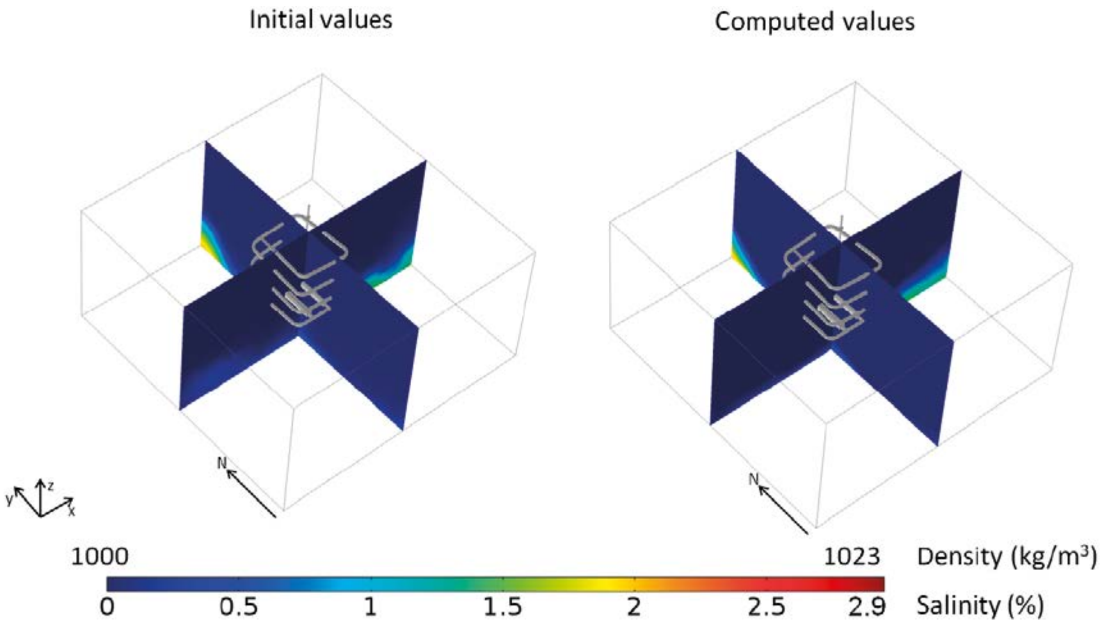

Figure 3-31. *Salinity and density at repository location 500_4, with initial values (left) and computed values (right).*

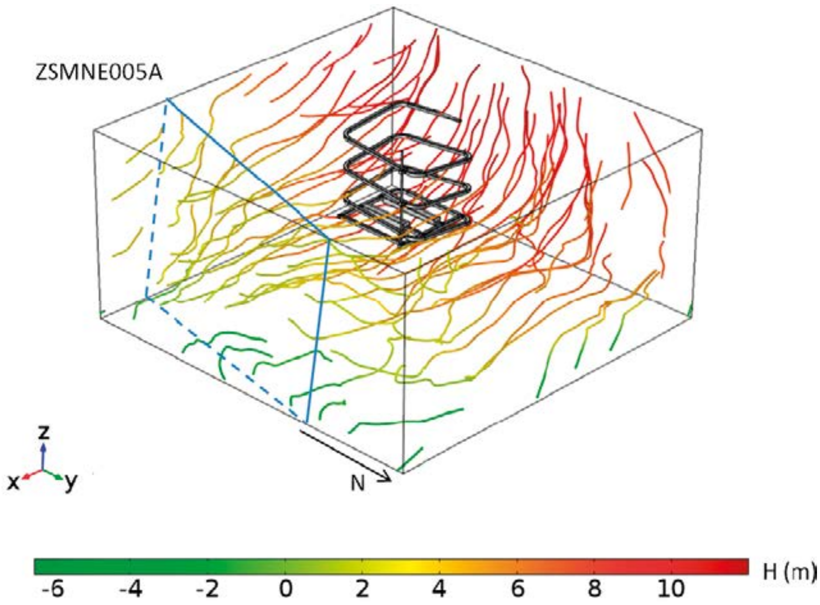

Figure 3-32. *Groundwater streamlines at location 500_4. The colour of the streamlines indicates the local hydraulic head (H). The location of the relevant deformation zones is indicated by blue plane traces.*

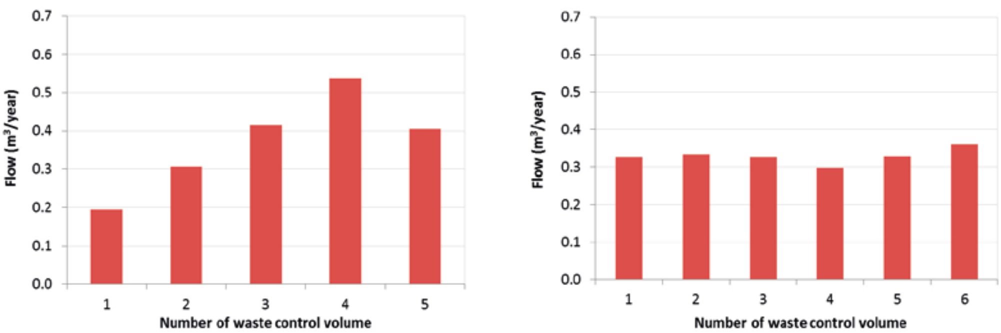

Figure 3-33. *Calculated flow through the waste control volumes of BHA (left) and BHK (right) at location 500_4.*

Table 3-7. Computed flow through waste control volumes and through the BHA and BHK vaults at location 500_4.

			Total flow (m^3/year)	Mass conservation error
BHA	**Waste**	BHA_1	0.194	3.05%
		BHA_2	0.306	0.93%
		BHA_3	0.414	1.14%
		BHA_4	0.537	0.45%
		BHA_5	0.404	−5.01%
	Vault	BHA	0.842	0.91%
BHK	**Waste**	BHK_1	0.325	0.21%
		BHK_2	0.332	1.52%
		BHK_3	0.325	−0.46%
		BHK_4	0.297	0.87%
		BHK_5	0.328	2.42%
		BHK_6	0.360	2.74%
	Vault	BHK	3.288	0.08%

Groundwater flow at the level of the vaults shows a strong horizontal component from west to east (Figure 3-35). Water reaches the BHA vault transversally. The low hydraulic conductivity of BHA backfill acts as a hydraulic barrier and prevents water from reaching BHK as well.

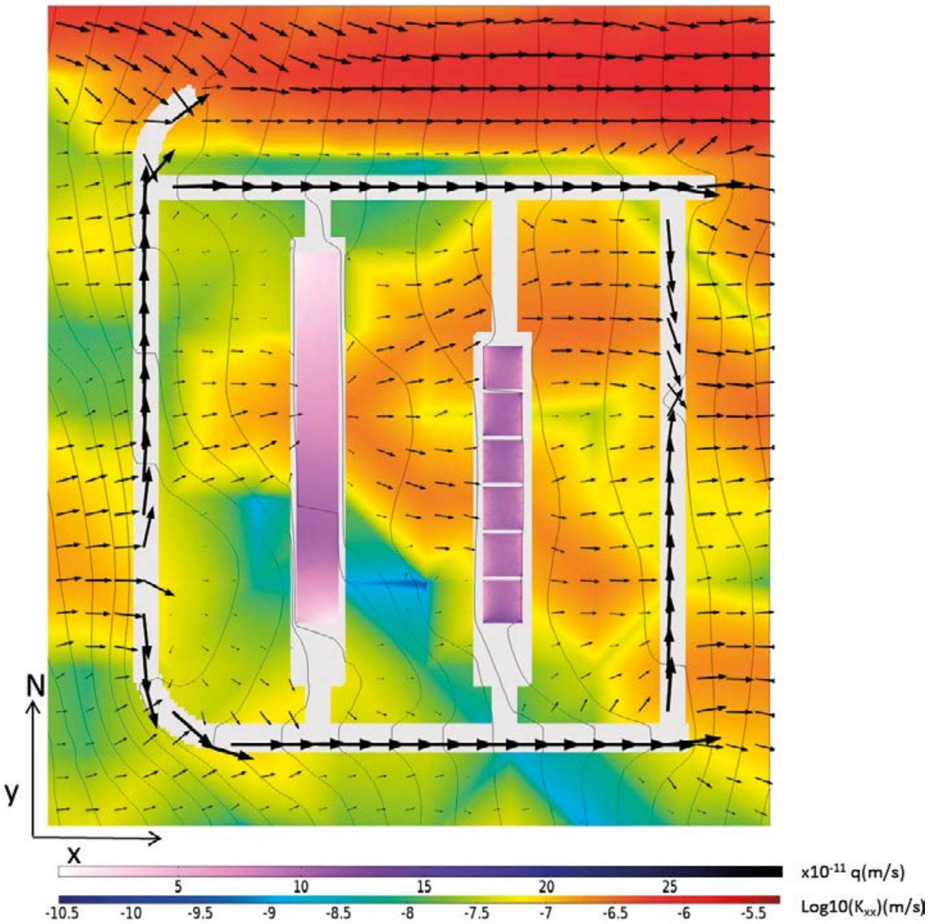

***Figure 3-34.** Magnitude of the Darcy velocity through the waste control volumes, hydraulic conductivity of the rock, hydraulic head (isolines) and Darcy velocity (arrows) at location 500_4. Additional cross-section plots are available in Appendix D (Figure D-7 and Figure D-8).*

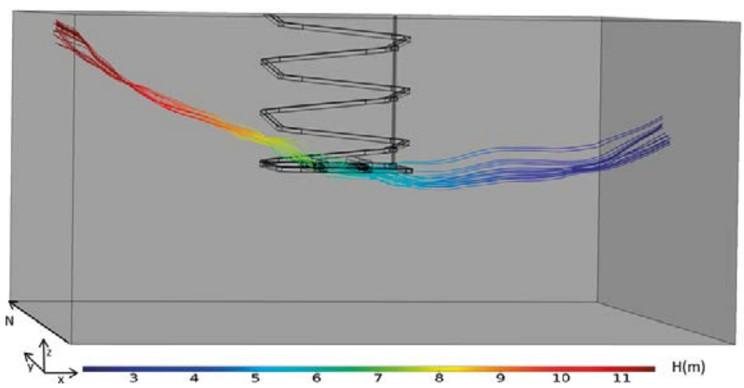

***Figure 3-35.** Streamlines crossing the waste control volumes of the BHA and BHK vault at location 500_4.*

3.4.5 Tracer transport

Figure 3-35 shows the extent of the two tracer plumes released at the vault/rock interface at steady state. The 500_4 domain has a horizontal groundwater flow from west to east, crossing first BHA and then BHK. This flow field results in elongated plumes from west to east. The interaction between the BHA tracer (located upstream) and the BHK vault is about 10%. The BHK tracer does not interact with the BHA vault.

Table 3-8. Calculated tracer interaction at location 500_4.

	From BHA to BHK	From BHK to BHA
m_r (kg/yr)	57.4	72.5
m_v (kg/yr)	5.93	7.1E−7
Ratio	0.1033	0.0000

3.5 700_1

3.5.1 Description of the host rock

The host rock at 700_1 has the lowest hydraulic conductivity values of all investigated locations. Vertical penetrative faults (north-south strike) outcropping at the surface (ZSMN001C and ZSMN005A) can be observed (Figure 3-39). Other deformation zones can be observed in Figure 3-37 and Figure 3-38. D11_Z1 presents an east-west strike and north dip and does not reach the surface. The hydraulic conductivity values of D11_Z1 range from 4.9×10^{-9} m/s to 2.94×10^{-8} m/s and the hydraulic conductivity of D12_Z1 ranges from 4.91×10^{-7} m/s to 9.81×10^{-8} m/s.

The same deformation zones affect the BHK and BHA vaults with similar hydraulic conductivity (Figure 3-37 and Figure 3-38). D11_Z1 crosses the BHA vault at waste control volume 5 and the BHK between waste control volume 4 and 5.

At 700 m depth deformation zone ZSMN001C has low hydraulic conductivity values (Figure 3-39). The ZSMN005A deformation zone also shows lower values of hydraulic conductivity at this depth. Deformation zones D11_Z11, D13_Z1 and D14_Z1 can also be observed in Figure 3-39.

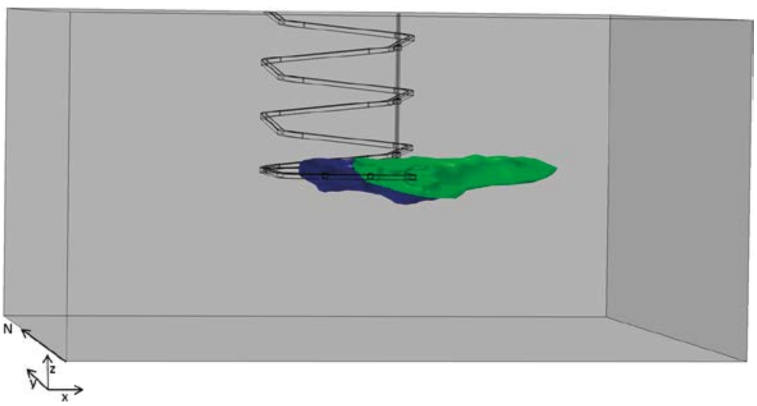

Figure 3-36. *Extent of tracer plumes illustrated by the 20% isosurface of the released concentration (c_r) at location 500_4. The tracer plume released from BHK is shown in green and tracer plume from BHA in blue.*

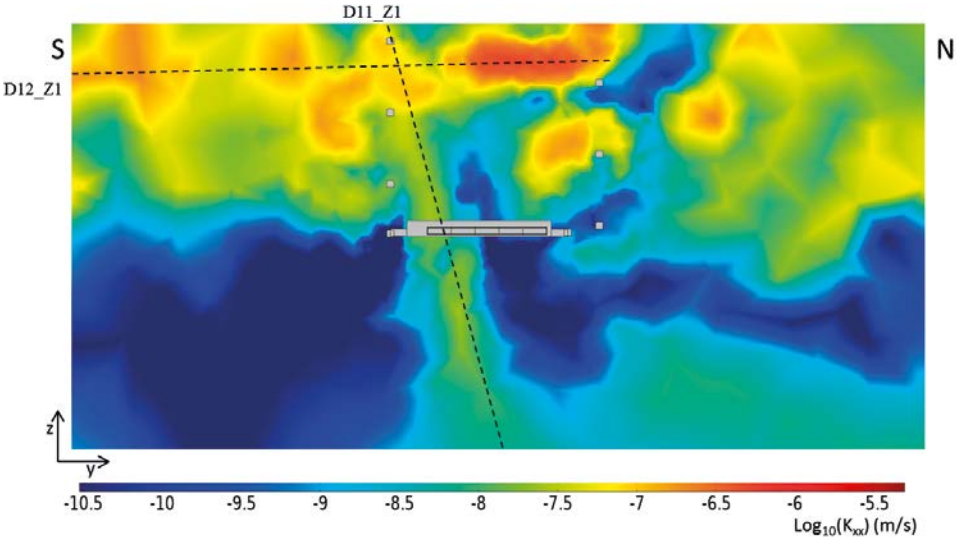

Figure 3-37. *Rock hydraulic conductivity field (K_{xx}) represented in an yz-plane intersecting the BHA vault at location 700_1.*

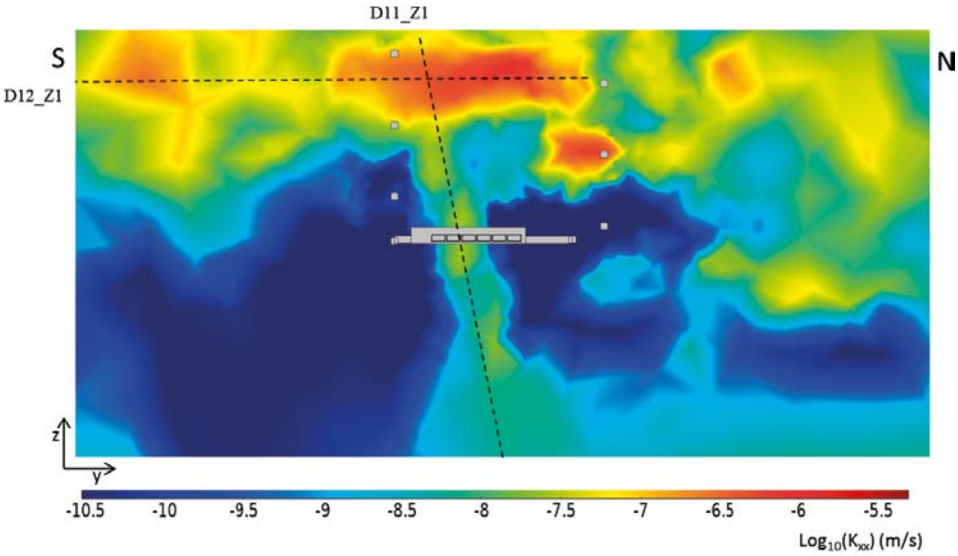

Figure 3-38. *Rock hydraulic conductivity field (K_{xx}) represented in an yz-plane intersecting the BHK vault at location 700_1.*

3.5.2 Salinity

The salinity distribution at location 700_1, computed from the regional model, is used both as initial conditions and boundary condition for the density driven flow simulation. Salinity is stratified and large variations are observed in the model domain. Therefore, a density dependent flow model is needed to properly analyse the flow dynamics. The salinity at 950 m depth, where the bottom model boundary was initially located, shows spatial variation with a maximum value of 2.6%. Simulations revealed boundary effects due to the movement of the interface in response to local pressure changes at the repository location. To avoid these effects the model domain was extended vertically an additional 350 m, with the lower boundary at 1,300 m depth. The salinity at the lower surface of the extended model domain reaches a maximum value of 4.13%. The salinity distribution resulting from a steady state density dependent flow simulation is shown in the right-hand plot of Figure 3-40.

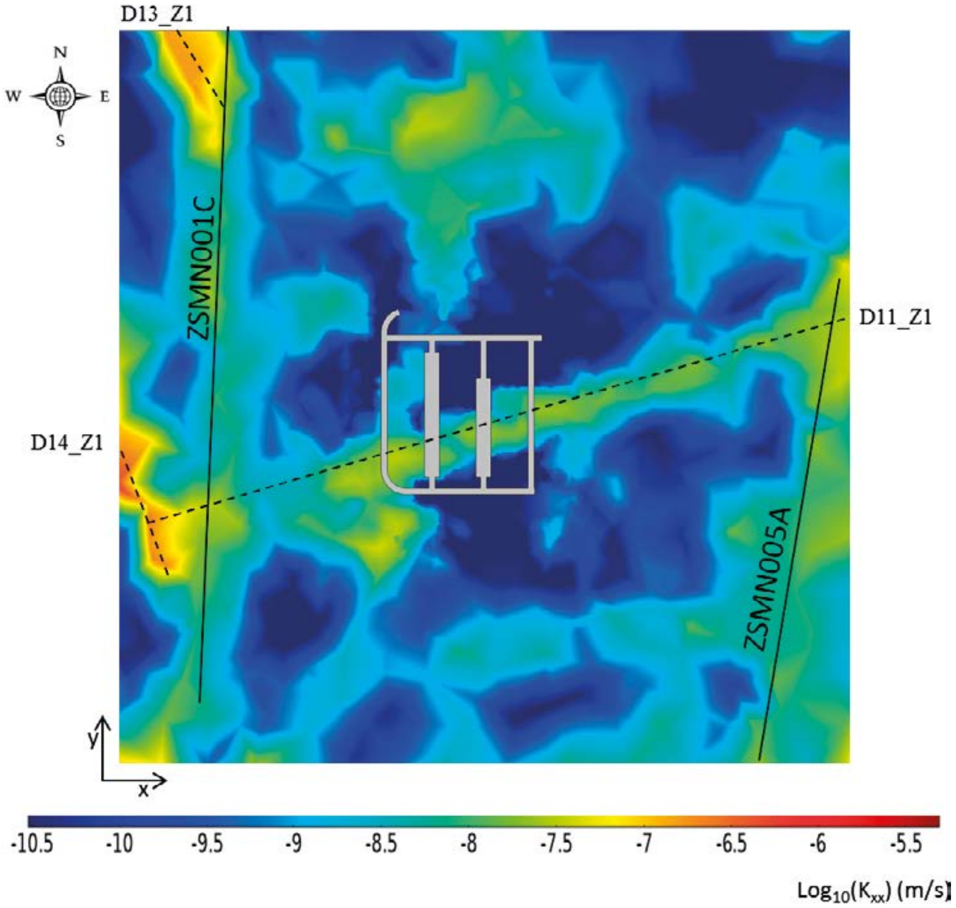

Figure 3-39. *Rock hydraulic conductivity field (K_{xx}) represented in a xy-plane intersecting BHA and BHK at location 700_1.*

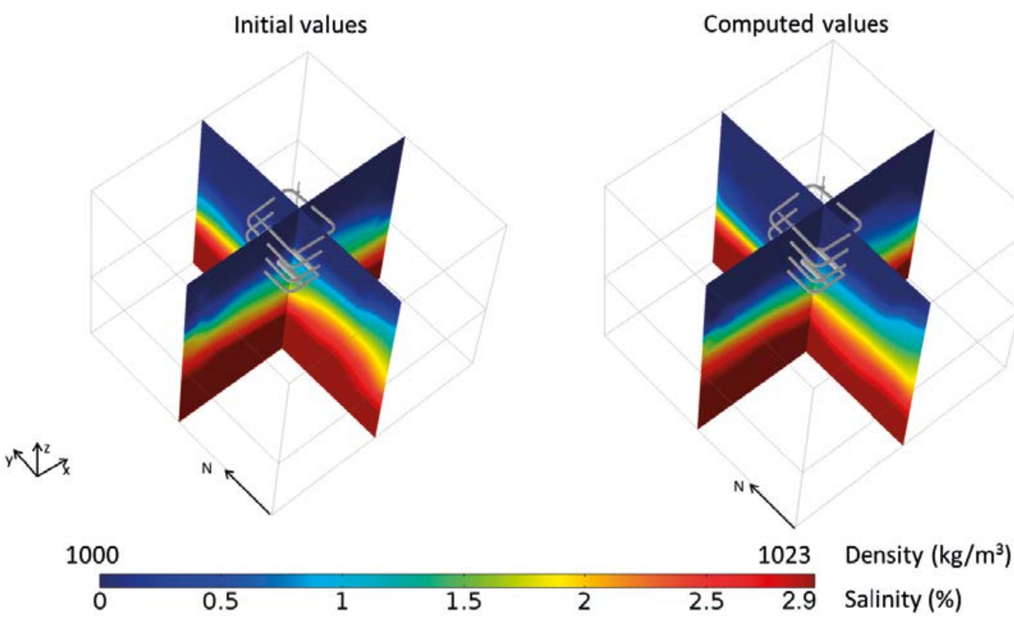

Figure 3-40. *Salinity and density at repository location 700_1 comparison between initial values (left) and computed values (right).*

3.5.3 Dispersivity

Dispersivity is a scale dependent parameter (Gelhar et al. 1992) and, in heterogeneous media, it depends on the correlation scale of heterogeneities (Gelhar and Axness 1983). In this highly heterogeneous model, the effective dispersivity has been chosen to be a combination of a local dispersivity term plus a term that depends on the element size. This implies that the Peclet number is nearly constant throughout the model domain. The dispersivity is defined as $\alpha = 15+\beta\cdot h$, where h is the element size (m) and β a constant set to 3. The resulting values of the dispersivity range between 15.5 to 155 m. In the present system the velocity-dependent dispersion is small compared to diffusion. Nevertheless, given the uncertainty related to the dispersivity values, a sensitivity analysis on the β parameter has been carried out.

A set of four additional simulations has been performed, with β = 12, 16.5, 21 and 30. The groundwater calculated flows through the vaults are presented in Table 3-9. The results show little sensitivity to the dispersivity values.

Table 3-9. Flow differences with respect to the base case for different values of β.

	Differences		30	21	16.5	12
BHA	**Waste**	BHA_1	0.15%	0.12%	0.10%	0.07%
		BHA_2	0.17%	0.13%	0.11%	0.08%
		BHA_3	0.16%	0.12%	0.10%	0.08%
		BHA_4	0.14%	0.11%	0.09%	0.07%
		BHA_5	0.10%	0.08%	0.07%	0.05%
	Tunnel	BHA	0.18%	0.14%	0.11%	0.08%
BHK	**Waste**	BHK_1	−0.37%	−0.25%	−0.19%	−0.13%
		BHK_2	−0.14%	−0.11%	−0.10%	−0.07%
		BHK_3	−1.23%	−0.85%	−0.66%	−0.45%
		BHK_4	−3.00%	−2.00%	−1.51%	−1.01%
		BHK_5	−2.02%	−1.32%	−0.98%	−0.66%
		BHK_6	−1.43%	−0.87%	−0.62%	−0.41%
	Tunnel	BHK	0.07%	0.04%	0.03%	0.02%

Figure 3-41 and Figure 3-42 compare the salt distribution at repository level for the cases β = 3 and 30. Results show only a minor effect of velocity-dependent dispersion in the computed results.

3.5.4 Groundwater flow field

Groundwater flow at location 700_1 is mainly horizontal, from north to south, influenced by the salinity stratification (Figure 3-43). The freshwater in the upper part of the model domain shows a subhorizontal flow. There is downward flow associated with the ZSMN005A and ZSMN001C deformation zones. The saline deep water flows from north to south with a slight vertical upwards component. The calculated total groundwater flow entering the model domain 700_1 is 4.09×10^3 m^3/year.

3.5.5 Flow through the vaults and waste

Figure 3-44 and Table 3-10 show the calculated groundwater flow per waste control volume and the total flow per vault. The total flow through BHA is five times greater than through BHK. The hydraulic conductivity of the rock is similar to hydraulic conductivity of the BHA backfill (Figure 3-45) and a part of the flow from northwest to southeast is forced through the northern part of the BHA vault. However, BHK is intersected by high hydraulic conductivity zone D11_Z1, which drives groundwater flow from northeast to southwest, reducing the flow across the BHK vault (Figure 3-45).

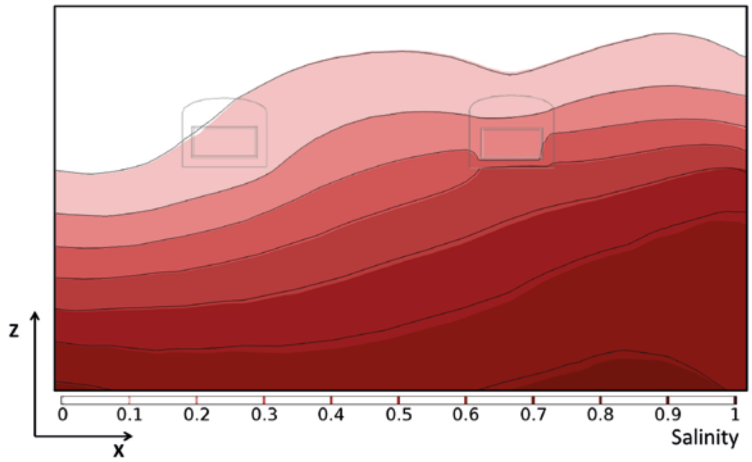

Figure 3-41. *Salinity contours in a vertical plane perpendicular to the vaults for location 700_1. Colour contours represent the base case solution (β = 3) and the black lines a solution with a higher dispersivity (β = 30).*

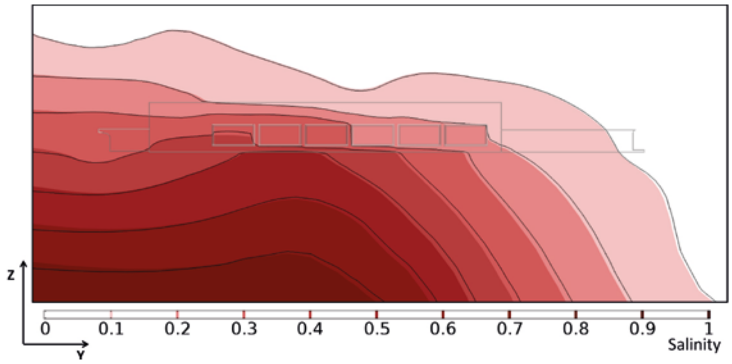

Figure 3-42. *Salinity contours in a vertical plane across the BHK for location 700_1. Colour contours represent the base case solution (β = 3) and the black lines a solution with a higher dispersivity (β = 30).*

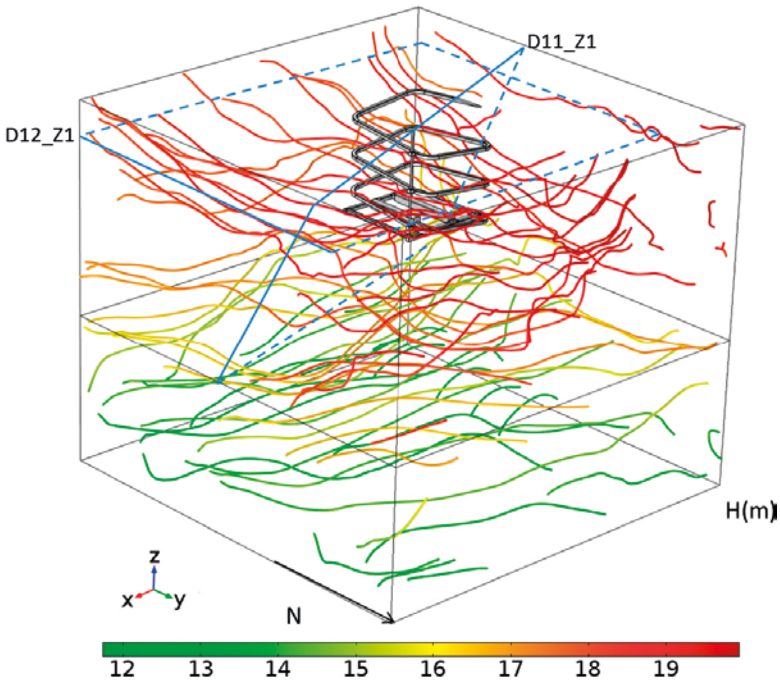

Figure 3-43. *Groundwater streamlines at location 700_1. The colour of the streamlines indicates the local hydraulic head (H). The location of the relevant deformation zones is indicated by blue plane traces.*

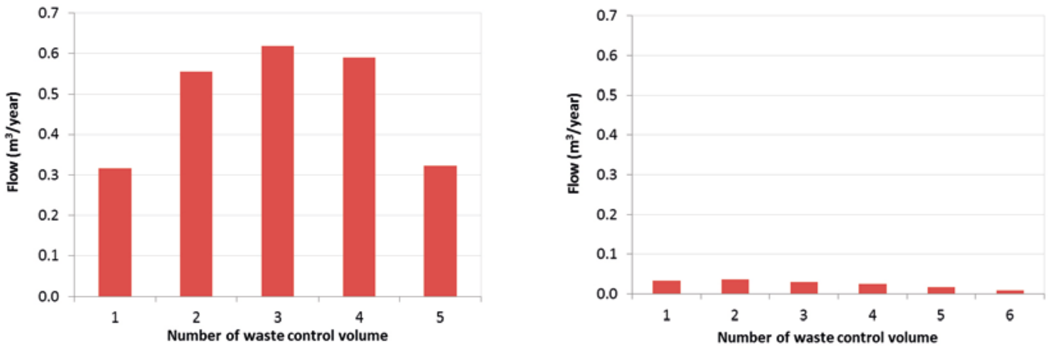

***Figure 3-44.** Calculated flow through the waste control volumes of BHA (left) and BHK (right) at location 700_1.*

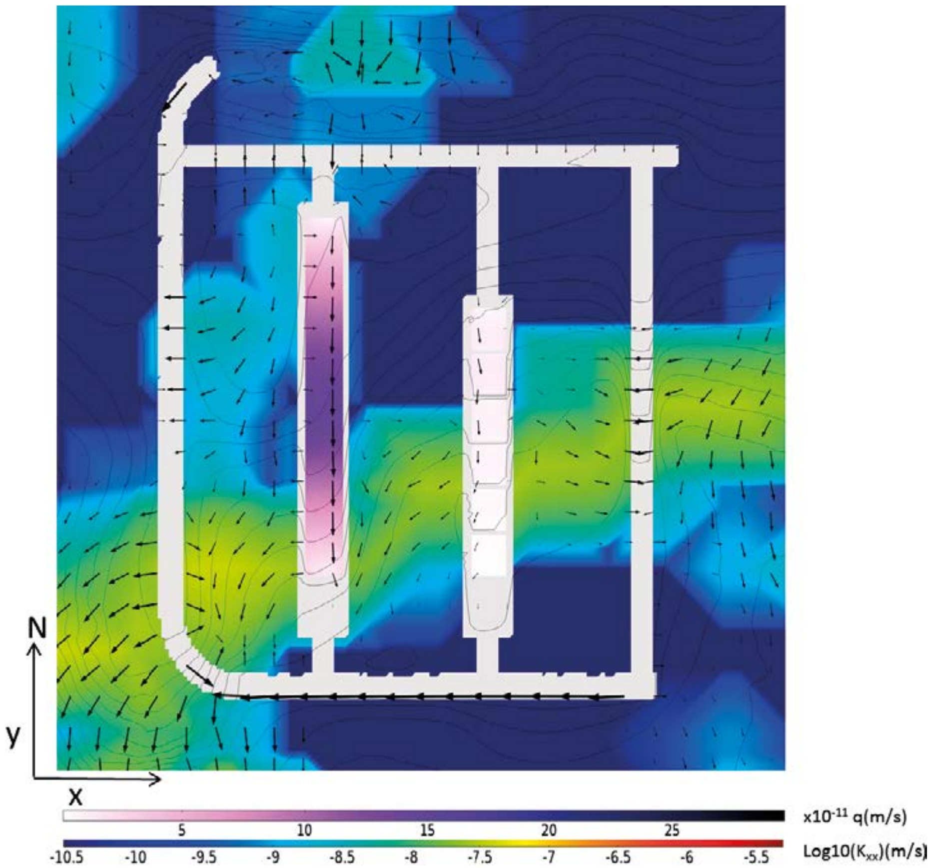

***Figure 3-45.** Magnitude of the Darcy velocity through the waste control volumes, hydraulic conductivity of the rock, hydraulic head (isolines) and Darcy velocity (arrows) at location 700_1. Additional cross-section plots are available in Appendix D (Figure D-9 and Figure D-8).*

On average, 72% of the flow through the BHA vault goes through the waste domain, while the corresponding number for the BHK is 23% (Figure 3-45). The central waste control volumes in BHA vault experience the highest groundwater flow. These control volumes are surrounded by rock of relatively low hydraulic conductivity. The control volumes (BHA_1 and BHA_5) are surrounded by more permeable rock and show lower flow vaules.

The flow streamlines reaching and leaving the vaults show a convoluted flow system (Figure 3-43, Figure 3-45, Figure 3-46), influenced by the freshwater/saltwater interface.

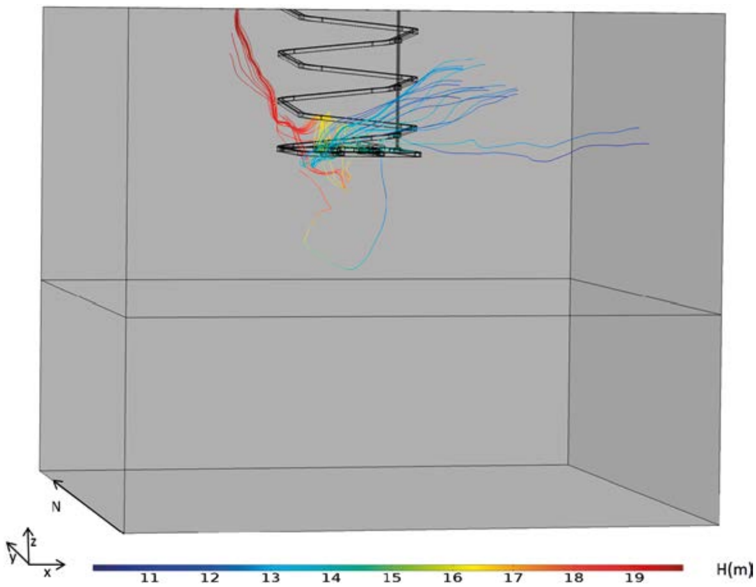

Figure 3-46. *Groundwater flow streamlines crossing the waste control volumes of the BHA and BHK vaults at location 700_1.*

Table 3-10. Computed flow through waste control volumes and through the BHA and BHK vaults at location 700_1.

			Total flow (m^3/year)	Mass conservation error
BHA	**Waste**	BHA_1	0.317	−3.45%
		BHA_2	0.556	−2.14%
		BHA_3	0.619	−0.59%
		BHA_4	0.590	1.44%
		BHA_5	0.324	3.14%
	Vault	BHA	0.671	0.16%
BHK	**Waste**	BHK_1	0.034	4.80%
		BHK_2	0.037	5.37%
		BHK_3	0.031	6.14%
		BHK_4	0.026	4.30%
		BHK_5	0.017	6.81%
		BHK_6	0.009	12.92%
	Vault	BHK	0.114	6.6%

3.5.6 Tracer transport

Figure 3-47 shows the extent of the two steady state tracer plumes released at the vault/rock interface. The 700_1 domain has low groundwater flows and the main mass transport mechanism is diffusion (Figure 3-47). The tracer distribution reveals two quasi stagnant spherical plumes around the vaults. The BHA tracer interacts slightly with the BHK vault (ratio m_r/m_v =0.0005 in Table 3-11). The BHK tracer shows an interaction with the BHA vault of 1% (ratio m_r/m_v =0.0011 in Table 3-11).

Table 3-11. Calculated tracer interaction at location 700_1.

	From BHA to BHK	From BHK to BHA
m_r (kg/yr)	8.07E+2	2.22E+2
m_v (kg/yr)	3.88E−1	2.46E−1
Ratio	0.0005	0.0011

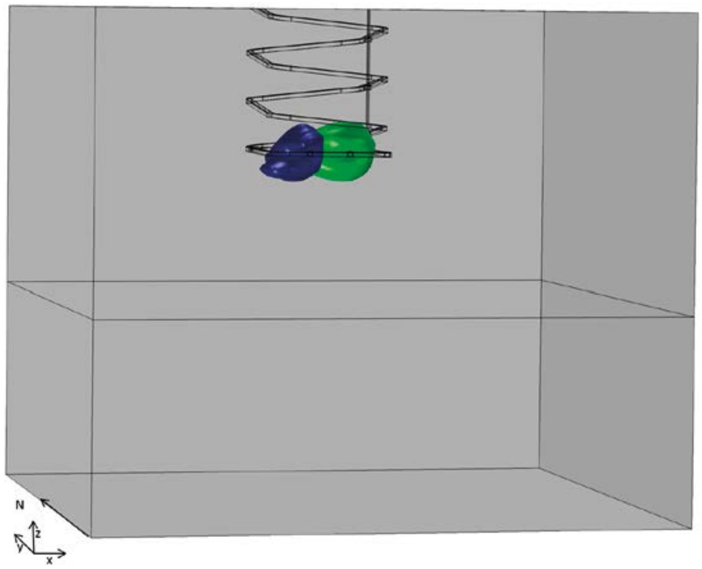

Figure 3-47. Extent of tracer plumes illustrated by the 20% isosurface of the released concentration (c_r) at location 700_1. The tracer plume released from BHK is shown in green and tracer plume from BHA in blue.

3.6 700_4

3.6.1 Description of the host rock

The host rock at location 700_4 has three main deformation zones with high hydraulic conductivity values (maximum values of hydraulic conductivity around 4.91×10^{-7} m/s). Two of these deformation zones are located south-southeast of the repository and outcrop at the surface. They are identified as ZSMEW005A and ZSMEW007A. The ZSMEW007A deformation zone dips approximately 45 degrees north (Figure 3-48 and Figure 3-49). D5_Z4 is a subvertical deformation zone with an east-west strike. It affects the northern part of the repository (Figure 3-50) crossing BHA and BHK at their northern end (Figure 3-48 and Figure 3-49). Other minor deformation zones, D8_Z4 and D6_Z4, parallel to D5_Z4 can be observed in Figure 3-48. The vertical deformation zones reach a depth of 700 m and are illustrated in Figure 3-50.

3.6.2 Salinity

The salinity distribution from the regional model is used both as initial conditions and boundary condition for the density driven flow simulation. Salinity ranges from 0.0% to 2.9%. A vertical stratification is observed. The interface between the fresh and the saltwater is subhorizontal, slightly dipping to the south. Maximum salinities are found to the northeast and reach repository depth.

The salinity distribution resulting from a steady-state density-dependent flow simulation is shown in Figure 3-51 (right). The computed salinity agrees well with the initial distribution of salinity from the regional model Figure 3-51, (left).

3.6.3 Groundwater flow field

Groundwater flows from west to east at location 700_4 (Figure 3-52). Groundwater enters the model domain through the west and top west boundaries. The streamlines show an eastward subhorizontal flow system controlled by the freshwater/saltwater interface. Flow is parallel to the subhorizontal salinity interface (Figure 3-51). At the southeast corner, streamlines show the influence of ZSMN005A in the flow field. The calculated total groundwater flow entering the model domain 700_4 is 1.55×10^4 m^3/year.

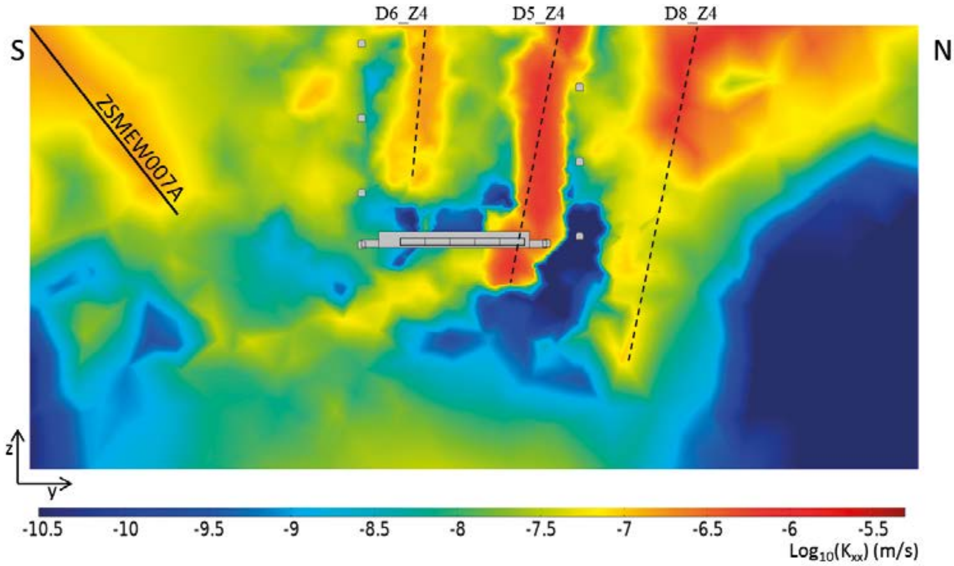

Figure 3-48. *Rock hydraulic conductivity field (K_{xx}) represented in an yz-plane intersecting the BHA vault at location 700_4.*

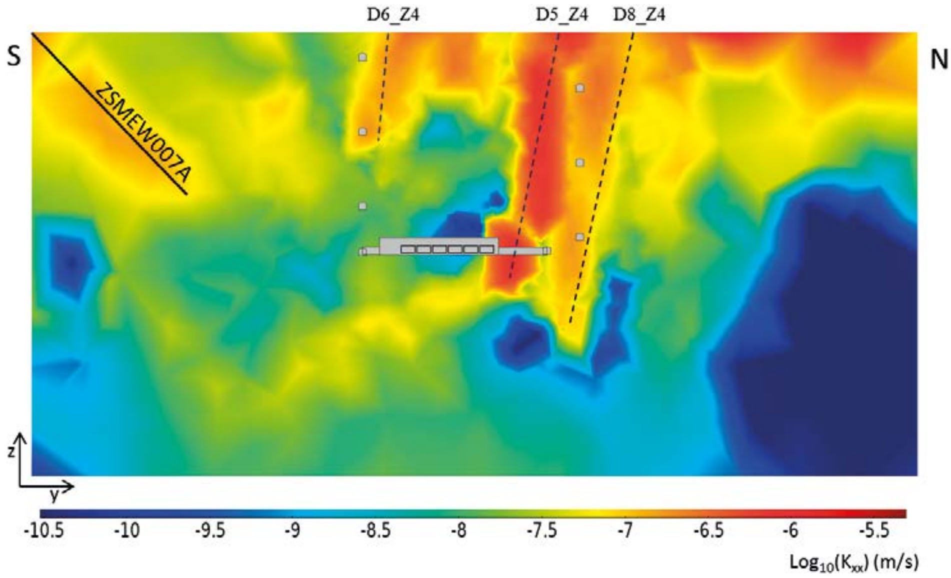

Figure 3-49. *Rock hydraulic conductivity field (K_{xx}) represented in an yz-plane intersecting the BHK vault at location 700_4.*

3.6.4 Flow through the vaults and waste packages.

Figure 3-53 and Table 3-12 show the calculated groundwater flow per waste control volume and the total flow per vault. In terms of the total flow through the vaults, BHK collects twice the flow of BHA.

On average, 15% of the flow entering the vaults passes through a waste domain for both BHA and BHK. In the case of BHA, the inflow is uniformly distributed between the waste control volumes, with the maximum inflow in BHA_2, affected by deformation zone D5_Z4 (Figure 3-54). In the BHK vault, waste control volume 1 collects the highest flow. This control volume borders on zone D5_Z4 (Figure 3-54).

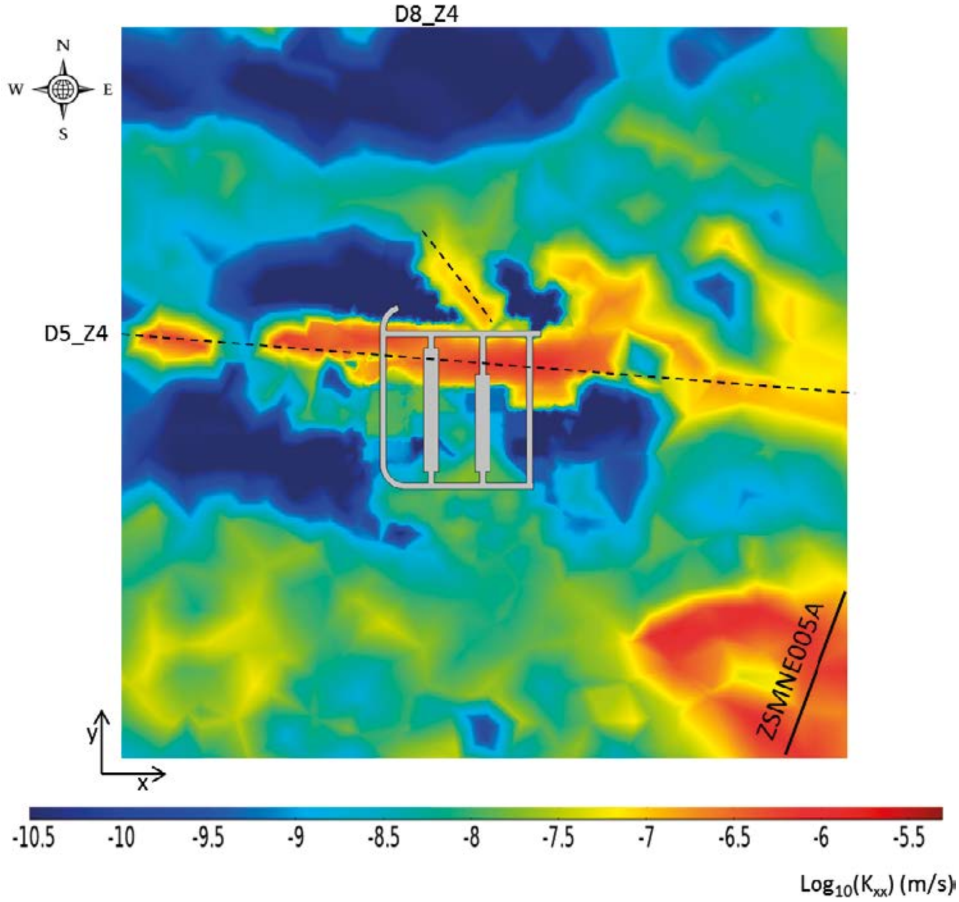

Figure 3-50. *Rock hydraulic conductivity field (K_{xx}) represented in a xy-plane intersecting BHA and BHK at location 700_4.*

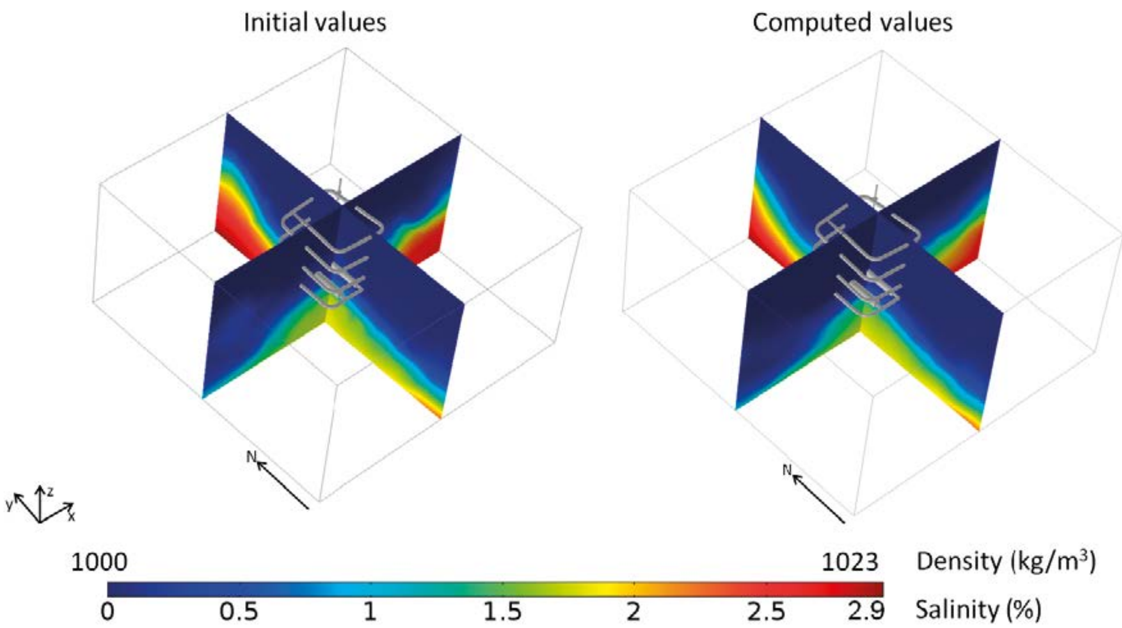

Figure 3-51. *Salinity and density at repository location 700_4, with initial values (left) and computed values (right).*

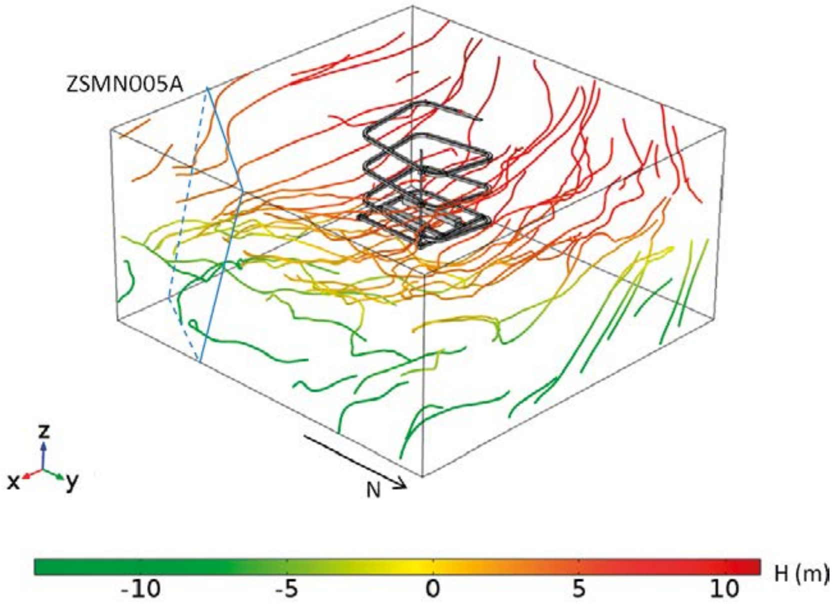

Figure 3-52. *Groundwater streamlines at location 700_4. The colour of the streamlines indicates the local hydraulic head (H). The location of the relevant deformation zones is indicated by blue plane traces.*

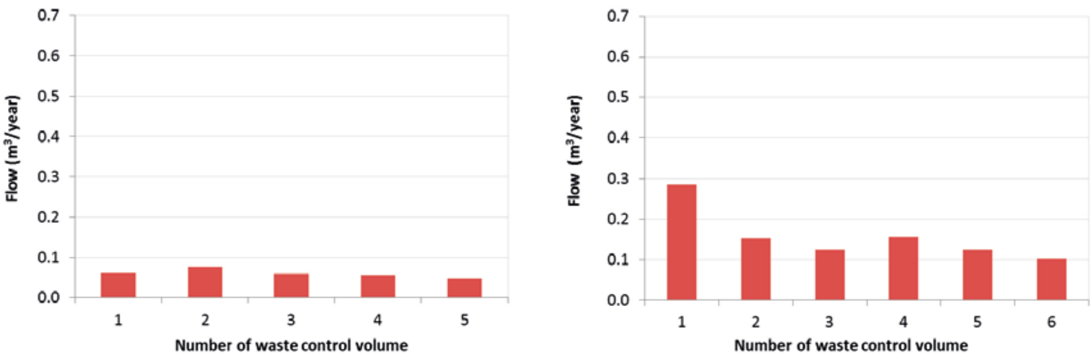

Figure 3-53. *Calculated flow through the waste control volumes of BHA (left) and BHK (right) at location 700_4.*

Table 3-12. Computed flow through waste control volumes and through the BHA and BHK vaults at location 700_4.

			Total flow (m^3/year)	Mass conservation error
BHA	**Waste**	BHA_1	0.061	−3.67%
		BHA_2	0.076	−2.74%
		BHA_3	0.060	−2.21%
		BHA_4	0.056	−1.71%
		BHA_5	0.047	−0.78%
	Vault	BHA	0.416	−0.78%
BHK	**Waste**	BHK_1	0.287	1.12%
		BHK_2	0.153	−0.65%
		BHK_3	0.125	−0.07%
		BHK_4	0.156	1.02%
		BHK_5	0.125	0.36%
		BHK_6	0.104	−0.19%
	Vault	BHK	1.016	−0.09%

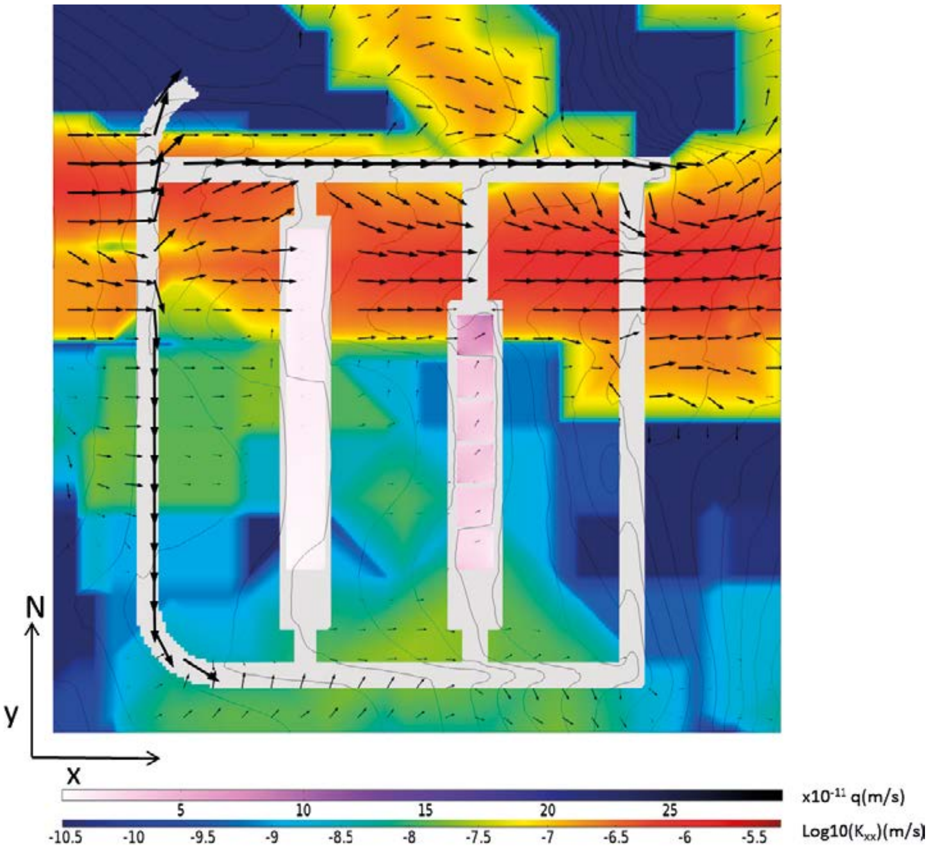

Figure 3-54. *Magnitude of the Darcy velocity through the waste control volumes, hydraulic conductivity of the rock, hydraulic head (isolines) and Darcy velocity (arrows) at location 700_4. Additional cross-section plots are available in Appendix D (Figure D-11 and Figure D-12).*

Figure 3-54 shows the Darcy velocity field together with the magnitude of the flow entering the waste. This figure illustrates how the flow from west to east occurs mainly through the high hydraulic conductivity deformation zone D5_Z4. When the zone encounters the access tunnels, most of that flow is redirected to the more permeable acess tunnels. The access tunnels act as a hydraulic ring that protects the waste vaults.

Figure 3-55 shows flow lines of water reaching and leaving the waste control volumes. The observed streamlines indicate a flow from west to east with a strong horizontal component.

3.6.5 Tracer transport

Figure 3-56 shows the extent of the two steady state tracer plumes released at the vault/rock interface. The 700_4 domain is characterized by horizontal flow controlled by the salinity stratification. The horizontal direction of groundwater flow from west to east puts BHA vault upstream of BHK (Figure 3-55 and Figure 3-56). BHK is affected by a 0.0163 fraction of the total mass flux released from BHA (Table 3-13). The interaction between the BHK tracer and BHA is only about 0.0001 of the mass released.

Table 3-13. Calculated tracer interaction at location 700_4.

	From BHA to BHK	From BHK to BHA
m_r (kg/yr)	8.80E+1	3.69E+1
m_v (kg/yr)	1.43	2.42E−3
Ratio	0.0163	0.0001

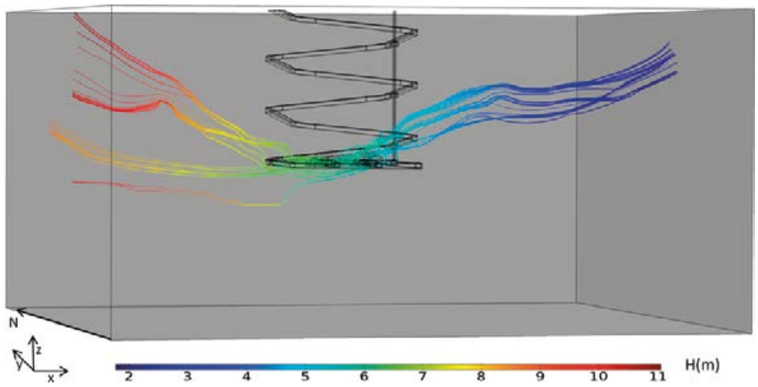

Figure 3-55. *Groundwater flow streamlines crossing the waste control volumes of the BHA and BHK vaults at location 700_4.*

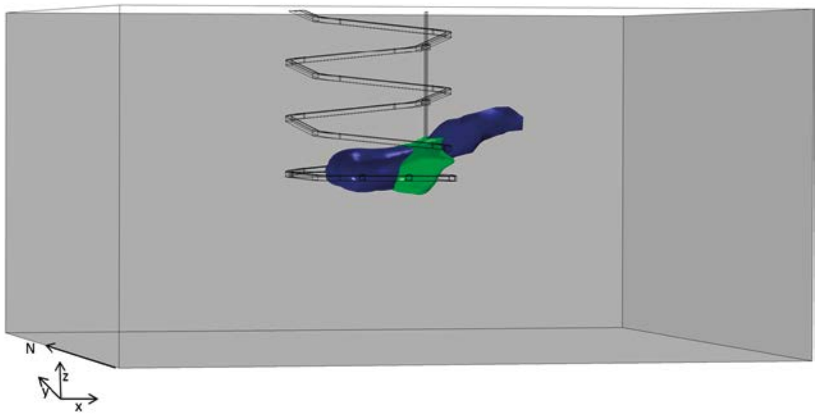

Figure 3-56. *Extent of tracer plumes illustrated by the 20% isosurface of the released concentration (c_r) at location 700_4. The tracer plume released from BHK is shown in green and tracer plume from BHA in blue.*

3.7 Summary

3.7.1 Description of the host rock

Figure 3-57 shows the vertical distribution of the geometric mean of the hydraulic conductivity (K_{xx}) within rock domain 1. Figure 3-58 shows the corresponding distribution for rock domain 4. Rock domain 1 has lower hydraulic conductivity values than rock domain 4. Hydraulic conductivity decreases with depth, with a difference of three orders of magnitude going from 300 m to 700 m depth. All the locations have between one and two deterministic deformation zones within the model domain. The number of stochastic deformation zones within the different locations range from 3 (700_4) to 8 (300_1). In most locations there is one stochastic deformation zone intersecting the repository. At location 300_1 there are two deformation zones affecting the repository.

3.7.2 Groundwater flow

Total flow

The total groundwater flow entering to the six model domains have been evaluated. Results are summarized in Figure 3-59. There is a reduction in the total flow with depth, consistent with the hydraulic conductivity reduction for the rock. In general, the total flow is higher in rock domain 4.

Water salinity

Groundwater salinity increases with depth in both rock domains. The vertical salinity gradient is greater for rock domain 4. Density differences do not impact groundwater flow for locations 300_1 and 300_4 but do so in the remaining cases. For location 700_1, the repository becomes positioned at the freshwater/saltwater interface, which creates upwards movement of the saline water. In that case, a larger vertical domain is needed to properly evaluate the upward migration of the saline water.

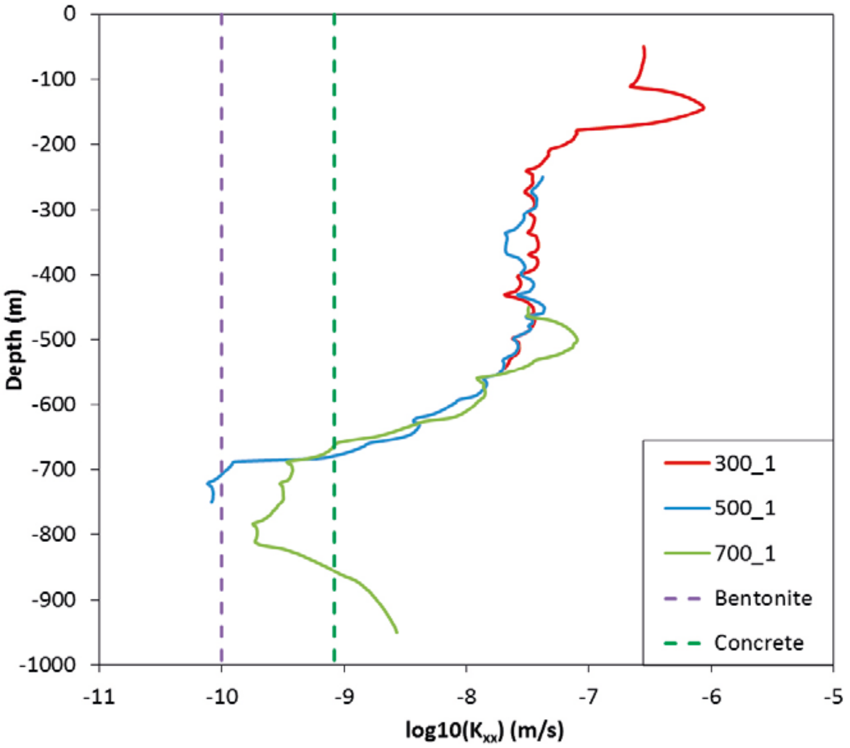

Figure 3-57. *Vertical distribution of the geometric mean hydraulic conductivity (K_{xx}) in rock domain 1. Dashed lines indicate concrete and bentonite backfill hydraulic conductivities.*

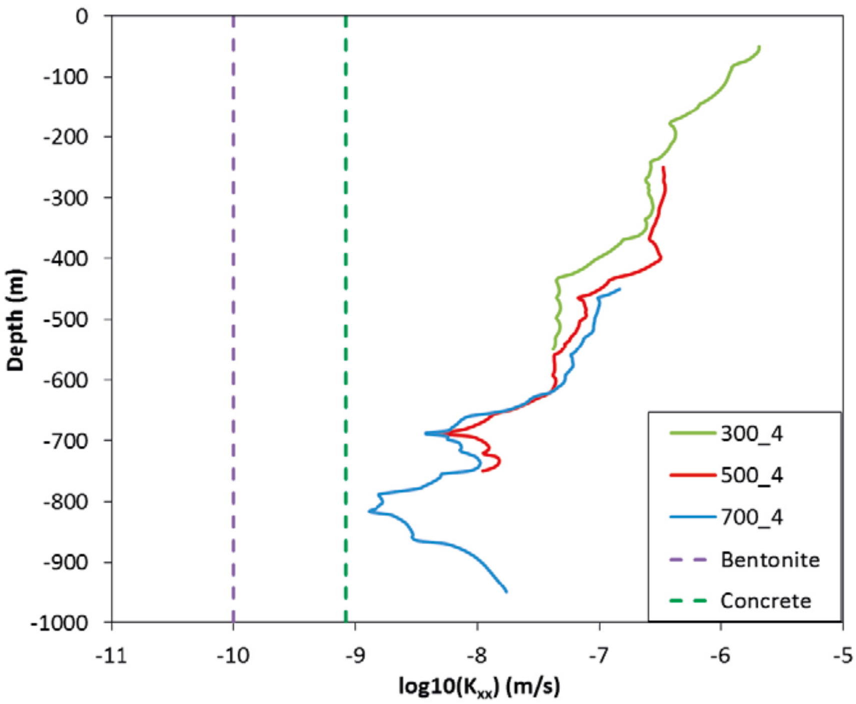

Figure 3-58. *Vertical distribution of the geometric mean hydraulic conductivity (K_{xx}) in rock domain 4. Dashed lines indicate concrete and bentonite backfill hydraulic conductivities.*

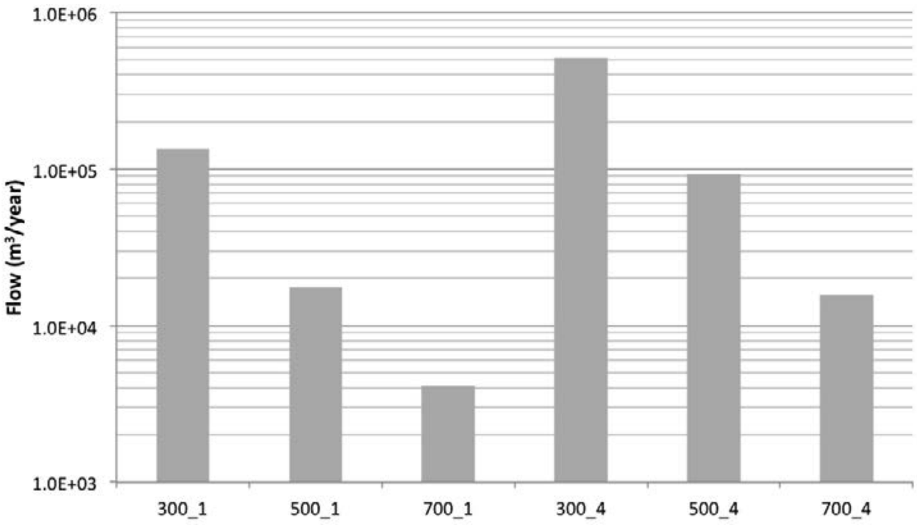

Figure 3-59. *Calculated groundwater flow through the rock domain in the six model domains.*

Main flow component

In locations 700_1, 700_4 and 500_4 the flow system is controlled by the salinity distribution. Flow is mainly horizontal in these cases and parallel to the salinity interface. The remaining cases show a main vertical flow component.

3.7.3 Vault flow

Flow through the BHA vault is fairly similar for all 6 locations (Figure 3-60). A minimum value of 0.425 m^3/year is calculated for location 700_4 and a maximum value of 0.861 m^3/year for location 500_4. The hydraulic conductivity of the bentonite backfill is lower than the rock hydraulic conductivity (Figure 3-57 and Figure 3-58) at all depths and acts as an efficient flow barrier.

Flow through the BHK vault shows a greater dependency on location, with a minimum value of 0.13 m^3/year at location 700_1 and a maximum value of 4.7 m^3/year at location 300_4. BHK vault flows are higher in rock domain 4, correlating with the higher hydraulic conductivity of this rock domain compared to domain 1. The BHK flow decreases with depth, although the difference is at most one order of magnitude going from 300 to 700 m. This limited sensitivity to the depth reflects the fact the concrete hydraulic conductivity is lower than the rock hydraulic conductivity for most locations (Figure 3-57 and Figure 3-58). At location 700_1, the deformation zone D11_Z1 crosses the BHK vault and serves as by-pass to the northeast to southwest flow, minimizing the flow across the BHK vault.

In four locations (300_1, 300_4, 500_4 and 700_4), the calculated flow through the BHK waste is greater than through the BHA waste (Figure 3-60). This is expected since the hydraulic conductivity of the concrete backfill is almost one order of magnitude higher than the bentonite backfill of BHA. At locations 500_1 and 700_1, the flow in the BHA waste is larger than in BHK. In both cases, the flow at the repository depth is parallel to the BHA vault. Furthermore, the upstream end of the vault is situated in rock with a hydraulic conductivity similar to that of the bentonite backfill. Water that passes the bentonite backfill will move through the entire waste volume in this case, as no internal flow barriers are assumed in BHA.

Interaction between vaults

The interaction between vaults has been analysed based on the results of two non-reactive tracer transport simulations. The non-reactive tracers have been released at the vault/rock interface. The ratio of tracer released from each vault (m_r), reaching the neighbouring vault (m_v) has been used to quantify the interaction. The computed interaction between vaults is negligible for most repository locations. Only location 500_4 yields a notable interaction (10%) between the upstream BHA vault and the BHK vault. At location 700_4 the interaction is 1%.

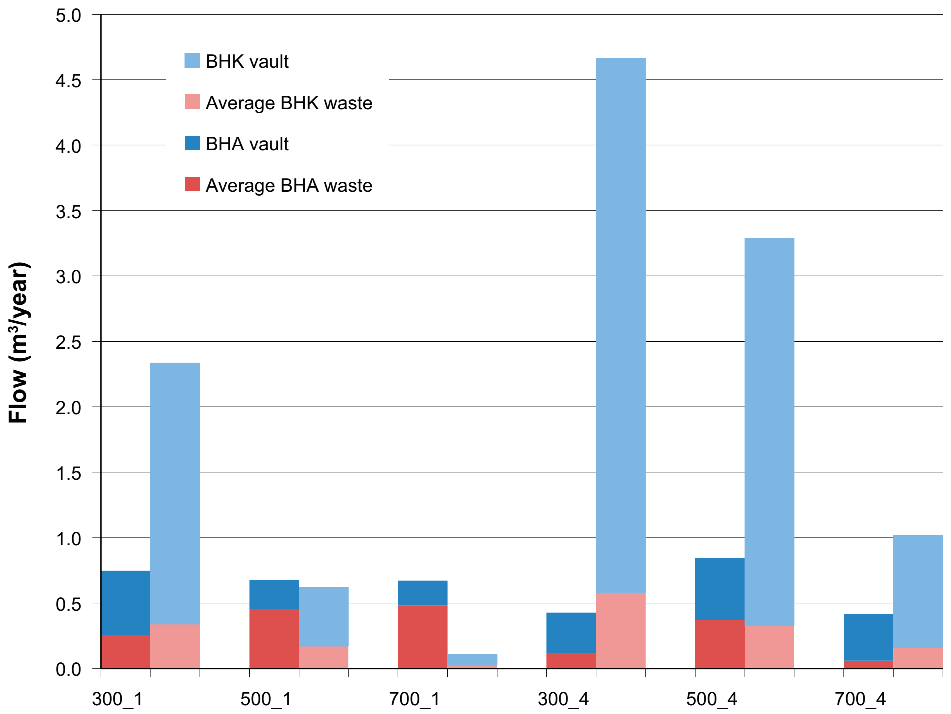

Figure 3-60. *Calculated groundwater flows through the BHA and BHK vaults and waste in the six model domains.*

4 Repository orientation

The repository orientation with respect to the flow field, can affect the flow through the vaults and waste as well as the interaction between the vaults. The influence of repository orientation has been investigated for one case where the flow is mainly vertical and one case where the flow is mainly horizontal.

4.1 Repository rotation under vertical flow conditions

At location 300_1, groundwater flow reaching the repository is mainly vertical. To analyse the effect of the repository orientation, a simulation with a repository rotation of 90° compared to the base case has been performed.

No appreciable changes are observed in the groundwater flow when the repository is rotated (Figure 4-1). However, the streamlines leaving and reaching the repository waste illustrate how groundwater flow changes direction when passing through the waste domain (Figure 4-2). The flow upstream of the repository remains unchanged. Flow is directed through the vaults and exits at their eastern end. The discharging streamlines reach deeper in the case of flow perpendicular to the vaults (base case). In the case of flow parallel to the vaults, the discharging streamlines are shorter indicating faster paths to the discharge areas.

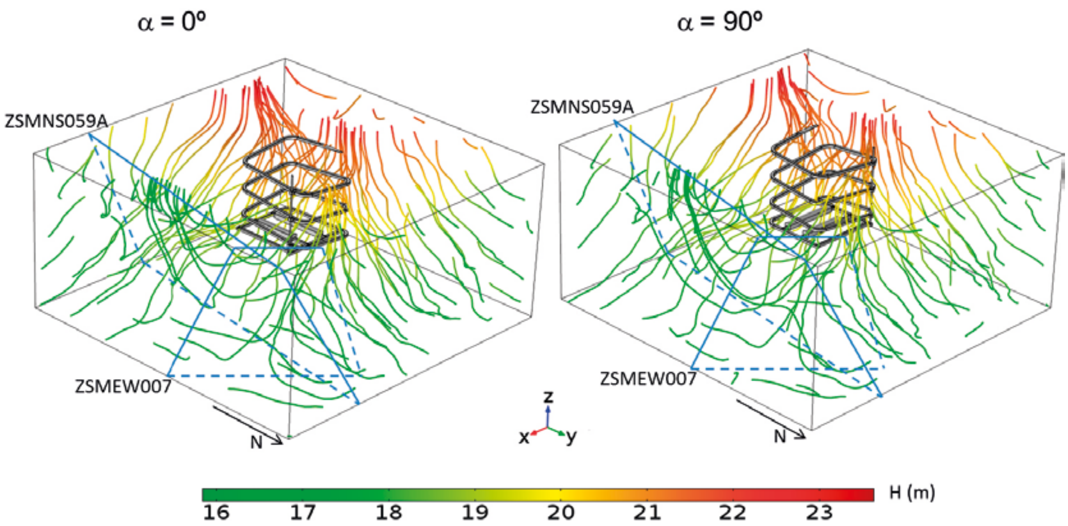

Figure 4-1. Groundwater flow field at location 300_1 for the base case and 90° rotation case.

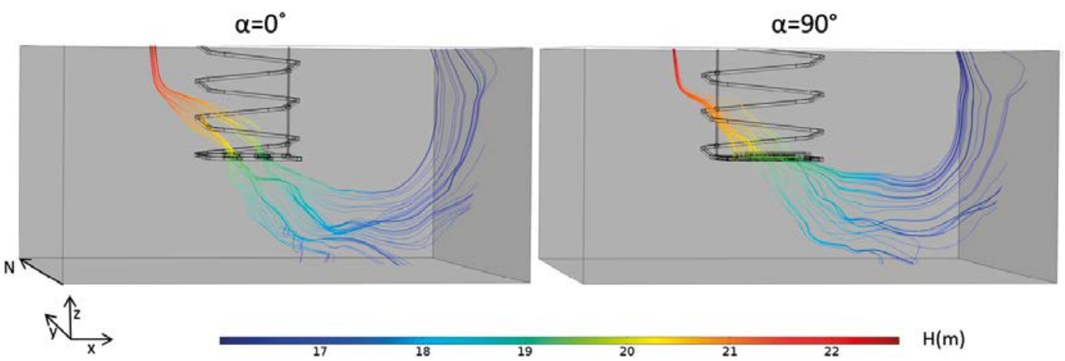

Figure 4-2. Streamlines of the groundwater flow crossing the waste control volumes of BHA and BHK at location 300_1 for the base case and 90° rotation case.

4.1.1 Flow through vault and waste control volumes

In the case of 90° repository rotation, the local groundwater flow is parallel to the vaults. The flow through the BHK vault is twice that of the BHA vault flow (see Table 4-1). The calculated waste flow is similar in both vaults and maximum flows occur at the central waste control volumes (Table 4-1). Approximately 66% of the groundwater flow entering BHA passes through the waste domain while the corresponding number for BHK is 17%. The fact that the BHA waste has no internal barriers facilitates groundwater to flow through the waste control volumes in the longitudinal direction.

Table 4-1. Computed flow through waste control volumes and through the BHA and BHK vaults at location 300_1 (90° repository rotation).

			Total flow (m^3/year)	Mass conservation error
BHA	**Waste**	BHA_1	0.527	−4.4%
		BHA_2	0.793	−0.9%
		BHA_3	0.865	−0.3%
		BHA_4	0.760	1.4%
		BHA_5	0.467	3.8%
	Vault	BHA	1.042	1.9%
BHK	**Waste**	BHK_1	0.369	−0.5%
		BHK_2	0.387	1.6%
		BHK_3	0.406	1.5%
		BHK_4	0.423	−0.1%
		BHK_5	0.431	0.6%
		BHK_6	0.393	−0.1%
	Vault	BHK	2.428	4.6%

Figure 4-4 compares the vault flows for the base case and the 90° rotation case. Groundwater flow through the vaults increases when the flow is parallel to the vaults. The increase is greater for BHA (around 0.25 m^3/year) than for BHK (around 0.15 m^3/year), corresponding to a 28% and a 4% increase, respectively.

The total groundwater flow through the waste is increased when flow is parallel to the vaults (90° rotation at Figure 4-5). This increase is greater for the BHA waste control volumes (about 60%) as no internal flow barriers are assumed. For the BHK, waste control volumes 4-6 experience greater groundwater flow for the 90° rotation case. Differences are due to the hydraulic conductivity the surrounding rock (Figure 4-3). In the base case, the southern part of the BHK vault is situated in a more permeable rock, which allows water to bypass the vault.

4.1.2 Tracer transport

The interaction between vaults is analysed based on the results of two non-reactive tracer transport simulations. The non-reactive tracers are released at the vault/rock interface of each vault. Figure 4-6 shows the extent of the tracer plumes at steady state, illustrated by the iso-surface with 20% of the released concentration (c_r). The plume's extent follows the flow paths shown in Figure 4-2. In the case of α=0°, the plumes extend downwards from the vaults illustrating the vertical direction of the outflowing water. However, the case of α=90° results in two parallel tracer plumes with a more horizontal outflow, especially for the tracer from the BHA vault (blue in Figure 4-6).

The computed mass of a tracer released from each vault (m_r) under the different repository orientations is presented in Table 4-2 for the tracer released from BHA, and in Table 4-3 for the tracer released from BHK. The mass of tracer released from the BHA vault is similar for both orientations. However, the mass of tracer released from the BHK, when the flow is perpendicular to the vaults, is 1.5 times larger than in the case of parallel flow. The mass of tracer that reaches the neighbouring vault is also computed (m_v), as well as the ratio between m_r and m_v. These two observables quantify the interaction between vaults. The computed interaction between vaults is negligible for both repository orientations (Table 4-2 and Table 4-3).

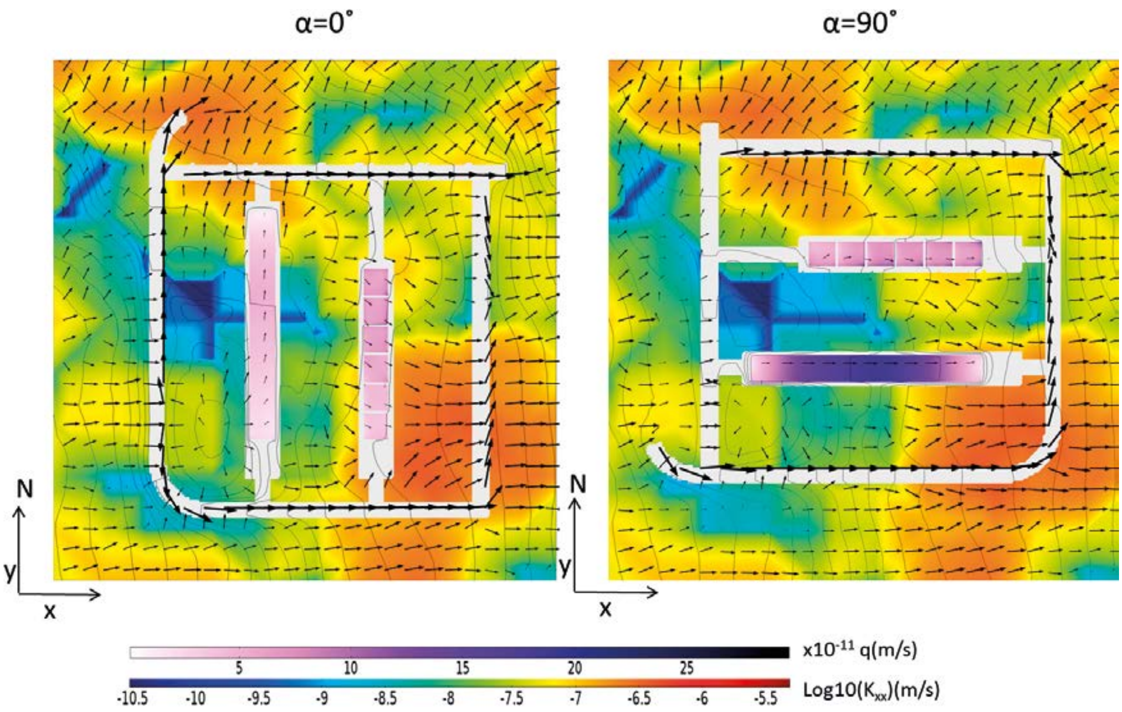

Figure 4-3. *Magnitude of the Darcy velocity through the waste control volumes, hydraulic conductivity of the rock, hydraulic head (isolines) and Darcy velocity (arrows) at location 300_1 for each rotation case.*

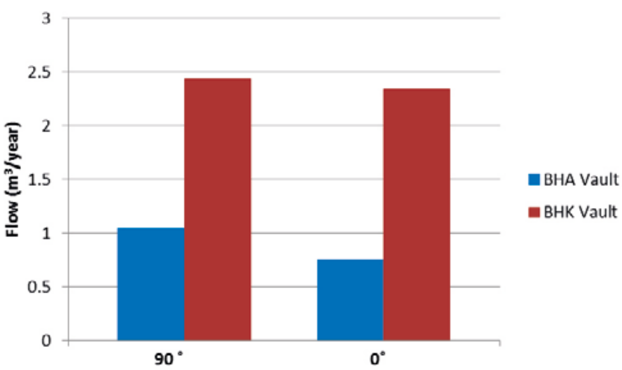

Figure 4-4. *Calculated flow through the BHA and BHK vaults for all rotation cases, at location 300_1.*

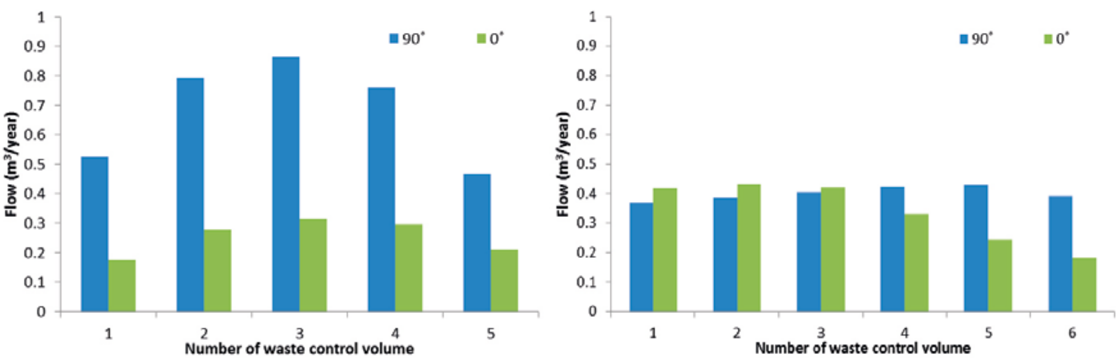

Figure 4-5. *Calculated flow through the waste control volumes for both rotation cases at location 300_1.*

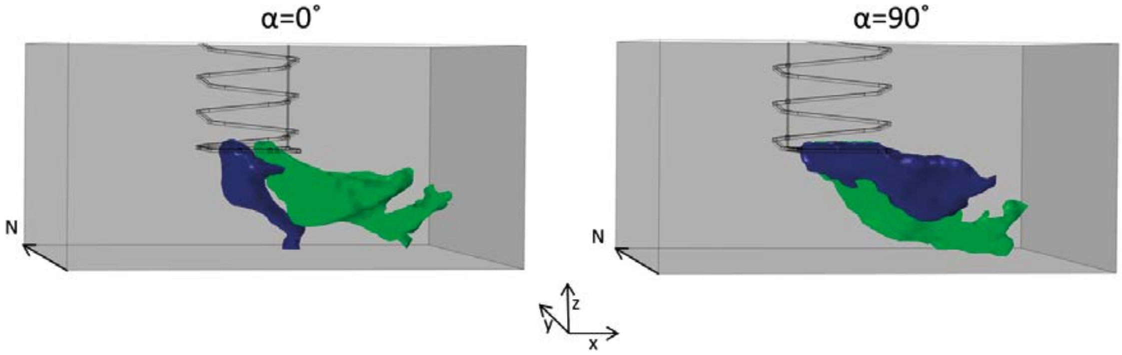

Figure 4-6. Extent of tracer plumes illustrated by the 20% isosurface of the released concentration (c_r) at location 300_1 for two repository orientations. The tracer plume released from the BHK is shown in green and tracer plume from the BHA in blue.

Table 4-2. Calculated tracer interaction at location 300_1 for the base case and 90° rotation case.

From BHA to BHK	m_r (kg/yr)	m_v (kg/yr)	Ratio
α=0°	2.24E+1	5.68E−4	0.0002
α=90°	2.69E+1	5.74E−3	0.0002

Table 4-3. Calculated tracer interaction at location 300_1 for the base case and 90° rotation case.

From BHK to BHA	m_r (kg/yr)	m_v (kg/yr)	Ratio
α=0°	3.82E+1	8.36E−6	0.0000
α=90°	2.58E+1	2.58E−4	0.0000

4.2 Repository rotation under horizontal flow conditions

The groundwater flow reaching the repository at location 500_4 is mainly horizontal. The flow through the vaults can be affected by the orientation of the vaults with respect to the flow field and by which vault is located upstream. The results from four simulations have been compared:

- α = 0° (base case): Vaults are perpendicular to the flow field with the BHA vault located upstream.
- α = 90° : Vaults are oriented parallel to the flow field with their loading areas located downstream.
- α = 180° : Vaults are perpendicular to the flow field with the BHK vault located upstream.
- α = 270° : Vaults are oriented parallel to the flow field with their loading areas located upstream.

4.2.1 Groundwater flow in the rock domain

The local flow in the 500_4 domain shows a strong horizontal component from west to east. This flow is not affected by rotation of the repository (Figure 4-7). Most of the groundwater flow enters the model domain through the top western boundary and quickly becomes horizontal. Near the repository the groundwater flow is mainly parallel to the vaults. Small changes in the streamlines crossing the waste compartments are observed for the different repository orientations (Figure 4-8).

4.2.2 Flow through vault and waste control volumes

The groundwater flow is directed from west to east. Near the repository, part of groundwater flow is diverted through the access tunnels and across the high permeability deformation zones located north of the repository (Figure 4-9). The flows through the BHA and BHK vaults and waste control volumes for each repository orientation are presented in Appendix E (Table E-1 through Table E-4).

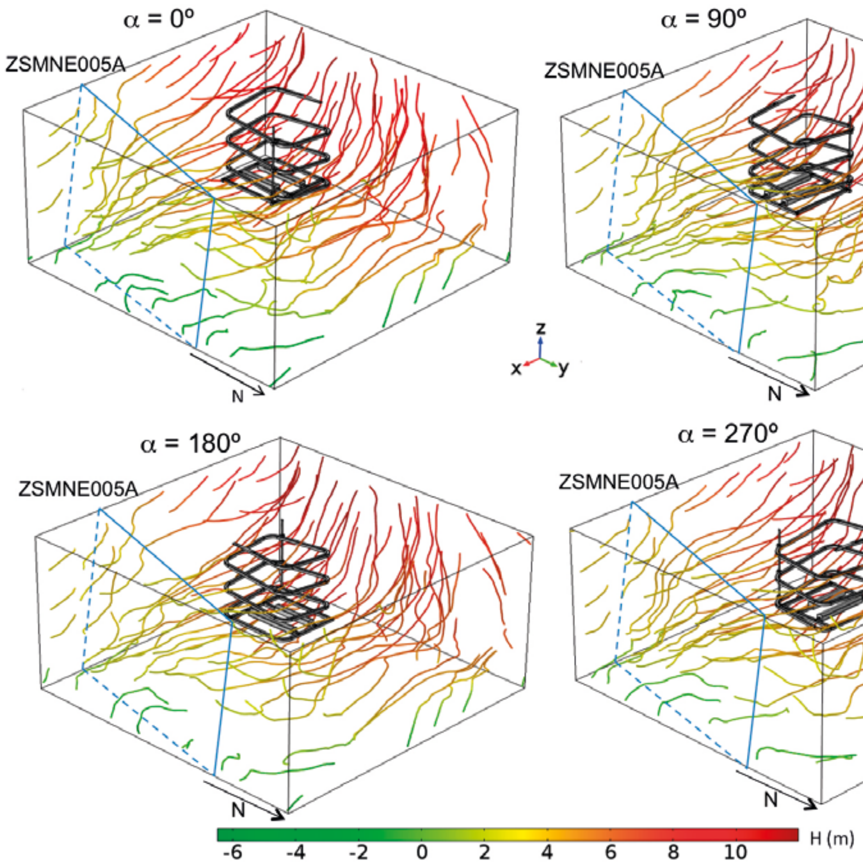

Figure 4-7. Groundwater flow field at location 500_4 for different repository orientations.

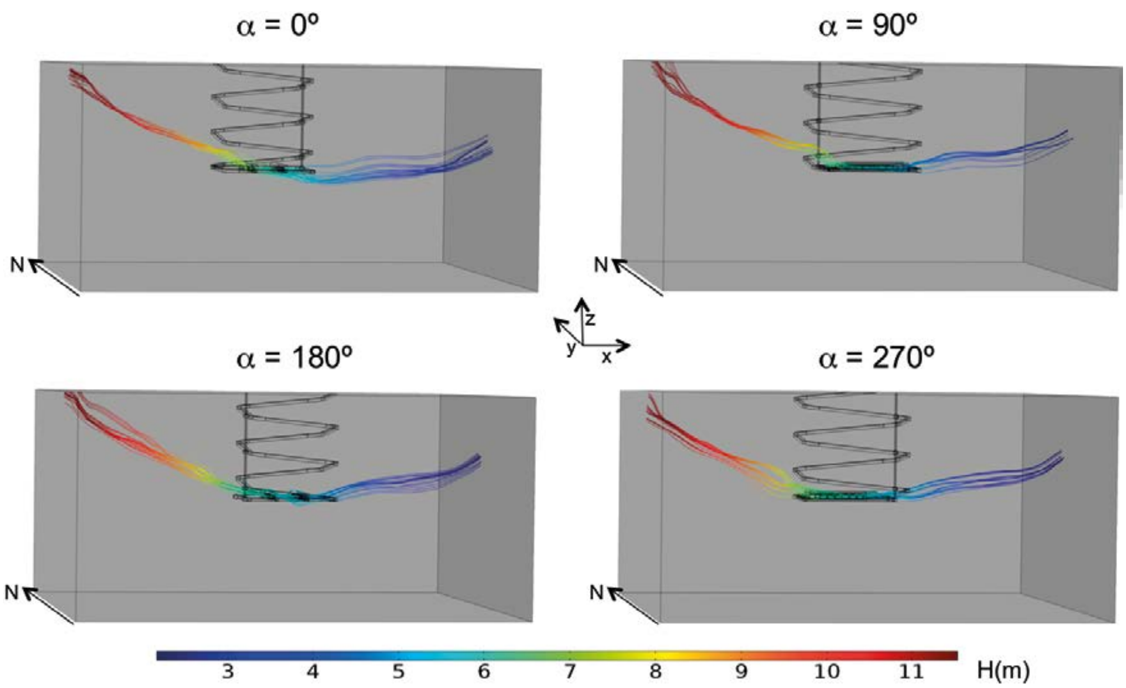

Figure 4-8. Streamlines of the groundwater flow crossing the waste control volumes of the BHA and BHK vaults at location 500_4 for different repository orientations.

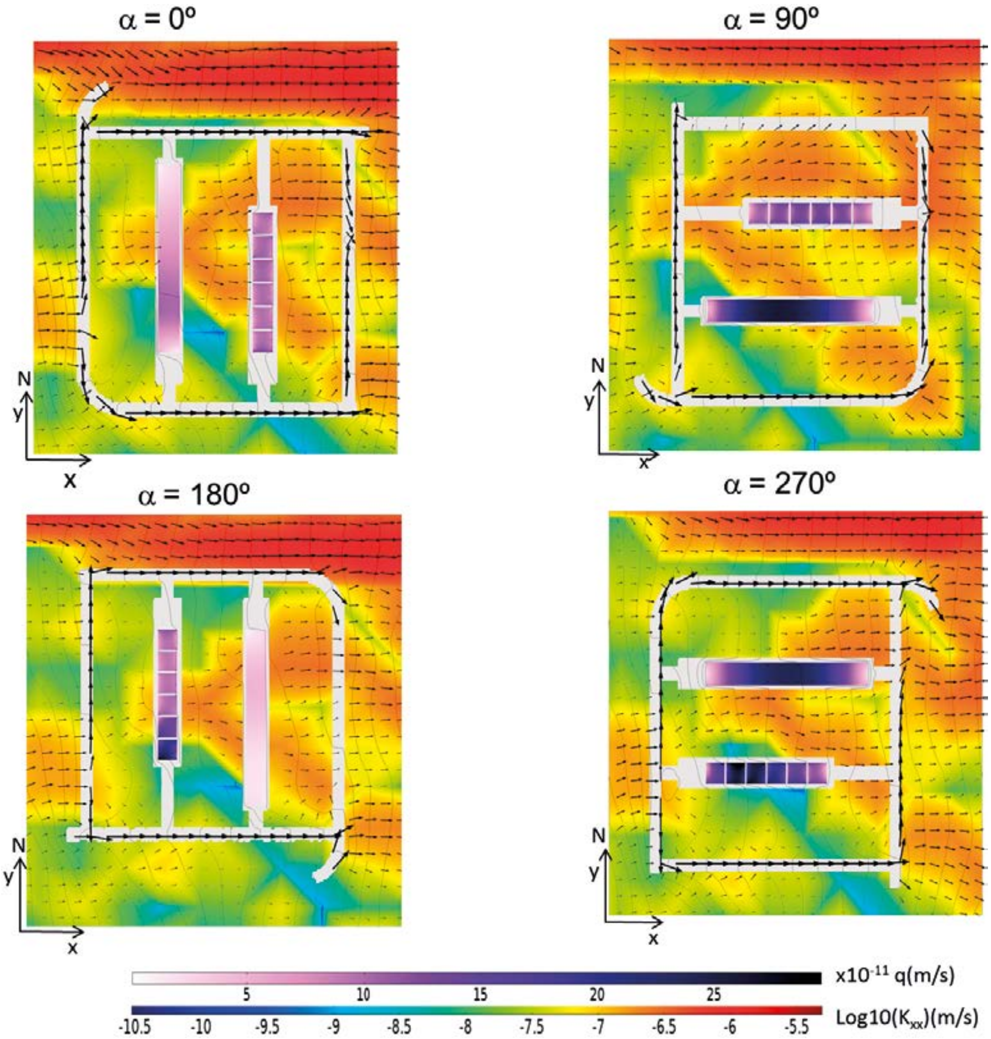

Figure 4-9. *Magnitude of the Darcy velocity through the waste control volumes, hydraulic conductivity of the rock, hydraulic head (isolines) and Darcy velocity (arrows) at location 500_4 for different repository orientations.*

For the base case (α = 0°) results show three times higher flows through BHK (3.2 m^3/year) than through BHA (0.85 m^3/year).

For the 90° rotation case, flows of approximately 1.3 m^3/year are calculated for both vaults. The comparatively low waste flow values in BHK are related to the backfill barriers between the waste compartments and also to the high rock hydraulic conductivity surrounding the vault. On the other hand, the BHA waste shows relatively high flow values induced by the low hydraulic conductivity of the rock near the upstream waste control volume (BHA_1). Most of the groundwater enters the waste through BHA_1 and flows along the waste to the downstream waste compartment (BHA_5).

For the 180° rotation case, the northern access tunnel is located within a high hydraulic conductivity zone that concentrates the flow in the rock. The access tunnel drives flow from the west to the deformation zone. This configuration leads to the lowest flow through BHA for all investigated orientations. BHA is furthermore protected by BHK located upstream and acting as a flow barrier. BHK, on the other hand, experiences the highest vault flows for the 180° rotation case. The flow through the BHK waste compartments is three times larger than for the BHA waste. The highest waste flows occur in BHK_1 and BHK_2, located in rock of low hydraulic conductivity.

For the 270° rotation case, the access tunnels again serve as by-pass for flow from west to east. The BHK vault experiences a groundwater inflow three times greater than calculated for the BHA vault.

The BHK waste flow is higher in the waste control volumes BHK_2, BHK_3 and BHK_4, located in low hydraulic conductivity rock zones. The BHA waste channels flow from west to east.

Groundwater flow in the BHK vault increases when vaults are oriented perpendicular to the flow direction (Figure 4-10). In that case, flow increases through the waste compartments surrounded by low hydraulic conductivity rock. The highest flows through BHK are observed for the 180° rotation case, when BHK is located upstream of BHA.

The flow through BHA is in general lower than through BHK (Figure 4-10) because of the lower hydraulic conductivity of the BHA backfill. Higher flows through the BHA are computed when the vault is parallel to the flow direction (90° and 270°). The absence of internal barriers along the BHA waste facilitates groundwater to flow through the waste control volumes in the longitudinal direction. The lowest flow through the BHA vault is found when the groundwater flow is perpendicular to the vaults and the BHA is located downstream of BHK (180°). In this case, the BHA is protected by the BHK located upstream and acting as a flow barrier and also by the north access tunnels, which channel flow from west to east.

In BHA, there is a correlation between the orientation of the repository and the flow through the waste. The BHA waste flow is higher when the vault is oriented parallel to the flow (Figure 4-11), due to the absence of internal flow barriers between waste. In BHK waste flow is not affected by the vault orientation. Rather, differences in the rock hydraulic conductivity surrounding the vault affect the local waste flow (Figure 4-12).

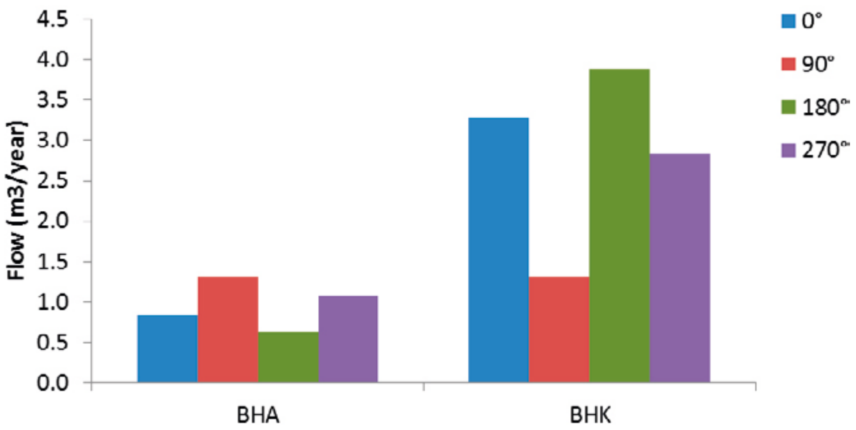

Figure 4-10. *Groundwater flow through the BHA and BHK vaults for the different rotation cases.*

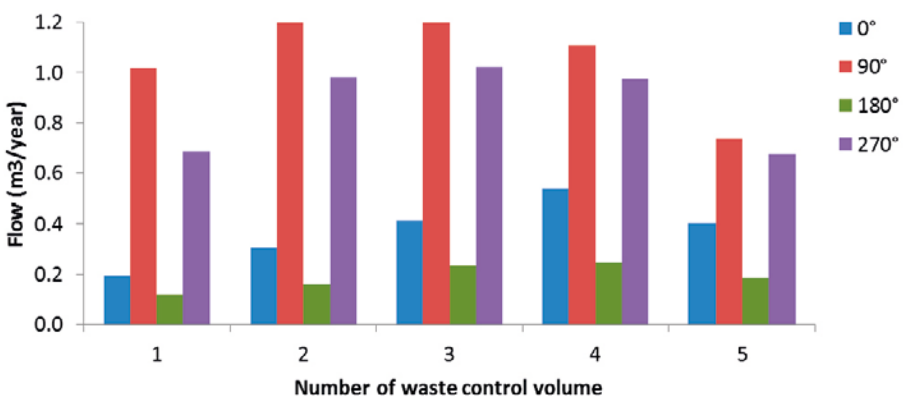

Figure 4-11. *Calculated flows through waste control volumes of BHA for all rotation cases.*

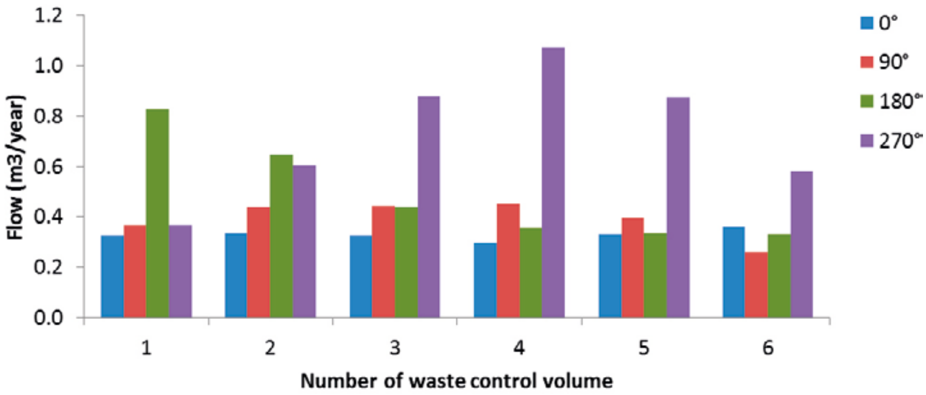

Figure 4-12. Calculated flows through waste control volumes of BHK for all rotation cases.

4.2.3 Tracer transport

Figure 4-13 shows the extent of two steady state tracer plumes released at the vault/rock interface of both vaults for the different rotation cases. The isosurface illustrating 20% of the released concentration (c_r) is shown in blue for BHK and green for BHA. The computed mass of tracer released from each vault (m_r), reaching the neighbouring vault (m_v) is presented in Table 4-4 for a tracer released from BHA, and in Table 4-5 for a tracer released from BHK.

Table 4-4. Calculated tracer interaction at location 500_4 for each rotation case.

From BHA to BHK	m_r (kg/yr)	m_v (kg/yr)	Ratio
α=0°	57.4	5.93	0.1033
α=90°	45.7	2.13E−2	0.0005
α=180°	91.5	1.3E−6	0
α=270°	59.0	4.6E−3	0.0001

Table 4-5. Calculated tracer interaction at location 500_4 for each rotation case.

From BHK to BHA	m_r (kg/yr)	m_v (kg/yr)	Ratio
α=0°	89.2	7.10E−7	0
α=90°	64.3	7.19E−5	0
α=180°	42.9	5.55	0.1295
α=270°	24.3	1.82E−2	0.0008

For the 0° rotation case, approximately 10% of the water released by the BHA (blue) reaches the BHK backfill. A tracer released from BHK will not reach BHA.

For the 90° rotation case, the two plumes are parallel, in the direction of the flow. The BHK tracer plume (green) is more elongated than the BHA plume. The mass of tracer that reaches the neighbouring vault indicates minimal interaction between vaults.

For the 180° rotation case, the BHK is located upstream of the BHA. According to the computed ratio m_r/m_v, approximately 13% of the discharging flow from BHK will reach the BHA backfill. A tracer released from BHA will not reach BHK.

For the 270° rotation case, the plumes are parallel to the vaults and negligible interaction between the vaults is found (ratio lower than 0.0008).

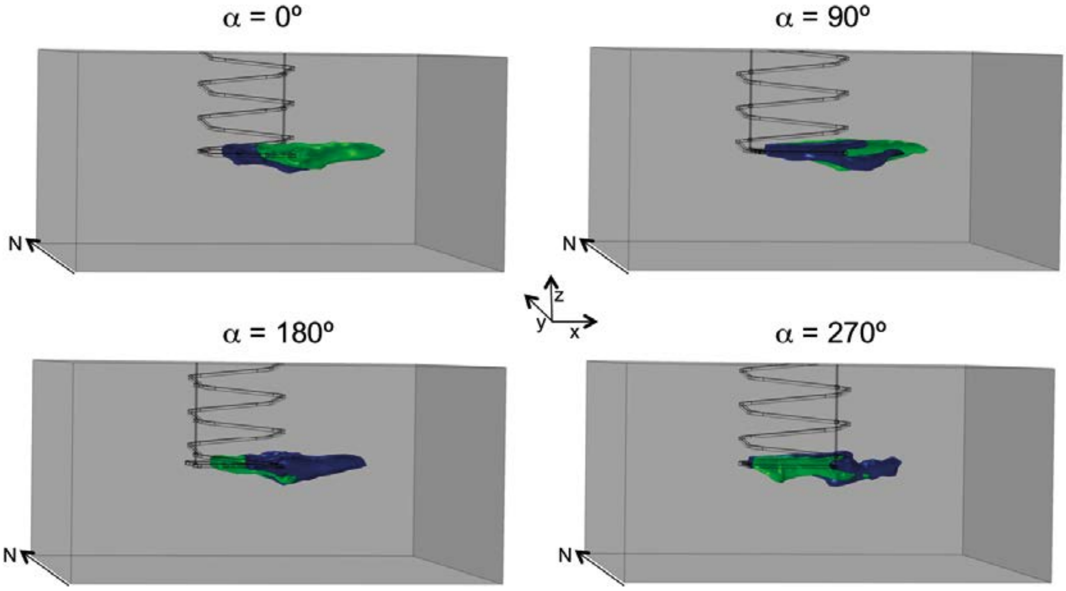

Figure 4-13. Extent of tracer plumes illustrated by the 20% isosurface of the released concentration (c_r) at location 500_4 for different repository orientations. The tracer plume released from the BHK is shown in green and tracer plume from the BHA in blue.

4.3 Summary

Two locations have been selected to study the influence of repository orientation with respect to the direction of groundwater flow. At location 300_1 the flow is mainly vertical, directed downward. At location 500_4 the flow is mainly horizontal.

In the vertical flow regime (300_1), a 90° rotation of the repository directs the horizontal component of the flow through the vaults. This increases the BHA waste flow relative to the base case. The BHK waste is more sensitive to local changes in hydraulic conductivity of the surrounding rock than to the orientation. The computed interaction between vaults is negligible for both repository orientations.

In the horizontal flow regime (500_4), the repository has been rotated 0°, 90°, 180° and 270°. Groundwater flow through BHK increases when the vault is perpendicular to the flow direction. The flow through BHA is in general lower than flow through the BHK vault. Higher waste flows are computed in the BHA when the vaults are parallel to the flow (90° and 270°). The flow through the BHK waste control volumes is mainly controlled by the rock hydraulic conductivity surrounding the vault. The interaction between vaults is negligible in the cases of vaults oriented parallel to the flow. When the flow is perpendicular, 10% of the water from BHA reaches the BHK backfill downstream. With the BHK vault upstream, 13% of the water from the BHK vault reaches the BHA backfill.

5 Influence of backfill hydraulic properties

The concrete backfill in BHK and the bentonite backfill in BHA are central barriers limiting groundwater flow through the SFL waste. This chapter details results from parametric investigations where the hydraulic properties of the backfills have been varied to evaluate the influence on flow through the vault and waste. Flow simulations have been carried out at locations 300_4, 500_4 and 700_1.

5.1 Hydraulic conductivity of vault backfills

The hydraulic properties assigned to repository materials in the simulation base case are described in Section 2.1. Three additional calculation cases are analysed here:

- A degraded case that assumes a hydraulic conductivity of the backfill equal to the hydraulic conductivity of the waste domain (1.0×10^{-7} m/s).
- A hydraulic cage case that considers a hydraulic conductivity of the backfill equal to the hydraulic conductivity of the crushed rock filling the access tunnels (1.0×10^{-5} m/s).
- An alternative initial state representing a backfill material with lower hydraulic conductivity than that assigned in the base case.

The hydraulic conductivity values of the backfills are summarised in Table 5-1.

Table 5-1. Hydraulic conductivity values (m/s) for different calculation cases.

	Alternative initial state	Base case	Degraded case	Hydraulic cage case
$K_{Concrete}$ (m/s)	1.00E−12	8.30E−10	1.00E−07	1.00E−05
$K_{Bentonite}$ (m/s)	1.00E−13	1.00E−10	1.00E−07	1.00E−05

When changing the hydraulic conductivity of the backfill in a given vault, the hydraulic conductivity of the remaining materials retained the values assigned in the base case.

5.2 Increasing hydraulic conductivity of the concrete backfill

This section explores how an increasing hydraulic conductivity of the concrete backfill in the BHK vault affects the flow through the vaults and waste compartments.

Location 300_4

The computed flows through the BHK vault and waste control volumes are presented in Table 5-2 and Figure 5-1. The flow through the BHK vault increases with increasing hydraulic conductivity of the backfill. The flow through the BHK in the hydraulic cage case is 4 times that of the degraded concrete case and 164 times that of the base case.

The degraded concrete case leads to an increase in groundwater flow entering the BHK waste control volumes (see Figure 5-2 and Figure 5-3). The increase in flow is similar for the six compartments (between 18 and 28 times higher than the flow in the base case).

In the hydraulic cage case, the backfill hydraulic conductivity is higher than the hydraulic conductivity of the waste domain. In the base case, the backfill acts as a barrier and water gets diverted from deformation zone D1_Z4 to the access tunnels south of the BHK vault. However, in the hydraulic cage case, groundwater flows from west to east through deformation zone D1_Z4, and through the BHK vault (Figure 5-4 and Figure 5-5). The waste compartments, with lower hydraulic conductivity, are protected to some extent by the hydraulic cage that channels flow from west to east through the backfill. The decrease in flow is more pronounced in the waste control volumes not affected by deformation zone D1_Z4.

Table 5-2. Groundwater flow through the BHK vault and waste control volumes for location 300_4. The flow ratio is calculated with respect to the base case.

	Base case	Degraded concrete case		Hydraulic cage case	
Flow control volume	Total flow (m^3/yr)	Total flow (m^3/yr)	Ratio	Total flow (m^3/yr)	Ratio
BHK vault	4.66E+00	2.00E+02	42.81	7.63E+02	163.76
BHK_1 waste	4.50E−01	8.49E+00	18.88	7.54E−01	1.68
BHK_2 waste	4.97E−01	1.25E+01	25.21	1.70E+00	3.42
BHK_3 waste	5.86E−01	1.57E+01	26.81	2.85E+00	4.86
BHK_4 waste	6.45E−01	1.73E+01	26.84	3.71E+00	5.74
BHK_5 waste	6.71E−01	1.79E+01	26.73	3.93E+00	5.86
BHK_6 waste	6.41E−01	1.82E+01	28.44	3.88E+00	6.05

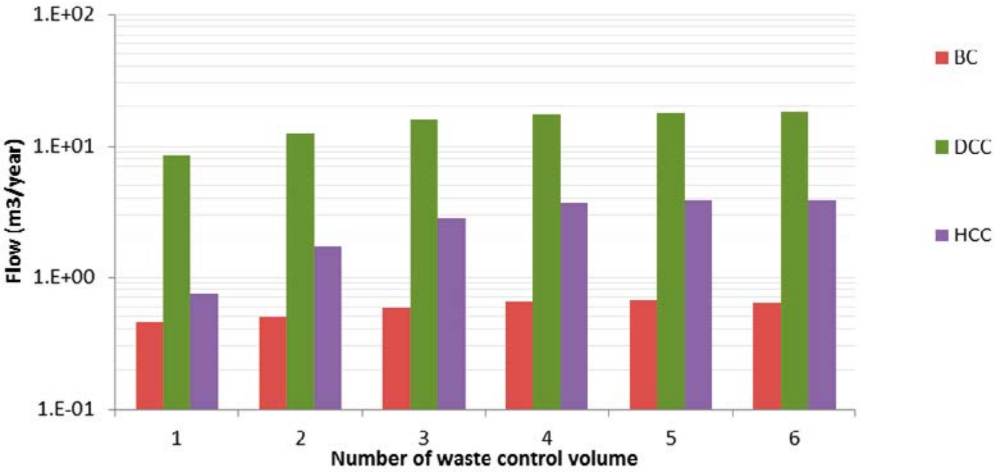

Figure 5-1. Groundwater flow through the BHK waste control volumes at location 300_4. BC = base case, DCC = degraded concrete case and HCC=hydraulic cage case.

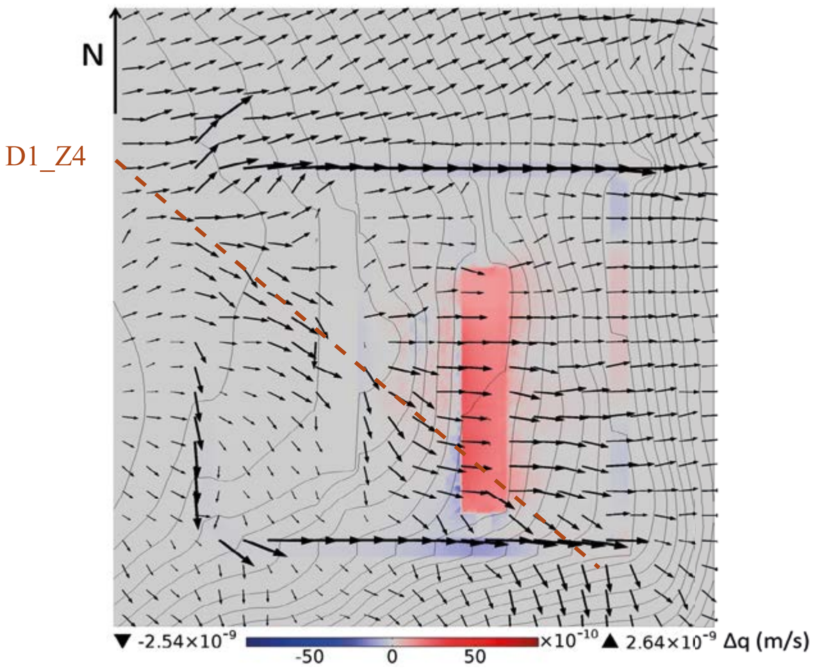

Figure 5-2. Difference in the magnitude of the Darcy velocity at location 300_4 calculated as $q - q_0$, where q = Darcy flux for the degraded concrete case and q_0 = Darcy flux for the base case. Arrows and hydraulic head isolines are plotted for the degraded concrete case.

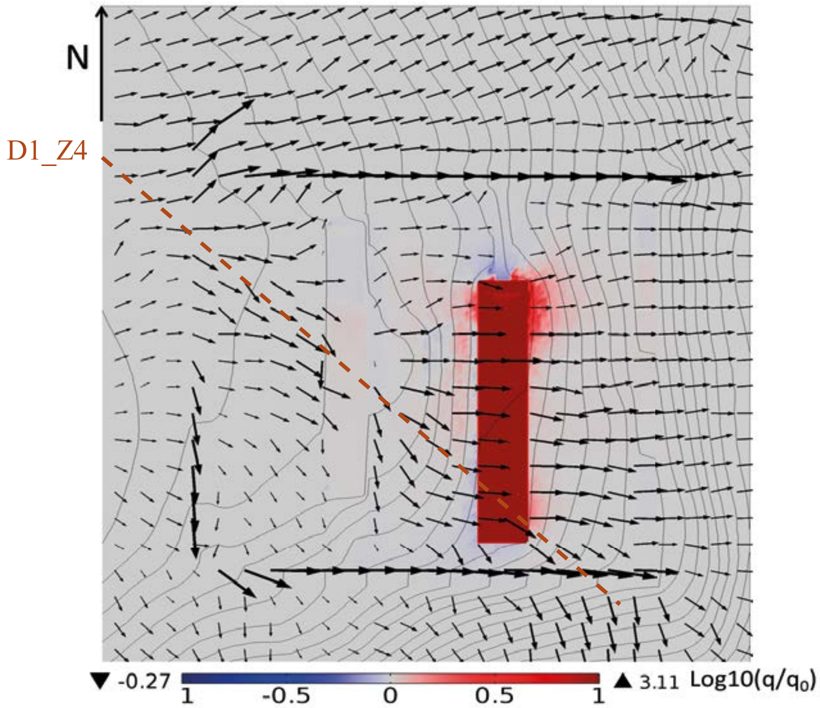

Figure 5-3. *Ratio of the Darcy velocity magnitude at location 300_4 calculated as* $log_{10}(q/q_0)$*, where* q *= Darcy velocity magnitude for the degraded concrete case and* q_0*=Darcy velocity for base case. Arrows and hydraulic head isolines are plotted for the degraded concrete case.*

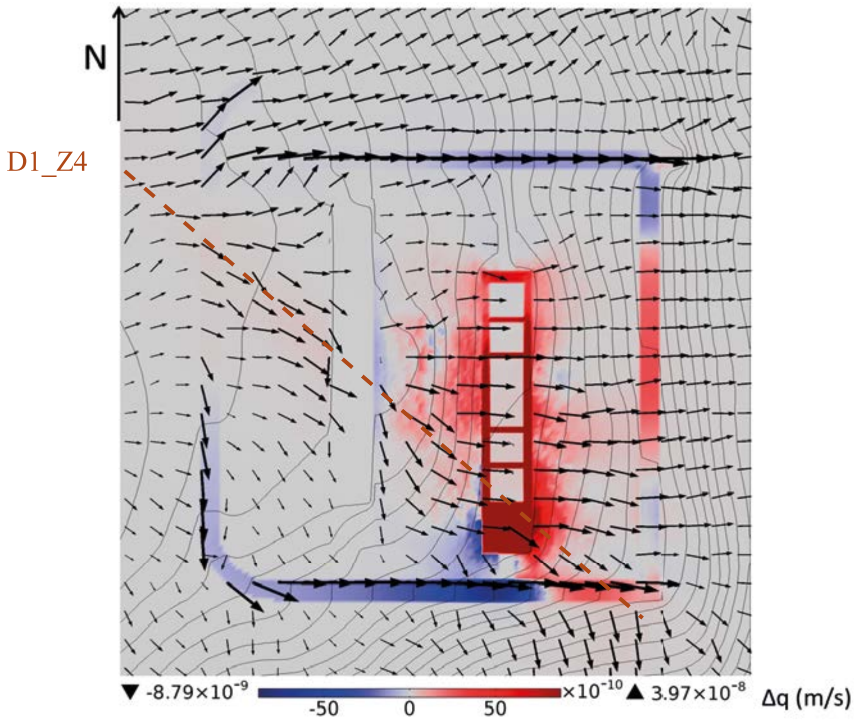

Figure 5-4. *Difference in the magnitude of the Darcy velocity at location 300_4 calculated as* $q - q_0$*, where* q *= Darcy flux for the BHK hydraulic cage case and* q_0 *= Darcy flux for the base case. Arrows and hydraulic head isolines are plotted for the BHK hydraulic cage case.*

The BHK backfill degradation has a small effect on the groundwater flow entering the BHA vault. The increase is about 2% for the degraded concrete case and 11% for the hydraulic cage case. This effect is due to BHA being located upstream of BHK at this location.

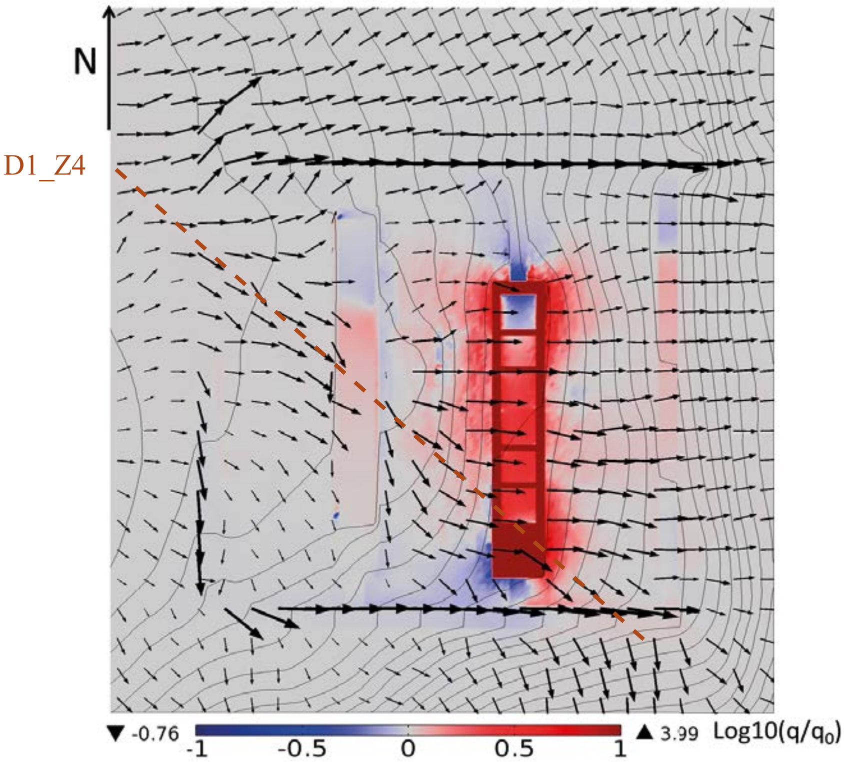

Figure 5-5. *Ratio of the Darcy velocity magnitude at location 300_4 calculated as $log_{10}(q/q_0)$, where q = Darcy velocity magnitude for hydraulic cage case and q_0 = Darcy velocity for base case. Arrows and hydraulic head isolines are plotted for the BHK hydraulic cage case.*

Location 500_4

At location 500_4, the flow through the BHK vault increases by a factor of 23, comparing the degraded concrete case to the base case. It doubles going from the degraded concrete case to the hydraulic cage case (Table 5-3).

At this location groundwater flows from west to east, mainly through deformation zone D5_Z4. In the base case flow is perpendicular to the vaults and the access tunnels act as a drainage system diverting groundwater from the vaults (see Section 3.4.4). The groundwater flow entering the waste control volumes is approximately one order of magnitude higher in the degraded concrete case compared to the base case (Figure 5-6, Figure 5-7 and Figure 5-8). However, waste flows decrease going from the degraded concrete case to the hydraulic cage case. Here, the backfill collects flow from deformation zone D6_Z4 but diverts the water from the waste domain due to the relatively high hydraulic conductivity of the backfill material (Figure 5-9 and Figure 5-10).

Table 5-3. Groundwater flow through the BHK vault and waste control volumes at location 500_4. The flow ratio is calculated with respect to the base case.

	Base case	Degraded concrete case		Hydraulic cage case	
Flow control volume	**Total flow (m^3/yr)**	**Total flow (m^3/yr)**	**Ratio**	**Total flow (m^3/yr)**	**Ratio**
BHK vault	3.29E+00	7.61E+01	23.14	1.67E+02	50.71
BHK_1 waste	3.25E−01	6.06E+00	18.64	6.71E−01	2.06
BHK_2 waste	3.32E−01	4.27E+00	12.87	3.80E−01	1.15
BHK_3 waste	3.25E−01	4.45E+00	13.69	4.20E−01	1.29
BHK_4 waste	2.97E−01	4.77E+00	16.07	3.86E−01	1.30
BHK_5 waste	3.28E−01	4.81E+00	14.67	4.04E−01	1.23
BHK_6 waste	3.60E−01	4.46E+00	12.41	3.19E−01	0.89

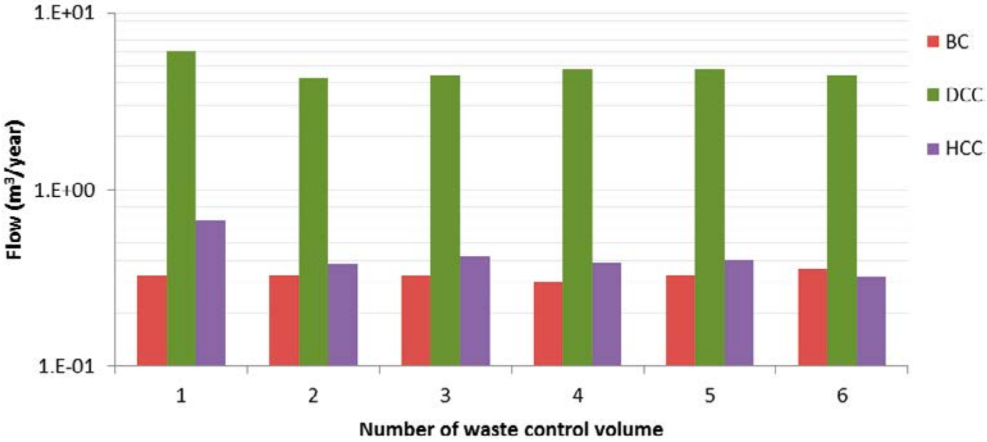

Figure 5-6. Groundwater flow through the BHK waste control volumes at location 500_4. BC = base case, DCC = degraded concrete case and HCC = hydraulic cage case.

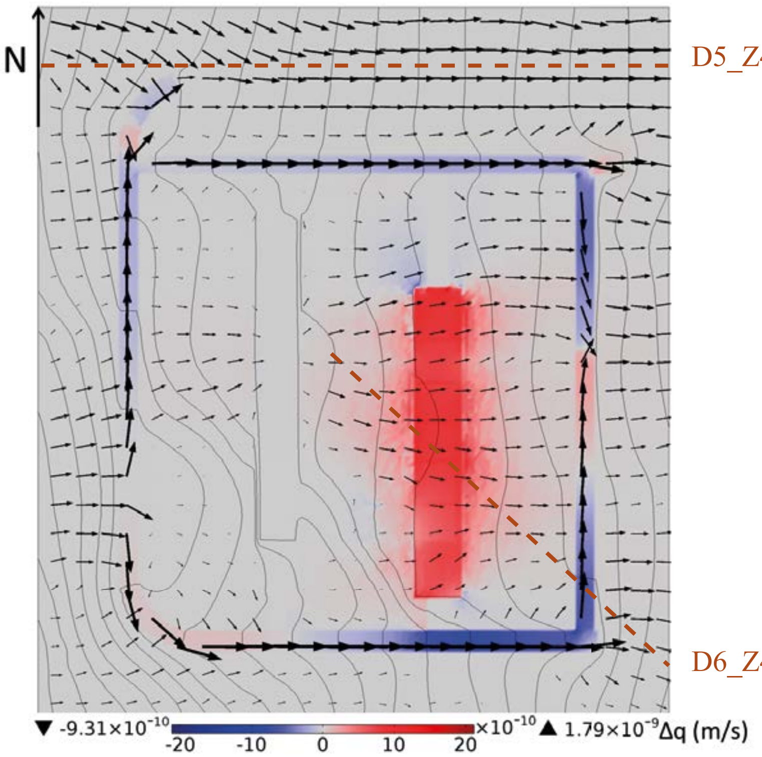

Figure 5-7. Difference in the magnitude of the Darcy velocity at location 500_4 calculated as $q - q_0$, where q = Darcy flux for the degraded concrete case and q_0 = Darcy flux for the base case. Arrows and hydraulic head isolines are plotted for the degraded concrete case.

Concrete degradation has negligible effect on the groundwater flow entering BHA. A difference of about 2% is observed for the degraded state and of 4% for the hydraulic cage state. This small effect is due to the BHA location, upstream of the BHK vault.

Location 700_1

Domain 700_1 is characterized by horizontal groundwater flow mainly from north to south, that is, parallel to the vaults (see Section 3.5.5). The hydraulic conductivity of the rock is lower, on average, compared to the hydraulic conductivity of the concrete backfill.

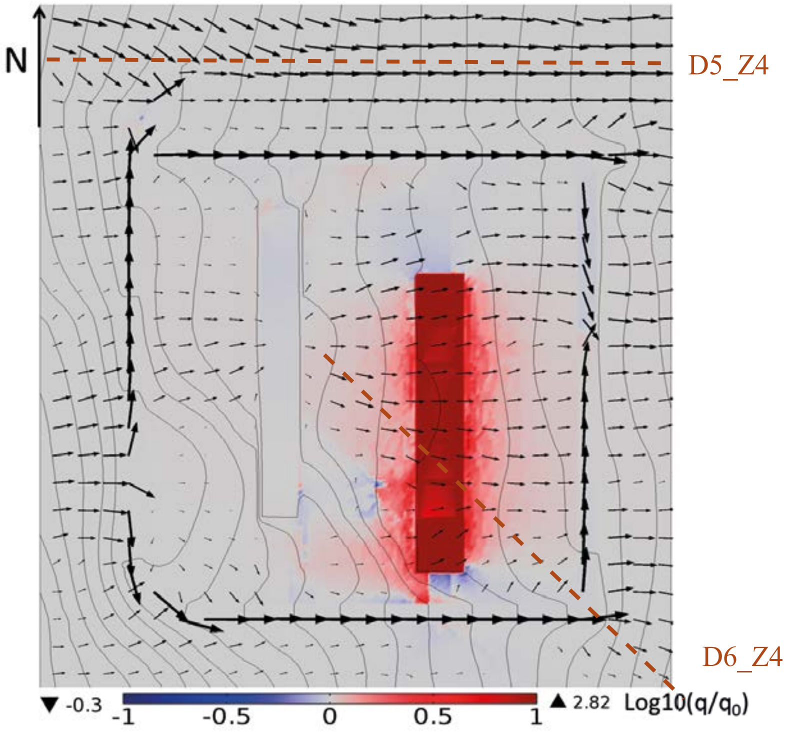

Figure 5-8. *Ratio of the Darcy velocity magnitude at location 500_4 calculated as* $log_{10}(q/q_0)$*, where* q *= Darcy velocity magnitude for the degraded concrete case and* q_0*=Darcy velocity for base case. Arrows and hydraulic head isolines are plotted for the degraded concrete case.*

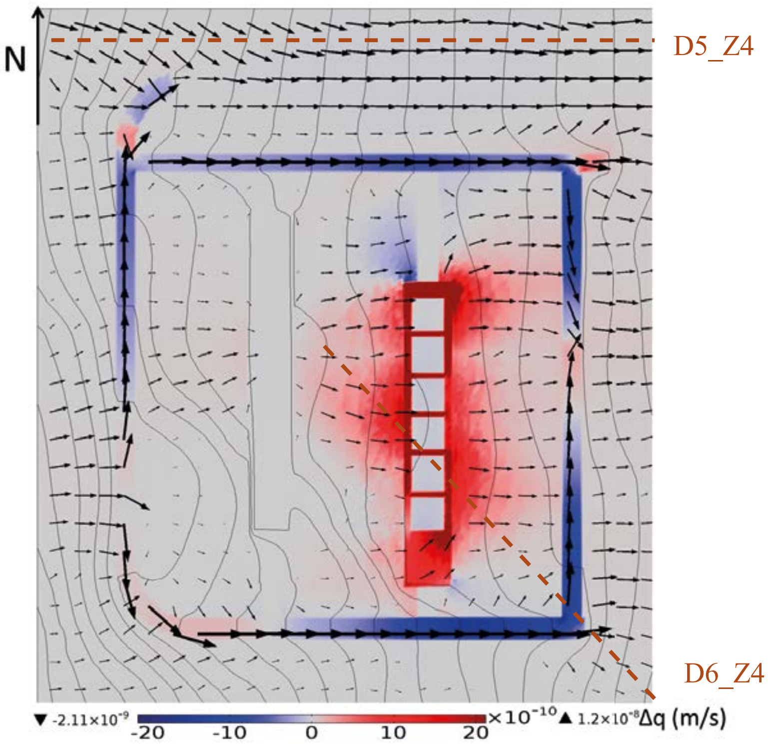

Figure 5-9. *Difference in the magnitude of the Darcy velocity at location 500_4 calculated as* $q - q_0$*, where* q *= Darcy flux for the BHK hydraulic cage case and* q_0 *= Darcy flux for the base case. Arrows and hydraulic head isolines are plotted for the BHK hydraulic cage case.*

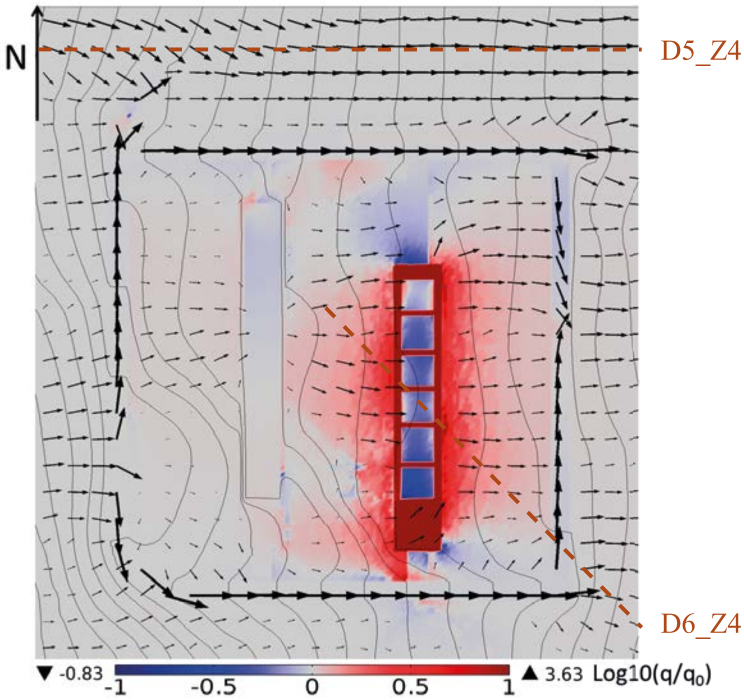

Figure 5-10. Ratio of the Darcy velocity magnitude at location 500_4 calculated as $log_{10}(q/q_0)$, where q = Darcy velocity magnitude for hydraulic cage case and q_0=Darcy velocity for base case. Arrows and hydraulic head isolines are plotted for the BHK hydraulic cage case.

Flow through the BHK vault increases approximately three times when comparing the base case to the degraded concrete case, and increases four times comparing with the hydraulic cage case (Table 5-4). The moderate influence on the vault flow indicates that the rock is the main flow barrier at this location.

Table 5-4. Groundwater flow through the BHK vault and waste control volumes at location 700_1. The flow ratio is calculated with respect to the base case.

	Base case	Degraded concrete case		Hydraulic cage case	
Flow control volume	**Total flow (m^3/yr)**	**Total flow (m^3/yr)**	**Ratio**	**Total flow (m^3/yr)**	**Ratio**
BHK vault	1.10E−01	2.92E−01	2.65	4.71E−01	4.28
BHK_1 waste	3.38E−02	2.00E−02	0.59	6.34E−03	0.19
BHK_2 waste	3.67E−02	3.16E−02	0.86	9.02E−03	0.25
BHK_3 waste	3.07E−02	6.40E−02	2.09	1.42E−02	0.46
BHK_4 waste	2.63E−02	8.77E−02	3.34	1.54E−02	0.59
BHK_5 waste	1.74E−02	7.44E−02	4.29	1.15E−02	0.67
BHK_6 waste	9.11E−03	4.77E−02	5.23	1.14E−02	1.25

Concrete degradation does not affect the waste control volumes equally (Table 5-4 and Figure 5-11). The flow through control volumes 1 and 2 decreases for the degraded concrete case. However, waste control volumes 3 through 6, affected by the deformation zone D11_Z1, experience a flow increase going from the base case to the degraded concrete case (Figure 5-12 and Figure 5-13) and a flow decrease going from the degraded concrete case to the hydraulic cage case (Figure 5-14 and Figure 5-15). In the degraded concrete case and hydraulic cage case, the hydraulic conductivity is higher in the vault than in the surrounding rock. Therefore the backfill acts as a preferential flow zone downstream of deformation zone D11_Z1.

The BHK concrete degradation does not produce any change in the groundwater flow through the BHA vault.

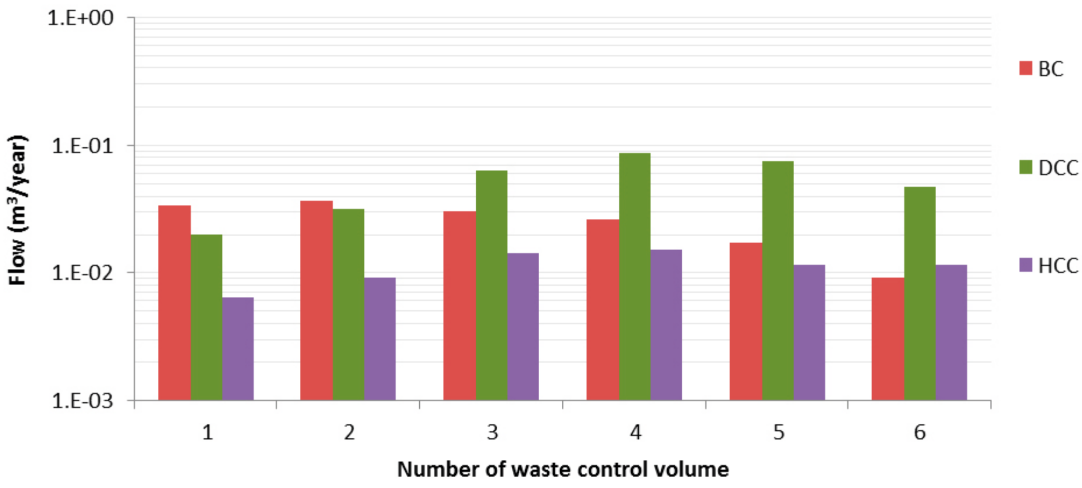

Figure 5-11. Groundwater flow through the BHK waste control volumes at location 700_1. BC = base case, DCC = degraded concrete case and HCC = hydraulic cage case.

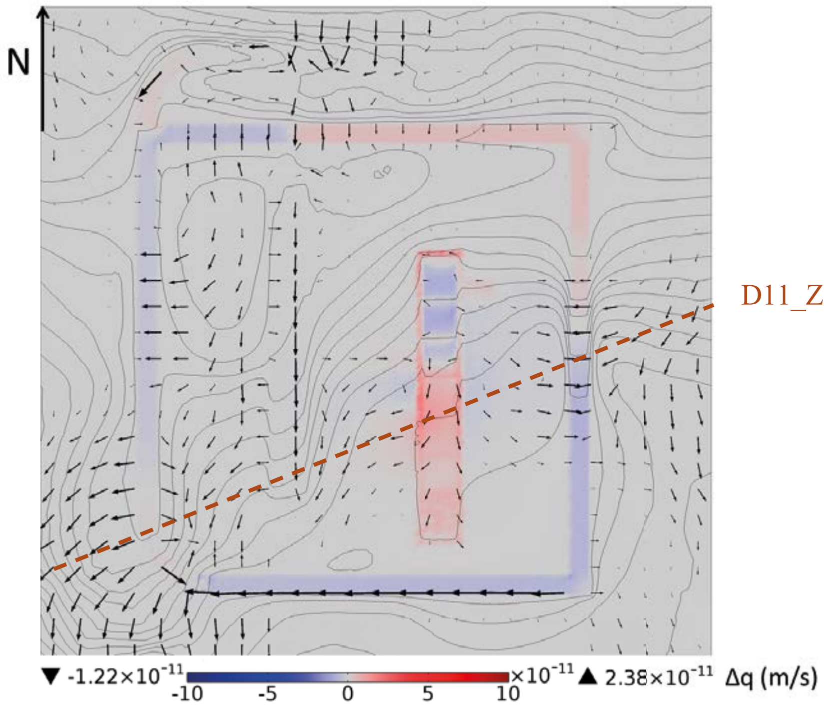

Figure 5-12. *Difference in the magnitude of the Darcy velocity at location 700_1 calculated as $q - q_0$, where q = Darcy flux for the degraded concrete case and q_0 = Darcy flux for the base case. Arrows and hydraulic head isolines are plotted for the degraded concrete case.*

5.3 Increasing hydraulic conductivity of the bentonite backfill

This section explores how an increasing hydraulic conductivity of the bentonite backfill in BHA affects the flow through the vaults and waste.

Location 300_4

The degraded bentonite case leads to an increase in the flow through the BHA vault of more than two orders of magnitude compared to the base case. Going from the degraded bentonite case to the hydraulic cage case leads to a six-fold increase in the flow through the vault (Table 5-5).

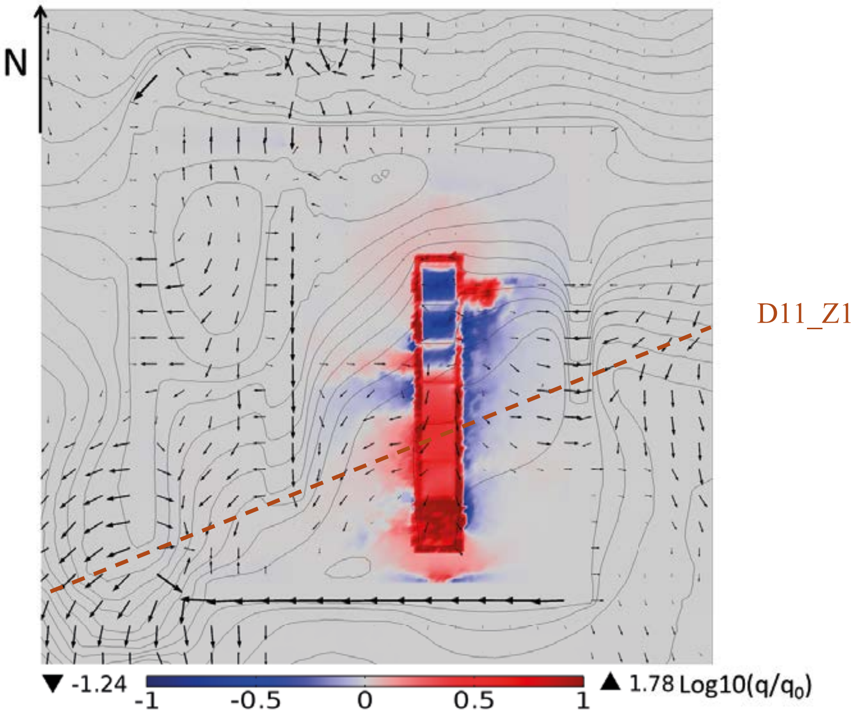

Figure 5-13. *Ratio of the Darcy velocity magnitude at location 700_1 calculated as* $log_{10}(q/q_0)$*, where* q *= Darcy velocity magnitude for the degraded concrete case and* q_0*=Darcy velocity for base case. Arrows and hydraulic head isolines are plotted for the degraded concrete case.*

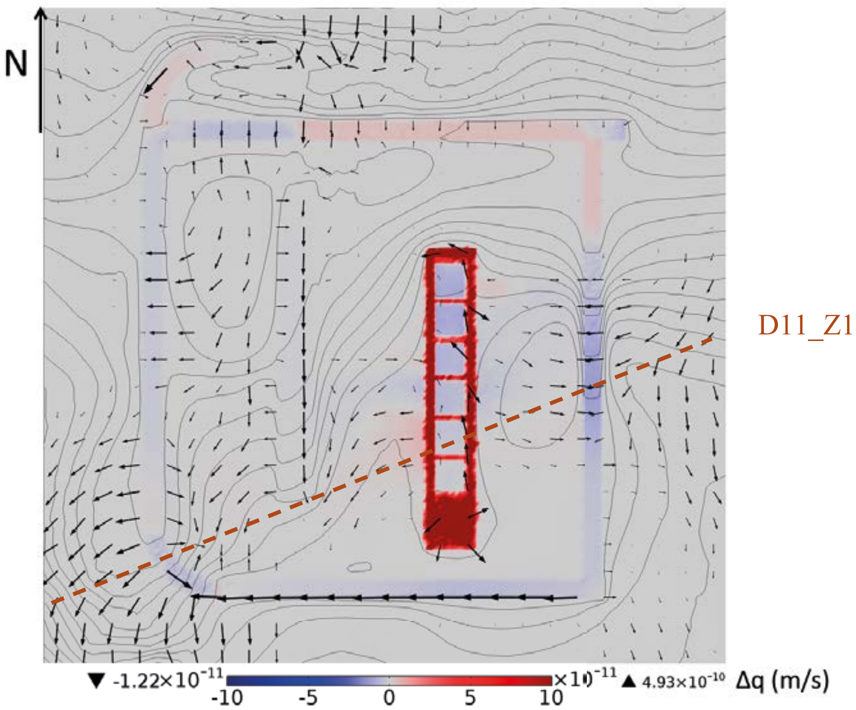

Figure 5-14. *Difference in the magnitude of the Darcy velocity at location 700_1 calculated as* $q - q_0$*, where* q *= Darcy flux for the degraded concrete case and* q_0 *= Darcy flux for the base case. Arrows and hydraulic head isolines are plotted for the BHK hydraulic cage case.*

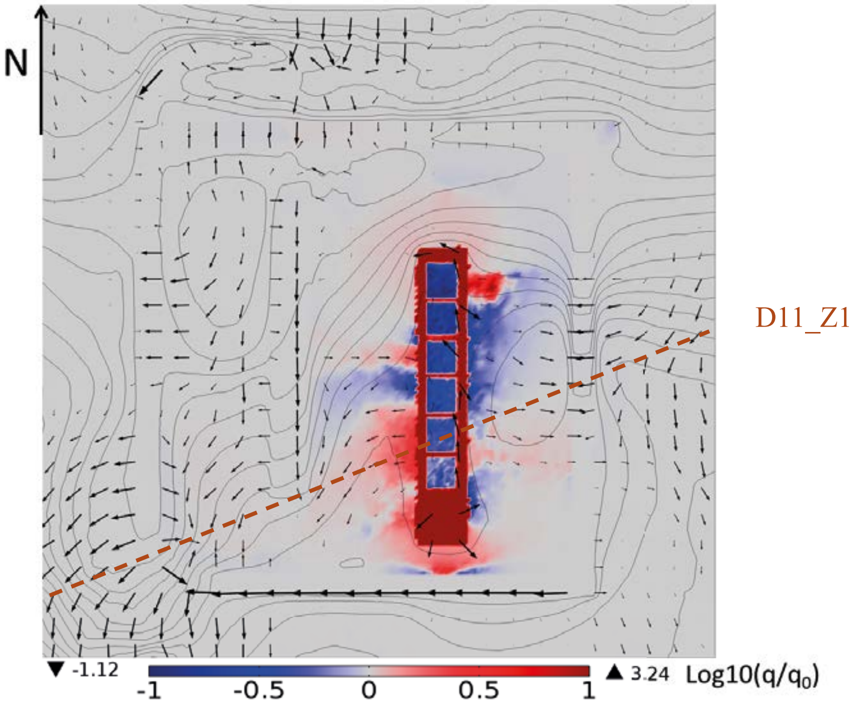

Figure 5-15. *Ratio of the Darcy velocity magnitude at location 700_1 calculated as log10(q/q_0), where q = Darcy velocity magnitude for hydraulic cage case and q_0=Darcy velocity for base case. Arrows and hydraulic head isolines are plotted for the BHK hydraulic cage case.*

Table 5-5. Groundwater flow through the BHA vault and waste control volumes at location 300_4. The flow ratio is calculated with respect to the base case.

	Base case	Degraded bentonite case		Hydraulic cage case	
Flow control volume	Total flow (m^3/yr)	Total flow (m^3/yr)	Ratio	Total flow (m^3/yr)	Ratio
BHA vault	4.26E−01	1.44E+02	339.00	7.63E+02	1,791.71
BHA_1 waste	9.57E−02	1.53E+01	160.15	4.29E+00	44.79
BHA_2 waste	8.61E−02	1.52E+01	176.87	8.01E+00	93.10
BHA_3 waste	1.09E−01	1.55E+01	142.15	1.14E+01	103.94
BHA_4 waste	1.55E−01	1.63E+01	104.85	9.70E+00	62.42
BHA_5 waste	1.38E−01	1.63E+01	118.22	4.64E+00	33.65

Groundwater flow through the waste control volumes increases by one order of magnitude, comparing the degraded bentonite case to the base case. It decreases going from the degraded case to the hydraulic cage case (Table 5-5 and Figure 5-16). Groundwater flows from the northwest to the southeast and is channeled through deformation zone D1_Z4 (see Section 3.2.4). In the base case, higher flows are observed in the waste control volumes located downstream of the deformation zone D1_Z4. In the degraded bentonite case groundwater flows through the BHA from west to east, homogenizing the flow between compartments and reducing the flow through deformation zone D1_Z4 located upstream of the vault (Figure 5-17 and Figure 5-18). In the hydraulic cage case flow through the waste is lower than in the degraded case and is concentrated to the central control volume, aligned with the deformation zone D1_Z4 (Figure 5-19 and Figure 5-20).

The degradation of the BHA backfill does not have a significant effect on the flow through the BHK. The increase is about 0.2% for the degraded bentonite case and 0.7% for the hydraulic cage case.

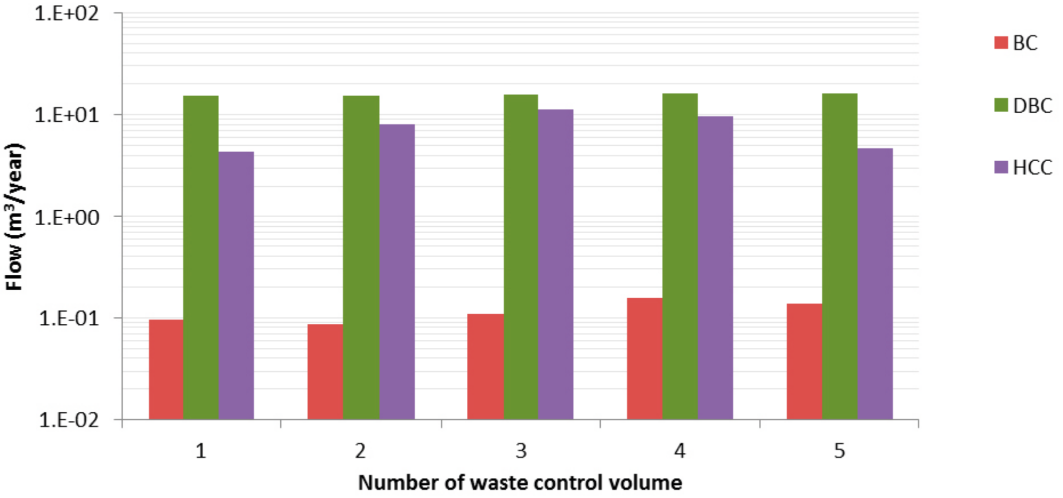

Figure 5-16. *Groundwater flow through the BHA waste control volumes at location 300_4. BC = base case, DBC = degraded bentonite case and HCC = hydraulic cage case.*

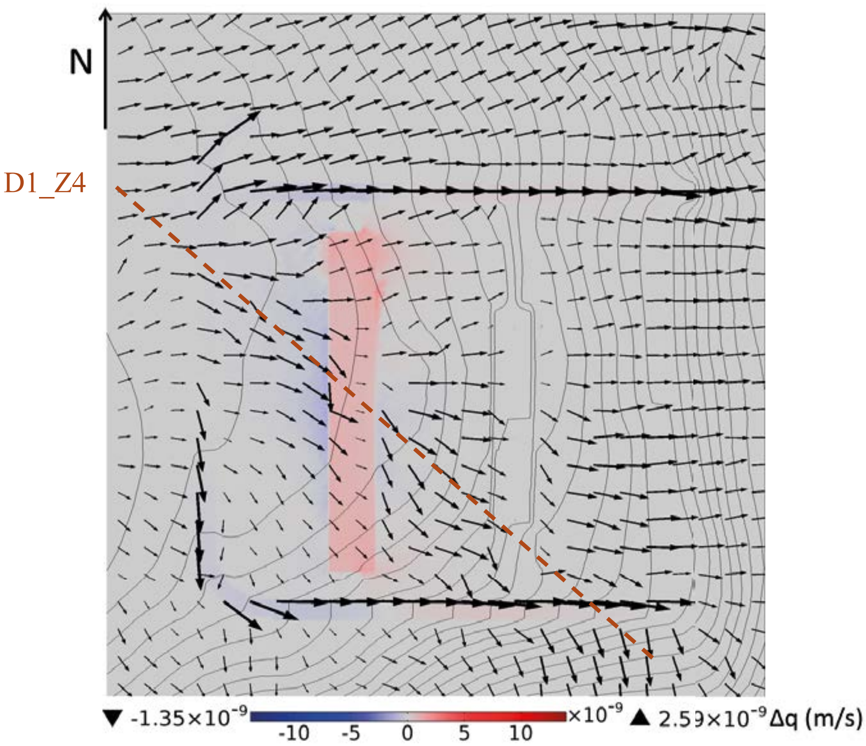

Figure 5-17. *Difference in the magnitude of the Darcy velocity at location 300_4 calculated as $q - q_0$, where q = Darcy flux for the degraded bentonite case and q_0 = Darcy flux for the base case. Arrows and hydraulic head isolines are plotted for the degraded bentonite case.*

Location 500_4

At location 500_4, the groundwater flow through BHA increases by two orders of magnitude when comparing the degraded bentonite case to the base case, and doubles going from the degraded bentonite case to the hydraulic cage case (Table 5-6). The increase of flow through the waste control volumes is approximately 20-fold, comparing the base case to the degraded bentonite case. The flow decreases by one order of magnitude when comparing the degraded case to the hydraulic cage case (Table 5-6 and Figure 5-21).

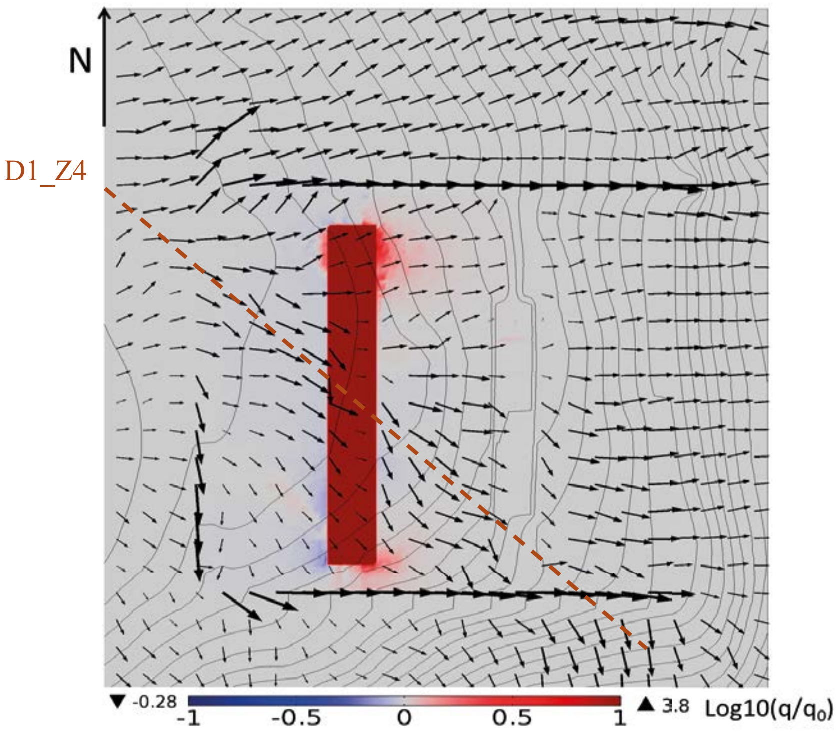

Figure 5-18. *Ratio of the Darcy velocity magnitude at location 300_4 calculated as $log_{10}(q/q_0)$, where q = Darcy velocity magnitude for the degraded bentonite case and q_0=Darcy velocity for base case. Arrows and hydraulic head isolines are plotted for the degraded bentonite case.*

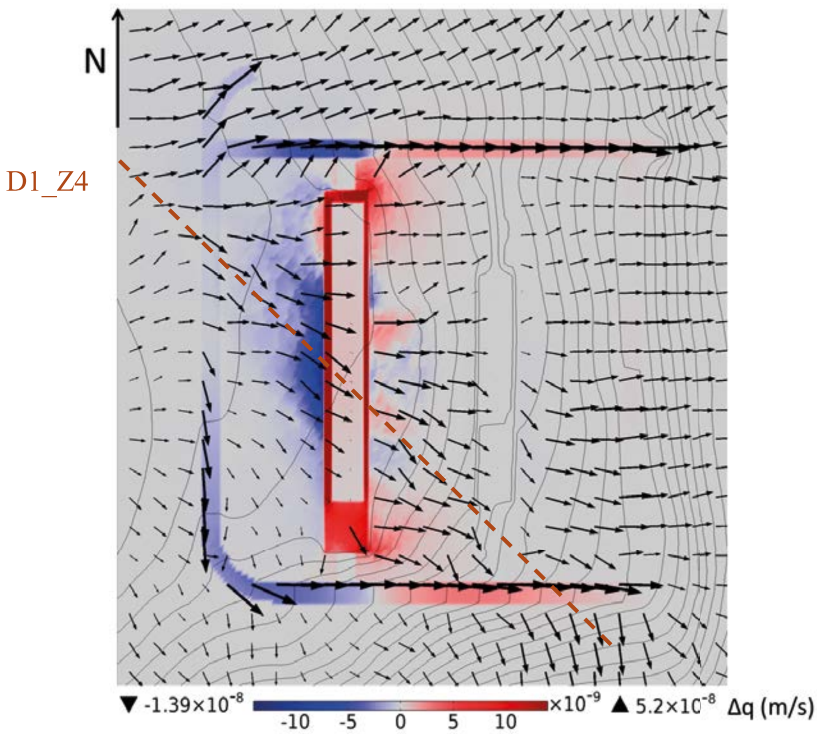

Figure 5-19. *Difference in the magnitude of the Darcy velocity at location 300_4 calculated as $q - q_0$, where q = Darcy flux for the hydraulic cage case and q_0 = Darcy flux for the base case. Arrows and hydraulic head isolines are plotted for the hydraulic cage case.*

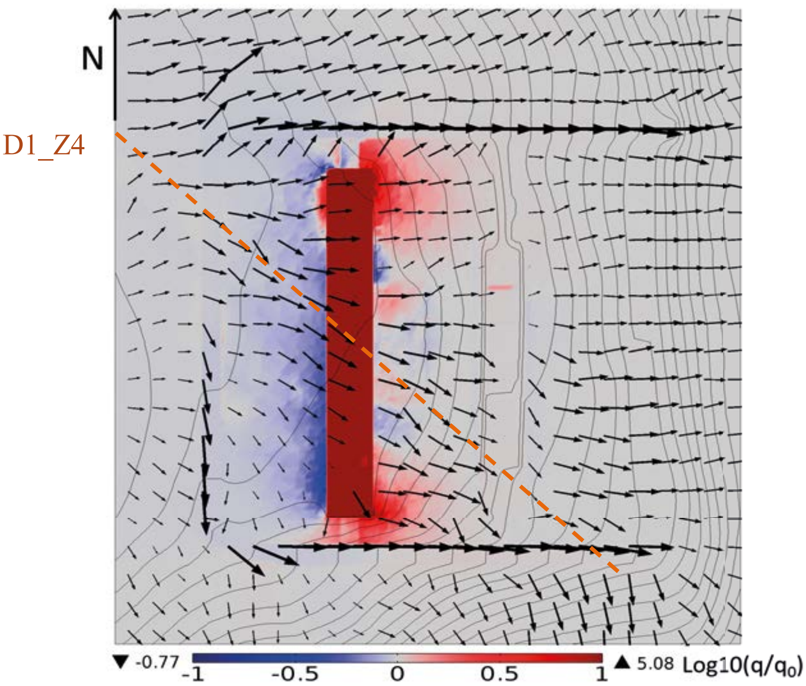

Figure 5-20. *Ratio of the Darcy velocity magnitude at location 300_4 calculated as $log_{10}(q/q_0)$, where q = Darcy velocity magnitude for the hydraulic cage case and q_0=Darcy velocity for base case. Arrows and hydraulic head isolines are plotted for the hydraulic cage case.*

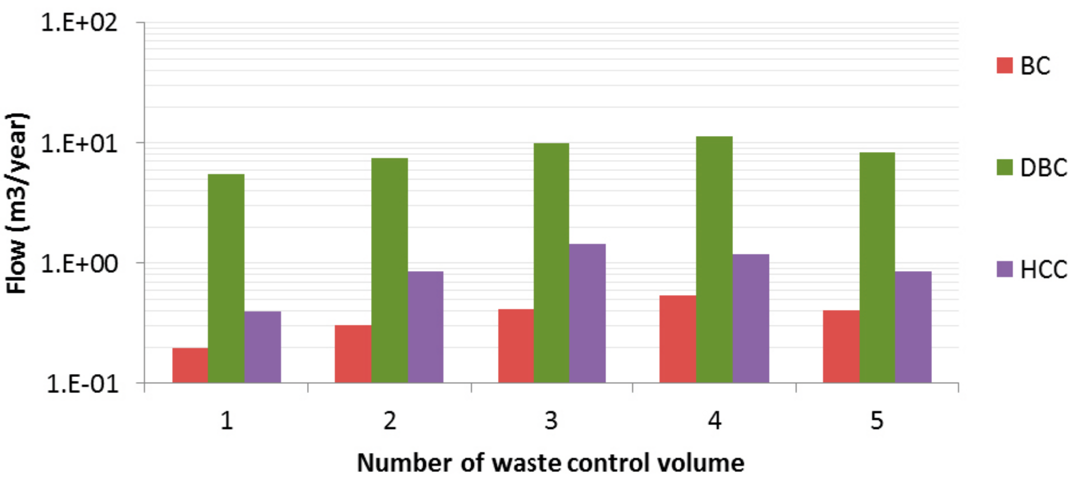

Figure 5-21. *Groundwater flow through the BHA waste control volumes at location 500_4. BC = Base case, DBC = degraded bentonite case and HCC = hydraulic cage case.*

Table 5-6. Groundwater flow through the BHA vault and waste control volumes at location 500_4. The flow ratio is calculated with respect to the base case.

	Base case	Degraded bentonite case		Hydraulic cage case	
Flow control volume	Total flow (m^3/yr)	Total flow (m^3/yr)	Ratio	Total flow (m^3/yr)	Ratio
BHA vault	8.42E−01	8.20E+01	97.35	1.41E+02	167.03
BHA_1 waste	1.94E−01	5.45E+00	28.07	3.99E−01	2.05
BHA_2 waste	3.06E−01	7.52E+00	24.57	8.63E−01	2.82
BHA_3 waste	4.14E−01	9.96E+00	24.03	1.44E+00	3.46
BHA_4 waste	5.37E−01	1.14E+01	21.22	1.19E+00	2.21
BHA_5 waste	4.04E−01	8.34E+00	20.63	8.49E−01	2.10

For the base case, the highest flow is observed for waste control volume 4. It is located to the south of deformation zone D6_Z4 and is surrounded by low hydraulic conductivity rock (see Section 3.4.4). As bentonite degrades, flow increases in the BHA waste domain and also in the surrounding rock to the north of deformation zone D6_Z4 (Figure 5-22 and Figure 5-23). In the hydraulic cage case the zone showing the highest flows shifts towards the central waste control volume, which is affected by deformation zone D6_Z4 (Figure 5-24 and Figure 5-25). Flow in the surrounding rock increases in the high hydraulic conductivity zones and decreases in the low hydraulic conductivity zones.

The degradation of the BHA backfill leads to an increase of groundwater flow into the BHK waste control volumes of about 2% for the degraded bentonite case and about 10% for the hydraulic cage case.

Location 700_1

At location 700_1, flow through BHA is less sensitive to bentonite degradation. The increase in flow through the vault is five-fold, comparing the degraded bentonite case to the base case. It then doubles going from the degraded bentonite case to the hydraulic cage case (Table 5-7). This result confirms that the low hydraulic conductivity rock controls groundwater flow.

Table 5-7. Groundwater flow through the BHA vault and waste control volumes at location 700_1. The flow ratio is calculated with respect to the base case.

	Base case	Degraded bentonite case		Hydraulic cage case	
Flow control volume	**Total flow (m^3/yr)**	**Total flow (m^3/yr)**	**Ratio**	**Total flow (m^3/yr)**	**Ratio**
BHA vault	6.71E−01	3.34E+00	4.98	5.72E+00	8.52
BHA_1 waste	3.17E−01	8.14E−01	2.57	3.80E−02	0.12
BHA_2 waste	5.56E−01	1.29E+00	2.33	5.54E−02	0.10
BHA_3 waste	6.19E−01	1.41E+00	2.27	8.61E−02	0.14
BHA_4 waste	5.90E−01	1.32E+00	2.24	7.85E−02	0.13
BHA_5 waste	3.24E−01	1.07E+00	3.30	7.37E−02	0.23

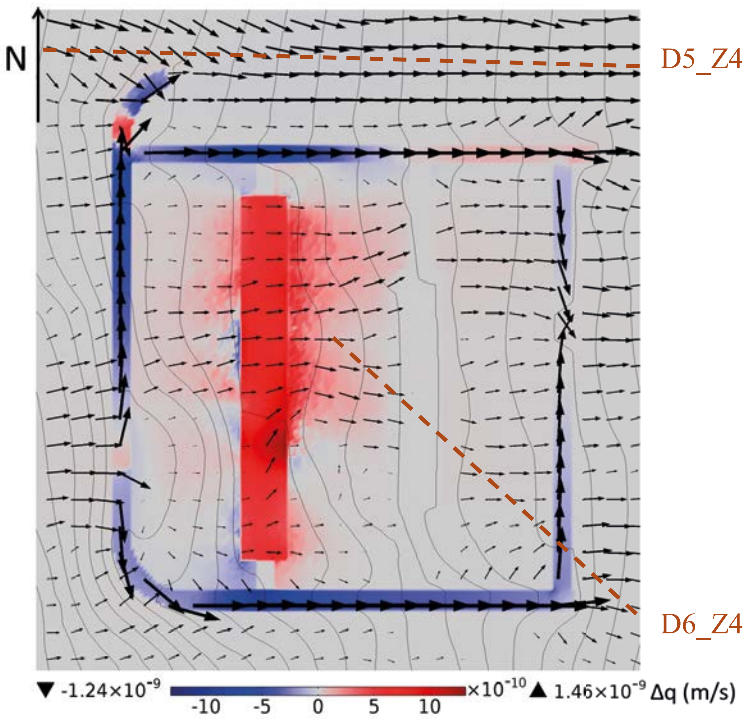

***Figure 5-22.** Difference in the magnitude of the Darcy velocity at location 500_4 calculated as $q - q_0$, where q = Darcy flux for the degraded bentonite case and q_0 = Darcy flux for the base case. Arrows and hydraulic head isolines are plotted for the degraded bentonite case.*

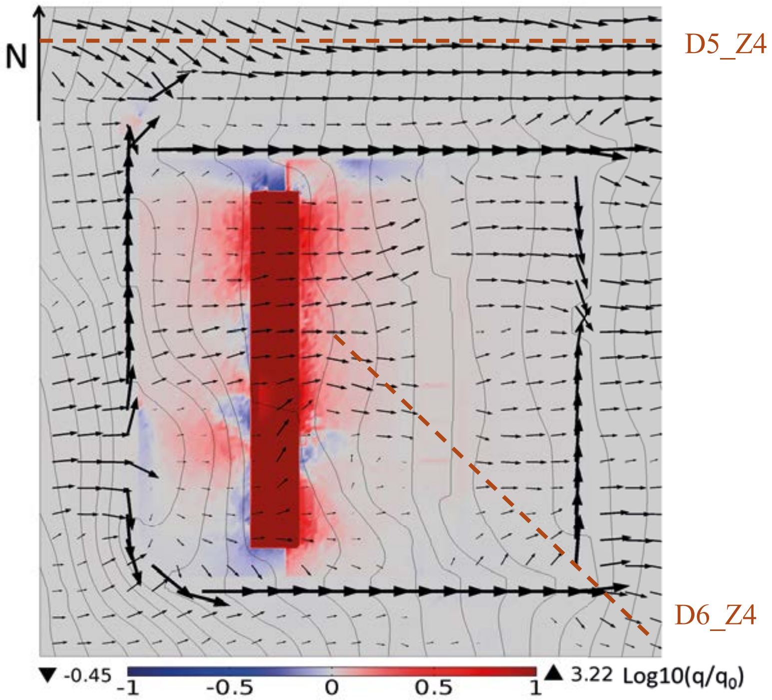

Figure 5-23. *Ratio of the Darcy velocity magnitude at location 500_4 calculated as* $log_{10}(q/q_0)$*, where* q *= Darcy velocity magnitude for the degraded bentonite case and* q_0*=Darcy velocity for base case. Arrows and hydraulic head isolines are plotted for the degraded bentonite case.*

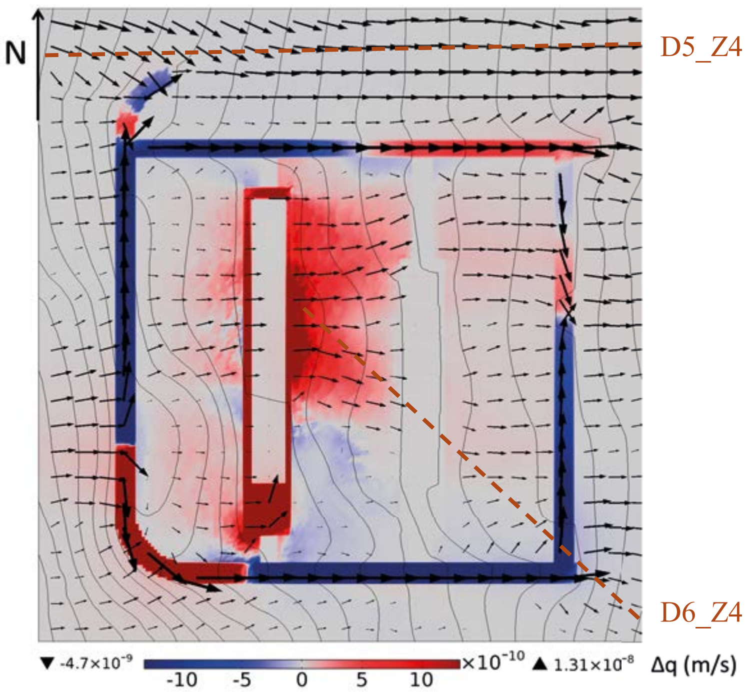

Figure 5-24. *Difference in the magnitude of the Darcy velocity at location 500_4 calculated as* $q - q_0$*, where* q *= Darcy flux for the hydraulic cage case and* q_0 *= Darcy flux for the base case. Arrows and hydraulic head isolines are plotted for the hydraulic cage case.*

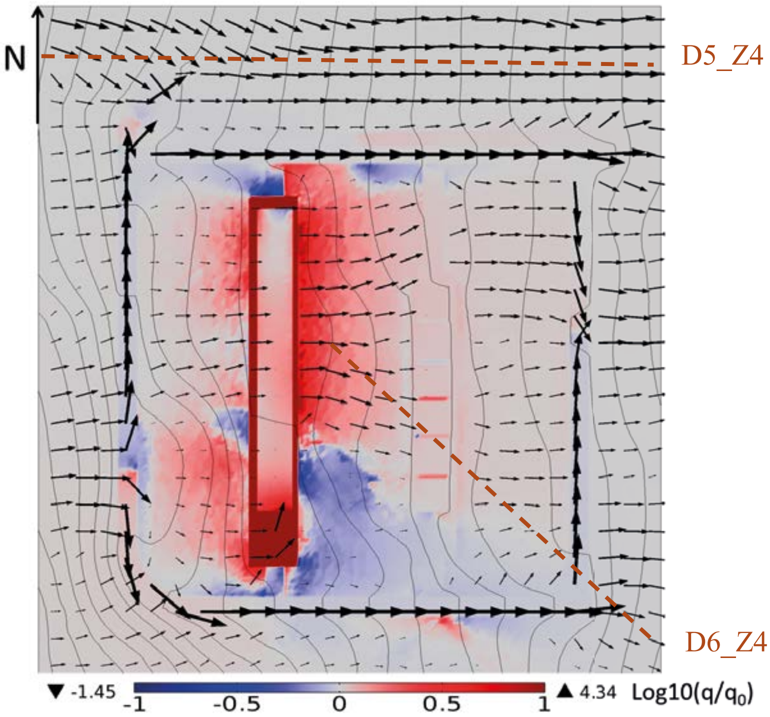

Figure 5-25. *Ratio of the Darcy velocity magnitude at location 500_4 calculated as* $log_{10}(q/q_0)$*, where q = Darcy velocity magnitude for the hydraulic cage case and* q_0*=Darcy velocity for base case. Arrows and hydraulic head isolines are plotted for the hydraulic cage case.*

Flow through the waste domain more than doubles comparing the base case to the degraded bentonite case. It decreases around one order of magnitude going from the degraded bentonite case to the hydraulic cage case (Table 5-7). A backfill material more permeable than the waste domain, together with the low hydraulic conductivity of the rock, yields an efficient combination to reduce the flow through the waste. The central waste compartment, BHA_3, experiences the highest flow for all cases (Figure 5-26). This compartment is affected by deformation zone D11_Z1 (Figure 5-27). In the base case (see Section 3.5.5), the waste flow is inversely proportional to the hydraulic conductivity of the surrounding rock. The distribution of flow is more homogeneous in the degraded bentonite case, where hydraulic conductivity of the backfill equals the hydraulic conductivity of the waste domain (Figure 5-26). The redistribution of flow is illustrated by the difference in the magnitude of the Darcy velocity between the degraded bentonite case and the base case (see Figure 5-27 and Figure 5-28), and between the hydraulic cage case and the base case (see Figure 5-29 and Figure 5-30).

The case with degraded bentonite in the BHA vault results in a 35% decrease in the BHK vault flow and a decrease of up to 21% in the waste control volumes. Flows decrease even further for the hydraulic cage case.

5.4 Alternative initial state of concrete backfill

The alternative initial state considers a concrete backfill in BHK with a hydraulic conductivity equal to 1.0×10^{-12} m/s, that is, approximately three orders of magnitude lower than for the base case.

The computed flow through the vaults and waste control volumes for the concrete backfill alternative initial state are presented in Table 5-8 for location 300_4, in Table 5-9 location 500_4 and Table 5-10 for location 700_1. The flow through the BHK vault decreases by three orders of magnitude compared to the base case for locations 300_4 and 500_4. The decrease in flow is proportional to the decrease in the concrete hydraulic conductivity. The flow decreases by two orders of magnitude at location 700_1. The flow through the waste control volumes decreases by three orders of magnitude for locations 300_4 and 500_4 and by two orders of magnitude for location 700_1. The lower sensitivity to the concrete hydraulic conductivity at location 700_1 is related to the low hydraulic conductivity of the rock at this location.

BHA is located upstream of BHK and is not affected by the changes in the hydraulic conductivity of the BHK backfill.

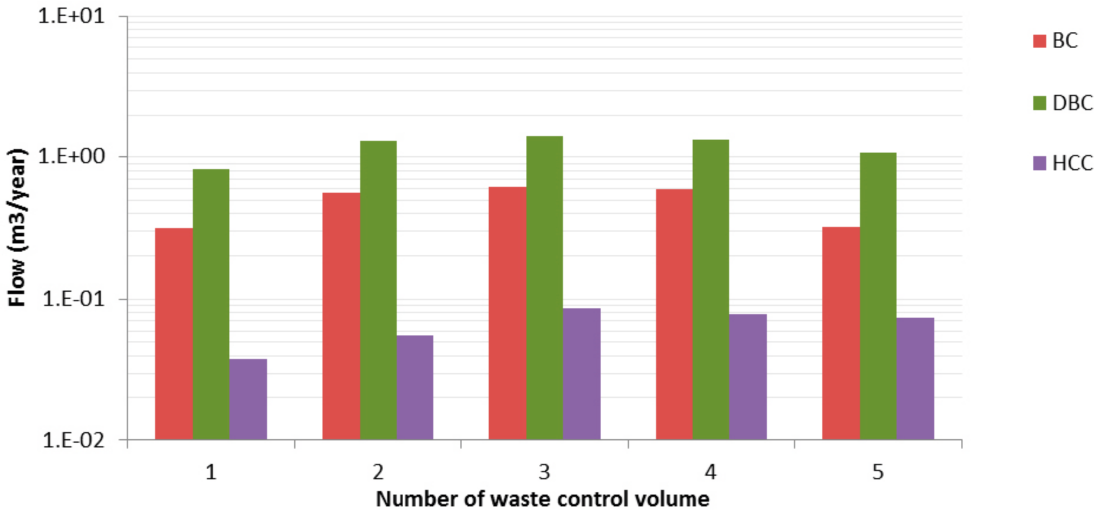

Figure 5-26. *Groundwater flow through the BHA waste control volumes at location 700_1. BC = Base case, DBC = degraded bentonite case and HCC = Hydraulic cage case.*

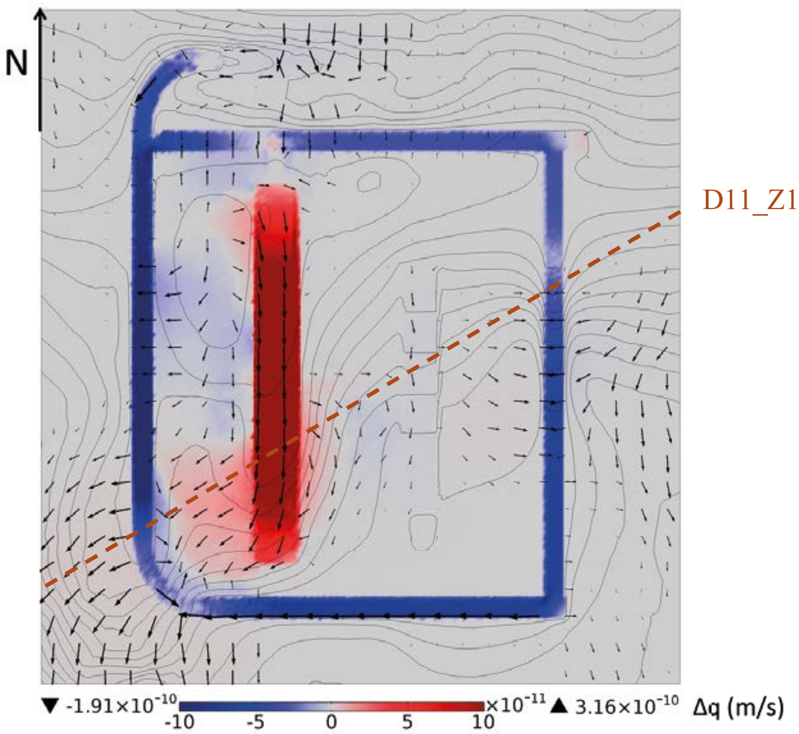

Figure 5-27. *Difference in the magnitude of the Darcy velocity at location 700_1 calculated as $q - q_0$, where q = Darcy flux for the degraded bentonite case and q_0 = Darcy flux for the base case. Arrows and hydraulic head isolines are plotted for the degraded bentonite case.*

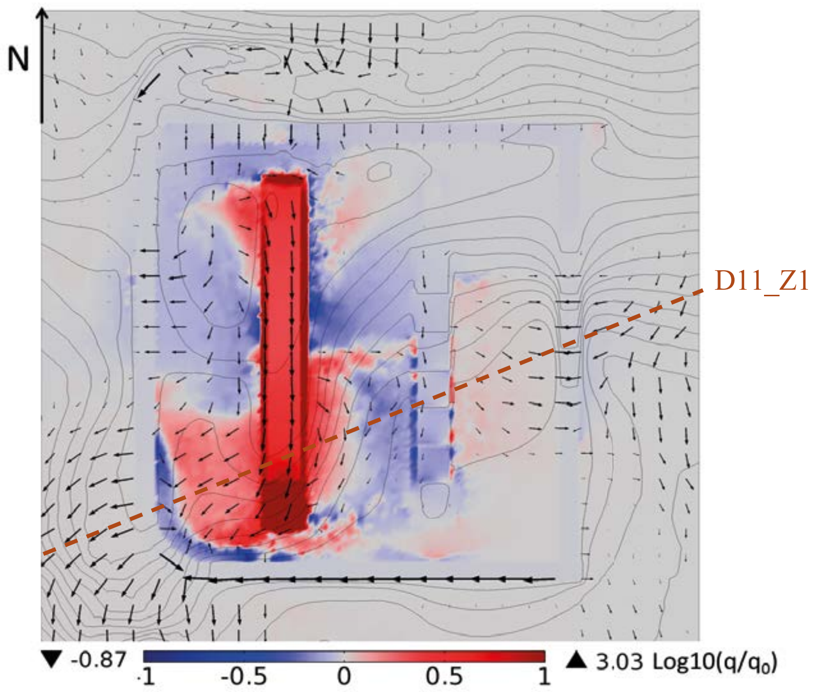

Figure 5-28. *Ratio of the Darcy velocity magnitude at location 700_1 calculated as $log_{10}(q/q_0)$, where q = Darcy velocity magnitude for the degraded bentonite case and q_0=Darcy velocity for base case. Arrows and hydraulic head isolines are plotted for the degraded bentonite case.*

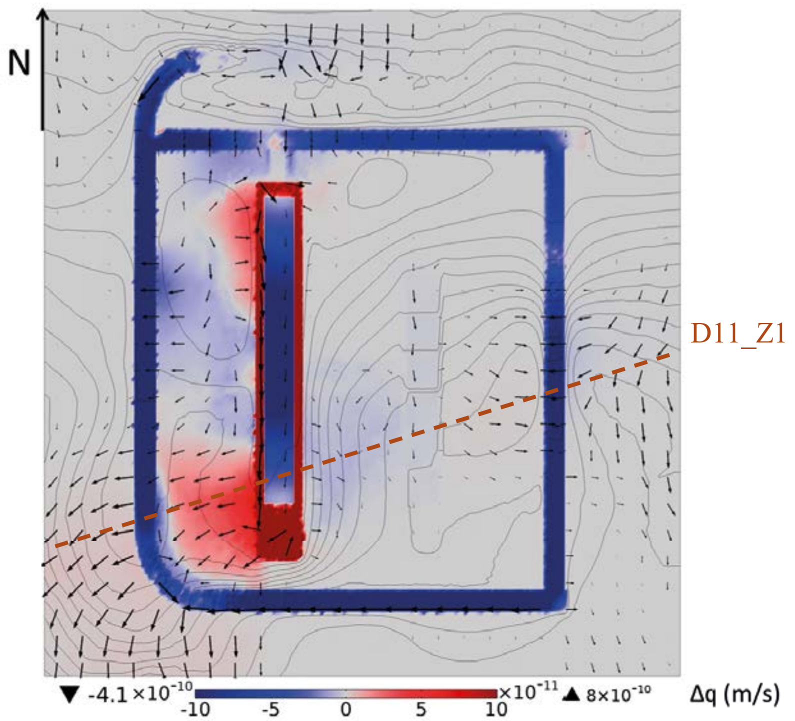

Figure 5-29. *Difference in the magnitude of the Darcy velocity at location 700_1 calculated as $q - q_0$, where q = Darcy flux for the hydraulic cage case and q_0 = Darcy flux for the base case. Arrows and hydraulic head isolines are plotted for the hydraulic cage case.*

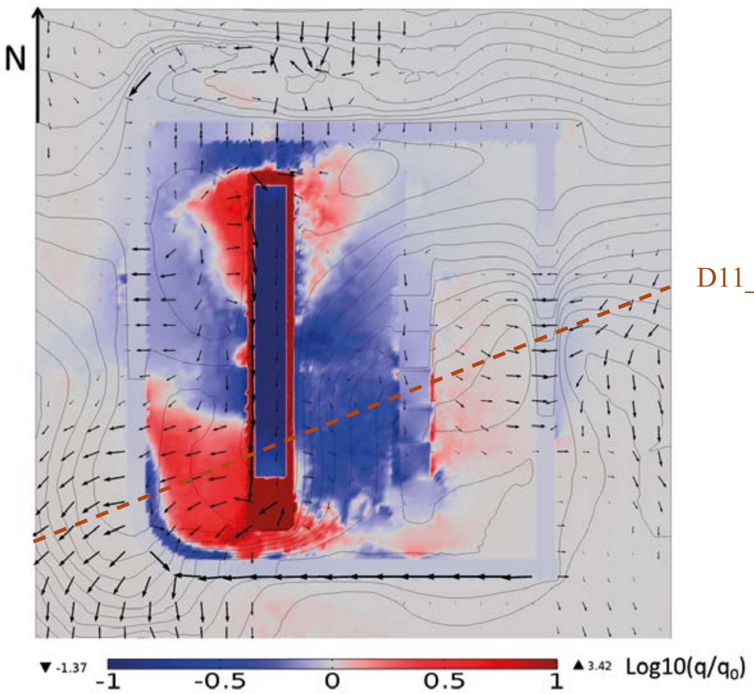

***Figure 5-30.** Ratio of the Darcy velocity magnitude at location 700_1 calculated as $log_{10}(q/q_0)$, where q = Darcy velocity magnitude for the hydraulic cage case and q_0=Darcy velocity for base case. Arrows and hydraulic head isolines are plotted for the hydraulic cage case.*

Location 300_4

Table 5-8. Computed flows for the alternative initial state and the base case at location 300_4. The ratio is calculated with respect to the base case.

	Base case	Alternative initial state	
Flow control volume	Total flow (m^3/yr)	Total flow (m^3/yr)	Ratio
BHK vault	4.66E+00	5.87E−03	1.26E−03
BHK_1 waste	4.50E−01	5.76E−04	1.28E−03
BHK_2 waste	4.97E−01	6.30E−04	1.27E−03
BHK_3 waste	5.86E−01	7.44E−04	1.27E−03
BHK_4 waste	6.45E−01	8.22E−04	1.27E−03
BHK_5 waste	6.71E−01	8.54E−04	1.27E−03
BHK_6 waste	6.41E−01	8.13E−04	1.27E−03

Location 500_4

Table 5-9. Computed flows for the alternative initial state and the base case at location 500_4. The ratio is calculated with respect to the base case.

	Base case	Alternative initial state	
Flow control volume	Total flow (m^3/yr)	Total flow (m^3/yr)	Ratio
BHK vault	3.29E+00	4.26E−03	1.30E−03
BHK_1 waste	3.25E−01	4.20E−04	1.29E−03
BHK_2 waste	3.32E−01	4.34E−04	1.31E−03
BHK_3 waste	3.25E−01	4.22E−04	1.30E−03
BHK_4 waste	2.97E−01	3.82E−04	1.29E−03
BHK_5 waste	3.28E−01	4.24E−04	1.29E−03
BHK_6 waste	3.60E−01	4.73E−04	1.32E−03

Location 700_1

Table 5-10. Computed flows for the alternative initial state and the base case at location 700_1. The ratio is calculated with respect to the base case.

	Base case	Alternative initial state	
Flow control volume	**Total flow (m^3/yr)**	**Total flow (m^3/yr)**	**Ratio**
BHK vault	1.10E−01	1.13E−03	1.03E−02
BHK_1 waste	3.38E−02	7.38E−04	2.18E−02
BHK_2 waste	3.67E−02	7.20E−04	1.96E−02
BHK_3 waste	3.07E−02	7.63E−04	2.49E−02
BHK_4 waste	2.63E−02	8.44E−04	3.21E−02
BHK_5 waste	1.74E−02	7.47E−04	4.31E−02
BHK_6 waste	9.11E−03	6.43E−04	7.06E−02

5.5 Alternative initial state of bentonite backfill

The alternative initial state considers a bentonite backfill in BHA with a hydraulic conductivity equal to 1.0×10^{-13} m/s, that is, three orders of magnitude lower than for the base case.

The computed flows through the vaults and waste control volumes for the bentonite backfill alternative initial state are presented in Table 5-11 for location 300_4, in Table 5-12 for location 500_4 and for location 700_1. For all locations, the flow through the BHA vault decreases by three orders of magnitude compared to the flow in the base case. This decrease in flow is proportional to the decrease in the bentonite hydraulic conductivity. The flow through the waste control volumes decreases by three orders of magnitude at locations 300_1 and 500_4 and by two orders at location 700_1.

BHK is located downstream of the BHA and is not affected by the changes in the hydraulic conductivity of the BHA backfill for domains 300_4 and 500_4. However, at location 700_1, the flow through the BHK vault increases 5% and the flow through the waste between 3 to 16%, with the maximum values observed for waste control volumes 5 and 6.

Location 300_4

Table 5-11. Computed flows for the alternative initial state and the base case for location 300_4. The ratio is calculated with respect to the base case.

	Base case	Alternative initial state	
Flow control volume	**Total flow (m^3/yr)**	**Total flow (m^3/yr)**	**Ratio**
BHA vault	4.26E−01	4.35E−04	1.02E−03
BHA_1 waste	9.57E−02	9.16E−05	9.57E−04
BHA_2 waste	8.61E−02	9.46E−05	1.10E−03
BHA_3 waste	1.09E−01	1.30E−04	1.19E−03
BHA_4 waste	1.55E−01	1.79E−04	1.15E−03
BHA_5 waste	1.38E−01	1.51E−04	1.09E−03

Location 500_4

Table 5-12. Computed flows for the alternative initial state and the base case for location 500_4. The ratio is calculated with respect to the base case.

	Base case	Alternative initial state	
Flow control volume	Total flow (m^3/yr)	Total flow (m^3/yr)	Ratio
BHA vault	8.42E−01	9.03E−04	1.07E−03
BHA_1 waste	1.94E−01	2.56E−04	1.32E−03
BHA_2 waste	3.06E−01	4.23E−04	1.38E−03
BHA_3 waste	4.14E−01	5.49E−04	1.33E−03
BHA_4 waste	5.37E−01	6.45E−04	1.20E−03
BHA_5 waste	4.04E−01	4.93E−04	1.22E−03

Location 700_1

Table 5-13. Computed flows for the alternative initial state and the base case for location 700_1. The ratio is calculated with respect to the base case.

	Base case	Alternative initial state	
Flow control volume	Total flow (m^3/yr)	Total flow (m^3/yr)	Ratio
BHA vault	6.71E−01	1.21E−03	1.80E−03
BHA_1 waste	3.17E−01	4.82E−03	1.52E−02
BHA_2 waste	5.56E−01	5.63E−03	1.01E−02
BHA_3 waste	6.19E−01	6.10E−03	9.85E−03
BHA_4 waste	5.90E−01	9.03E−03	1.53E−02
BHA_5 waste	3.24E−01	1.00E−02	3.10E−02

5.6 Summary

For each vault, four calculation cases have been analysed, assigning different values to the hydraulic conductivity of the backfill material (Table 5-1.) The backfill hydraulic conductivity is lower than the host rock hydraulic conductivity for the two least permeable cases (alternative initial case and base case). The degraded concrete and bentonite cases are characterized by a backfill hydraulic conductivity set equal to the hydraulic conductivity of the waste domain (1.0×10^{-7} m/s). This case therefore represents a homogeneous vault. Moreover, this value is on the same order as the hydraulic conductivity of the host rock. In the hydraulic cage case, the hydraulic conductivity of the backfill is higher than that of the waste and the host rock. In this case the backfill acts as a hydraulic cage surrounding the waste domain.

Location 300_4

Figure 5-31 summarizes the results of the flows through the vault for all the studied cases at location 300_4. The curves for the BHA and BHK vaults overlap. This overlap indicates that flows are controlled by the hydraulic conductivity of the backfill materials rather than by the upstream/downstream position of the vaults, or by local hydraulic conductivity of the rock.

When the hydraulic conductivity of the backfill is lower than the hydraulic conductivity of the rock (to the left of the blue area in Figure 5-31), there is a 1:1 relationship between the hydraulic conductivity of the backfill and the flow through the vault. The backfill is the main flow barrier and controls the flow through the vault. However, for the degraded backfill and hydraulic cage cases, the sensitivity to the hydraulic conductivity of the backfill is reduced. In the hydraulic cage cases, the rock is less permeable than the backfill and acts as the main flow barrier.

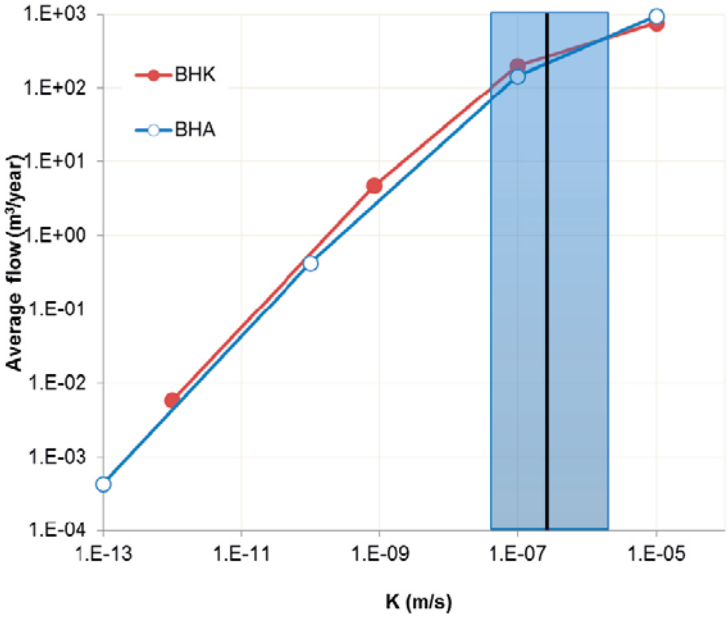

Figure 5-31. *Average flows through the BHA and BHK vaults considering different hydraulic conductivities of the backfills. The blue zone indicates the range of hydraulic conductivities in the rock at location 300_4. The black line shows the average hydraulic conductivity of the rock at repository depth.*

Figure 5-32 shows the relationship between the average flow through the waste and the backfill hydraulic conductivity. A 1:1 relationship on the log scale is observed between the flow through the waste and the backfill hydraulic conductivity in the cases where the backfill acts as a barrier (alternative initial state and base case). The maximum waste flow is calculated for the case of a homogeneous vault (degraded cases). The flow through the waste decreases as the hydraulic conductivity of the backfill becomes greater than that of the waste domain.

Location 500_4

At location 500_4, the groundwater flow through the vaults increases with the hydraulic conductivity of the backfill (Figure 5-33). A linear relationship between the flow and the hydraulic conductivity of the backfill (1:1 in log scale) is observed between the alternative initial state and the base case. The slope decreases slightly between the base case and the degraded case. Note that in the degraded case the hydraulic conductivity of the backfill is on the same order as the rock, such that both are equally effective as hydraulic barriers. The slope decreases further between the degraded case and the hydraulic cage case. When the backfill is more permeable than the host rock, the rock constitutes the flow barrier. Therefore the flow through the vault is relatively insensitive to the permeability of the backfill.

For both vaults, the flow through the waste increases linearly between the alternative initial state and the base case, with a slope of approximately 1 (Figure 5-34). The slope decreases between the base case and the degraded case. The maximum flow through the waste occurs for the degraded case, where the backfill hydraulic conductivity equals the waste hydraulic conductivity (1×10^{-7} m/s). Flow through the waste decreases when the hydraulic conductivity of the backfill becomes greater than that of the waste domain. The backfill then acts as a hydraulic cage reducing the groundwater flow through the waste.

The flow through the waste is lower through BHK than through BHA for the alternative initial state and for the base case. This difference decreases for the degraded and hydraulic cage cases. For degraded backfills, the hydraulic conductivity is homogeneous within the vault, minimizing the effect of the local hydraulic conductivity in the host rock. It also limits the impact of the upstream/downstream location of the vaults.

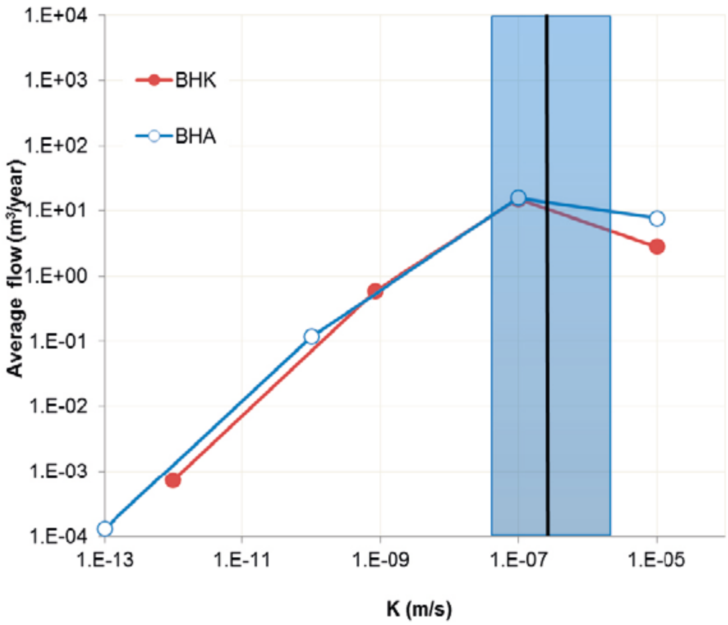

Figure 5-32. *Average flows through the BHA and BHK waste domain considering different hydraulic conductivities of the backfills. The blue zone indicates the range of hydraulic conductivities in the rock at location 300_4. The black line shows the average hydraulic conductivity of the rock at repository depth.*

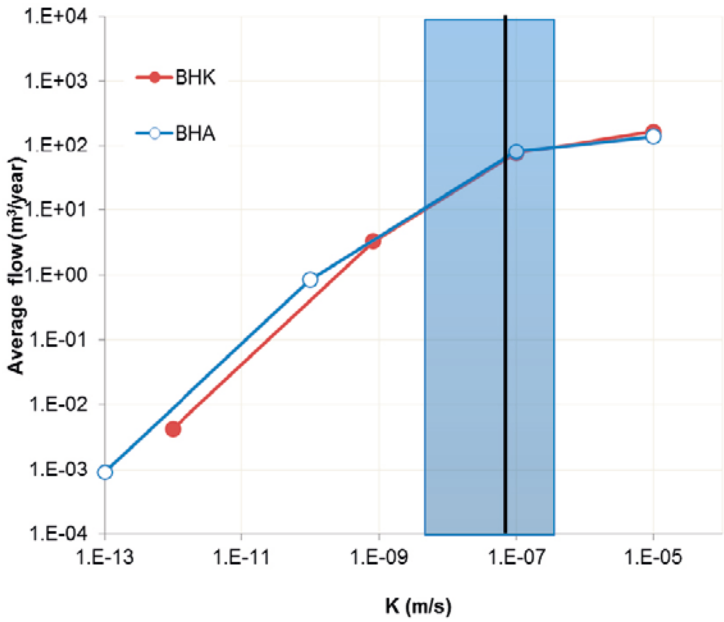

Figure 5-33. *Average flows through the BHA and BHK vaults considering different hydraulic conductivities of the backfills. The blue zone indicates the range of hydraulic conductivities in the rock at location 500_4. The black line shows the average hydraulic conductivity of the rock at repository depth.*

Location 700_1

The rock at location 700_1 has the lowest hydraulic conductivity of all investigated locations. For the base case, the hydraulic conductivity of concrete backfill in BHK is higher than the average hydraulic conductivity of the surrounding rock (Figure 5-35).

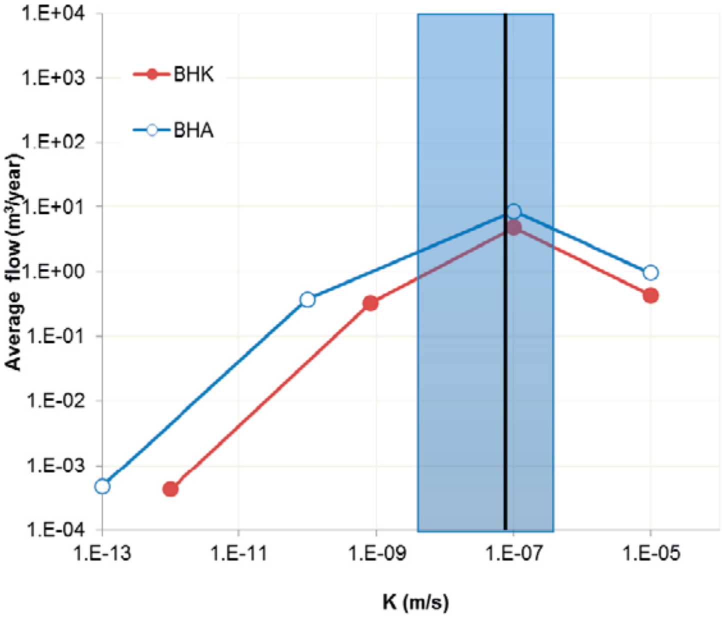

Figure 5-34. *Average flows through the BHA and BHK waste domain considering different hydraulic conductivities of the backfills. The blue zone indicates the range of hydraulic conductivities in the rock at location 500_4. The black line shows the average hydraulic conductivity of the rock at repository depth.*

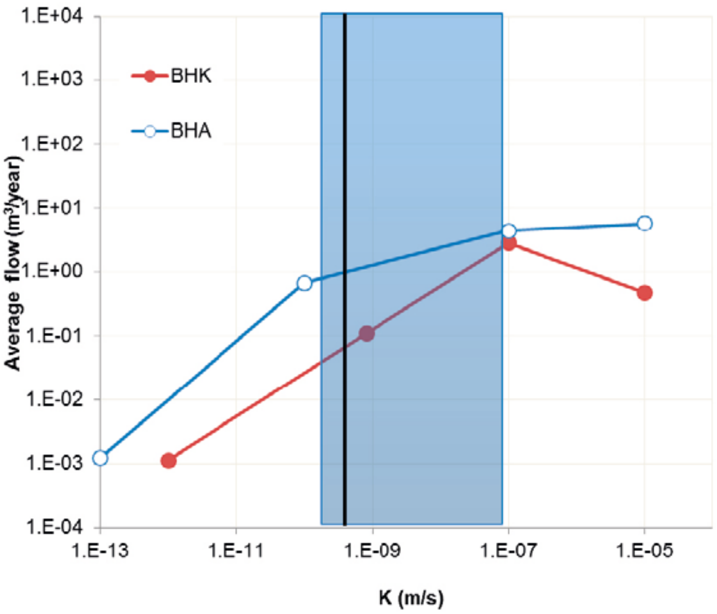

Figure 5-35. *Average flows through the BHA and BHK vaults considering different hydraulic conductivities of the backfills. The blue zone indicates the range of hydraulic conductivities in the rock at location 700_1. The black line shows the average hydraulic conductivity of the rock at repository depth.*

Flow through the vaults increases with increasing backfill hydraulic conductivity, going from the alternative initial cases to the degraded cases (Figure 5-35). Flows through BHA are higher than through BHK. For the BHA alternative initial state as well as the base case, the hydraulic conductivity is lower than the average hydraulic conductivity of the rock. Therefore the backfill acts as the main hydraulic barrier. When the hydraulic conductivity of the bentonite backfill in BHA is within the range of rock hydraulic conductivity (blue area in Figure 5-35) both backfill and rock act as hydraulic barriers. The hydraulic cage cases reveal a modest increase in flow through the BHA vault and a reduction in flow through the BHK vault.

At location 700_1, groundwater flows parallel to the vaults, from north to south. For such a flow regime the BHA waste domain experiences higher flows than the BHK (Figure 5-36). In contrast, the BHK waste domain is relatively unaffected by axial flow as the individual waste compartments are separated by concrete backfill. Again, for backfill conductivities lower than the rock hydraulic conductivity, it is the backfill that controls the flow through the waste (Figure 5-36). The impact of the backfill hydraulic conductivity within the range of the rock hydraulic conductivity (blue area in ***Figure 5-36***) is moderate. When the backfill hydraulic conductivity is higher than that of the waste domain, the backfill acts as a hydraulic cage and the flow through the waste is reduced for both vaults.

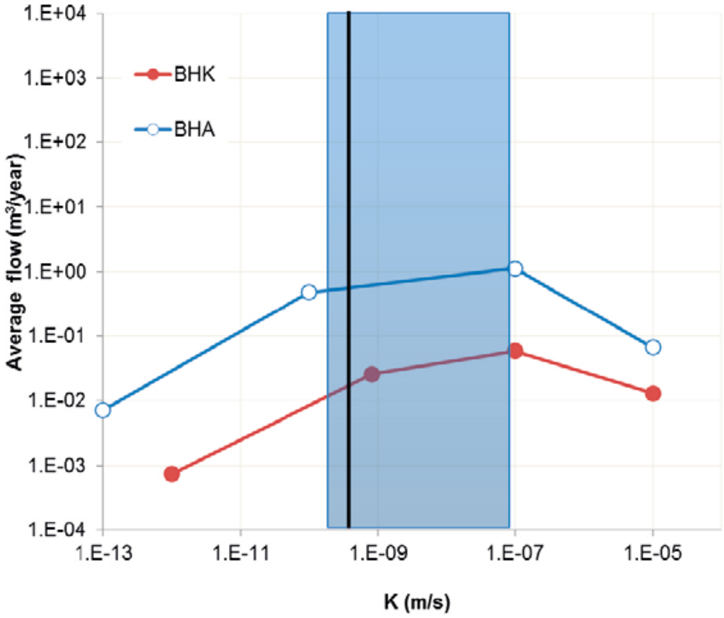

Figure 5-36. *Average flows through the BHA and BHK waste domain considering different hydraulic conductivities of the backfills. The blue zone indicates the range of hydraulic conductivities in the rock at location 700_1. The black line shows the average hydraulic conductivity of the rock at repository depth.*

6 Alternative repository closure approaches

In addition to the engineered barriers in the waste vaults, plugs may be installed in repository tunnels and shaft to further restrict groundwater flow. The closure installations assumed for the base case are described in Section 2.1. In addition, two alternative closure approaches have been considered in order to evaluate the influence on groundwater flow through the vaults and waste:

- A case without plugs in the access ramp and shaft.
- An extended closure case with bentonite in the access tunnels at repository depth.

The three closure alternatives are summarized in Figure 6-1.

6.1 No plugs in the access ramp and shaft

This closure case assumes that no sealing plugs are installed in the access ramp and in the shaft of the repository. Rather, crushed rock of high hydraulic conductivity (1.0×10^{-5} m/s) fills these volumes. The material properties assigned to installations in BHA and BHK are equal to those set for the base case.

Groundwater can enter the repository through the ramp and shaft when no plugs are present. The vertical variability of the flow through the host rock has been used to set plausible prescribed inflow values where the ramp and shaft intersect the top model boundary. The vertical distribution of the geometric mean of Darcy velocities in the rock (q_{GM}), averaged over the model domains 300_4, 500_4 and 700_1, has been calculated according to

$$q_{GM}(z) = \exp\left[\frac{1}{A(z)}\iint \log_{10} q(x,y,z)\,dxdy\right] \qquad (6\text{-}1)$$

Above, *q(x,y,z)* is the magnitude of the Darcy velocity (m/s) and *A(z)* the area of the model domain. Results are shown in Figure 6-2. Above a depth of 700 m the Darcy velocities range from 1×10^{-11} to 2×10^{-8} m/s.

Based on this, a set of five simulations with different prescribed values of groundwater inflow through the shaft and ramp (1×10^{-7}, 1×10^{-8}, 1×10^{-9}, 1×10^{-10} and 1×10^{-11} m/s) was performed for each of the locations 300_4, 500_4 and 700_1. Calculated flows through the BHA and BHK vaults and waste domains are presented in the section below.

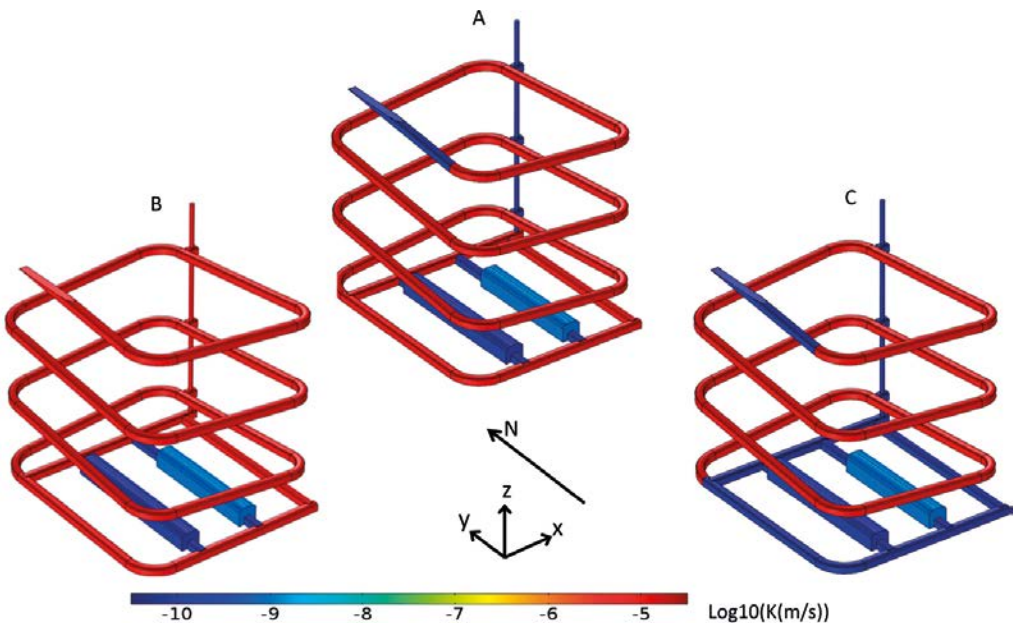

Figure 6-1. *Hydraulic conductivity of repository materials. A = Base case, B = No plugs in access ramp and shaft, and C = Extended closure case.*

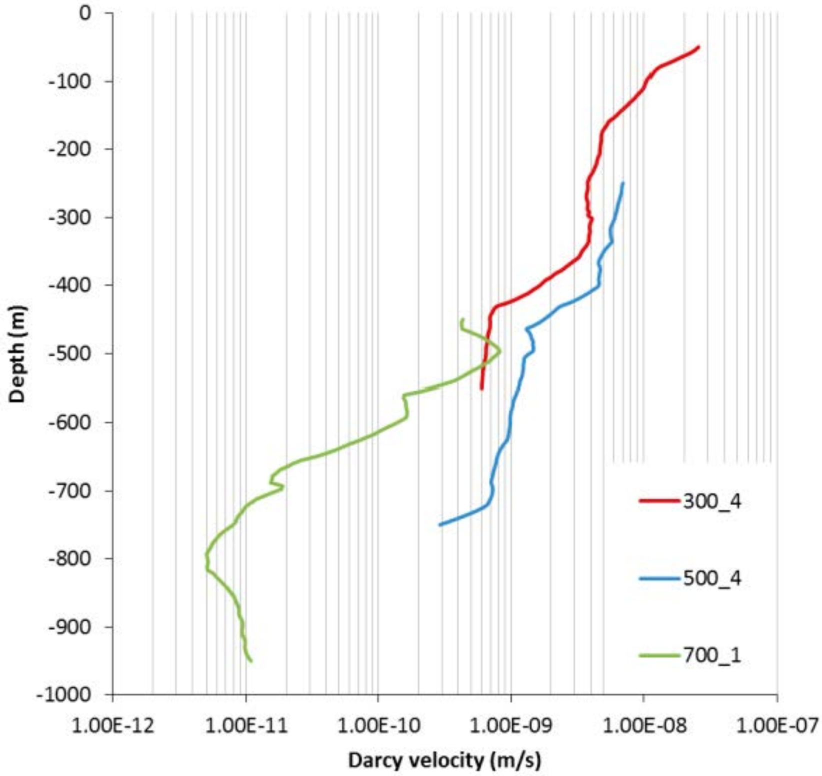

Figure 6-2. *Vertical distribution of the geometric mean of the Darcy velocity for the different model locations.*

Location 300_4

Table 6-1 shows that there is no significant change in the flow that enters the vaults and waste domain compared to the base case. The inflow surface area is small (19 m^2) and the considered inflow values are of the same order of magnitude (or lower) as the flow through the rock at the top of the model domain. Consequently, the amount of water entering the access ramp is small compared to the water flowing through the rock.

Table 6-1. Total flow through the BHA and BHK vaults and waste domains (m3/year) for different prescribed values of groundwater inflow through the shaft and ramp.

	Base case	q = 1e−7(m/s)	q = 1e−8(m/s)	q = 1e−9(m/s)	q = 1e−10(m/s)	q = 1e−11(m/s)
Flow control volume	**Total flow (m^3/yr)**	**Total flow (m^3/ yr)**	**Total flow (m^3/ yr)**	**Total flow (m^3/ yr)**	**Total flow (m^3/ yr)**	**Total flow (m^3/ yr)**
BHA vault	4.27E−01	4.27E−01	4.26E−01	4.26E−01	4.26E−01	4.26E−01
BHA 1 waste	9.60E−02	9.58E−02	9.55E−02	9.55E−02	9.55E−02	9.55E−02
BHA 2 waste	8.61E−02	8.62E−02	8.60E−02	8.60E−02	8.60E−02	8.60E−02
BHA 3 waste	1.09E−01	1.10E−01	1.10E−01	1.10E−01	1.10E−01	1.10E−01
BHA 4 waste	1.55E−01	1.56E−01	1.56E−01	1.56E−01	1.56E−01	1.56E−01
BHA 5 waste	1.38E−01	1.38E−01	1.38E−01	1.38E−01	1.38E−01	1.38E−01
BHK vault	4.66E+00	4.66E+00	4.65E+00	4.65E+00	4.65E+00	4.65E+00
BHK 1 waste	4.50E−01	4.48E−01	4.47E−01	4.47E−01	4.47E−01	4.47E−01
BHK 2 waste	4.98E−01	4.98E−01	4.97E−01	4.97E−01	4.97E−01	4.97E−01
BHK 3 waste	5.86E−01	5.87E−01	5.86E−01	5.86E−01	5.86E−01	5.86E−01
BHK4 waste	6.46E−01	6.46E−01	6.45E−01	6.45E−01	6.45E−01	6.45E−01
BHK 5 waste	6.71E−01	6.72E−01	6.71E−01	6.70E−01	6.70E−01	6.70E−01
BHK 6 waste	6.41E−01	6.42E−01	6.41E−01	6.40E−01	6.40E−01	6.40E−01

Location 500_4

Table 6-2 shows that there is no significant change in the flow that enters the vaults and waste domain compared to the base case. As for location 300_4, the amount of water entering the access ramp is small compared to the water flowing through the rock.

Table 6-2. Total flow through the BHA and BHK vaults and waste domains (m3/year) for different prescribed values of groundwater inflow through the shaft and ramp.

	Base case	q = 1e−7(m/s)	q = 1e−8(m/s)	q = 1e−9(m/s)	q = 1e−10(m/s)	q = 1e−11(m/s)
Flow control volume	**Total Flow (m^3/year)**	**Total Flow (m^3/ year)**	**Total Flow (m^3/ year)**	**Total Flow (m^3/ year)**	**Total Flow (m^3/ year)**	**Total Flow (m^3/ year)**
BHA vault	8.42E−01	8.46E−01	8.44E−01	8.44E−01	8.43E−01	8.43E−01
BHA 1 waste	1.94E−01	1.96E−01	1.96E−01	1.96E−01	1.96E−01	1.96E−01
BHA 2 waste	3.06E−01	3.08E−01	3.08E−01	3.08E−01	3.08E−01	3.08E−01
BHA 3 waste	4.14E−01	4.16E−01	4.16E−01	4.16E−01	4.16E−01	4.16E−01
BHA 4 waste	5.37E−01	5.39E−01	5.38E−01	5.38E−01	5.38E−01	5.38E−01
BHA 5 waste	4.04E−01	4.05E−01	4.05E−01	4.05E−01	4.05E−01	4.05E−01
BHK vault	3.29E+00	3.31E+00	3.30E+00	3.30E+00	3.30E+00	3.30E+00
BHK 1 waste	3.25E−01	3.29E−01	3.28E−01	3.27E−01	3.27E−01	3.27E−01
BHK 2 waste	3.32E−01	3.34E−01	3.34E−01	3.33E−01	3.33E−01	3.33E−01
BHK 3 waste	3.25E−01	3.27E−01	3.26E−01	3.26E−01	3.26E−01	3.26E−01
BHK4 waste	2.97E−01	2.98E−01	2.97E−01	2.97E−01	2.97E−01	2.97E−01
BHK 5 waste	3.28E−01	3.30E−01	3.28E−01	3.28E−01	3.28E−01	3.28E−01
BHK 6 waste	3.60E−01	3.62E−01	3.60E−01	3.60E−01	3.60E−01	3.60E−01

Location 700_1

For this location, the average flow through the rock is 1×10^{-9} m/s at the top boundary and 1×10^{-11} m/s at repository depth (Figure 6-2). The flow through the rock is thus in the lower range of prescribed fluxes through the access ramp. In this case, an influence on the flow through vaults and the waste domains can be observed (Table 6-3). An inflow of 1×10^{-7} m/s yields a 2% flow decrease through the BHA vault whereas the inflow of 1×10^{-11} m/s yields a 9% flow decrease. Flow similarly decreases somewhat in all the BHA waste control volumes. In contrast, the flow through the BHK vault increases between a 32% for an inflow of 1×10^{-7} m/s and a 41% 1×10^{-11} m/s. The flow through the waste increases up to a 160%. The maximum increase is located at the southernmost waste control volume (BHK_6).

Table 6-3. Total flow through the BHA and BHK vaults and waste domains (m3/year) for different prescribed values of groundwater inflow through shaft and ramp.

	Base case	q= 1e−7(m/s)	q= 1e−8(m/s)	q= 1e−9(m/s)	q= 1e−10(m/s)	q= 1e−11(m/s)
Flow control volume	**Total flow (m^3/ yr)**	**Total flow (m^3/ yr)**	**Total flow (m^3/ yr)**	**Total flow (m^3/ yr)**	**Total flow (m^3/ yr)**	**Total flow (m^3/ yr)**
BHA vault	6.71E−01	6.55E−01	6.15E−01	6.11E−01	6.11E−01	6.11E−01
BHA 1 waste	3.17E−01	3.15E−01	3.01E−01	2.99E−01	2.99E−01	2.99E−01
BHA 2 waste	5.56E−01	5.46E−01	5.15E−01	5.12E−01	5.11E−01	5.11E−01
BHA 3 waste	6.19E−01	6.06E−01	5.69E−01	5.66E−01	5.65E−01	5.65E−01
BHA 4 waste	5.90E−01	5.73E−01	5.41E−01	5.38E−01	5.38E−01	5.38E−01
BHA 5 waste	3.24E−01	3.11E−01	2.96E−01	2.95E−01	2.94E−01	2.94E−01
BHK vault	1.10E−01	1.45E−01	1.54E−01	1.55E−01	1.56E−01	1.56E−01
BHK 1 waste	3.38E−02	3.53E−02	3.51E−02	3.51E−02	3.51E−02	3.51E−02
BHK 2 waste	3.67E−02	3.84E−02	3.61E−02	3.59E−02	3.59E−02	3.58E−02
BHK 3 waste	3.07E−02	3.80E−02	3.64E−02	3.71E−02	3.72E−02	3.72E−02
BHK4 waste	2.63E−02	3.62E−02	4.31E−02	4.38E−02	4.39E−02	4.39E−02
BHK 5 waste	1.74E−02	3.04E−02	3.48E−02	3.54E−02	3.54E−02	3.54E−02
BHK 6 waste	9.11E−03	1.84E−02	2.34E−02	2.39E−02	2.39E−02	2.39E−02

For the highest water inflows in the ramp and shaft, the absence of plugs results in a change in the local flow and the salinity at repository level. The difference in the flow field at repository depth for the case of prescribed inflow equal to 1×10^{-7} m/s is illustrated in Figure 6-3 and the changes in salinity in Figure 6-4. The prescribed inflow in this case is much higher than the flow within the 700_1 rock domain. The flow reaches the repository depth through the northwestern access tunnels. The groundwater flow is directed along the access tunnels towards the south and east. The direction of flow changes in the eastern access tunnel (Figure 6-3). In the base case the easternmost access tunnel drains water from the rock east of the BHK vault. In the alternative closure case water flows west from the access tunnel reaching BHK and increasing the vault and waste flow. At the southern and east access tunnels water accumulates and groundwater head increases. This decreases the salinity locally and affects the position of the interface to deeper, more saline waters (Figure 6-4 and Figure 6-5).

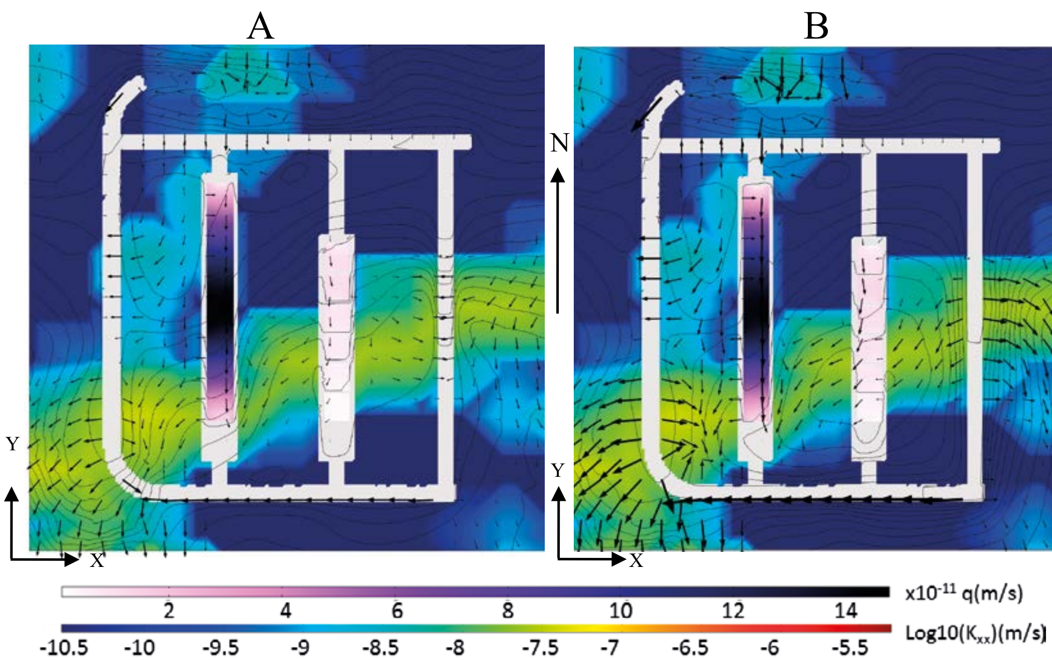

__Figure 6-3.__ Magnitude of the Darcy velocity through the waste control volumes (displayed only within the waste domain), hydraulic conductivity of the rock (displayed only in the rock domain), hydraulic head (isolines) and Darcy velocity (arrows) at location 700_1 for the base case (A) and the closure alternative with no plugs in the access ramp and a prescribed inflow at the ramp of 1×10^{-7} m/s (B).

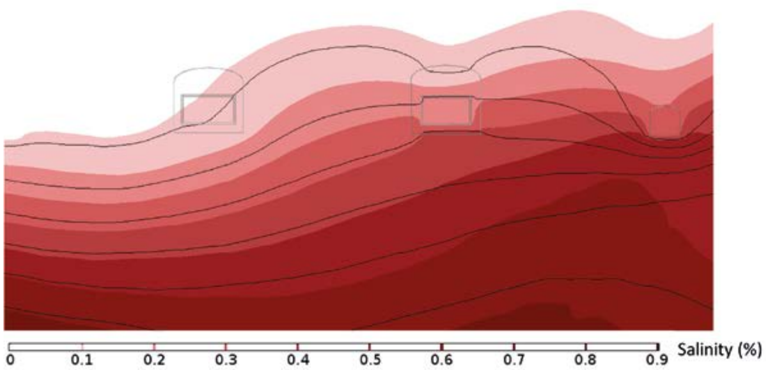

__Figure 6-4.__ Salinity contours in a vertical plane perpendicular to the vaults at location 700_1. Colour contours represent the base case solution and the black lines a solution for the no plugs case with a prescribed inflow through the ramp and shaft of 1×10^{-7} m/s. A downward movement of the salinity contours is observed for the no plugs case, in particular under the access tunnels.

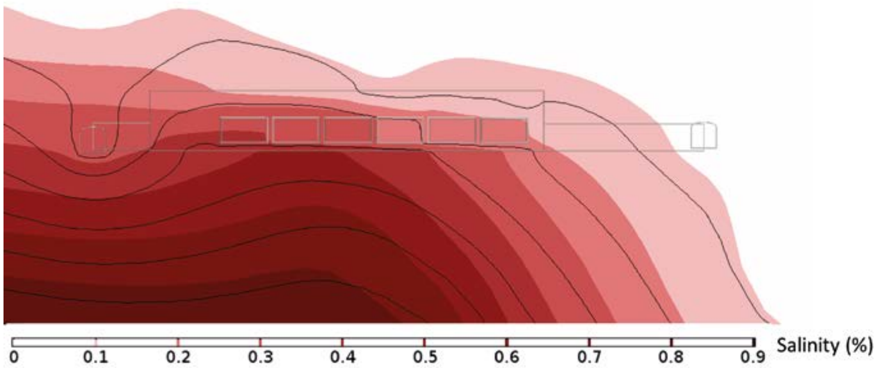

__Figure 6-5.__ Salinity contours in a vertical plane across the BHK at location 700_1. Colour contours represent the base case solution and the black lines a solution for the no plugs case with a prescribed inflow through the ramp and shaft of 1×10^{-7} m/s. A downward movement of the salinity contours is observed for the no plugs case, in particular under the access tunnels.

6.2 Extended closure

In the extended closure case it has been assumed that the access tunnels at repository depth are filled with bentonite (K=1×10^{-10} m/s). Other repository materials have the hydraulic conductivities assigned in the base case (see Figure 6-1).

Location 300_4

Table 6-4 shows that the computed flows through vaults and waste control volumes are approximately the same as for the base case.

Table 6-4. Total flow through the BHA and BHK vaults and waste domains (m3/year) for the base case and extended closure at location 300_4. The ratio is calculated with respect to the base case.

	Base case	Extended closure	Ratio
Flow control volume	**Total flow (m^3/yr)**	**Total flow (m^3/yr)**	**Total flow (m^3/yr)**
BHA vault	4.27E−01	4.26E−01	1.00
BHA_1 waste	9.60E−02	8.99E−02	0.94
BHA_2 waste	8.61E−02	8.41E−02	0.98
BHA_3 waste	1.09E−01	1.14E−01	1.04
BHA_4 waste	1.55E−01	1.57E−01	1.01
BHA_5 waste	1.38E−01	1.39E−01	1.01
BHK vault	4.66E+00	4.75E+00	1.02
BHK_1 waste	4.50E−01	4.63E−01	1.03
BHK_2 waste	4.98E−01	5.04E−01	1.01
BHK_3 waste	5.86E−01	5.93E−01	1.01
BHK_4 waste	6.46E−01	6.53E−01	1.01
BHK_5 waste	6.71E−01	6.80E−01	1.01
BHK_6 waste	6.41E−01	6.52E−01	1.02

In the base case, the access tunnels act as preferential flow paths redistributing the horizontal flow, while in the extended closure case they act as a flow barriers (Figure 6-6). However, groundwater flow at domain 300_4 is mainly vertical (see Section 3.2.4) and therefore, the repository sensitivity to the extended sealing is minimal.

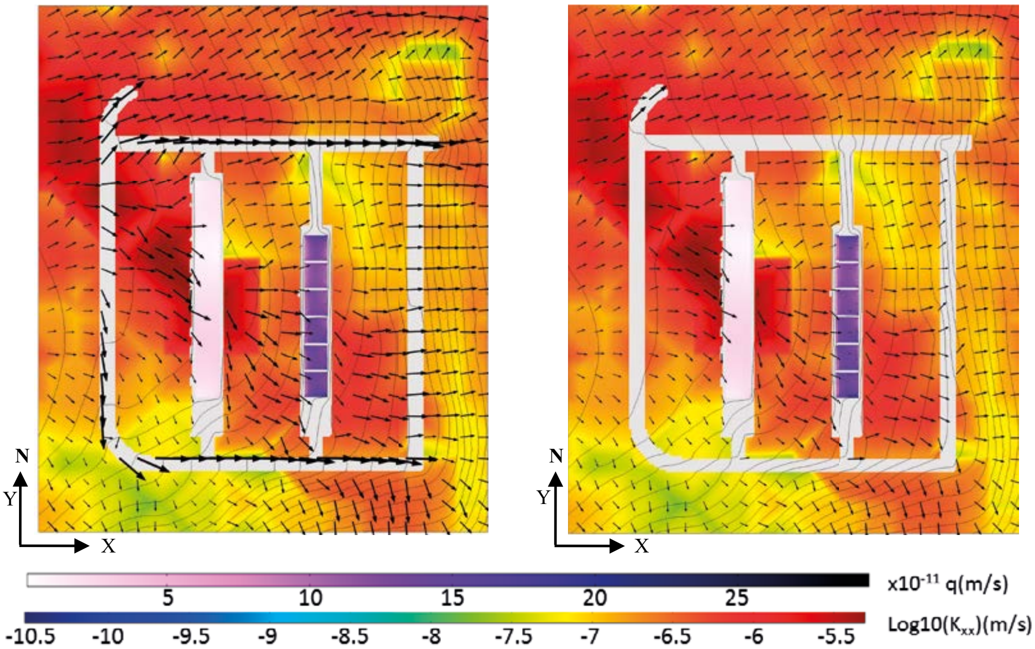

Figure 6-6. *Magnitude of the Darcy velocity through the waste control volumes (displayed only within the waste domain), hydraulic conductivity of the rock (displayed only in the rock domain), hydraulic head (isolines) and Darcy velocity (arrows) at location 300_4 for the base case (left) and the extended closure case (right).*

Location 500_4

At location 500_4, the extended closure increases the groundwater flow by 13–25% for BHA and by 6–13% for BHK (Table 6-5).

Table 6-5. Total flow through the BHA and BHK vaults and waste domains (m3/year) for the base case and extended closure case at location 500_4. The ratio is calculated with respect to the base case.

	Base case	Extended closure	Ratio
Flow control volume	Total flow (m^3/yr)	Total flow (m^3/yr)	Total flow (m^3/yr)
BHA vault	8.42E−01	9.70E−01	1.15
BHA_1 waste	1.94E−01	2.20E−01	1.13
BHA_2 waste	3.06E−01	3.61E−01	1.18
BHA_3 waste	4.14E−01	5.04E−01	1.22
BHA_4 waste	5.37E−01	6.54E−01	1.22
BHA_5 waste	4.04E−01	5.06E−01	1.25
BHK vault	3.29E+00	3.60E+00	1.09
BHK_1 waste	3.25E−01	3.46E−01	1.07
BHK_2 waste	3.32E−01	3.52E−01	1.06
BHK_3 waste	3.25E−01	3.51E−01	1.08
BHK_4 waste	2.97E−01	3.30E−01	1.11
BHK_5 waste	3.28E−01	3.70E−01	1.13
BHK_6 waste	3.60E−01	4.09E−01	1.14

Figure 6-7 shows the redistribution of flow at repository depth due to the extended bentonite sealing. The arrow size in the plots, proportional to the magnitude of the Darcy velocity, illustrates lower flows in the sealed tunnels but higher flows in the central rock domain and repository vaults. At location 500_4, the groundwater flow is mainly horizontal at repository depth (see Section 3.4.4). This explains the more notable effects of the extended closure, as compared to the 300_4 location.

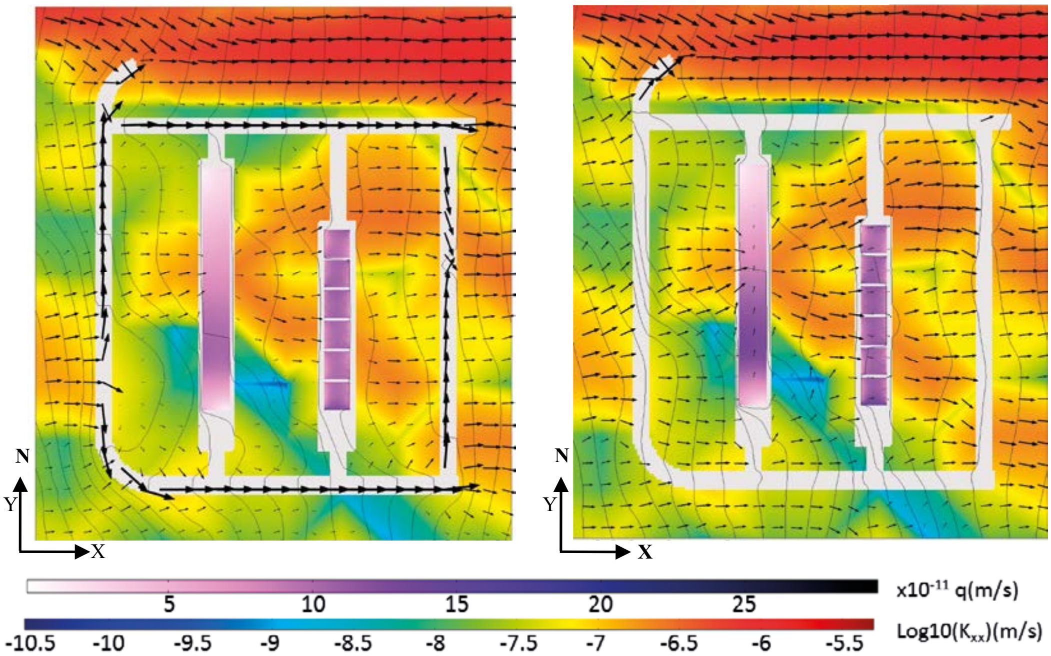

Figure 6-7. *Magnitude of the Darcy velocity through the waste control volumes (displayed only within the waste domain), hydraulic conductivity of the rock (displayed only in the rock domain), hydraulic head (isolines) and Darcy velocity (arrows) at location 500_4 for the base case (left) and the extended closure case (right).*

Location 700_1

Location 700_1 is characterized by horizontal flow and a saline stratification at repository depth. Here, the extended closure leads to an increase in flow through the vaults and waste (Table 6-6). The relative increase in flow through the vault is higher in the BHK (95%) than in the BHA (26%). The flow through the waste follows the same trend, with the largest increase (up to 233%) in the BHK southernmost waste control volumes. These control volumes are affected by deformation zone D11_Z1. Nevertheless, the flow through the BHK waste remains one order of magnitude smaller than the corresponding flow through the BHA.

Table 6-6. Total flow through the BHA and BHK vaults and waste domains (m3/year) for the base case and extended closure case at domain 700_1. The ratio is calculated with respect to the base case.

	Base case	Extended closure	Ratio
Flow control volume	**Total flow (m^3/yr)**	**Total flow (m^3/yr)**	**Total flow (m^3/yr)**
BHA vault	6.71E−01	8.49E−01	1.27
BHA_1 waste	3.17E−01	4.43E−01	1.40
BHA_2 waste	5.56E−01	7.15E−01	1.29
BHA_3 waste	6.19E−01	7.84E−01	1.27
BHA_4 waste	5.90E−01	7.48E−01	1.27
BHA_5 waste	3.24E−01	4.14E−01	1.28
BHK vault	1.10E−01	2.15E−01	1.95
BHK_1 waste	3.38E−02	4.58E−02	1.35
BHK_2 waste	3.67E−02	4.63E−02	1.26
BHK_3 waste	3.07E−02	5.04E−02	1.64
BHK_4 waste	2.63E−02	5.93E−02	2.26
BHK_5 waste	1.74E−02	4.79E−02	2.76
BHK_6 waste	9.11E−03	3.03E−02	3.33

Figure 6-8 illustrates how the access tunnels redirect the flow from east to west in the base case. Most of the velocity arrows are directed towards the access tunnels and the hydraulic head isolines show a draining effect of the access tunnels in the east part of the repository. In the extended closure case, groundwater flow near the repository increases. The hydraulic conductivity values for the rock at 700_1 are similar to the hydraulic conductivity of the closure bentonite (1×10^{-10} m/s). Therefore, flow is controlled by the more permeable deformation zones.

6.3 Summary

For the investigated closure alternative with no plugs in the shaft and ramp, inflow boundary conditions replace the no flow conditions set for the base case. The average Darcy velocities evaluated in the rock domain have been used as a guide to assign inflow velocities in the ramp and shaft. At locations 300_4 and 500_4, no significant effect is observed on the flow through vaults or waste. At location 700_1, changes in the local flow and the salinity at repository level can be observed, primarily affecting the flow through the BHK vault and waste.

In the extended closure case the access tunnels at the repository level are assumed to be filled with bentonite. At location 300_4 the groundwater flow is mainly vertical. In such a regime the effect on the flow through the vaults and waste is small, comparing to the base case. At locations 500_4 and 700_1 the groundwater flow is mainly horizontal. In such instances the flow through vaults and waste increases, as compared to the base case. In the base case the access tunnels redirect water past the repository vaults. When sealing off the access tunnels with bentonite, groundwater is concentrated to high permeability zones of the rock, increasing the flow near the vaults.

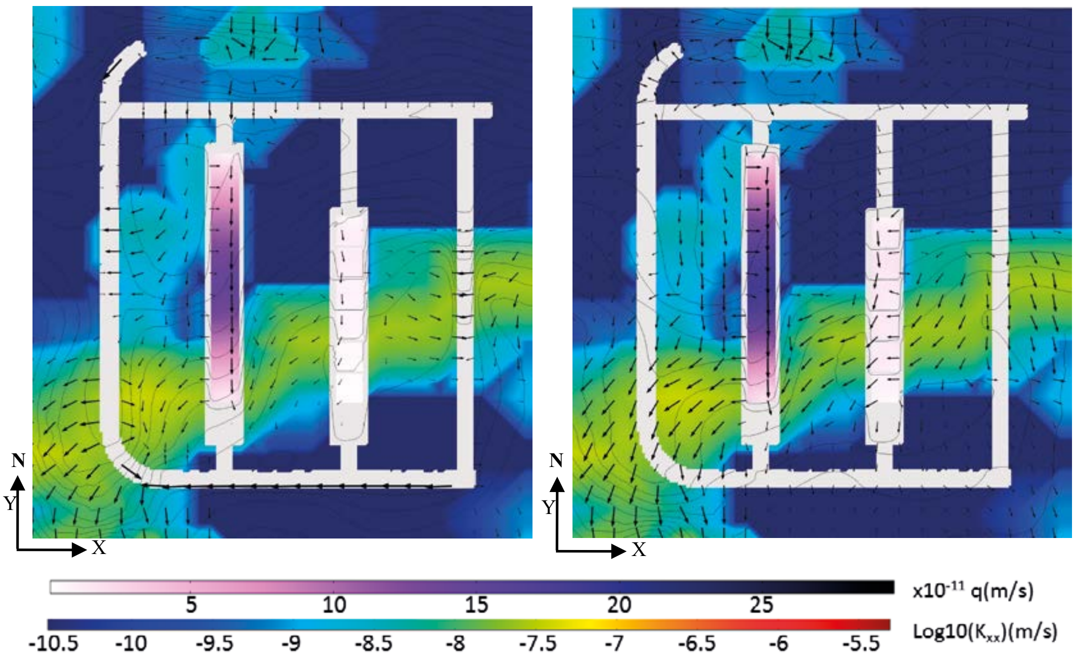

Figure 6-8. *Magnitude of the Darcy velocity through the waste control volumes (displayed only within the waste domain), hydraulic conductivity of the rock (displayed only in the rock domain), hydraulic head (isolines) and Darcy velocity (arrows) at location 700_1 for the base case (left) and the extended closure case (right).*

References

SKB's (Svensk Kärnbränslehantering AB) publications can be found at www.skb.se/publications.

Abarca E, Idiart A, de Vries L M, Silva O, Molinero J, von Schenck H, 2013. Flow modelling on the repository scale for the safety assessment SR-PSU. SKB TR-13-08, Svensk Kärnbränslehantering AB.

COMSOL, 2013. COMSOL Subsurface flow module v 5.0. COMSOL AB, Stockholm, Sweden.

Elfwing M, Evins L Z, Gontier M, Grahm P, Mårtensson P, Tunbrant S, 2013. SFL concept study. Main report. SKB TR-13-14, Svensk Kärnbränslehantering AB.

Gelhar L W, Axness C L, 1983. Three-dimensional stochastic analysis of macrodispersion in aquifers. Water Resources Research 19, 161–180.

Gelhar L W, Welty C, Rehfeldt K R, 1992. A critical review of data on field-scale dispersion in aquifers. Water Resources Research 28, 1955–1974.

Nardi A, Idiart A, Trinchero P, de Vries L.M. and Molinero J, 2014. Interface COMSOL-PHREEQC (iCP), an efficient numerical framework for the solution of coupled multiphysics and geochemistry. Computers & Geosciences 69, 10–21.

Rhén I, Hartley L, 2009. Bedrock hydrogeology Laxemar. Site descriptive modelling, SDM-Site Laxemar. SKB R-08-92, Svensk Kärnbränslehantering AB.

Rhén I, Forsmark T, Hartley L, Jackson C P, Roberts D, Swan D, Gylling B, 2008. Hydrogeological conceptualisation and parameterisation. Site descriptive modelling, SDM-Site Laxemar. SKB R-08-78, Svensk Kärnbränslehantering AB.

Rhén I, Forsmark T, Hartley L, Joyce S, Roberts D, Gylling B, Marsic N, 2009. Bedrock hydrogeolology. Model testing and synthesis. Site descriptive modelling, SDM-Site Laxemar. SKB R-08-91, Svensk Kärnbränslehantering AB.

SKB, 2001. Project SAFE. Compilation of data for radionuclide transport analysis. SKB R-01-14, Svensk Kärnbränslehantering AB.

SKB, 2010. Buffer, backfill and closure process report for the safety assessment SR-Site. SKB TR-10-47, Svensk Kärnbränslehantering AB.

SKB, 2011. Site selection – siting of the final repository for spent nuclear fuel. SKB R-11-07, Svensk Kärnbränslehantering AB.

SKB, 2014. Data report for the safety assessment SR-PSU. SKB TR-14-10, Svensk Kärnbränslehantering AB.

Svensson U, 2010. DarcyTools, version 3.4. Verification, validation and demonstration. SKB R-10-71, Svensk Kärnbränslehantering AB.

Svensson U, Ferry M, 2010. Darcy Tools version 3.4. User's guide. SKB R-10-72, Svensk Kärnbränslehantering AB.

Vidstrand P, Rhén I, Zugec N, 2010. Groundwater flow modelling of periods with periglacial and glacial climate conditions – Laxemar. SKB R-09-25, Svensk Kärnbränslehantering AB.

Appendix A

Consistent coupling of regional and near-field flow models

The model for the groundwater flow in the near-field is coupled to a model for the regional flow that is set up and solved using the software DarcyTools (Svensson and Ferry 2010, Svensson 2010). The regional flow model supplies the repository-scale model with pressure boundary conditions, initial conditions, as well as the hydraulic conductivity field of the bedrock.

The near-field model in COMSOL and far-field model in DarcyTools are connected by means of the iDC interface (Abarca et al. 2013). A benchmark exercise is presented here to illustrate that the models have been consistently coupled.

A common model geometry shared by DarcyTools and COMSOL has been created based on the undisturbed 300_1 rock domain (see Section 3.1). An inner box has been included for post processing purposes. The dimensions of the inner box were set to $350 \times 350 \times 32\ m^3$ and with a position defined by X_{min} = 7,975 m, Y_{min} = 7,075 m, Z_{min} = −320 m. A representation of the COMSOL model domain is shown in Figure A-1.

The steady-state groundwater flow has been computed using the driving pressure boundary conditions and hydraulic conductivity field of the bedrock, taken from the regional flow model. The outflowing groundwater has been computed for the inner box according to:

$$Q_{box,out} = \sum \iint_{(\vec{q}\cdot\vec{n})>0} \vec{q} \cdot \vec{n} \qquad \text{(A-1)}$$

and the inflow as:

$$Q_{box,in} = \sum \iint_{(\vec{q}\cdot\vec{n})>0} \vec{q} \cdot \vec{n} \qquad \text{(A-2)}$$

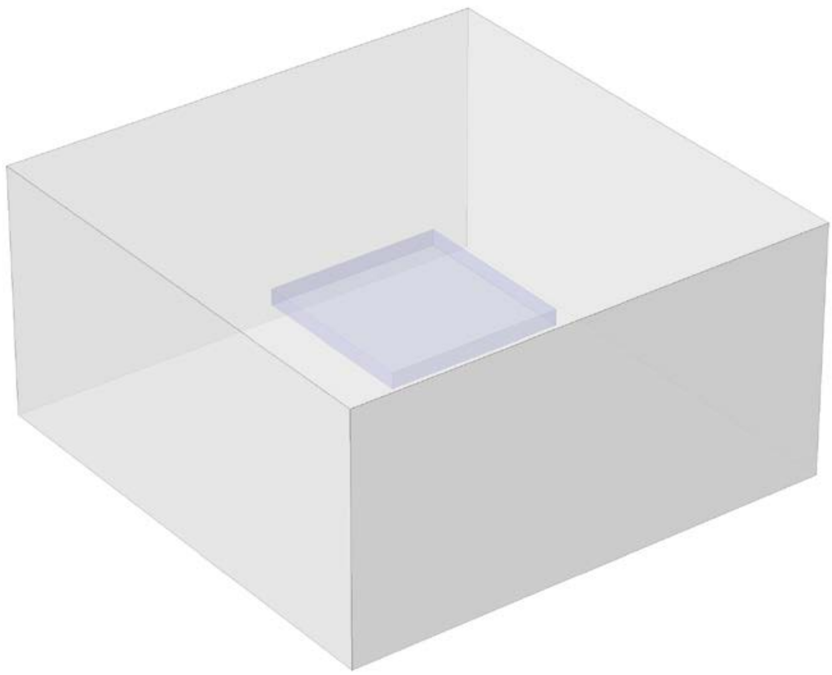

Figure A-1. *Model domain for validation test as represented in COMSOL. The inner blue box indicates the location of the surfaces where normal fluxes have been evaluated.*

The same calculation has also been carried out using DarcyTools. In DarcyTools, a patch of coordinates x_{min}= 7,975.0, x_{max}= 8,325.0, y_{min}=7,075.0, y_{max}= 7,425.0, z_{min}= −300, z_{max}= −300.0 has been defined to delimit the control volume for computing the incoming flow. The patch property gathers all cells intersecting with the defined plane. Due to the method of assignment, there is some uncertainty in the final dimensions of the control volume. The volume depends on the size of all the cells intersected by the plane, which can vary in with location. The volume can be approximated to $350 \times 350 \times 32$ m^3. The computed flows across this control volume are presented in Table A-1 and compared with the flows calculated for the control volume in COMSOL.

Table A-1. Comparison between the groundwater flow values calculated with COMSOL and DarcyTools at the same location.

	Outflow (m^3/s)	Inflow (m^3/s)	Mass balance error
COMSOL	3.02E−05	3.04E−05	0.5%
DarcyTools	2.59E−05	2.59E−05	0.0%
Difference	4.30E−05	4.50E−06	

The mass balance closing errors are small for both COMSOL and DarcyTools models. The difference in the computed inflow between the COMSOL and DarcyTools models is 17%. This discrepancy can be attributed to difference in dimension between the COMSOL and DarcyTools control volumes.

Results confirm that the COMSOL model, taking boundary conditions and property fields from the regional DarcyTools model, can reproduce the groundwater flow in the near-field.

Appendix B

Determination of near-field model domain size

Models of the SFL near-field hydrology receive their boundary conditions from regional hydrogeological models. The near-field model domain should be large enough such that changes in hydraulic properties of repository materials have negligible effect on the imposed boundary conditions. The aim of the calculations presented here is to determine the domain size for the SFL near-field model, adequate for all investigated locations.

Calculations have been performed to evaluate the radius of influence on local groundwater flow due to the presence of a schematic repository structure in the host rock. In theory, the radius of influence of a pressure perturbation in the subsurface tends to infinity. In practice, a cut-off value is defined below which the pressure perturbation is assumed to be negligible. The cut-off value is used to define the necessary distance between the repository and the boundaries of the near-field model. To ensure the validity of the cut-off value, the pressure boundary conditions of the near-field model are perturbed around the proposed cut-off value and the impact in the flow through the repository is assessed. The described procedure is followed here.

Calculation cases

Hydrogeological simulations have been performed using DarcyTools (Svensson and Ferry 2010, Svensson 2010), which is a computer code for the simulation of flow and transport in porous and/or fractured media. The calculations present a recapture of the Laxemar SR-Site model for periglacial and glacial conditions (Vidstrand et al. 2010), assessed for present day conditions. The SR-Site model has been updated to run with DarcyTools version v3.5. In addition, a finer discretisation between 600 and 800 metres of depth has been created.

SFL has been represented by a rectangular block of volume $350 \times 350 \times 32$ m^3. This volume is sufficient to enclose the repository at the depth of the rock vaults, irrespective of their orientation. A homogeneous hydraulic conductivity has been assigned to the block. In the simulations, the repository volume has been placed at depths of 300 m, 500 m and 700 m in each of rock domains 1 and 4 (see Section 2.2).

For each repository location, groundwater flows have been calculated for two cases, with different values of hydraulic conductivity assigned to the repository volume. The results have been compared with reference calculations where the rock has remained undisturbed also in the repository volume.

Each model is identified by a name/ID of the form "*depth_j_str*", where:

- *depth* is an integer value that specifies the approximate depth of the repository (i.e. 300, 500 or 700 m depth),
- *j* is a categorical variable that can take on two values (1 or 4) that identify the repository location,
- *str* is a string equal to "lp" or "hp". The string "lp" refers to a "low permeability" case, where the repository volume is assigned an isotropic hydraulic conductivity of 10^{-12} m/s. The string "hp" refers to a "high permeability" case, where the repository volume is assigned an isotropic hydraulic conductivity of 10^{-3} m/s.

The values for hydraulic conductivity in the original model have been modified in PROPGEN by looping over all the cell-walls of the domain. The model, with modified hydraulic properties, has then been restarted and run until new steady-state conditions were reached.

The location of the repository volumes at each depth are shown in Figure B-1 through Figure B-3, below.

Volumetric flow

The simulations have been carried out under steady-state conditions with no source or sink terms present. Assuming that differences in density in the repository volume are small, then:

$$\nabla \cdot \boldsymbol{q} = 0 \quad \text{(B-1)}$$

where $\boldsymbol{q}$ (m/s) is the Darcy velocity. This equation states that the total inflow into the repository volume, Q_{in} (m^3/s), must be equal to the total outflow, Q_{out} (m^3/s). For each model, Q_{in} and Q_{out} have been computed and compared to the values obtained using the model with undisturbed rock properties.

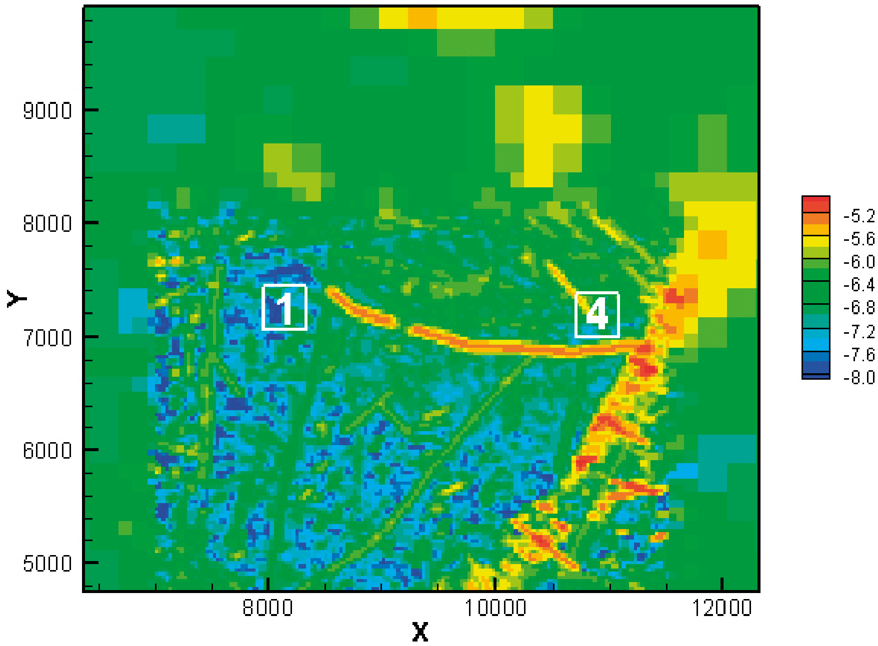

Figure B-1. *Logarithm of the hydraulic conductivity (K_{xx} (m/s)) in a cross section of the model at 300 m depth. Repository locations 300_1 and 300_4 are indicated.*

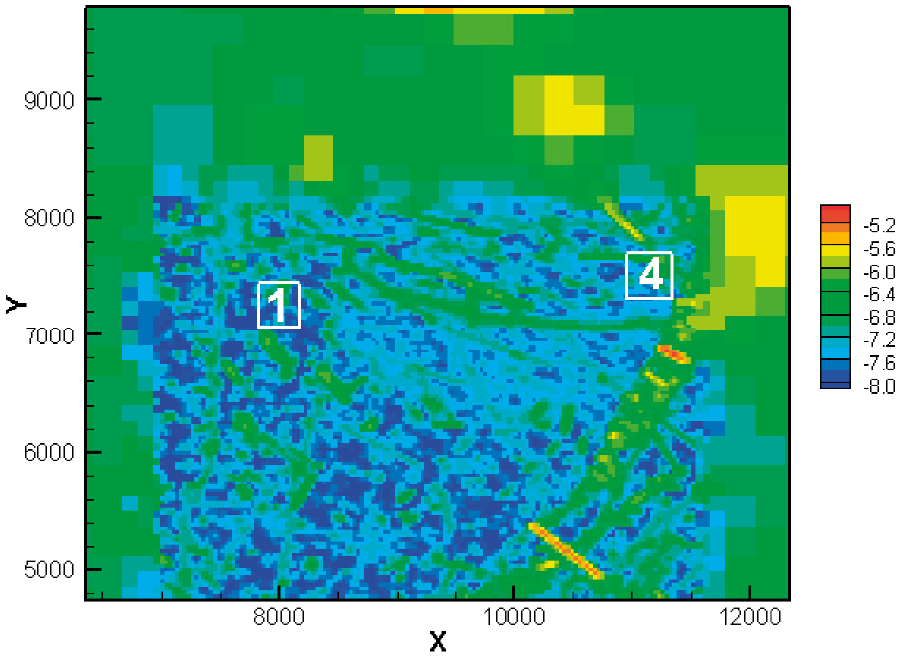

Figure B-2. *Logarithm of the hydraulic conductivity (K_{xx} (m/s)) in a cross section of the model at 500 m depth. Repository locations 500_1 and 500_4 are indicated.*

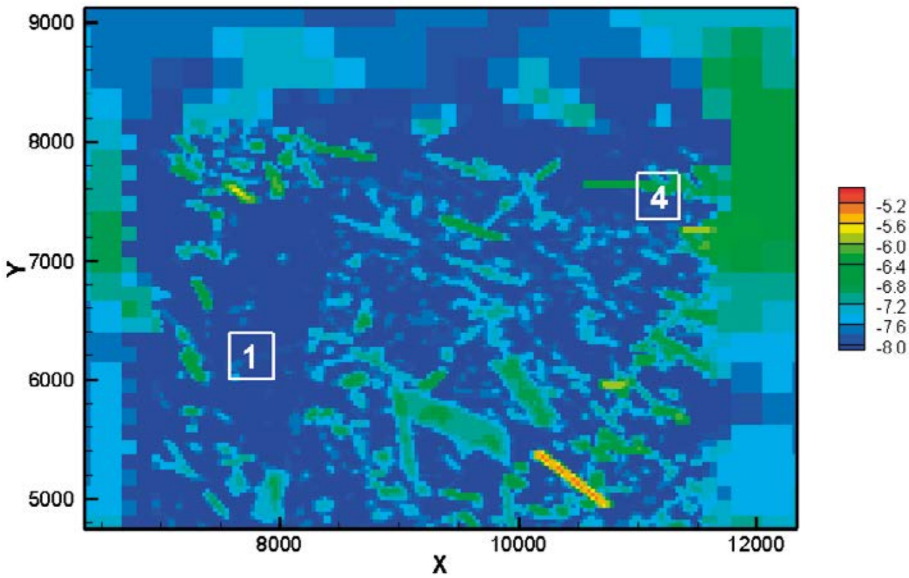

Figure B-3. *Logarithm of the hydraulic conductivity (K_{xx} (m/s)) in a cross section of the model at 700 m depth. Repository locations 700_1 and 700_4 are indicated.*

Table B-1 and Figure B-4 summarize the groundwater mass balances in the repository volumes. The difference between the inflow and outflow is the absolute mass balance error. The absolute error divided by the average between the inflow and the outflow is the relative mass balance error.

Table B-1. Total inflow into the repository volume (Qin), outflow from the repository volume (Qout) and computed differences.

Repository location	Model ID	Q_{in} (kg/s)	Q_{out} (kg/s)	$Q_{in} - Q_{out}$ (kg/s)
300_1	undisturbed	2.59×10^{-2}	2.59×10^{-2}	-3.82×10^{-8}
	300_1_hp	6.06×10^{-2}	6.06×10^{-2}	2.83×10^{-5}
	300_1_lp	5.74×10^{-3}	5.74×10^{-3}	-2.81×10^{-8}
300_4	undisturbed	2.79×10^{-1}	2.79×10^{-1}	-7.50×10^{-7}
	300_4_hp	6.78×10^{-1}	6.78×10^{-1}	1.90×10^{-5}
	300_4_lp	4.90×10^{-2}	4.90×10^{-2}	-1.63×10^{-6}
500_1	undisturbed	9.73×10^{-3}	9.73×10^{-3}	-1.17×10^{-7}
	500_1_hp	2.11×10^{-2}	2.11×10^{-2}	1.11×10^{-5}
	500_1_lp	3.00×10^{-3}	3.00×10^{-3}	-4.44×10^{-9}
500_4	undisturbed	1.39×10^{-2}	1.39×10^{-2}	9.00×10^{-9}
	500_4_hp	1.14×10^{-1}	1.15×10^{-1}	1.02×10^{-3}
	500_4_lp	3.39×10^{-3}	3.39×10^{-3}	-8.90×10^{-8}
700_1	undisturbed	3.05×10^{-4}	3.06×10^{-4}	3.30×10^{-7}
	700_1_hp*	2.08×10^{-3}	2.07×10^{-3}	-4.82×10^{-6}
	700_1_lp	8.03×10^{-5}	8.03×10^{-5}	1.62×10^{-8}
700_4	undisturbed	1.58×10^{-2}	1.58×10^{-2}	-1.32×10^{-6}
	700_4_hp	2.96×10^{-2}	2.89×10^{-2}	-7.09×10^{-4}
	700_4_lp	4.65×10^{-3}	4.65×10^{-3}	1.05×10^{-7}

*hydraulic conductivity in the repository volume set equal to 10^{-5} m/s.

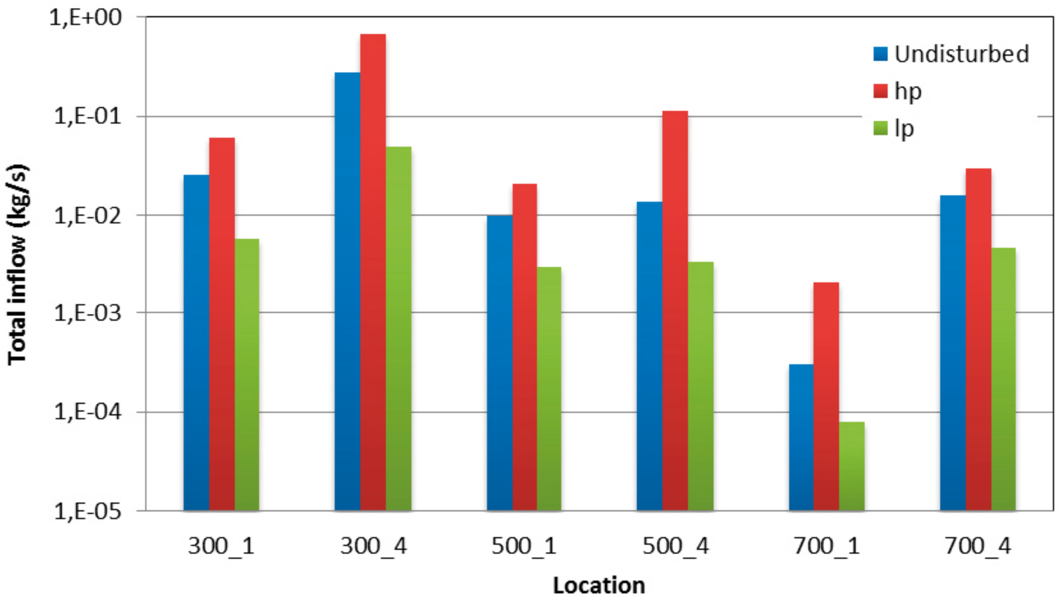

Figure B-4. *Total inflow into the repository volume for the undisturbed case, high permeability case (hp) and low permeability case (lp) for different locations.*

The computed relative mass balance errors are very small (<<1‰) for the undisturbed and all the "low permeability" models (*str*=lp). Relative errors of a few percent or less are observed for most of the "high permeability" models (*str*=hp). This is due to a greater permeability contrast between the repository volume and the surrounding bedrock. When the repository volume was located at 700 m depth, the permeability contrast along with the coarser mesh refinement used in the lower part of the model domain, caused convergence issues that decreased the accuracy of the calculations. To overcome these numerical problems, a hydraulic conductivity of 10^{-5} m/s was assigned to the repository volume for the 700_1_hp model.

When the repository volume is filled with high-permeability material, the total flow into and out of the volume increases by a factor of about 2, except for 500_4_hp, where the total flow is around one order of magnitude higher compared to the undisturbed flow. In contrast, the total flow computed for the different "lp" models is about 70–80% lower compared to the undisturbed flow.

Pressure perturbation and cut-off

In a groundwater flow model, a change of the hydraulic properties within the domain results in a perturbation of the computed state variable. When the change applies over a limited part of the domain, the spatial extent of the perturbation signature is likely to be limited as well. Here, the perturbation signature of each repository volume has been analyzed by computing the relative difference between the undisturbed and the disturbed pressure fields, according to:

$$p_{diff}(\boldsymbol{x}) = \frac{|p_{rep}(\boldsymbol{x}) - p_{nat}(\boldsymbol{x})|}{p_{nat}(\boldsymbol{x})} \cdot 100 \qquad \text{(B-2)}$$

The extent of the hydrogeological perturbation has been visualized by representing the spatial distribution of $p_{diff}(\boldsymbol{x})$ along representative cross sections.

Figure B-5 through Figure B-28 show contour plots of p_{diff} = 1%, 2%, 5% and 10%, computed for all locations. Results are plotted on a horizontal (*z=constant*) and a vertical (*y=constant*) cross section that pass through the middle of the repository volume (black lines). A domain of size of 1,000 × 1,000 × 500 m^3 is indicated by gray lines in the figures.

The pressure difference at the near-field boundaries (grey rectangle) is less than 5% for most cases. For some locations, the highly permeable repository case yield pressure differences slightly above 5% but never reaching the 10% difference. The extent of the 5% pressure perturbation zone for each case is provided in Table B-2.

Table B-2. Coordinates of boxes that enclose the 5% pressure difference isosurfaces (i.e. pdiff = 5%) of the different models. No values are specified for those models where pressure differences higher than 5% are not observed.

Model ID	x_{min}	y_{min}	z_{min}	x_{max}	y_{max}	z_{max}
300_1_hp	7,938	7,064	−351	8,344	7,446	−288
300_1_lp	–	–	–	–	–	–
300_4_hp	10,578	6,940	−605	11,279	7,479	−194
300_4_lp	10,770	7,033	−511	11,152	7,383	−255
500_1_hp	–	–	–	–	–	–
500_1_lp	–	–	–	–	–	–
500_4_hp	10,544	7,230	−830	11,535	7,829	−357
500_4_lp	10,994	7,354	−511	11,375	7,670	−451
700_1_hp	7,538	5,977	−799	7,918	6,390	−641
700_1_lp	–	–	–	–	–	–
700_4_hp	10,769	7,035	−791	11,657	7,827	−548
700_4_lp	10,962	7,160	−894	11,535	7,796	−641

The 5% pressure difference is assumed as the cut-off value to define the radius of influence of due to changes in hydraulic properties of repository materials. Based on the cut-off, a $1{,}000 \times 1{,}000 \times 500$ m^3 rock domain is proposed to be adequate for the near-field hydrogeological models at the investigated locations. Calculations to validate this selection are presented in the following section.

It should be noted that the repository volume in the current simulations (3.92×10^6 m^3) is considerably greater than the volume of the actual repository geometry (the repository vaults and access tunnels at deposition level total approximately 1.9×10^5 m^3). Therefore, it is expected that the hydraulic perturbation of the repository is conservatively estimated.

Validation

To check the validity of the near-field model domain size, a test has been performed for location 300_1. A model of dimensions $1{,}000 \times 1{,}000 \times 500$ m^3 has been set up in COMSOL. The DarcyTools model has supplied the pressure boundary conditions and the bedrock hydraulic conductivity field to the COMSOL model. An inner box of dimensions $350 \times 350 \times 32$ m^3 has been included for post processing purposes.

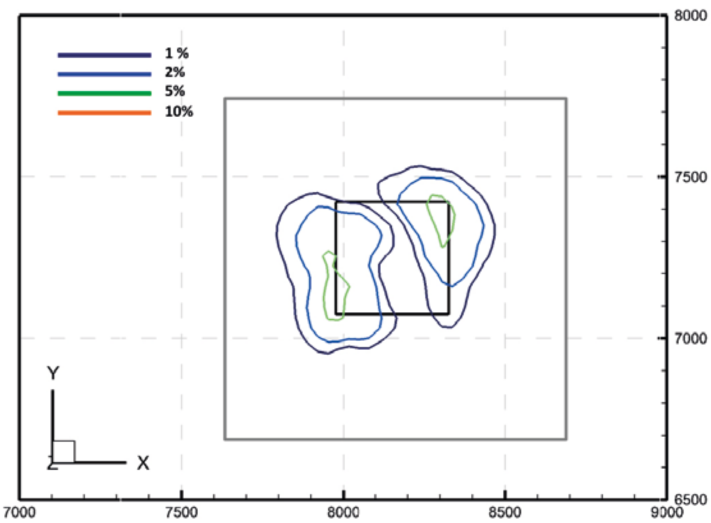

***Figure B-5.** Model 300_1_hp: isolines showing different values of $p_{diff}(x)$ along a horizontal cross section (z = −300 m). The size of the repository volume (black square) and of the related near-field nested domain (gray square) are also indicated. The 10% isoline does not appear in the graph because the maximum pressure difference is lower than 10%.*

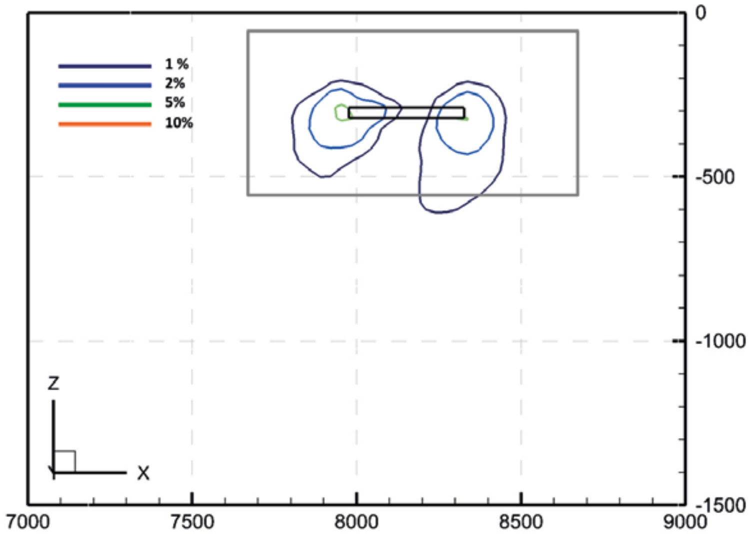

***Figure B-6.** Model 300_1_hp: isolines showing different values of $p_{diff}(x)$ along a vertical cross section (y = 7,256 m). The size of the repository volume (black rectangle) and of the related near-field nested domain (gray rectangle) are also indicated. The 10% isoline does not appear in the graph because the maximum pressure difference is lower than 10%.*

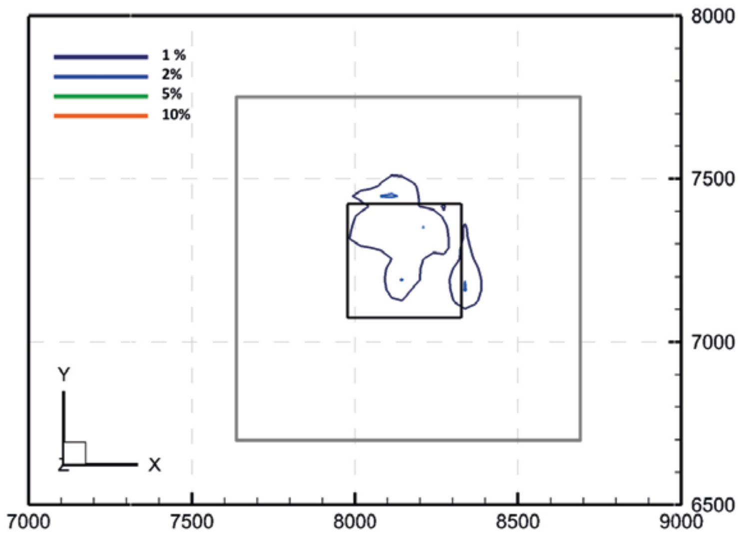

***Figure B-7.** Model 300_1_lp: isolines showing different values of p_{diff} along a horizontal cross section (z = −300 m). The size of the repository volume (black square) and of the related near-field nested domain (grey square) are also indicated.*

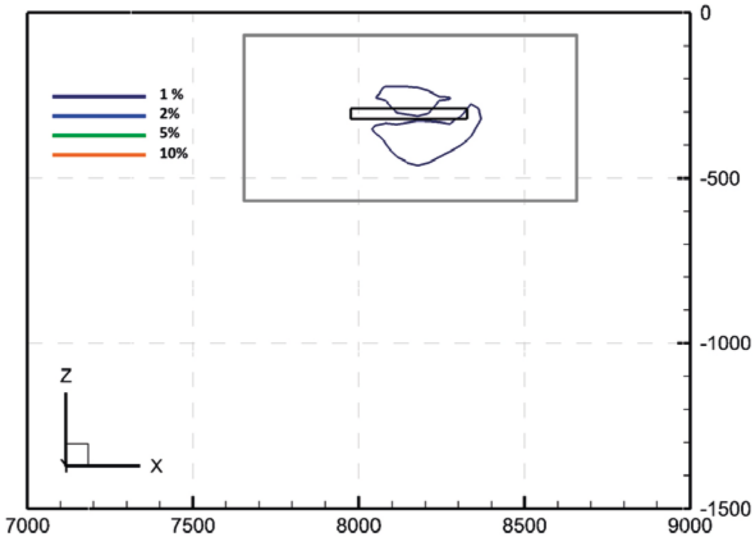

Figure B-8. *Model 300_1_lp: isolines showing different values of* p_{diff} *along a horizontal cross section (z = 7,256 m). The size of the repository volume (black rectangle) and of the related near-field nested domain (grey rectangle) are also indicated.*

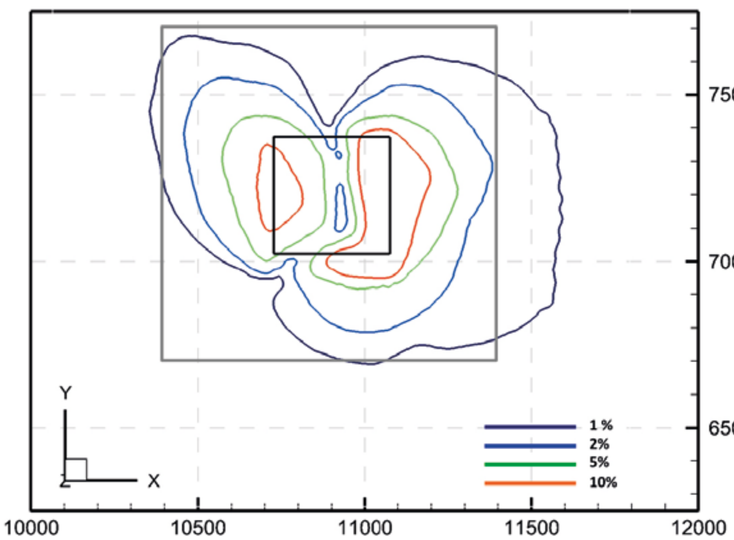

Figure B-9. *Model 300_4_hp: isolines showing different values of* p_{diff} *along a horizontal cross section (z = −300 m). The size of the repository volume (black square) and of the related near-field nested domain (grey square) are also indicated*

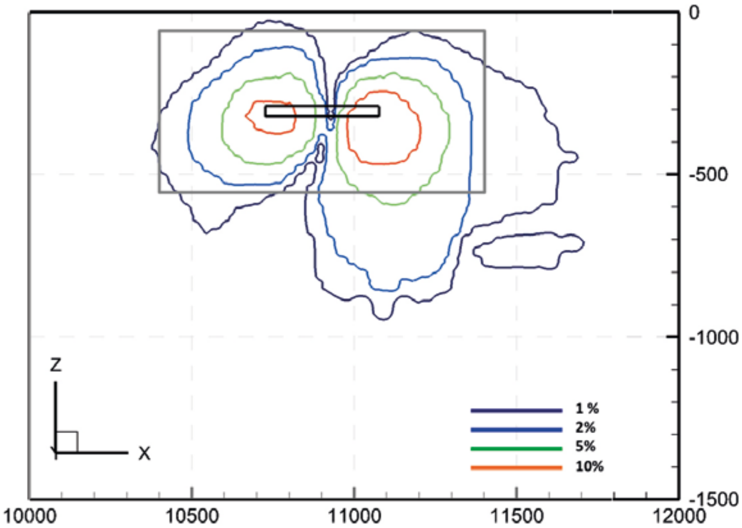

Figure B-10. *Model 300_4_hp: isolines showing different values of* p_{diff} *along a horizontal cross section (y = 7,192 m). The size of the repository volume (black rectangle) and of the related near-field nested domain (grey rectangle) are also indicated.*

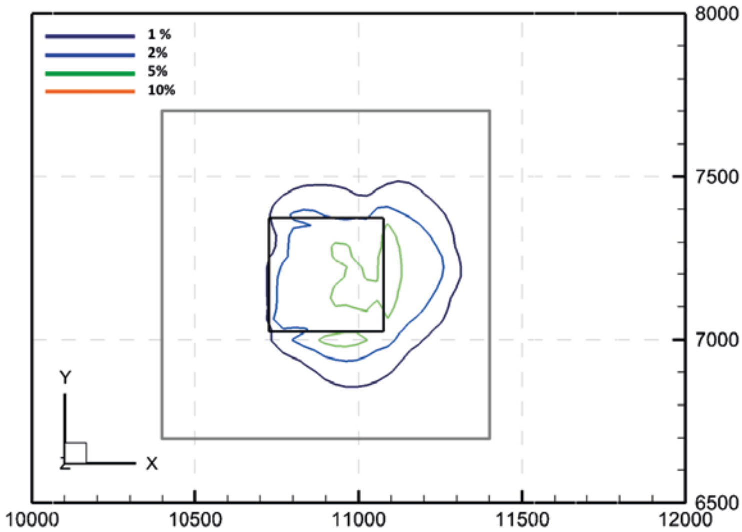

Figure B-11. *Model 300_4_lp: isolines showing different values of* p_{diff} *along a horizontal cross section (z = −300 m). The size of the repository volume (black square) and of the related near-field nested domain (grey square) are also indicated.*

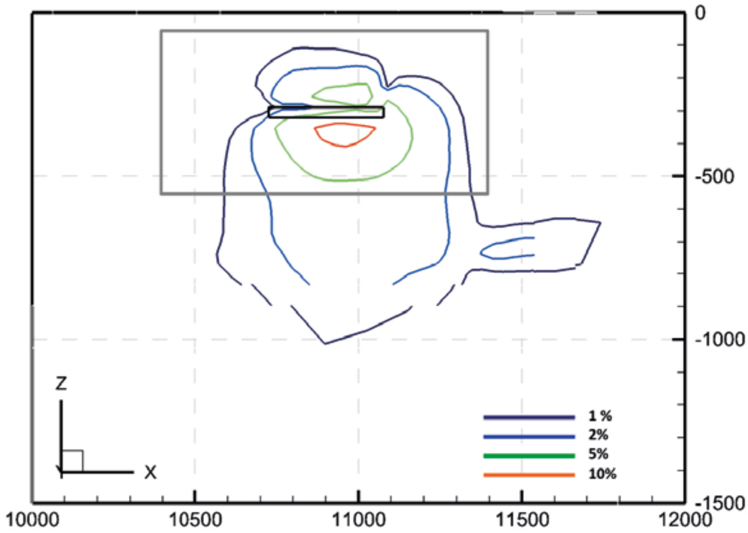

Figure B-12. *Model 300_4_lp: isolines showing different values of p_{diff} along a horizontal cross section (y = 7,192 m). The size of the repository volume (black rectangle) and of the related near-field nested domain (grey rectangle) are also indicated.*

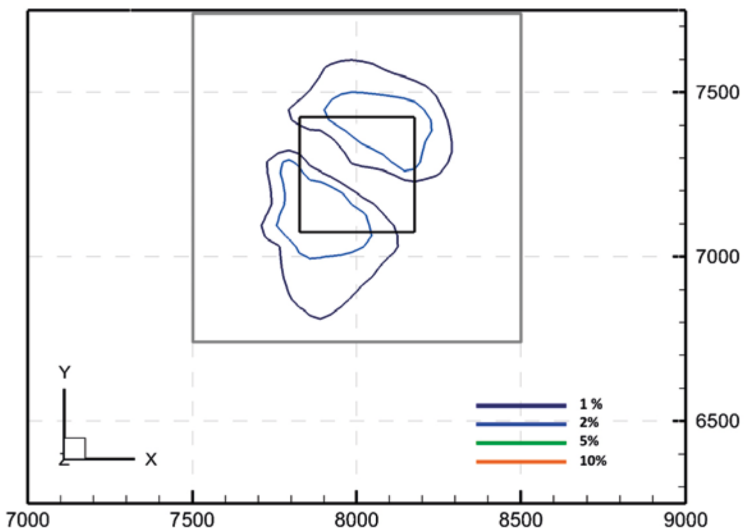

Figure B-13. *Model 500_1_hp: isolines showing different values of p_{diff} along a horizontal cross section (z = −500 m). The size of the repository volume (black square) and of the related near-field nested domain (grey square) are also indicated.*

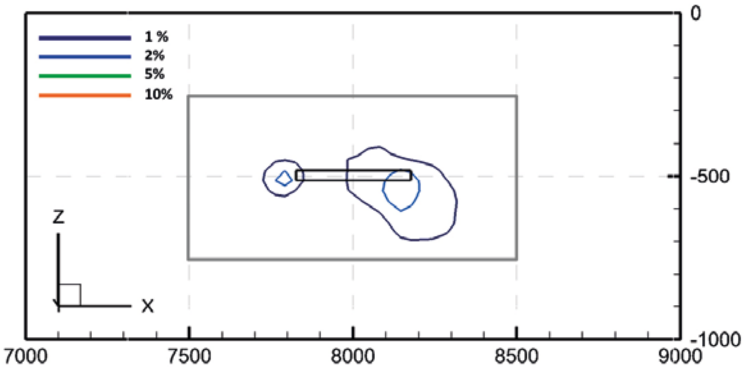

Figure B-14. *Model 500_1_hp: isolines showing different values of* p_{diff} *along a horizontal cross section (y = 7,288 m). The size of the repository volume (black rectangle) and of the related near-field nested domain (grey rectangle) are also indicated.*

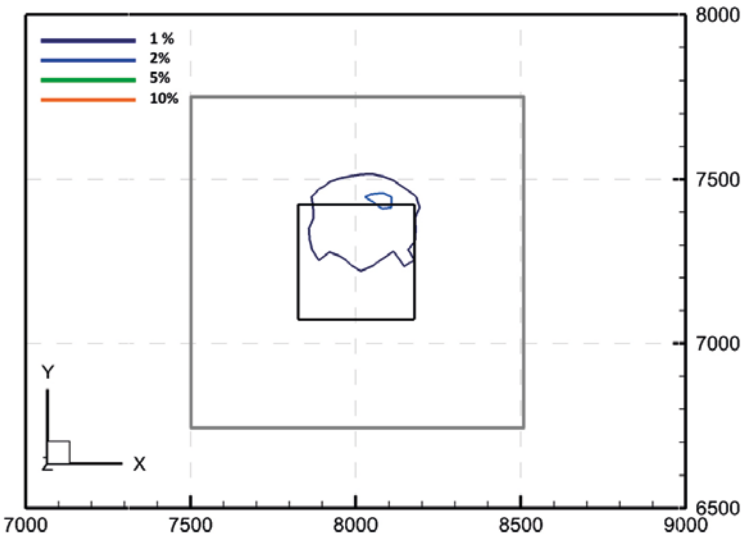

Figure B-15. *Model 500_1_lp: isolines showing different values of* p_{diff} *along a horizontal cross section (z = −500 m). The size of the repository volume (black square) and of the related near-field nested domain (grey square) are also indicated.*

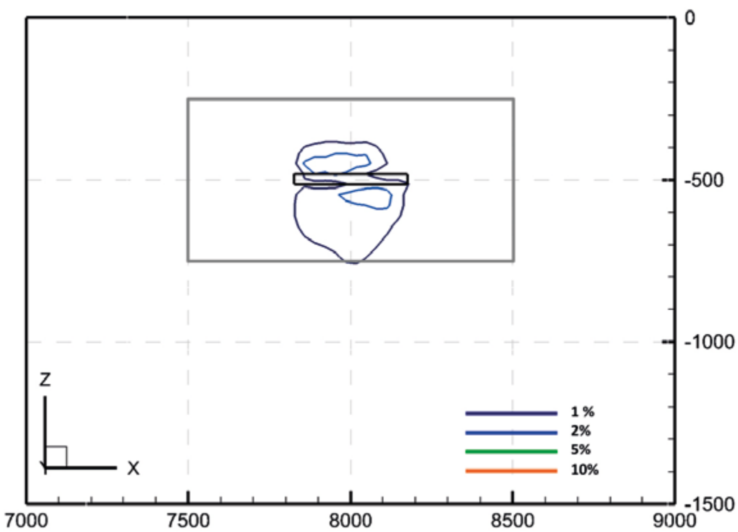

Figure B-16. *Model 500_1_lp: isolines showing different values of* p_{diff} *along a horizontal cross section (y = 7,288 m). The size of the repository volume (black rectangle) and of the related near-field nested domain (grey rectangle) are also indicated.*

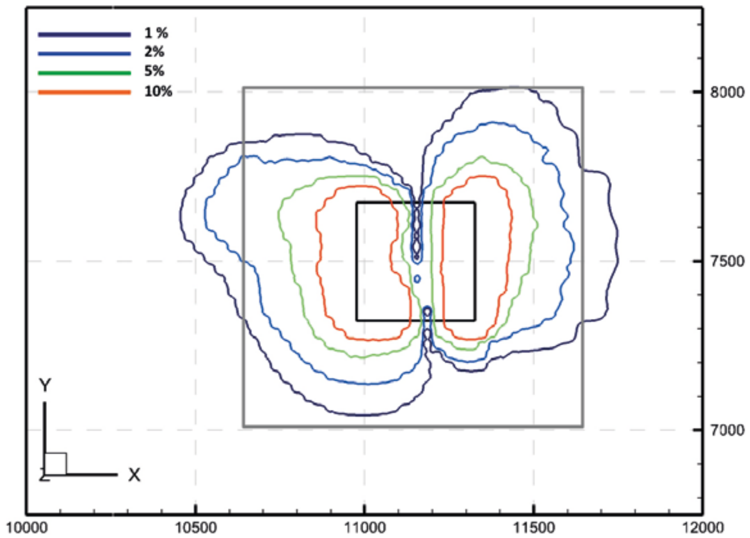

Figure B-17. Model 500_4_hp: isolines showing different values of p_{diff} along a horizontal cross section (z = −500 m). The size of the repository volume (black square) and of the related near-field nested domain (grey square) are also indicated.

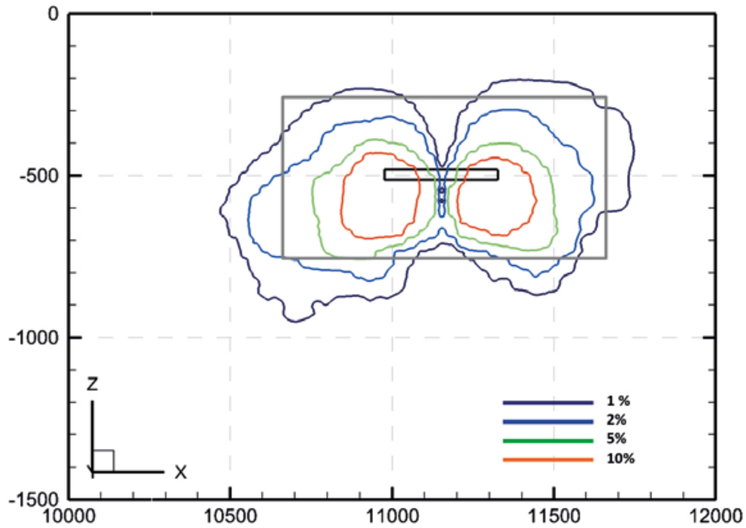

Figure B-18. Model 500_4_hp: isolines showing different values of p_{diff} along a horizontal cross section (y = 7,500 m). The size of the repository volume (black rectangle) and of the related near-field nested domain (grey rectangle) are also indicated.

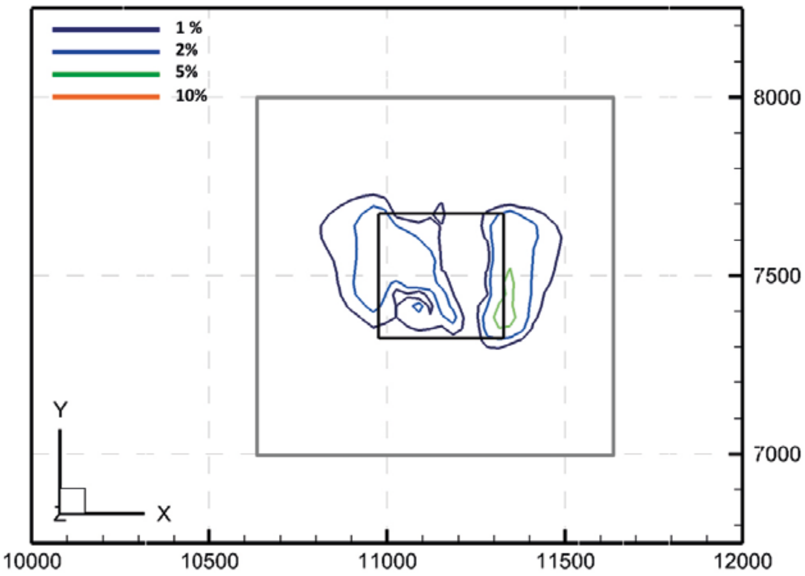

Figure B-19. *Model 500_4_lp: isolines showing different values of* p_{diff} *along a horizontal cross section (z = −500 m). The size of the repository volume (black square) and of the related near-field nested domain (grey square) are also indicated.*

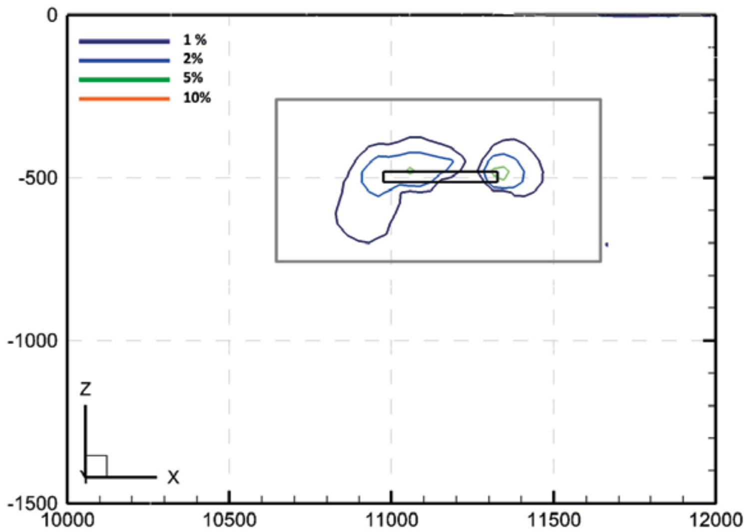

Figure B-20. *Model 500_4_lp: isolines showing different values of* p_{diff} *along a horizontal cross section (y = 7,500 m). The size of the repository volume (black rectangle) and of the related near-field nested domain (grey rectangle) are also indicated.*

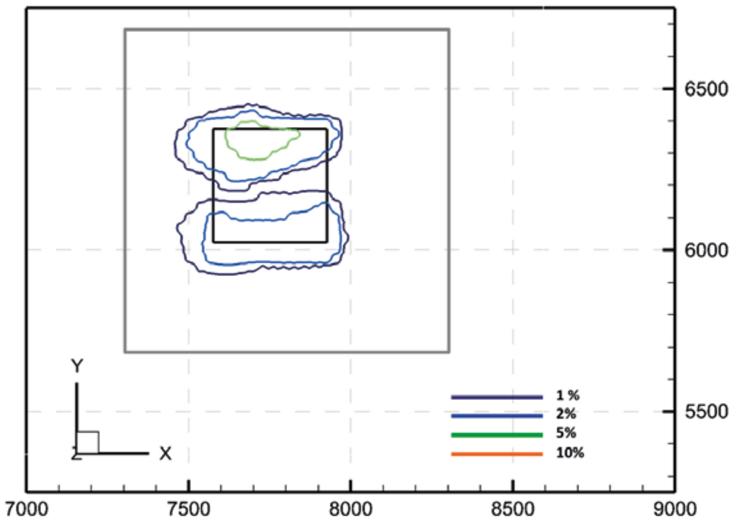

***Figure B-21.** Model 700_1_hp: isolines showing different values of p_{diff} along a horizontal cross section (z = −700 m). The size of the repository volume (black square) and of the related near-field nested domain (grey square) are also indicated*

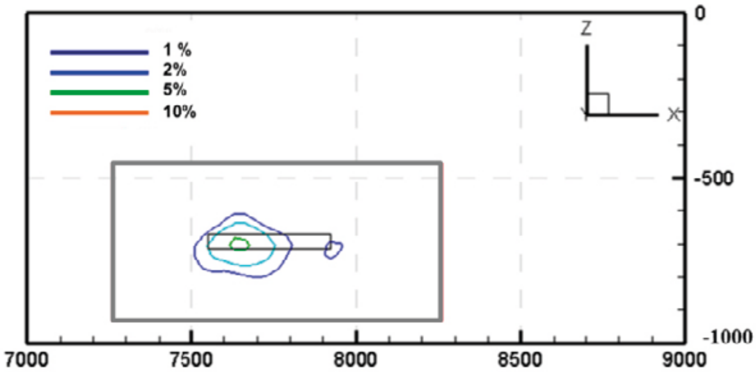

***Figure B-22.** Model 700_1_hp: isolines showing different values of p_{diff} along a horizontal cross section (y = 6,200 m). The size of the repository volume (black rectangle) and of the related near-field nested domain (grey rectangle) are also indicated.*

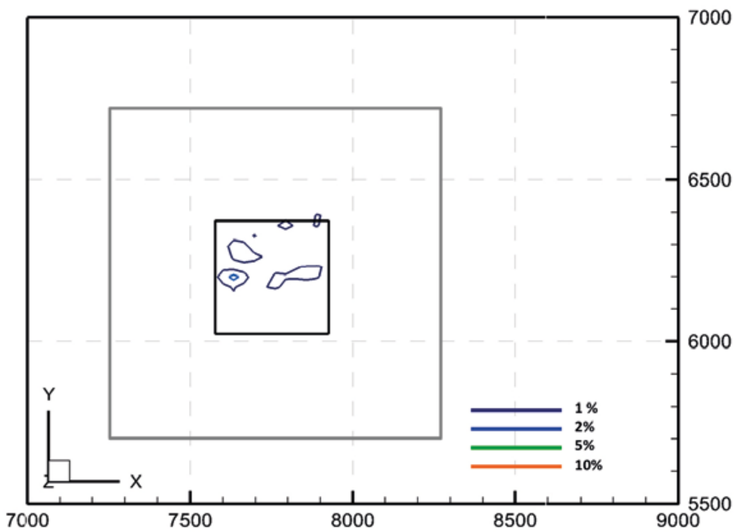

***Figure B-23.** Model 700_1_lp: isolines showing different values of p_{diff} along a horizontal cross section (z = −700 m). The size of the repository volume (black square) and of the related near-field nested domain (grey square) are also indicated.*

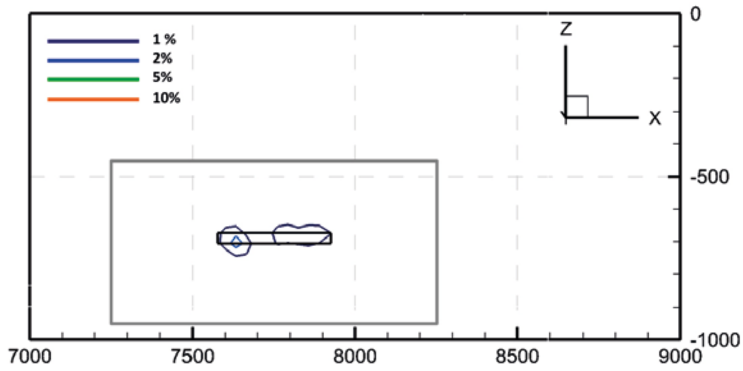

Figure B-24. *Model 700_1_lp: isolines showing different values of p_{diff} along a horizontal cross section (y = 6,200 m). The size of the repository volume (black rectangle) and of the related near-field nested domain (grey rectangle) are also indicated.*

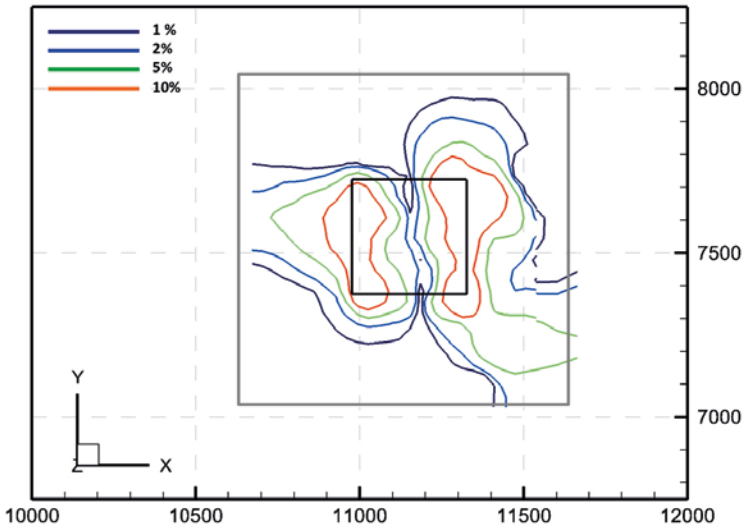

Figure B-25. *Model 700_4_hp: isolines showing different values of p_{diff} along a horizontal cross section (z = −700 m). The size of the repository volume (black square) and of the related near-field nested domain (grey square) are also indicated.*

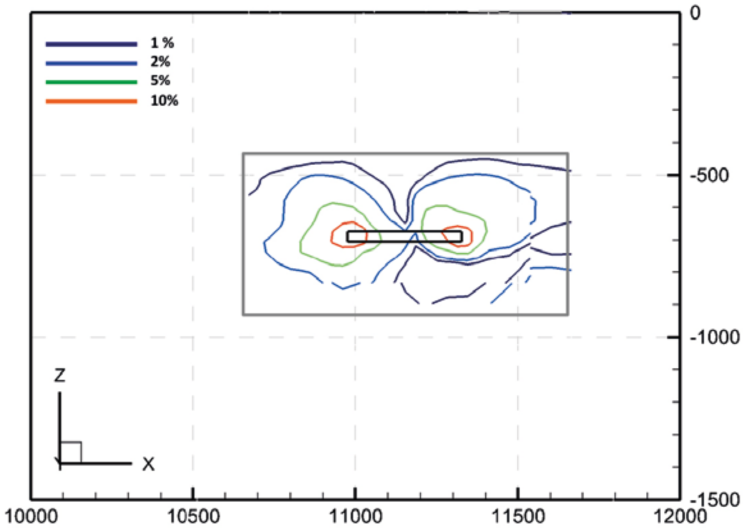

Figure B-26. *Model 700_4_hp: isolines showing different values of p_{diff} along a horizontal cross section (y = 7,500 m). The size of the repository volume (black rectangle) and of the related near-field nested domain (grey rectangle) are also indicated.*

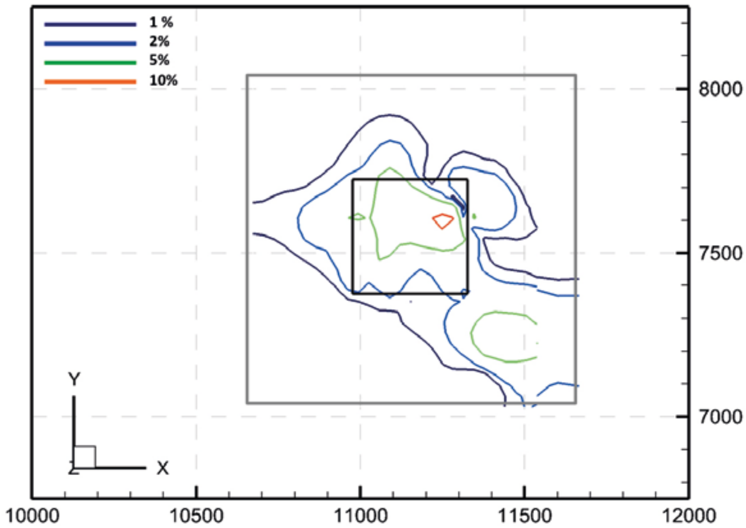

Figure B-27. *Model 700_4_lp: isolines showing different values of* p_{diff} *along a horizontal cross section (z = −700 m). The size of the repository volume (black square) and of the related near-field nested domain (grey square) are also indicated.*

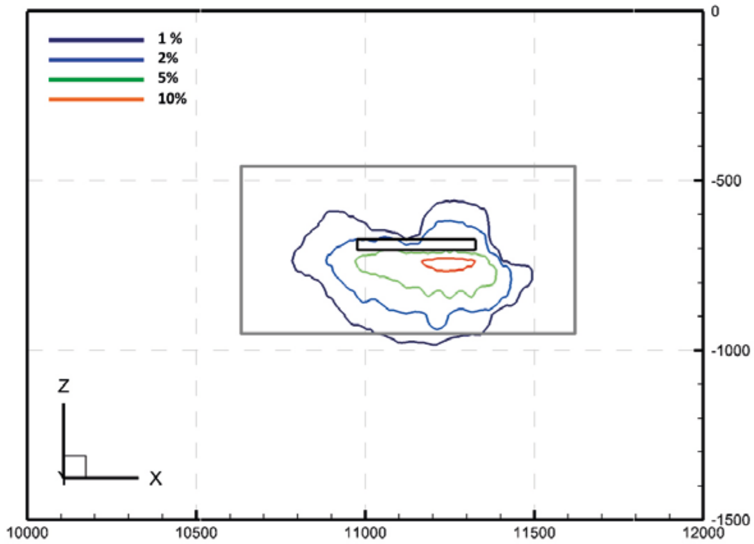

Figure B-28. *Model 700_4_lp: isolines showing different values of* p_{diff} *along a horizontal cross section (y = 7,500 m). The size of the repository volume (black rectangle) and of the related near-field nested domain (grey rectangle) are also indicated.*

Several steady-state groundwater flow simulations have been carried out where the prescribed pressure field at the model boundaries has been modified. The new pressure fields have been generated by perturbing the pressure field from the regional flow model according to the expression:

$$p' = (1 + rW)p_{DT} \qquad \text{(B-3)}$$

Above, p_{DT} is the original pressure field from the DarcyTools model, r is a random function ranging from 1 to −1 (see Figure B-30), and W is a perturbation factor. Five simulations were carried out, with W set to 0.01, 0.02, 0.05, 0.1 and 0.2. The maximum pressure difference at the boundary is $2W$.

The groundwater entering the model domain and the inner box has been calculated for the unperturbed case and the five increasingly perturbed cases (Table B-3). Results show a notable increase in the flow entering the model domain with increasing perturbation. Nevertheless, differences observed for the flow across the inner box are modest, even for a pressure perturbation of 20%.

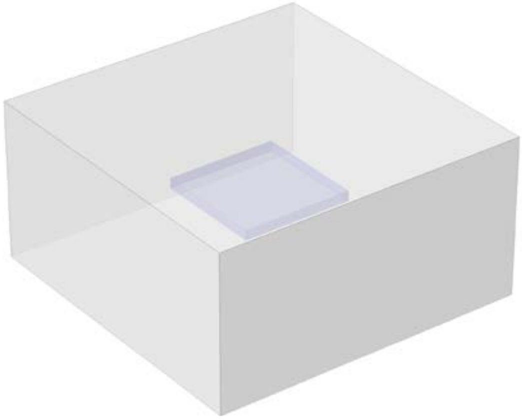

Figure B-29. Model domain for the validation test. The inner blue box indicates the location of the surfaces where fluxes have been evaluated.

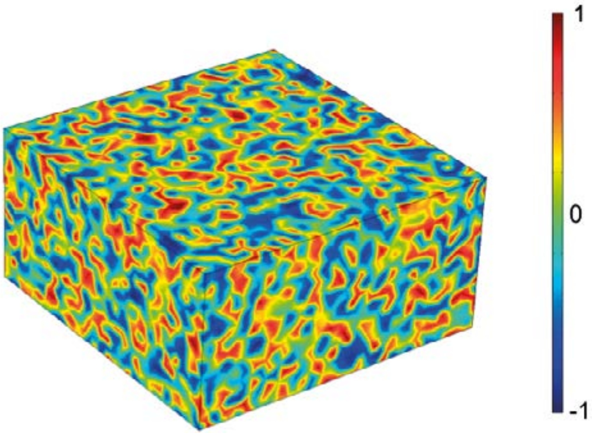

Figure B-30. Random function applied to perturb the pressure field at the boundary condition.

Table B-3. Flow entering the inner box and the model domain for increasingly perturbed pressure fields at the boundaries.

Perturbation factor	Flow (m^3/s)	
	Inner box	Model domain
Base Case	3.02E−05	3.44E−03
0.01	3.02E−05	3.70E−03
0.02	3.02E−05	4.20E−03
0.05	3.01E−05	6.30E−03
0.1	3.00E−05	1.05E−02
0.2	2.97E−05	1.97E−02

Figure B-31 shows the differences in the flow through the model domain, relative to the unperturbed case, as a function of the perturbation factor. Similarly, Figure B-32 shows the relative difference in the flow across the inner box. An increase in flow of almost 500% occurs in the model domain for a perturbation factor of 20%. However, this corresponds to a flow variation of less than 2% in the inner box.

The 5% pressure difference contours calculated with the DarcyTools model correspond to a perturbation factor of 0.05. This perturbation yields a maximum variation of flow in the outer model boundary of approximately 80% and of less than 0.4% in the inner box. This shows that the domain dimensions ($1,000 \times 1,000 \times 500$ m^3) are sufficient to prevent boundary effects when calculating groundwater flow through the repository.

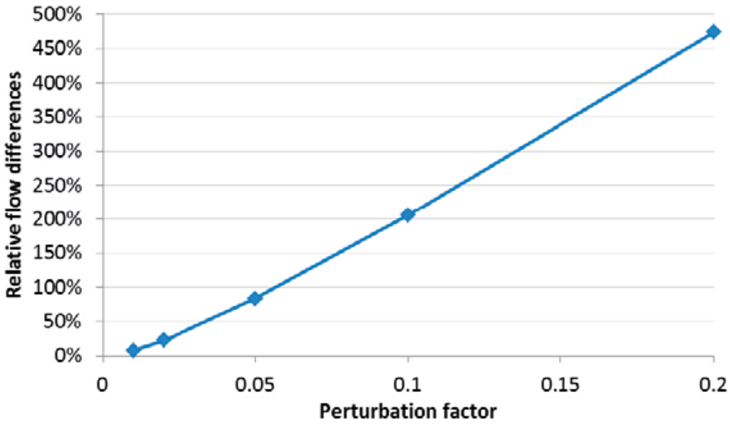

Figure B-31. *Differences in inflow through the model domain with respect to the base case.*

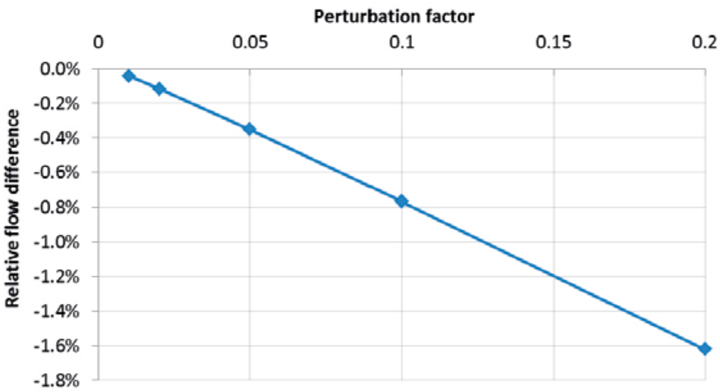

Figure B-32. *Differences in inflow through the inner box with respect to the base case.*

Appendix C

Model discretization

Near-field models are discretized by an unstructured mesh. The number of tetrahedral elements used for each model is given in Table C-1.

Table C-1. Number of tetrahedral elements discretising the model domain.

Model	Number of elements
300_1	1,650,798
500_1	1,650,538
700_1	1,786,736
300_4	1,650,424
500_4	1,650,906
700_4	1,652,146

Hydraulic conductivity of the host rock

The hydraulic conductivity of the rock in the near-field models is specified as a tensor field. The K_{xx} component has been chosen to illustrate representative conductivity values of the rock in several plots presented in this report. Maximum and minimum conductivity values for all tensor components and model domains are presented in Table C-2.

Table C-2. Components of the hydraulic conductivity tensor.

Model	(K_{xx}) m/s		(K_{yy}) m/s		(K_{zz}) m/s	
	Maximum	Minimum	Maximum	Minimum	Maximum	Minimum
300_1	6.92E−05	2.99E−11	6.87E−05	6.87E−05	6.38E−05	2.99E−11
500_1	9.81E−06	2.99E−11	9.81E−06	9.81E−06	9.81E−06	2.99E−11
700_1	9.81E−06	2.99E−11	9.81E−06	9.81E−06	1.36E−06	2.99E−11
300_4	6.87E−05	2.99E−11	6.87E−05	6.87E−05	4.91E−05	9.81E−11
500_4	1.42E−05	2.99E−11	1.37E−05	1.37E−05	1.52E−05	2.99E−11
700_4	2.89E−06	2.99E−11	2.89E−06	2.89E−06	2.89E−06	2.99E−11

Appendix D

Supplementary result plots

Plots of the magnitude and the direction of the groundwater flow around and through the SFL repository are presented below. For each investigated location, the 2D results are presented for xz and yz-planes crossing the vaults.

Location 300_1

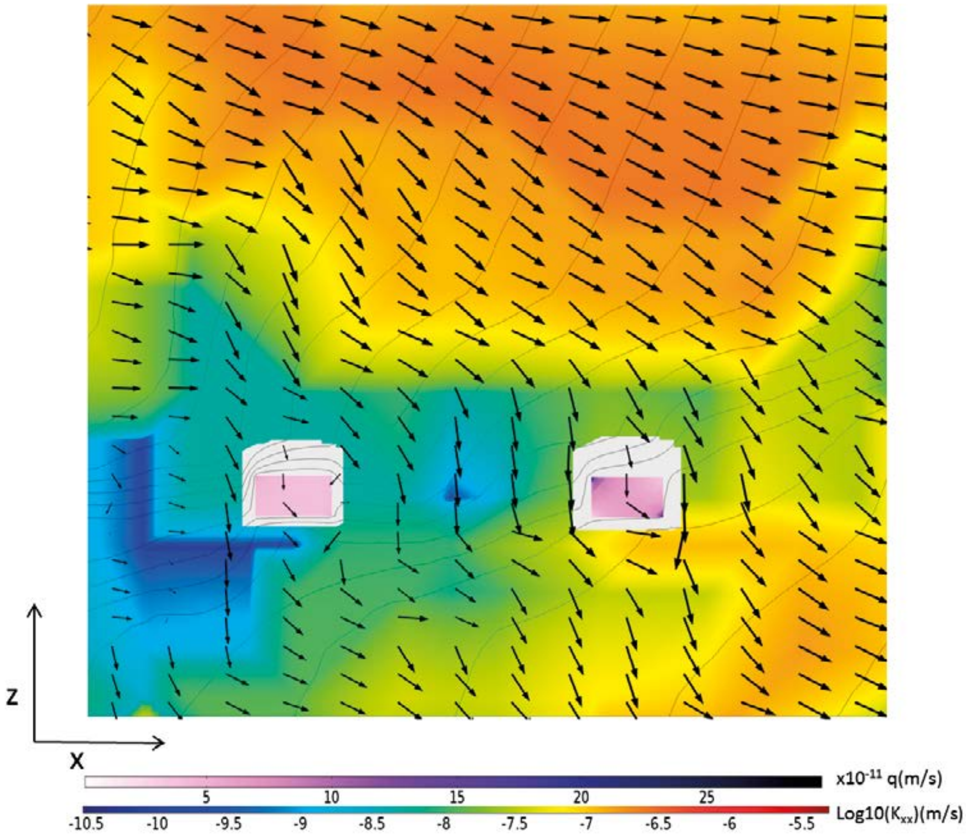

Figure D-1. *Magnitude of Darcy velocity through the waste control volumes (BHA left and BHK right), hydraulic conductivity of the rock, hydraulic head (isolines) and Darcy velocity (arrows) in xz-plane at location 300_1.*

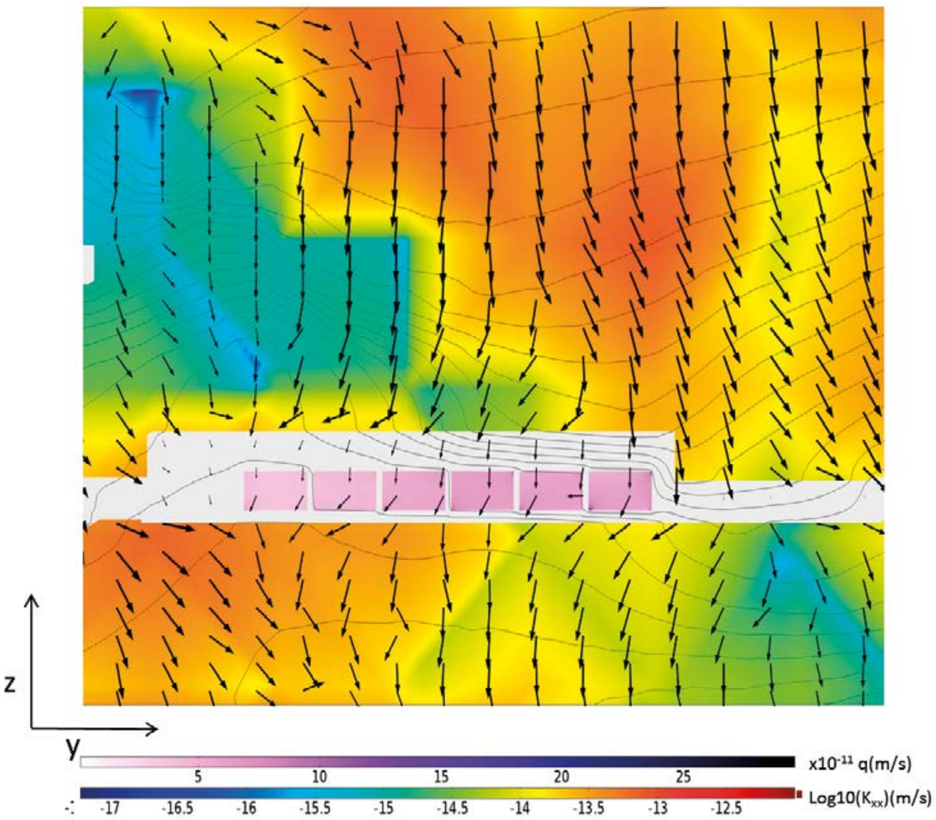

Figure D-2. Magnitude of Darcy velocity through the waste control volumes (BHK), hydraulic conductivity of the rock, hydraulic head (isolines) and Darcy velocity (arrows) in yz-plane at location 300_1.

Location 300_4

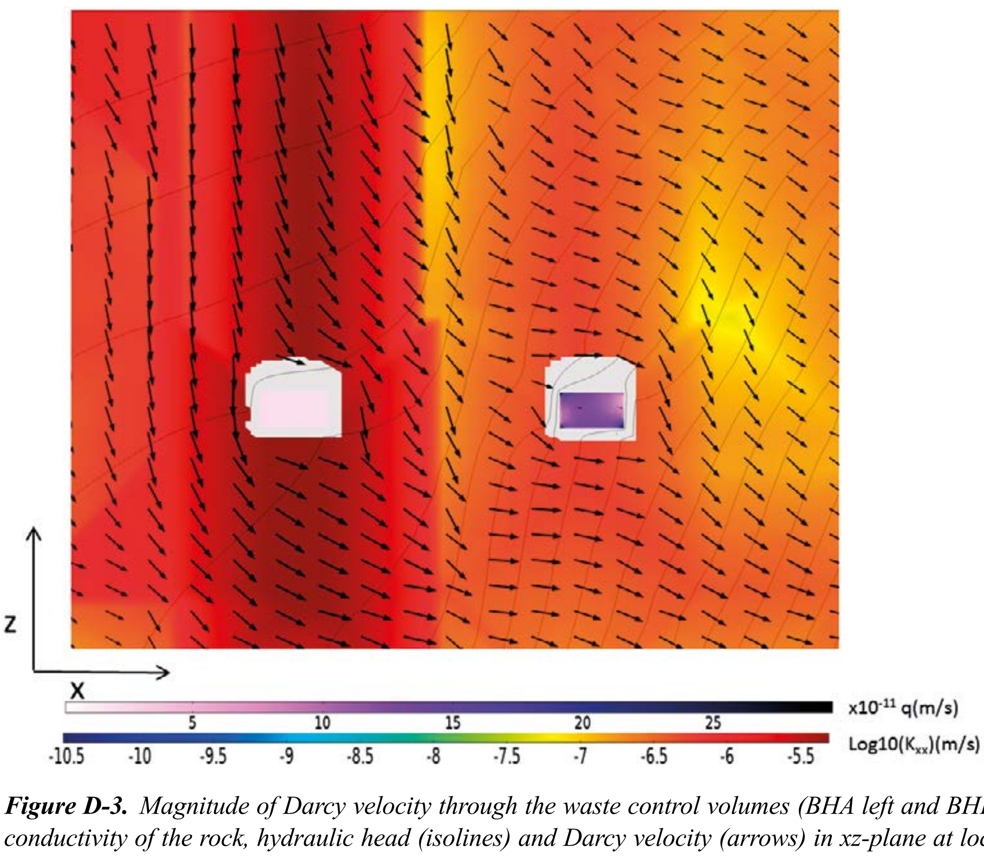

Figure D-3. Magnitude of Darcy velocity through the waste control volumes (BHA left and BHK right), hydraulic conductivity of the rock, hydraulic head (isolines) and Darcy velocity (arrows) in xz-plane at location 300_4.

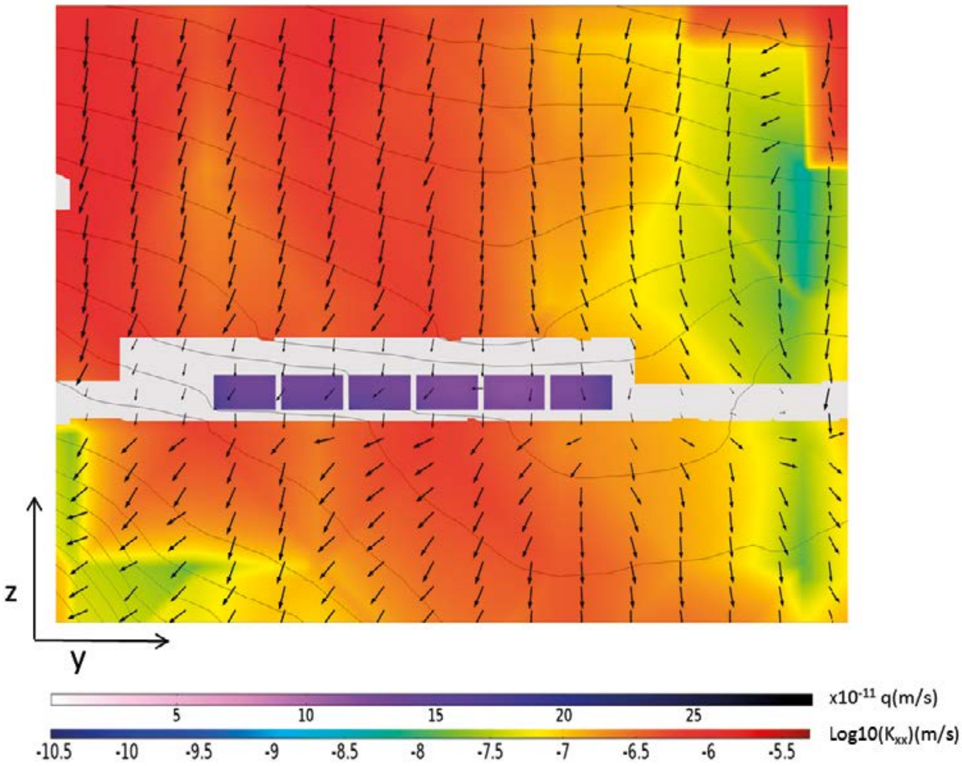

Figure D-4. *Magnitude of Darcy velocity through the waste control volumes (BHK), hydraulic conductivity of the rock, hydraulic head (isolines) and Darcy velocity (arrows) in yz-plane at location 300_4.*

Location 500_1

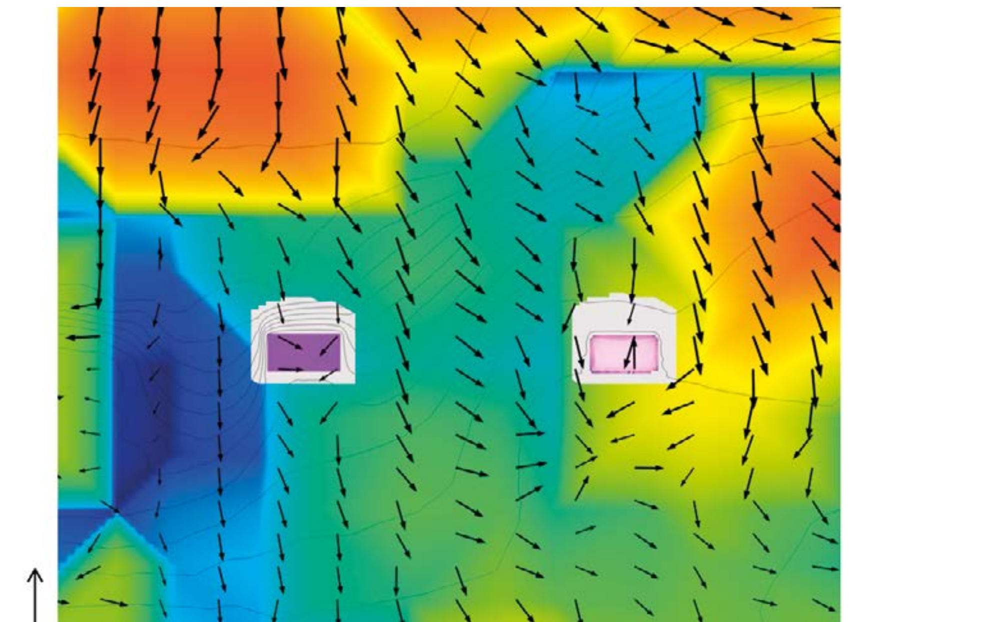

Figure D-5. *Magnitude of Darcy velocity through the waste control volumes (BHA left and BHK right), hydraulic conductivity of the rock, hydraulic head (isolines) and Darcy velocity (arrows) in xz-plane at location 500_1.*

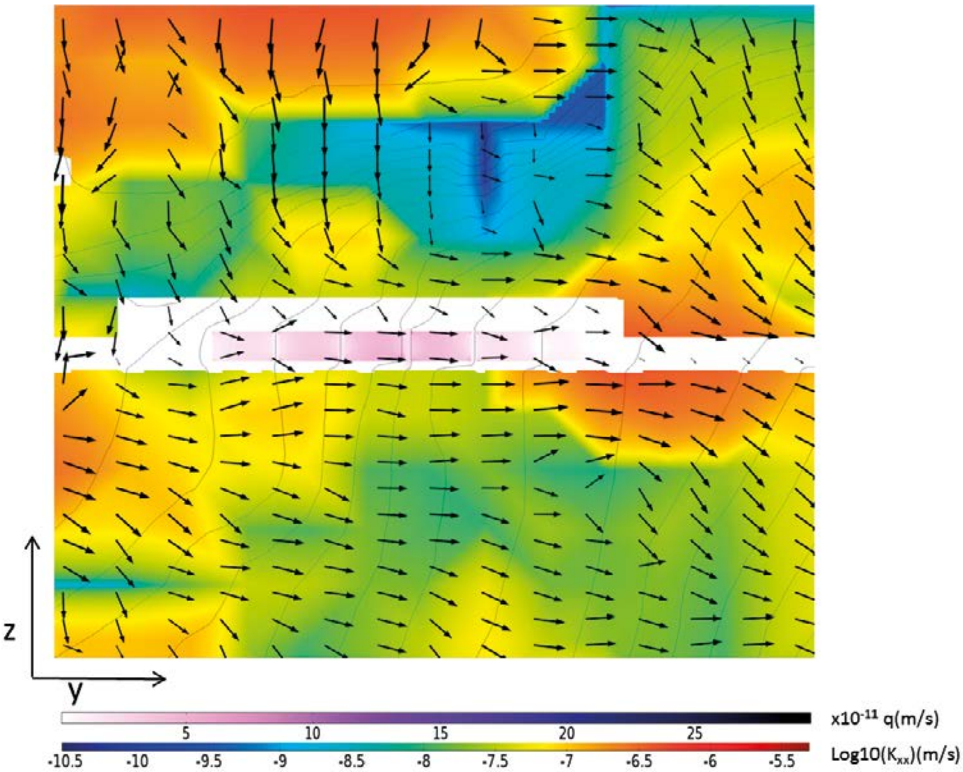

***Figure D-6.** Magnitude of Darcy velocity through the waste control volumes (BHK), hydraulic conductivity of the rock, hydraulic head (isolines) and Darcy velocity (arrows) in yz-plane at location 500_1.*

Location 500_4

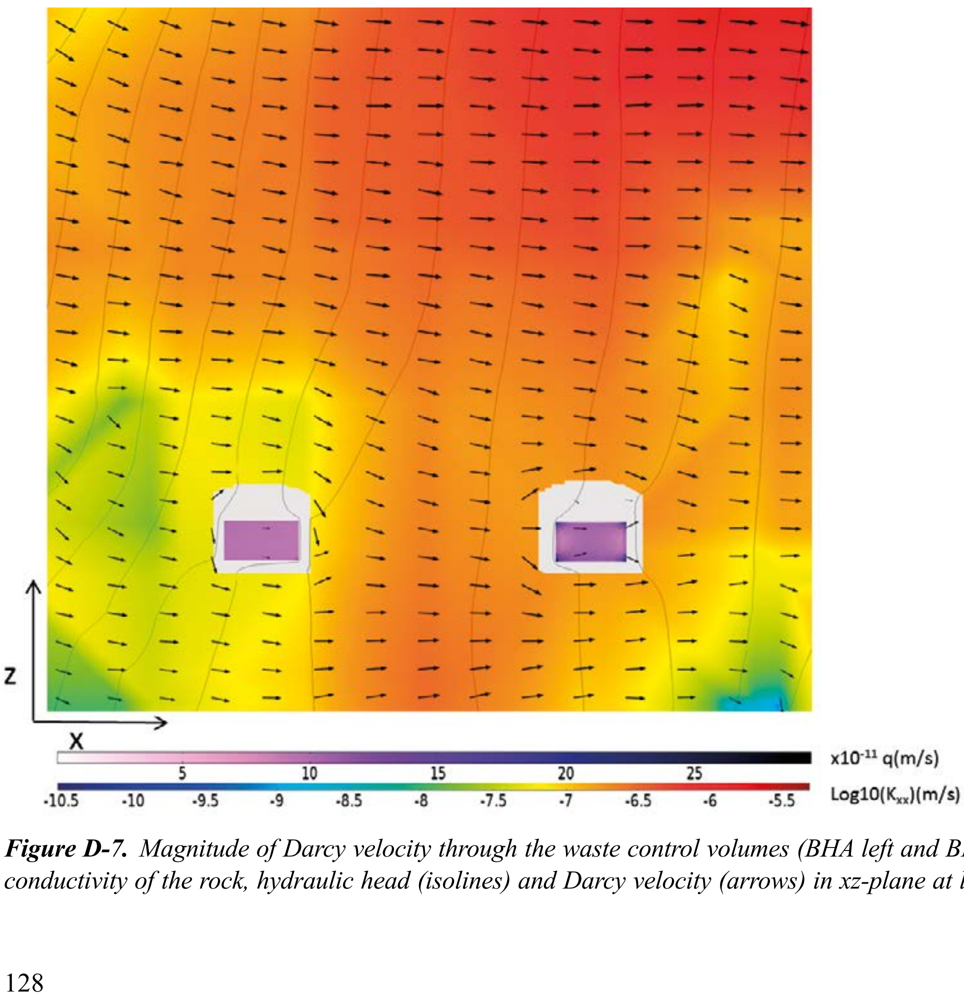

***Figure D-7.** Magnitude of Darcy velocity through the waste control volumes (BHA left and BHK right), hydraulic conductivity of the rock, hydraulic head (isolines) and Darcy velocity (arrows) in xz-plane at location 500_4.*

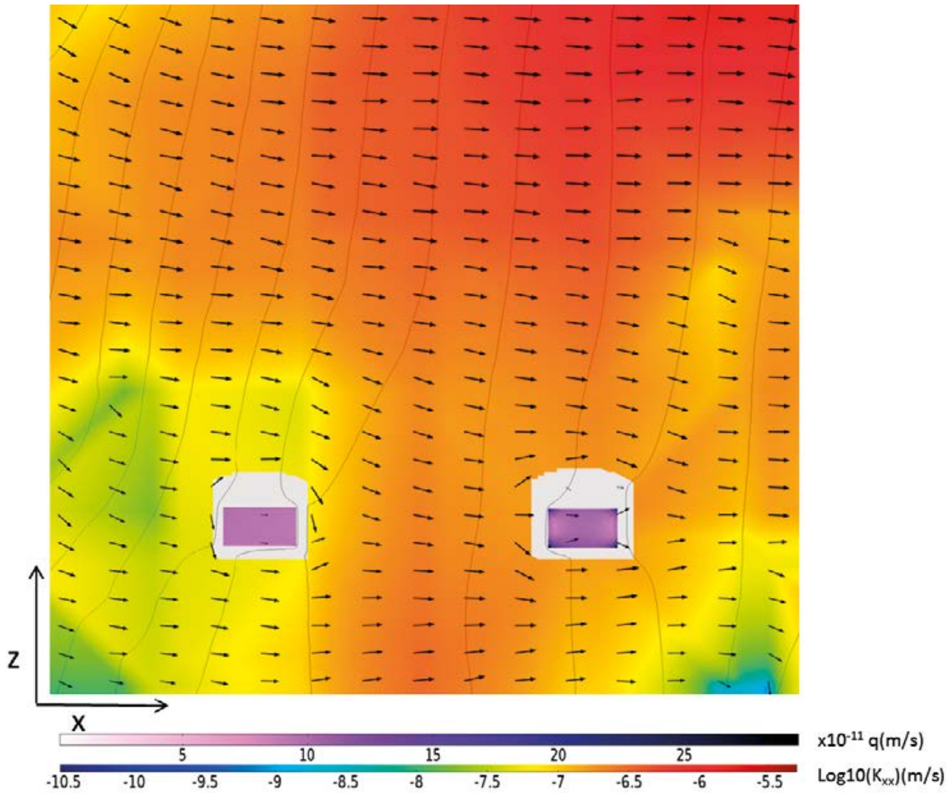

***Figure D-8.** Magnitude of Darcy velocity through the waste control volumes (BHK), hydraulic conductivity of the rock, hydraulic head (isolines) and Darcy velocity (arrows) in yz-plane at location 500_4.*

Location 700_1

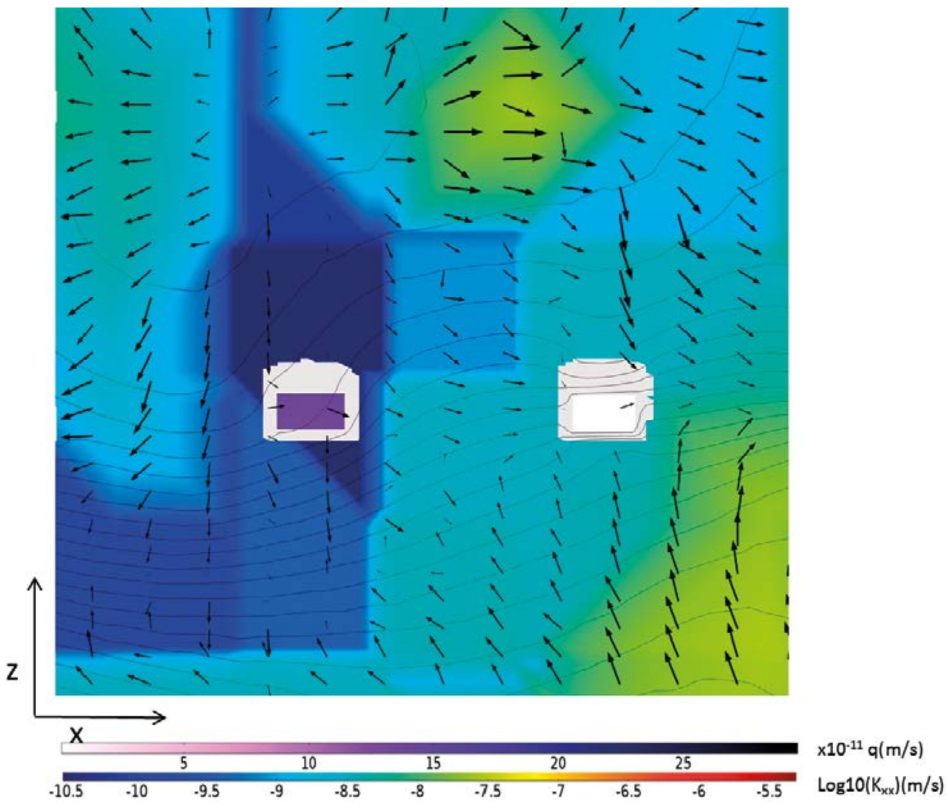

***Figure D-9.** Magnitude of Darcy velocity through the waste control volumes (BHA left and BHK right), hydraulic conductivity of the rock, hydraulic head (isolines) and Darcy velocity (arrows) in xz-plane at location 700_1.*

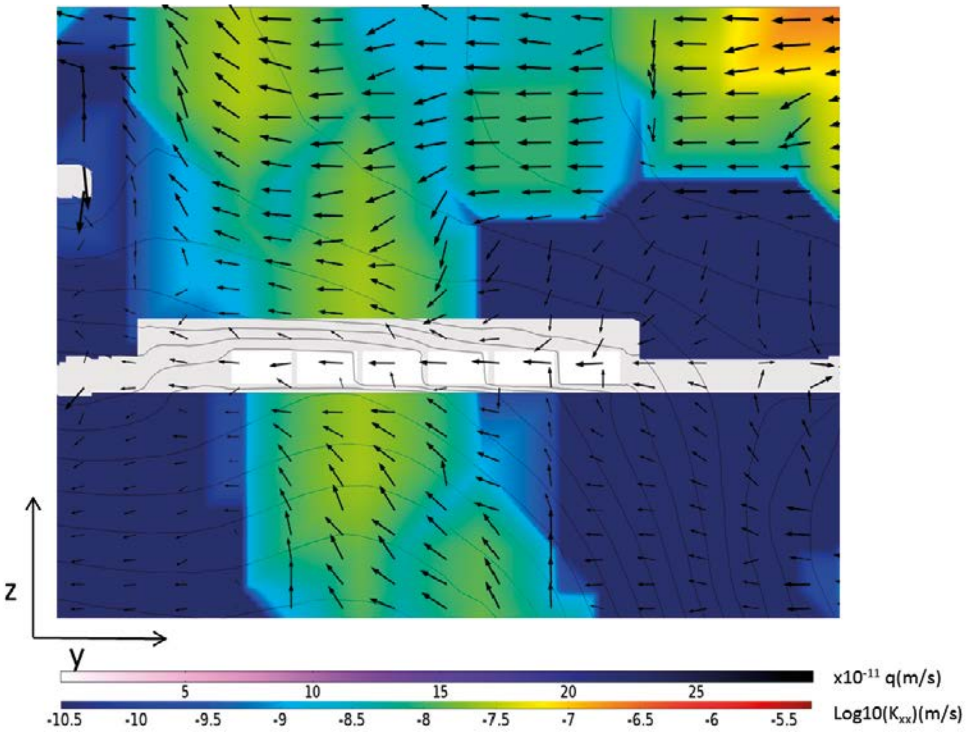

Figure D-10. *Magnitude of Darcy velocity through the waste control volumes (BHK), hydraulic conductivity of the rock, hydraulic head (isolines) and Darcy velocity (arrows) in yz-plane at location 700_1.*

Location 700_4

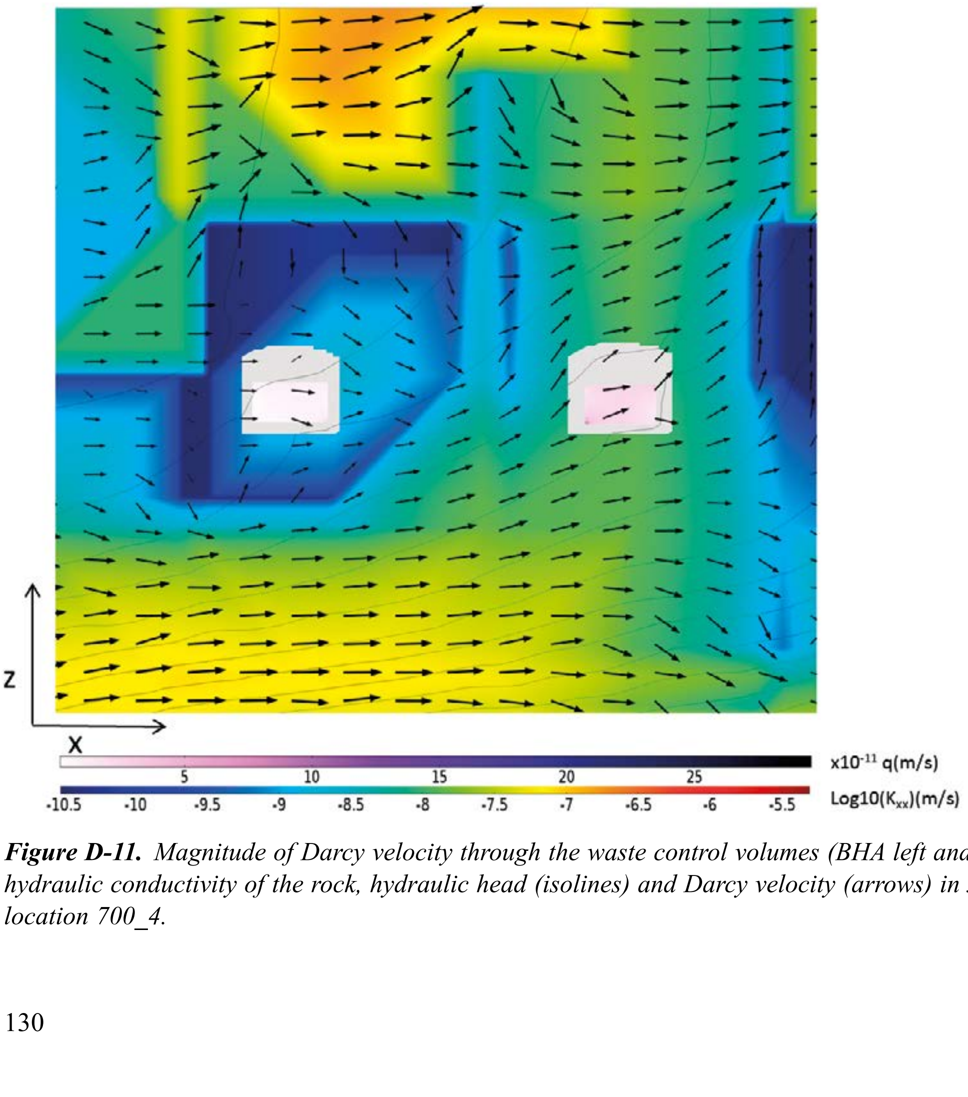

Figure D-11. *Magnitude of Darcy velocity through the waste control volumes (BHA left and BHK right), hydraulic conductivity of the rock, hydraulic head (isolines) and Darcy velocity (arrows) in xz-plane at location 700_4.*

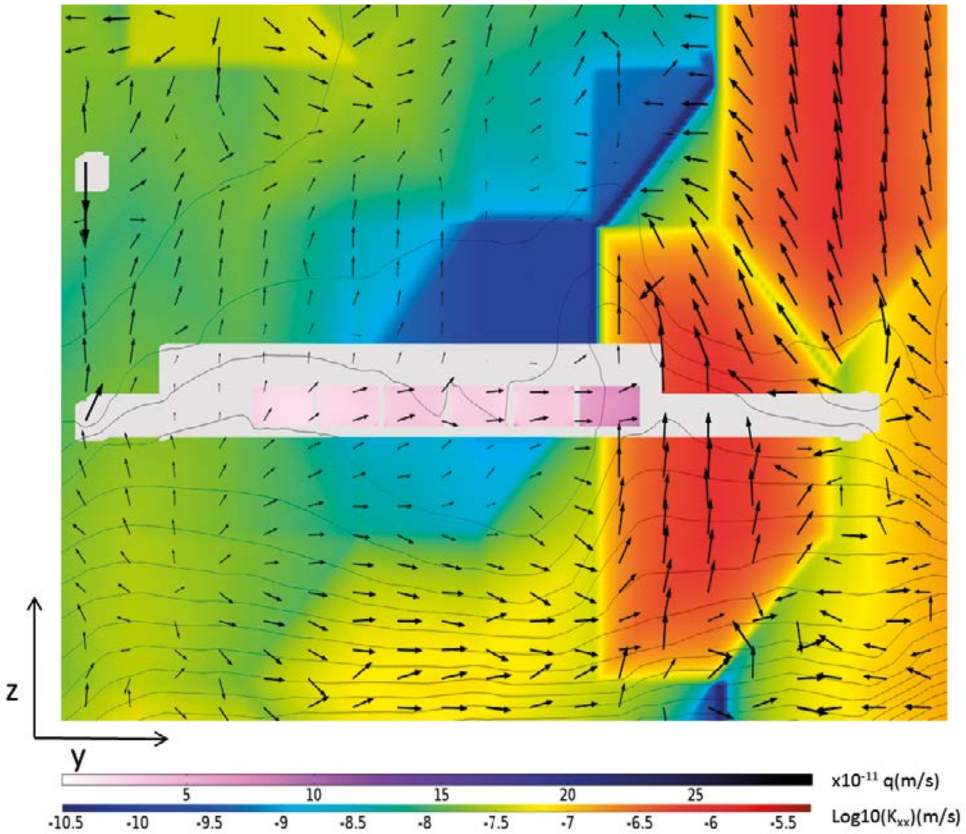

Figure D-12. *Magnitude of Darcy velocity through the waste control volumes (BHK), hydraulic conductivity of the rock, hydraulic head (isolines) and Darcy velocity (arrows) in yz-plane at location 700_4.*

Appendix E

Vault and waste flows as function of repository orientation at location 500_4

The flows through the BHA and BHK vaults and waste control volumes at location 500_4 is presented in Table E-1 for 0° rotation, in Table E-2 for 90° rotation, in Table E-3 for 180° rotation, and in Table E-4 for 270° rotation.

Table E-1. Calculated flow through waste control volumes and BHA and BHK vaults at location 500_4 for the case of 0° repository rotation.

			Total flow (m^3/year)	Mass conservation error
BHA	**Waste**	BHA_1	0.194	3.05%
		BHA_2	0.306	0.93%
		BHA_3	0.414	1.14%
		BHA_4	0.537	0.45%
		BHA_5	0.404	−5.01%
	Vault	BHA	0.842	0.91%
BHK	**Waste**	BHK_1	0.325	0.21%
		BHK_2	0.332	1.52%
		BHK_3	0.325	−0.46%
		BHK_4	0.297	0.87%
		BHK_5	0.328	2.42%
		BHK_6	0.360	2.74%
	Vault	BHK	3.288	0.08%

Table E-2. Calculated flow through waste control volumes and BHA and BHK vaults at location 500_4 for the case of 90° repository rotation.

			Total flow (m^3/year)	Mass conservation error
BHA	**Waste**	BHA_1	1.019	−3.96%
		BHA_2	1.244	−0.56%
		BHA_3	1.239	0.41%
		BHA_4	1.110	1.02%
		BHA_5	0.736	4.82%
	Vault	BHA	1.319	−0.51%
BHK	**Waste**	BHK_1	0.366	0.18%
		BHK_2	0.439	1.44%
		BHK_3	0.441	1.09%
		BHK_4	0.451	0.99%
		BHK_5	0.395	−0.51%
		BHK_6	0.260	3.25%
	Vault	BHK	1.310	2.50%

Table E-3. Calculated flow through waste control volumes and BHA and BHK vaults at location 500_4 for the case of 180° repository rotation.

			Total flow (m^3/year)	Mass conservation error
BHA	**Waste**	BHA_1	0.118	−0.41%
		BHA_2	0.161	−1.37%
		BHA_3	0.235	−1.43%
		BHA_4	0.248	−0.24%
		BHA_5	0.186	3.99%
	Vault	BHA	0.628	1.70%
BHK	**Waste**	BHK_1	0.826	0.26%
	0	BHK_2	0.649	0.41%
	0	BHK_3	0.436	−1.35%
	0	BHK_4	0.355	−1.90%
	0	BHK_5	0.331	−1.96%
	0	BHK_6	0.329	−2.39%
	Vault	BHK	3.884	2.01%

Table E-4. Calculated flow through waste control volumes and BHA and BHK vaults at location 500_4 for the case of 270° repository rotation.

			Total flow (m^3/year)	Mass conservation error
BHA	**Waste**	BHA_1	0.685	−1.47%
		BHA_2	0.981	−1.04%
		BHA_3	1.021	−0.36%
		BHA_4	0.975	−0.73%
		BHA_5	0.674	−0.78%
	Vault	BHA	1.081	1.83%
BHK	**Waste**	BHK_1	0.366	−1.47%
	0	BHK_2	0.605	−1.04%
	0	BHK_3	0.879	−0.36%
	0	BHK_4	1.071	−0.73%
	0	BHK_5	0.873	−0.78%
	0	BHK_6	0.584	0.13%
	Vault	BHK	2.839	3.14%

Appendix F

Vault and waste flows as function of backfill hydraulic properties

Concrete barrier

Table F-1. Calculated flow through the BHA and BHK waste and vaults at location 300_4 for the base case.

			Total flow (m^3/year)	Mass conservation error
BHA	**Waste**	BHA_1	9.59E−02	0.04%
		BHA_2	8.61E−02	−4.75%
		BHA_3	1.09E−01	−2.37%
		BHA_4	1.55E−01	−0.70%
		BHA_5	1.38E−01	3.33%
	Vault	BHA	4.27E−01	−1.82%
BHK	**Waste**	BHK_1	4.50E−01	0.32%
		BHK_2	4.97E−01	2.21%
		BHK_3	5.86E−01	0.67%
		BHK_4	6.45E−01	1.69%
		BHK_5	6.71E−01	2.20%
		BHK_6	6.41E−01	1.41%
	Vault	BHK	4.66E+00	1.52%

Table F-2. Calculated flow through the BHA and BHK waste and vaults at location 300_4 for the degraded concrete state.

			Total flow (m^3/year)	Mass conservation error
BHA	**Waste**	BHA_1	9.49E−02	−0.02%
		BHA_2	8.69E−02	−4.73%
		BHA_3	1.12E−01	−2.32%
		BHA_4	1.57E−01	−0.68%
		BHA_5	1.39E−01	3.34%
	Vault	BHA	4.29E−01	−1.84%
BHK	**Waste**	BHK_1	8.49E+00	0.42%
		BHK_2	1.25E+01	0.23%
		BHK_3	1.57E+01	−0.02%
		BHK_4	1.73E+01	−0.61%
		BHK_5	1.79E+01	−0.70%
		BHK_6	1.82E+01	−0.44%
	Vault	BHK	2.00E+02	0.79%

Table F-3. Calculated flow through the BHA and BHK waste and vaults at location 300_4 for the hydraulic cage state in the BHK.

			Total flow (m^3/year)	Mass conservation error
BHA	**Waste**	BHA_1	9.09E−02	13.85%
		BHA_2	9.04E−02	3.02%
		BHA_3	1.22E−01	−2.52%
		BHA_4	1.66E−01	−12.52%
		BHA_5	1.44E−01	−17.95%
	Vault	BHA	4.39E−01	−1.90%
BHK	**Waste**	BHK_1*	7.54E−01	0.24%
		BHK_2*	1.70E+00	−0.38%
		BHK_3*	2.85E+00	0.40%
		BHK_4*	3.71E+00	0.24%
		BHK_5*	3.93E+00	0.47%
		BHK_6*	3.88E+00	1.40%
	Vault	BHK**	7.63E+02	4.96%

Table F-4. Calculated flow through the BHA and BHK waste and vaults at location 300_4 for the alternative initial state in the BHK.

			Total flow (m^3/year)	Mass conservation error
BHA	**Waste**	BHA_1	9.59E−02	0.04%
		BHA_2	8.61E−02	−4.75%
		BHA_3	1.09E−01	−2.38%
		BHA_4	1.55E−01	−0.70%
		BHA_5	1.38E−01	3.32%
	Vault	BHA	4.27E−01	−1.82%
BHK	**Waste**	BHK_1	5.76E−04	0.42%
		BHK_2	6.30E−04	2.33%
		BHK_3	7.44E−04	0.69%
		BHK_4	8.22E−04	1.77%
		BHK_5	8.54E−04	2.34%
		BHK_6	8.13E−04	1.34%
	Vault	BHK	5.87E−03	1.50%

Table F-5. Calculated flow through the BHA and BHK waste and vaults at location 500_4 for the base case.

			Total flow (m^3/year)	Mass conservation error
BHA	**Waste**	BHA_1	1.94E−01	3.05%
		BHA_2	3.06E−01	0.93%
		BHA_3	4.14E−01	1.14%
		BHA_4	5.37E−01	0.45%
		BHA_5	4.04E−01	−5.01%
	Vault	BHA	8.42E−01	0.91%
BHK	**Waste**	BHK_1	3.25E−01	0.21%
		BHK_2	3.32E−01	1.52%
		BHK_3	3.25E−01	−0.46%
		BHK_4	2.97E−01	0.87%
		BHK_5	3.28E−01	2.42%
		BHK_6	3.60E−01	2.74%
	Vault	BHK	3.29E+00	0.08%

Table F-6. Calculated flow through the BHA and BHK waste and vaults at location 500_4 for the degraded concrete state.

			Total flow (m^3/year)	Mass conservation error
BHA	**Waste**	BHA_1	1.90E−01	3.00%
		BHA_2	3.01E−01	0.95%
		BHA_3	4.12E−01	1.18%
		BHA_4	5.38E−01	0.48%
		BHA_5	4.07E−01	−4.99%
	Vault	BHA	8.52E−01	0.90%
BHK	**Waste**	BHK_1	6.06E+00	−0.20%
		BHK_2	4.27E+00	0.29%
		BHK_3	4.45E+00	0.76%
		BHK_4	4.77E+00	1.09%
		BHK_5	4.81E+00	0.00%
		BHK_6	4.46E+00	−1.28%
	Vault	BHK	7.61E+01	1.44%

Table F-7. Calculated flow through the BHA and BHK waste and vaults at location 500_4 for the hydraulic cage state in the BHK.

			Total flow (m^3/year)	Mass conservation error
BHA	**Waste**	BHA_1	1.83E−01	−12.77%
		BHA_2	2.95E−01	7.00%
		BHA_3	4.12E−01	20.98%
		BHA_4	5.46E−01	18.72%
		BHA_5	4.14E−01	−14.22%
	Vault	BHA	8.72E−01	0.87%
BHK	**Waste**	BHK_1*	6.71E−01	1.16%
		BHK_2*	3.80E−01	−0.64%
		BHK_3*	4.20E−01	−1.42%
		BHK_4*	3.86E−01	−1.48%
		BHK_5*	4.04E−01	−0.04%
		BHK_6*	3.19E−01	0.00%
	Vault	BHK**	1.67E+02	1.71%

Table F-8. Calculated flow through the BHA and BHK waste and vaults at location 500_4 for the alternative initial state in the BHK.

			Total flow (m^3/year)	Mass conservation error
BHA	**Waste**	BHA_1	1.63E−01	3.05%
		BHA_2	2.81E−01	0.93%
		BHA_3	4.15E−01	1.14%
		BHA_4	5.37E−01	0.45%
		BHA_5	4.04E−01	−5.01%
	Vault	BHA	8.41E−01	0.91%
BHK	**Waste**	BHK_1	4.20E−04	0.20%
		BHK_2	4.34E−04	1.61%
		BHK_3	4.22E−04	−0.48%
		BHK_4	3.82E−04	0.83%
		BHK_5	4.24E−04	2.59%
		BHK_6	4.73E−04	2.93%
	Vault	BHK	4.26E−03	0.03%

Table F-9. Calculated flow through the BHA and BHK waste and vaults at location 700_1 for the base case.

			Total flow (m^3/year)	Mass conservation error
BHA	**Waste**	BHA_1	3.17E−01	−3.45%
		BHA_2	5.56E−01	−2.14%
		BHA_3	6.19E−01	−0.59%
		BHA_4	5.90E−01	1.44%
		BHA_5	3.24E−01	3.14%
	Vault	BHA	6.71E−01	0.16%
BHK	**Waste**	BHK_1	3.38E−02	4.80%
		BHK_2	3.67E−02	5.37%
		BHK_3	3.07E−02	6.14%
		BHK_4	2.63E−02	4.30%
		BHK_5	1.74E−02	6.81%
		BHK_6	9.11E−03	12.92%
	Vault	BHK	1.10E−01	−26.24%

Table F-10. Calculated flow through the BHA and BHK waste and vaults at location 700_1 for the degraded concrete state.

			Total flow (m^3/year)	Mass conservation error
BHA	**Waste**	BHA_1	3.17E−01	−3.45%
		BHA_2	5.55E−01	−2.14%
		BHA_3	6.18E−01	−0.59%
		BHA_4	5.89E−01	1.44%
		BHA_5	3.23E−01	3.15%
	Vault	BHA	6.70E−01	0.16%
BHK	**Waste**	BHK_1*	2.00E−02	16.40%
		BHK_2*	3.16E−02	13.06%
		BHK_3*	6.40E−02	3.99%
		BHK_4*	8.77E−02	3.41%
		BHK_5*	7.44E−02	7.12%
		BHK_6*	4.77E−02	11.22%
	Vault	BHK**	2.92E−01	2.89%

Table F-11. Calculated flow through the BHA and BHK waste and vaults at location 700_1 for the hydraulic cage state in the BHK.

			Total flow (m^3/year)	Mass conservation error
BHA	**Waste**	BHA_1	3.16E−01	85.02%
		BHA_2	5.55E−01	81.66%
		BHA_3	6.18E−01	84.26%
		BHA_4	5.87E−01	82.87%
		BHA_5	3.22E−01	82.44%
	Vault	BHA	6.69E−01	0.16%
BHK	**Waste**	BHK_1*	6.34E−03	−77.72%
		BHK_2*	9.02E−03	−109.90%
		BHK_3*	1.42E−02	−110.23%
		BHK_4*	1.54E−02	−82.98%
		BHK_5*	1.15E−02	−75.53%
		BHK_6*	1.14E−02	−35.20%
	Vault	BHK**	4.71E−01	16.05%

Table F-12. Calculated flow through the BHA and BHK waste and vaults at location 700_1 for the alternative initial state in the BHK.

			Total flow (m^3/year)	Mass conservation error
BHA	**Waste**	BHA_1	3.17E−01	−3.46%
		BHA_2	5.57E−01	−2.14%
		BHA_3	6.20E−01	−0.59%
		BHA_4	5.91E−01	1.44%
		BHA_5	3.25E−01	3.15%
	Vault	BHA	6.72E−01	0.16%
BHK	**Waste**	BHK_1	7.38E−04	−12.91%
		BHK_2	7.20E−04	−15.36%
		BHK_3	7.63E−04	−45.92%
		BHK_4	8.44E−04	−45.76%
		BHK_5	7.47E−04	−28.67%
		BHK_6	6.43E−04	−13.09%
	Vault	BHK	1.13E−03	2.16%

Bentonite barrier

Table F-13. Calculated flow through the BHA and BHK waste and vaults at location 300_4 for the degraded bentonite state.

			Total flow (m^3/year)	Mass conservation error
BHA	**Waste**	BHA_1	1.53E+01	1.53%
		BHA_2	1.52E+01	1.02%
		BHA_3	1.55E+01	−0.11%
		BHA_4	1.63E+01	−0.09%
		BHA_5	1.63E+01	0.75%
	Vault	BHA	1.44E+02	−3.74%
BHK	**Waste**	BHK_1	4.49E−01	0.32%
		BHK_2	4.98E−01	2.21%
		BHK_3	5.86E−01	0.67%
		BHK_4	6.45E−01	1.70%
		BHK_5	6.70E−01	2.20%
		BHK_6	6.40E−01	1.41%
	Vault	BHK	4.66E+00	1.50%

Table F-14. Calculated flow through the BHA and BHK waste and vaults at location 300_4 for the hydraulic cage state in the BHA.

			Total flow (m^3/year)	Mass conservation error
BHA	**Waste**	BHA_1*	4.29E+00	0.54%
		BHA_2*	8.01E+00	2.80%
		BHA_3*	1.14E+01	0.77%
		BHA_4*	9.70E+00	2.71%
		BHA_5*	4.64E+00	3.46%
	Vault	BHA**	9.39E+02	6.46%
BHK	**Waste**	BHK_1	4.52E−01	0.35%
		BHK_2	5.00E−01	2.24%
		BHK_3	5.86E−01	0.66%
		BHK_4	6.46E−01	1.71%
		BHK_5	6.72E−01	2.24%
		BHK_6	6.44E−01	1.44%
	Vault	BHK	4.71E+00	1.45%

Table F-15. Calculated flow through the BHA and BHK waste and vaults at location 300_4 for the alternative initial state in the BHA.

			Total flow (m^3/year)	Mass conservation error
BHA	**Waste**	BHA_1	9.16E−05	−0.52%
		BHA_2	9.46E−05	−4.96%
		BHA_3	1.30E−04	−2.27%
		BHA_4	1.79E−04	−0.59%
		BHA_5	1.51E−04	3.59%
	Vault	BHA	4.35E−04	−1.85%
BHK	**Waste**	BHK_1	4.49E−01	0.32%
		BHK_2	4.97E−01	2.21%
		BHK_3	5.85E−01	0.67%
		BHK_4	6.45E−01	1.69%
		BHK_5	6.70E−01	2.20%
		BHK_6	6.40E−01	1.41%
	Vault	BHK	4.66E+00	1.51%

Table F-16. Calculated flow through the BHA and BHK waste and vaults at location 500_4 for the degraded bentonite state.

			Total flow (m^3/year)	Mass conservation error
BHA	**Waste**	BHA_1	5.45E+00	0.36%
		BHA_2	7.52E+00	0.20%
		BHA_3	9.96E+00	−0.32%
		BHA_4	1.14E+01	−1.26%
		BHA_5	8.34E+00	1.60%
	Vault	BHA	8.20E+01	−1.94%
BHK	**Waste**	BHK_1	3.32E−01	0.21%
		BHK_2	3.41E−01	1.53%
		BHK_3	3.35E−01	−0.48%
		BHK_4	3.07E−01	0.86%
		BHK_5	3.35E−01	2.43%
		BHK_6	3.64E−01	2.77%
	Vault	BHK	3.36E+00	0.01%

Table F-17. Calculated flow through the BHA and BHK waste and vaults at location 500_4 for the hydraulic cage state in the BHA.

			Total flow (m^3/year)	Mass conservation error
BHA	**Waste**	BHA_1*	3.99E−01	0.61%
		BHA_2*	8.63E−01	3.23%
		BHA_3*	1.44E+00	1.81%
		BHA_4*	1.19E+00	−1.50%
		BHA_5*	8.49E−01	3.69%
	Vault	BHA**	1.41E+02	4.90%
BHK	**Waste**	BHK_1	3.48E−01	0.20%
		BHK_2	3.56E−01	1.61%
		BHK_3	3.54E−01	−0.47%
		BHK_4	3.29E−01	0.83%
		BHK_5	3.51E−01	2.39%
		BHK_6	3.65E−01	2.81%
	Vault	BHK	3.48E+00	−0.11%

Table F-18. Calculated flow through the BHA and BHK waste and vaults at location 500_4 for the alternative initial state in the BHA.

			Total flow (m^3/year)	Mass conservation error
BHA	**Waste**	BHA_1	2.56E−04	2.25%
		BHA_2	4.23E−04	−1.52%
		BHA_3	5.49E−04	−0.66%
		BHA_4	6.45E−04	−0.20%
		BHA_5	4.93E−04	−4.85%
	Vault	BHA	9.03E−04	0.89%
BHK	**Waste**	BHK_1	3.25E−01	0.21%
		BHK_2	3.31E−01	1.52%
		BHK_3	3.25E−01	−0.46%
		BHK_4	2.97E−01	0.87%
		BHK_5	3.28E−01	2.42%
		BHK_6	3.60E−01	2.74%
	Vault	BHK	3.29E+00	0.08%

Table F-19. Calculated flow through the BHA and BHK waste and vaults at location 700_1 for the degraded bentonite state.

			Total flow (m^3/year)	Mass conservation error
BHA	**Waste**	BHA_1*	8.14E−01	−4.21%
		BHA_2*	1.29E+00	−1.75%
		BHA_3*	1.41E+00	−0.66%
		BHA_4*	1.32E+00	0.12%
		BHA_5*	1.07E+00	0.91%
	Vault	BHA**	3.34E+00	2.29%
BHK	**Waste**	BHK_1	3.14E−02	4.93%
		BHK_2	3.41E−02	5.57%
		BHK_3	3.04E−02	6.25%
		BHK_4	2.33E−02	5.06%
		BHK_5	1.38E−02	8.83%
		BHK_6	5.92E−03	18.85%
	Vault	BHK	1.05E−01	−27.80%

Table F-20. Calculated flow through the BHA and BHK waste and vaults at location 700_1 for the hydraulic cage state in the BHA.

			Total flow (m^3/year)	Mass conservation error
BHA	**Waste**	BHA_1*	3.80E−02	2.50%
		BHA_2*	5.54E−02	0.88%
		BHA_3*	8.61E−02	2.60%
		BHA_4*	7.85E−02	−4.29%
		BHA_5*	7.37E−02	3.20%
	Vault	BHA**	5.72E+00	−0.69%
BHK	**Waste**	BHK_1	2.95E−02	5.02%
		BHK_2	3.16E−02	5.78%
		BHK_3	2.71E−02	6.75%
		BHK_4	2.00E−02	6.13%
		BHK_5	1.19E−02	10.41%
		BHK_6	5.96E−03	18.78%
	Vault	BHK	1.04E−01	−27.99%

Table F-21. Calculated flow through the BHA and BHK waste and vaults at location 700_1 for the alternative initial state in the BHA.

			Total flow (m^3/year)	Mass conservation error
BHA	**Waste**	BHA_1	4.82E−03	−29.91%
		BHA_2	5.63E−03	−110.77%
		BHA_3	6.10E−03	−45.33%
		BHA_4	9.03E−03	−94.09%
		BHA_5	1.00E−02	−127.36%
	Vault	BHA	1.21E−03	−1.92%
BHK	**Waste**	BHK_1	3.49E−02	4.75%
		BHK_2	3.80E−02	5.27%
		BHK_3	3.11E−02	6.08%
		BHK_4	2.79E−02	4.03%
		BHK_5	1.95E−02	6.06%
		BHK_6	1.06E−02	11.52%
	Vault	BHK	1.16E−01	−24.16%

SKB is tasked with managing Swedish nuclear and radioactive waste in a safe way.

skb.se

Arkitektkopia AB, Bromma, 2016